

DSE - Next Stop: Europa

Investigate the ice layer and subsurface ocean on Europa to establish the conditions for possible life

V. van den Bercken	4098862	R. Kok	4176111
S. Burger	4213971	T.A.H. Kranen	4148193
N.M. Dekkers	4224043	G.P. van Marrewijk	4137787
J.M. Hoogvliet	4135350	F.T. Melman	4229223
A.V. Kassem	4231848	B. Mulder	4100794

Detail Report

Design Synthesis Exercise

- This page intentionally left blank -

Preface

In 1610, Galileo discovered four satellites orbiting Jupiter. Only later they became known as Ganymede, Callisto, Io and Europa. These are the first bodies discovered that did not orbit the Sun or Earth. Due to the increasing level of space technology in recent decades, it has become feasible to perform a detailed investigation of the geological and mechanical properties of the ice and ocean on Europa for the first time.

The scientific community shows special interest in this moon, because it may contain the three ingredients needed for life. Water is present at least in the form of ice, and probably also in the subsurface ocean. Organic compounds may also be found, deduced from the signs of “claylike materials”. Finally, heat originating from tidal deformation could be a source of energy for life. Because of this, Europa can provide the scientific community with new insights on the presence of conditions for life. A team of 10 Aerospace Engineering students from Delft University of Technology in the Netherlands is intensively investigating the possibilities of scientific missions to the interesting moon Europa, in the context of the Design Synthesis Exercise to finish their Bsc degree.

As with any project, most motivation comes from learning and getting new insights. Therefore, the design team wants to give many thanks to Erwin Mooij, Fardin Esrail and Svenja Woicke for their willingness and patience to always provide us with advise and resources on many different topics. Without their guiding role, the quality of our work could never have reached this level. Special thanks to Hermes M. Jara Orue. Without his enthusiasm and knowledge, the wonders of Europa would not have been unveiled to us in such an inspiring way.

Finally, we gratefully thank Thomas Voirin from ESTEC in Noordwijk, to provide us with the information we need from our customer.

‘All truths are easy to understand once they are discovered; the point is to discover them’

– Galileo Galilei –

Contents

List of Symbols	vii
List of Abbreviations	x
Executive Overview	xi
Summary of the Mission	xi
1 Introduction	1
2 Concept Description & Top Level Requirements	2
2.1 Concept Description	2
2.2 Top Level Requirements	2
3 Design Considerations	4
3.1 Mission Functions	4
3.2 Resource Allocation and Budget Breakdown	4
4 Astrodynamic Characteristics	7
4.1 Interplanetary Transfer	7
4.2 Jovian Tour	8
4.3 Europa Orbit	10
4.4 De-orbiting	16
4.5 ΔV Budget	16
5 Guidance, Navigation and Control Subsystem	17
5.1 Subsystem Description	17
5.2 Functional Flow Block Diagram	19
5.3 Functional Breakdown Structure	20
5.4 Performance Analysis	21
5.5 Code Verification	25
5.6 Compliance Matrix	26
6 Propulsion Subsystem	28
6.1 Functional Breakdown Structure	28
6.2 Functional Flow Block Diagram	28
6.3 Performance	28
6.4 Verification	34
6.5 Compliance Matrix	35
7 Scientific Instrumentation	36
7.1 Orbiter & Lander Instrumentation Performance	36
7.2 Penetrator Instruments:	37
7.3 Objectives, Requirements and Instruments	37
7.4 Choosing a Landing Site	38
7.5 Payload Bay Layout	39
8 Power Subsystem	41
8.1 Subsystem Description	41
8.2 Functional Flow Diagram	41
8.3 Functional Breakdown	41
8.4 Performance Analysis	42
8.5 Sanity Check	46
8.6 Compliance Matrix	46

9	Telecommunication, Command & Data Handling Subsystem	49
9.1	Subsystem Description	49
9.2	Functional Flow Block Diagram	49
9.3	Functional Breakdown Structure	50
9.4	Performance Analysis	50
9.5	Hardware Block Diagram	53
9.6	Code Verification	54
9.7	Compliance Matrix	54
10	Thermal Control Subsystem	57
10.1	Thermal Control System Description	57
10.2	Functional Flow Block Diagram	57
10.3	Function Breakdown Structure	58
10.4	Performance Analysis	58
10.5	Code Verification	62
10.6	Compliance Matrix	63
11	Structural Subsystem	64
11.1	Subsystem Description	64
11.2	Functional Flow Block Diagram	64
11.3	Functional Breakdown Structure	64
11.4	Performance Analysis	64
11.5	Verification & Validation Structure Subsystem	71
11.6	Compliance Matrix	71
12	Radiation	72
12.1	Design Approach	72
12.2	Radiation Effects	72
12.3	Jovian Radiation Environment	73
12.4	Shielding	75
12.5	Radiation Monitoring Subsystem	78
12.6	Compliance & Recommendations	79
13	Technical Risk Assessment	80
13.1	Risk Elements	80
13.2	Risk Map	85
13.3	Risk Mitigation Results	85
13.4	Conclusion of Risk	86
14	System Performance	87
14.1	Spacecraft Systems Characteristics	87
14.2	Spacecraft Configuration	89
14.3	Compliance Matrix	92
14.4	Sensitivity Analysis	95
15	Mission Development & Operations	99
15.1	Manufacturing, Assembly and Integration Plan	99
15.2	Operations and Logistic Concept Description	102
15.3	Sustainable Development Strategy	107
15.4	Market Analysis	109
16	Programmatics	114
16.1	Project Design & Development Logic	114
16.2	Cost Break-down Structure	115
17	Conclusion	122
18	Recommendations	124
	Bibliography	128
A	Work Distribution	129

List of Symbols

A	Geometric Area	[m ²]	m_j	Number of critical functions (number of modules) of subsystem j	[-]
a	Acceleration	[m/s]	M	Magnetic Moment	[Tm ³]
a_{surf}	Albedo of surface	[-]	M	Mass of Celestial Body	[kg]
A_j	Additional components for subsystem j	[-]	M	Maximum Bending Moment	[Nm]
a	Semi-major axis	[km]	M_M	Molecular weight [g/Mol]	
A_e	Equatorial radius of planet	[km]	m	Mass	[kg]
B_e	Polar radius of planet	[km]	\dot{m}	Massflow	[kg/s]
C	Specific heat	[J/(kg K)]	m_b	Supported Mass	[kg]
c	Speed of Light	[m/s]	m_f	Final Mass	[kg]
ΔV	Delta V	[km/s]	m_p	Propellant Mass	[kg]
D	Dipole Moment	[Am ²]	n_j	Redundancy level for subsystem j	[-]
D	Diameter [m]		n	Mean motion	[rad/s]
dt	Time Step	[s]	M	Mean anomaly	[deg]
e	Eccentricity	[-]	P_{axial}	Axial Load	[N]
E	Eccentric anomaly	[deg]	P_{cr}	Critical Buckling Load	[N]
E	Young's Modulus	[Pa]	P_d	Power used during daytime	[W]
f_{nat}	Natural Frequency	[Hz]	P_e	Power used during eclipse	[W]
g_0	Gravitational Acceleration at Sea Level on Earth	[m/s ²]	P_{eq}	Equivalent Load	[N]
g	Gravitational Acceleration	[m/s ²]	P_{pl}	Payload Power	[W]
F	Visibility Factor	[-]	P_{sun}	Power Generated by Sun	[W]
G	Gravitational Constant	[N.m ² /kg ²]	P_t	Total Power	[W]
h	Orbit height	[km]	Q	Internal Dissipation	[W]
h	Momentum	[Nms]	q	Unitless Reflectance Factor	[-]
h	Conductivity	[W/K]	T_d	Daylight time	[s]
h	Panel Height	[m]	T_e	Eclipse time	[s]
h_{orbit}	Orbit height	[m]	X_d	Path losses during daytime	[-]
i	Inclination	[deg]	X_e	Path losses during eclipse	[-]
$I_{x,y,z}$	Moments of Inertia about the X, Y, and Z Axis Respectively	[kgm ²]	r	Radius	[km]
I_{sp}	Specific Impulse	[s]	r_{per}	Radius of Periapsis	[km]
J_2	J2 effect	[-]	r_{prop}	Propellant Arm	[m]
J_3	J3 effect	[-]	r_{SOI}	Radius of the Sphere of Influence	[km]
J_{alb}	Albedo flux	[W/m ²]	R	Distance of Spacecraft to Celestial Body	[m]
J_{rad}	Radiation flux	[W/m ²]	R_J	Jovian equatorial radius	71,492 [km]
J_{sun}	Sunlight flux	[W/m ²]	R_A	Universal gas constant	[J/(kg/kmol)]
k_j	Basic functional subsystem number of components of subsystem j	[-]	S	Shear Stress	[N]
k	Stiffness Factor	[-]	s	Distance	[m]
k_b	Beam - Bending Deflection Coefficient	[-]	s_{sun}	Distance Between S/C and the Sun	[m]
k_s	Beam - Shear Deflection Coefficient	[-]	T	Torque	[Nm]
L	Length	[m]	T	Temperature	[K]
L_p	Array pointing loss factor	[-]	T_{bb}	Blackbody Temperature	[K]
			t	Time	[sec]
			t_c	Core Thickness Honeycomb Beam	[mm]
			t_f	Facing Thickness Honeycomb Beam	[mm]
			v	Velocity	[m/s]
			V	Orbital Velocity	[m/s]
			V	Volume	[m ³]

w_n	Natural Frequency	[Hz]
Z	Relative atomic numver	[-]
α	Surface Absorptivity	[-]
Δt	Time Difference	[s]
ΔV	Velocity Difference	[m/s]
δ	Deflection	[mm]
η_{uv}	Power loss caused by UV discoloration	[-]
η_{cy}	Power loss caused by thermal cycling	[-]
η_m	Power loss caused by cell mismatch	[-]
η_l	Power loss caused by resistance in cell interconnects	[-]
η_{con}	Power loss caused by contamination from all sources	[-]
η_{rad}	Power loss caused by radiation damage	[-]
Γ	Vander Kerckhove function	[-]
γ	Reduction Factor	[-]
γ	Specific heat ratio	[-]
ϕ	Geometric Parameter	[-]
σ	Boltzmann Constant	228.6 [dB]
σ_{cr}	Critical Buckling Stress	[Pa]
σ_f	Stress in Skin Honeycomb Beam	[Pa]
τ_c	Shear Stress in Honeycomb Beam	[Pa]
ε	Surface Emissivity	[-]
ε	Expansion ratio	[-]
θ	Alignment Angle	[rad]
λ	Unitless Factor	[-]
μ	Standard Gravitational Parameter	[km^3/s^{-2}]
Φ	Solar Flux	[W/m ²]
ϕ	Angle of Incidence of the Sun	[rad]
ω_{spin}	Angular Velocity	[rad/s]
ρ	Pressure [Pa]	

List of Abbreviations

AO	Announcement of Opportunity
APR	Array Power Regulator
ASRG	Advanced Stirling Radioisotope Generator
ATP	Adenosine Triphosphate
BCDR	Battery Charge/Discharge Regulator
BPF	Band Pass Filter
BTE	Boltzmann Transport Equation
CBE	Current Best Estimate
CM	Command and Monitoring module
CMG	Control Moment Gyros
CMOS	Complementary Metal Oxide Semiconductor
COSPAR	Committee on Space Research
CRISM	Compact Reconnaissance Imaging Spectrometer for Mars
CST	Requirement of category <i>Cost</i>
CTS	Coaxial Transfer Switch
D&D	Design and Development
DDD	Damage Displacement Dose
DFE	Direct from Earth
DG83	Divine and Garrett 1983 model
DHMR	Dry Heat Microbial Reduction
DOT	Design Option Tree
DSE	Design Synthesis Exercise
DSN	Deep Space Network
DTE	Direct to Earth
EB	Engineering Budget
ECSS	European Cooperation on Space Standardization
EOL	End-of-Life
eqv	Equivalent
EUR	Euro
FBS	Functional Breakdown Structure
FFBD	Functional Flow Block Diagram
FY	Fiscal Year
GEO	Geostationary Earth Orbit
GIRE	Galileo Interim Radiation Environment
GNC	Guidance, Navigation & Control
HPBW	Half power beam width
IEUSD	Internal Electrostatic Discharge
IRU	Inertial Reference Unit
ITT	Invitation to Tender
JEO	Jupiter Europa Orbiter
JPL	Jet Propulsion Laboratory
LA	Laser Altimeter
LAL	Limulus Amebocyte Lysate
LGA	Low Gain Antenna
LNA	Low Noise Amplifier
LORRI	Long Range Reconnaissance Imager
LP	Langmuir Probe
MAG	Magnetometer
MC	Mapping Camera
MEA	Mean Error Amplifier
MGA	Medium Gain Antenna
MLA	Mercury Laser Altimeter
MLI	Multi-layer insulation
MPPT	Maximum Power Point Tracker
MRO	Mars reconnaissance orbiter
MSL	Mars science laboratory

NF	Noise Filter
NIEL	Non-Ionising Energy Loss
No.	Number
OTR	Requirement of category <i>Other</i>
PB	Piggyback
PCB	Printed Circuit Board
PCU	Power Conditioning Unit
PDU	Power Distribution Unit
PERF	Performance
PLL	Phase Lock Loop
RAMS	Reliability, Availability, Maintainability and Safety
RDF	Radiation Design Factor
RF	Radio frequency
RMS	Radiation Monitoring Subsystem
RS	Radio Science
RTG	Radioisotope Thermal Generator
RTOF	Reflectron Type Time-of-Flight Mass Spectrometer
S/C	Spacecraft
SCI	Science Requirement
SEE	Single Event Effects
SEGR	Single Event Gate Rupture
SEL	Single Event Latch-Up
SET	Single Event Transients
SEU	Single Event Upset
SNR	Signal to noise ratio
SOI	Sphere of influence
SPENVIS	Space Environment, Effects, and Education System
SR	Safety & Requirement of category <i>Safety and Reliability</i>
SSPA	Solid State Power Amplifier
STP	System Interface Temperature
SUS	Requirement of category <i>Sustainability</i>
SYS	System Requirement
TBD	To Be Determined
TMM	Thermal Mathematical Model
TC&DH	Telecommunication, Command & Data Handling
TCS	Thermal Control System
TID	Total Ionising Dose
TRL	Technology Readiness Level
TRP	Temperature Reference Point
UHF	Ultra high frequency
USE	User Requirement
USO	Ultra Stable Oscillator
V&V	Verification and Validation
VHP	Vapor Phase Hydrogen Peroxide
WBS	Work Breakdown Structure
WFD	Workflow Diagram
WTS	Waveguide Transfer Switch

Executive Overview

Europa, one of Jupiter's icy satellites, is considered one of the most promising sources for extraterrestrial life in the Solar System. Europa may hide life in the ocean beneath its icy crust, protecting organisms from the harsh radiation environment of Jupiter. Europa, discovered four hundred years ago by Galileo Galilei, is even believed to be internally active. A mission to Europa will provide insight into the origin of natural satellites to the possible emergence of habitats, greatly advancing the understanding of the potential of life emerging in our galactic neighbourhood. Europa is unique compared to its siblings as its ocean is believed to be in direct contact with the rocky mantle beneath it. This may lead to geothermal heat injection into the ocean. Life in the ocean could thus be fed by geothermal heat, similar to life on the bottom of Earth's ocean that occurs near black vents that emit a constant stream of methane and hydrocarbons. Convection flows, together with tidal heating, will provide good conditions and possibly supply enough chemical energy to sustain life. In addition to the abundance of water, NASA scientists concluded from the analysis of Galileo data, that clay-like materials are present on the surface [Mooij, 2015]. These clay-like materials are believed to be an important building block for life.

Summary of the Mission

A team of 10 TU Delft university students of Aerospace Engineering will conduct a feasibility study for a mission to Europa, capable of achieving the following science goals. The measurement duration shall be 3 months, with a launch no later than September 2025 and a total mission cost of maximum 2.5B EUR. September is the very last launch window in 2025, if not reached than the requirement for launch in 2025 is violated. Any exposure to hazardous materials shall be avoided for all personnel involved and mission success shall be larger than 95% (excluding launch). COSPAR regulations for Europa will be adhered to, which also requires that a clear end-of-life strategy will be included in the design. The Need Statement is defined as follows:

The scientific community wants to analyse the ice layer and the subsurface ocean on Europa to establish the conditions for possible life.

Following the Need Statement, the Mission Statement is defined as:

A team of 10 aerospace engineering students from Delft University of Technology will conduct a feasibility study for a space mission to analyse the ice layer and the subsurface ocean on Europa to establish the conditions for possible life, which is to be launched no later than 2025 and will not exceed a total cost of 2.5B EUR.

Investigating Europa's habitability includes investigating the presence of any water within and beneath Europa's ice shell, investigating the chemistry of the surface and ocean and evaluating geological processes that might deliver the chemical energy needed for life. To learn more about the habitability and history of Europa it is important to characterize the ice shell and any subsurface water. This can be either the ocean or pockets of water inside the ice layer. Also relevant is to characterize the nature of the exchange of material between the ocean and the surface ice. To achieve this goal, the ice properties, such as rigidity and thickness, will have to be analysed. Furthermore, the regional and global heat flow variations will have to be determined in conjunction with the composition and chemistry of the surface, subsurface and atmosphere. Determination of most recent geological sites will help in understanding the formation and habitability of the different sites and show insight in the history of Europa. It shall be established whether lateral variations in ice dynamics are present, what the depth of the subsurface ocean is and how the thickness and state of the (metal) moon core can be described.

Concept description

The mission developed is named Moonraker and will be a piggyback orbiter/lander mission attached to the Europa Clipper. Moonraker will detach from the Clipper before Jupiter orbit insertion and will therefore have limited influence on the design of the Clipper mission. The main purpose of the 'piggyback' concept is to share the same launcher and therefore reduce the mission cost. This because a market analysis showed that ESA would not support a large class mission until 2030. The mission will after detachment from Clipper first perform a Jovian tour of a year to reduce the required ΔV for

Jupiter orbit insertion. During this tour the orbiter will perform flybys around other Jovian moons, namely Callisto and Ganymede. During these flybys the orbiter will make images of these moons and will transmit these images directly towards Earth. After the Jovian tour the orbiter will perform a polar Europa orbit insertion. The orbiter will then deploy a penetrator and will then mainly function as a relay satellite. Because the data-rate for the orbiter is limited, the orbiter is not able to transmit the amount of instrument data.

Astrodynamics

The chosen piggyback mission profile is much dependent on the NASA Clipper mission to get to the Jovian system. On the 22nd November 2021 at 00:01:13, the Clipper mission is scheduled to take off on an Atlas V rocket along with the piggyback addition of an orbiter and penetrator lander and embark on a VEE-GA transfer to the Jovian system. The transfer will require a ΔV of 3.852 km/s to be launched towards Venus from an Earth orbit height of 200 km. The arrival date will be 6.37 years later on the 3rd April 2028. Following the transfer, the spacecraft will detach from Clipper and perform a Jovian tour, consisting of 15 flybys, to lower its energy and finally insert itself in a Europa orbit on the 3rd Jan 2030. The chosen orbit will be a polar orbit, with inclination of 90 degrees, orbit height of 244.29 km, eccentricity of 0.005, argument of periapsis of 270 degrees and a right ascension of the ascending node of 90 degrees. This orbit enables the orbit to pass the South pole 36 times for every Europa sidereal day, i.e. the ground repeat of the orbit is (36,1). Furthermore, the orbit is deemed frozen, but not free from orbital variation. Therefore a ΔV budget for counteracting inclination changes is computed to have a value of 371 m/s for the whole mission duration. Other orbital parameters are chosen not to be counteracted for. Finally, the mission will end on the 7th February 2030 by applying a ΔV of 100 m/s which will deorbit the orbiter and have a guided crash on the surface of Europa.

Guidance, Navigation and Control

For location determination and attitude determination and control, the instruments from Table 1 have been selected for the orbiter. The penetrator uses the same SIRU and thrusters as the orbiter. The penetrator will be stabilized using a spin speed of 0.28 rad/s. The descent will take 1 hour, 38 minutes and 6 seconds and the impact velocity will be 285 m/s.

Table 1: Estimated characteristics of the ADC system

Subpart	Mass [kg]	Power [W]	Performance	Amount
Thrusters	0.2	0	0.5 [N]	12
Star Tracker	0.05	0.22	30 [arcsecond]	2
SIRU	1.775	10.75	Bias: 0.006 [deg/hr]	1
Sun Sensor	0.215	0	0.3 [deg]	6
Total	5.565	11.19	[-]	21

Propulsion

The propulsion system includes one main engine attached to the penetrator. This 100 N engine performs the main orbit injections, inclination changes and the landing of the penetrator with an I_{sp} of 320 seconds. On both the penetrator and the orbiter, twelve 0.5 N reaction control thrusters are implemented. These reaction control thrusters perform 3-axis rotation manoeuvres and orbital correction manoeuvres for the orbiter after detachment of the penetrator with an I_{sp} of 227 seconds. Two cylindrical fuel tanks and two oxidiser tanks are located around the main structure. Two spherical tanks are located in the descent stage of the penetrator, which is located in the central structure of the orbiter. For all manoeuvres, 303.6 kg of bi-propellant of Hydrazine and NTO is needed for the orbiter and 47.7 kg for the penetrator. An additional 42.1 kg of monopropellant hydrazine is needed. These two fuel systems are both connected to the same engine, thus reducing weight. The dry mass of the propulsion system is estimated to be equal to 24.6 kg for the orbiter and 5.7 kg in the penetrator.

Instruments

The carefully selected science instruments will be able to look for the signs pointing to conditions for life on Europa. Table 7.1 gives the orbiter instruments and table 7.2 gives the lander instruments.

Table 2: Orbiter Instrumentation Specifics

Instrument Specifics	Accuracy	Unit
O1. Stereo Imager (SI) ^{1, 2}		
High resolution	2048x2048	pixels
Stereo imaging	1024x1024	pixels
O2. Laser Altimeter (LAT)	-	-
SILAT Total		
Average power	12	W
Weight	5	kg
Dimensions	0.3x0.3x0.3	m

Table 3: Instrumentation Specifics Lander

Penetrator Instruments	Specifics
P1. Seismometer ³	(3-axis)
P2. Descent Camera ⁴	
P3. Sampling drill ⁵	-
P4. Microbiology/Astrobiology Camera ⁶	six micron resolution
P5. Geochemistry package (incl. Mass spec.) ⁷	-
P6. Magnetometer ⁸	-

Penetrator:

The payload science instrumentation will take maximum advantage of landing on Europa by taking situ samples and processing them but also taking seismic and gravitational measurements for the duration of the entire mission. A total of 60 samples will be processed over the lifetime of the microbiology part of the penetrator, which will be between 12 and 24 hours, the drill will penetrate about 0.2-1 meter into the ice depending on the composition. After the 60 samples the primary payload bay will be switched off and only the communication part and the seismometer will stay active until all the data is transmitted and the batteries have run out.

For a landing site, the South Pole is chosen since this is an unknown potentially interesting site. Also where the forces acting on the icy layer are the largest at the poles. In terms of orbiter contact time landing at the poles is also advantageous, since it will give about 31 times more contact time compared to an equatorial orbit, and therefore more data can be transmitted when landing at the poles. Also the potential presents of water vapour plumes at the south pole contributed to this choice of landing site.

Power

The power system is based on a photovoltaic-battery system. It uses state of the art 33 % efficient multi-junction Gallium Arsenide cells. The power system is designed for daylight power of 71.9 W and eclipse power of 51.2 W, which gives a total design power of 122 W. This results in a total solar array size of 13.5 m². The panel is based on an aluminium honeycomb structure and uses 150 μm of fused silica cover glass to shield the cells for a 1 MeV equivalent electron fluence of 3.00 E+15. This results in a radiation degradation of 29 %. The solar array uses a deployment mechanism of 15 kg per panel and the attachment structure is 10 kg for both panels. This gives a total solar array mass of 74.2 kg. The dimensions per panel are 1.87 x 3.6 m when deployed, and 1.87 x 0.9 m when stowed during launch when it is folded four times. The battery stores 400 Wh whilst a only 188 Wh is required for a Jovian eclipse. Lithium-ion cells have been used with a capacity of 1.5 Ah per cell at a mass of 42 g per cell. The depth of discharge for the battery is 0.6 at approximately 500 cycles and the DOD can be higher when a battery failure occurs. The total mass of the batteries equals 4.70 kg. Finally the power conditioning and distribution unit is based on the power system design of Rosetta, Mars Express and Venus Express. This system is dual hot redundant for most components and has a mass of 10.6 kg whilst dissipating

¹ [Moon et al., 2009]

² [Kraft,]

³ [Gowen et al., 2007], [Gowen et al., 2011]

⁴ [Gao et al., 2008]

⁵ [Weiss et al., 2011]

⁶ [Thomas et al., 2003], [Luthi et al., 2004]

⁷ [Gowen et al., 2007], [Gowen et al., 2011]

⁸ [Gowen et al., 2007], [Gowen et al., 2011]

approximately 20 W. The total mass for the orbiter power system equals 89.5 kg. The penetrator has a primary Lithium/Carbon Monofluoride cells with a high specific power of 514 Wh/kg. The power mass for the penetrator power subsystem including a power conditioning unit is 0.9 kg for the penetrator and 0.25 kg for the penetrator delivery system.

Telecommunication and Data handling

The Telecommunications, Command and Data Handling (TCDH) subsystem is responsible for maintaining communication links between different parties. The TCDH subsystem on the orbiter acts as a data relay for transmission of the science data from the penetrator to Earth. It therefore consists of two systems. For close range communications with the penetrator, a UHF-Band transceiver unit is installed. For communications with Earth, an X-Band transceiver is used. The Ultra High Frequency (UHF) system operated at 400 MHz and communicates through a helical antenna with a beamwidth of ± 80 degrees to assure contact during flyover, and is nadir pointed. The X-Band communication system (8 GHz) makes use of four antennas. The high-gain antenna assembly incorporates a high-gain antenna (HGA) of 1.3 m diameter, a medium-gain antenna (MGA) with the same boresight, and a low-gain antenna (LGA). The other LGA can be found on the opposite side of the spacecraft to omni-directionally cover the space around the spacecraft. The HGA is body-fixed and thus relies on pointing accuracy of the spacecraft for pointing. Data rates achieved for direct to Earth (DTE) communication is 2943 bit/s. Data rate to and from the penetrator is 8 kbit/s. Total data gathered from the penetrator is 13 Mbit. In total 46 flybys are needed to relay this data considering 37 seconds of contact time per orbit. The systems data handling incorporates a 1750 A processing unit. Risk mitigation for the system is achieved by having a fully redundant, no single point of failure, subsystem.

Thermal control

The Thermal Control System (TCS) is designed to keep all S/C components within their required temperature range. For the orbiter, it is found that a total radiator surface area of 0.7 m² black painted aluminium is needed. Besides that, around 4 m of variable conductance heat pipes is used to transport heat from the payload, structure and propellant tanks to these radiators. The entire orbiter is wrapped in 25-layer insulation blankets that make efficient use of goldized kapton. A 20 W patch heater is used to keep the payload vault at the right temperature when the TC& DH and GNC system are not consuming power. The high-gain antenna is used as a heat shield during the part of the interplanetary trajectory where the S/C is closest to the sun. The temperature requirements and the predicted temperatures in three extreme cases are shown in Table 4. The TCS for the orbiter has to be analysed in more detail, to find its performance loss in the radiation environment around Jupiter.

	T_{min} allowed	T_{max} allowed	T Orb. (max)	T Orb. (min)	T Orb. En.	T MDS	Within range
1: Structure	252	323	264	262	263	281	Yes
2: Tanks	274	293	280	280	277	281	Yes
3: Vault	273	293	283	281	279	279	Yes
4: Antenna	103	394	150	150	149	303	Yes
5: Sol. panel	98	393	190	170	190	133	Yes
6: Radiator	100	368	146	146	164	277	Yes
7: Rocket Eng.	100	3500	249	233	430	243	Yes
8: Insulation	200	374	251	229	249	239	Yes

Table 4: Temperatures in [K] of the eight nodes as modelled by the TMM in three extreme cases. By using the described design, all temperature requirements are met. For the Europa Orbit (Orb.) case, temperatures vary during orbit, therefore max. and min. temperatures are provided. Some nodes are colder in the Minimum Distance to Sun (MDS) and Orbit Europa with Engine On (Orb. En.) case than in the Orb. case. This is caused by increased conduction to the radiator.

The penetrator uses a vacuum flask-like design, where a closed payload compartment is mounted with an offset from the outer shell wall. This is done with six titanium struts. To counteract the heat loss from conduction and thermal radiation, a small heater (10 W) is necessary. Further research has to be done to ensure the thermal design for the penetrator withstands the impact loads. The TCS mass is 11.1 kg for the orbiter and around 0.2 kg for the penetrator, and power consumption varies between 0 W to 20 W for the orbiter and 1 to 10 W for the penetrator, depending on the mission stage. The cost for testing the system may make the budget of 2.2M EUR limiting for the design.

Radiation

Like Earth, the presence of a magnetosphere has led to the formation of belts of trapped radiation. Radiation poses a unique technical challenge for any mission to Europa due to the flight system spending a significant time in these harsh Jovian radiation belts. Conventional engineering practice of multiplying the estimated TID level by a radiation design factor of 2 has been applied, accounting for uncertainties within the radiation environment models. The Divine and Garrett 1983 model has been used to model the Jovian radiation environment for the specific trajectory of the Moonraker mission. This leads to, for instance, a differential fluence of $9.8 \cdot 10^{14} \text{ cm}^{-2} \text{ MeV}^{-1}$ at a proton energy of 1 MeV and $1.36 \cdot 10^{15} \text{ cm}^{-2} \text{ MeV}^{-1}$ at 1 MeV electron energy. The resulting integral and differential fluences and fluxes have been imported in SHIELDOSE-2Q, a 1-D Monte Carlo simulation used to model the total ionising dose for electrons, protons and bremsstrahlung, resulting in a reference radiation design point of 1.63 Mrad behind a 100 mils aluminium shield. The most mass-efficient shielding material is found to be CW80, an alloy of 20% copper and 80% tungsten. The material combines low-Z copper to limit the buildup of bremsstrahlung and protons, with tungsten to shield for the dominating energetic electrons.

The shielding strategy for the Moonraker mission has led to the most mass-efficient system, utilizing a centralized chassis to house standard 6U chassis PCB cards, allowing PCB spot shielding where needed. Separate components that require shielding are housed in an enclosure, which prevents shielding the entire spacecraft down to its lowest common denominator. This approach proves to be especially beneficial to the telecommunications subsystem, allowing placement of components near the high-gain antenna to prevent cable losses and noise. This approach has led to a total radiation shielding mass of 35.93 kg for the Moonraker relay satellite. The penetrator itself does not require additional radiation shielding, its wall thickness to survive impact loads is thicker than the required radiation shielding thickness. The descent stage does require some additional enclosure shielding, combining to a total shielding mass of 1.69 kg.

To monitor the radiation exposure and to update the understanding of the Jovian radiation environment, a Radiation Monitoring Subsystem (RMS) is added to the system. The RMS will continuously monitor the real-time radiation and surface charging environment. It contains two principal sensors, one located at the star tracker and one inside of the 6U chassis. Its data will improve the understanding of radiation transport processes, single event effects and spacecraft charging.

Structure

For the structure subsystem, a preliminary design of the primary structure has been made. This study was limited to the components only. The joining methods have not been investigated. The structure has been sized to withstand all the loads during the launch of the spacecraft and doing so within the natural frequencies constraints of the Atlas V551 launcher. The PB is separated by a Lightband system. The primary structure components of the orbiter are listed in Table 5. The penetrator descent structure consists of the tank support structure, engine and nozzle support structure, subsystem support structure and the penetrator separation system.

Table 5: Structure Component Overview

Component	Dimensions [m]	Material	Weight [kg]
Lower Central Cylinder	(RxL)(0.19 x 1)	AL 6061 T6	4.19
Top Central Cylinder	(RxL)(0.11 x 0.6)	AL 6061 T6	1.12
Tank Support Beam (2x)	(Lxb)(0.7 x 0.14)	AL 6061 T6/ Carbon Steel 1017	2.62
Cylinder Support Beam	(Lxb)(0.26 x 0.14)	AL 6061 T6/AL 5052	0.62
Clipper Attachment Structure	n/a	AL 6061 T6	0.61
Base panel	(Lxb)(0.6 x 0.6)	AL 6061 T6	1.5
Top Tank Support (4x)	(RxL)(0.05 x 0.22)	AL 6061 T6	0.76
Joints	TBD	TBD	4.4
Total	-	-	16.54

Risk

A risk analysis was performed on the S/C subsystems, astrodynamics and planetary protection. Most risks that are considered have a low failure probability, but a critical or catastrophic consequence. By mitigation via analysis, testing or re-design, nearly all risks considered can be mitigated to a lower probability of occurrence and/or a lower impact on the mission. However, it is unlikely that all risks can

be mitigated within the cost budget and planning. Therefore, mitigation procedures should focus on the risk that have catastrophic impact and on the risks that have a high and moderate probability

Two possible events could not be mitigated from a high risk to a medium or low risk location. These risks are both associated with penetrator failure at impact. The first one is the situation that the instrumentation does not survive the impact, in which case no scientific data can be collected. This risk will always have catastrophic failure. Furthermore, as the surface roughness and density of the Europa ice are not known, penetrator tests on Earth can never fully guarantee a safe landing on Europa.

The second high risk event, associated with the penetrator landing, is the angle of impact with the surface. It is not known exactly where the penetrator will land, and the surface of Europa has a roughness up to the level of meters. A too large impact angle may cause structural failure, telecommunications pointing failure or scientific data collection failure.

It is concluded that these risks either should be accepted, or that the mass and cost budget should be increased to develop a dedicated mission. This mission could first make a high-resolution mapping of the landing location, and then safely deploy a penetrator at the selected, smooth location. This penetrator should have a more accurate landing guidance system than the current design. It should also be designed for all impact angles that are likely to happen.

Performance

The mass budget is an important parameter in the design of a spacecraft since it drives the cost to a large extent. The mass budget is much higher than the required 350 kg. This was caused by the high mass of the power subsystem. The mass budget for the orbiter and penetrator can be found in Table 6. As can be seen the total mass for the piggyback combination which is connected to Clipper equals 704 kg.

Table 6: Mass budget for the orbiter

Subsystem	Design Mass [kg]	Margin [kg]	Total Mass [kg]
Total Orbiter Dry Mass	218.2	43.6	261.8
Total Wet Orbiter Mass	507.4	101.5	608.9
Penetrator Wet Mass	79.0	15.8	94.8
Total Mass Added to Clipper	586.4	117.3	703.7

Cost breakdown

The cost estimation is based on NASA studies on a Europa multiple flyby, a Europa Orbiter and a Europa orbiter lander. Below in table 7 the cost per segment can be found. As can be seen the total cost for the spacecraft systems, which is what most of this report is about, is estimated to be 142.2M EUR

Table 7: Detailed cost break-down based on Europa mission studies

Cost Estimation Methodology ⁹	Flyby	Orbiter	Orbiter/Lander	Average	Piggyback
Spacecraft systems	427.9	421.8	693	514.2	142.2
Others	846.9	661.5	1045.7	851.4	260.1
Reserves (20%)	397.3	324.6	566.1	429.3	118.7
TOTAL	1672.1	1407.9	2304.8	1794.9	521

Conclusion

The conclusion of the detailed design of the Moonraker mission is that a ‘piggyback’ orbiter/lander combination is not feasible within 350 kg. The final system wet mass is 704 kg. This large mass is mainly attributed to four main factors. The low solar constant at Jupiter which makes the power system relatively heavy. The long transmission path towards Earth which makes the telecommunication system relatively heavy. The harsh radiation environment of Europa also requires a heavy radiation protection. Finally, the large ΔV budget causes a propellant mass which is more than half of the mission wet mass. To reduce the mass of the system, the orbiter only functions as a relay satellite for the penetrator. This reduces the telecommunications and the power subsystem mass which also reduces the propellant mass. The design can fit the 350 kg if the orbiter is dropped and the design of the trajectory of Clipper is changed such that it can send the data of the penetrator.

⁹In 10⁶ EUR (FY(2015))

1. Introduction

Europa, first discovered by Galileo Galilei in the year 1610, is one of Jupiter's 67 moons. It is believed that Europa could possibly sustain life underneath its icy exterior. Today, 405 years later, a team of 10 students is investigating possible missions to analyse the ice layer, subsurface ocean and the interior of Europa. This icy satellite, slightly smaller than Earth's moon, does it well in the public opinion, for example on NASA's website it is the public top choice for a future mission. After the data retrieved by the Galileo satellite Europa became popular because of it is in geoscience terms young surface and its liquid water subsurface ocean.

The first spacecraft to visit the Jovian system was the Pioneer 10 in 1973 and a year later the Pioneer 11. They were the first to take close-up pictures and measurements inside this Jovian system. The Voyager was the first to discover the icy exterior of Europa in 1979. In 1995 the Galileo spacecraft was the first to enter into an orbit of the Jovian system, making close approaches of the four large Galilean moons and discovering possible liquid water beneath Europa's icy exterior. Several missions specifically to Europa or flybys of the four largest moons of Jupiter have been considered by several space agencies. NASA is currently developing the Europa Clipper mission, which will be a multiple flyby mission investigating surface and subsurface composition and properties. The Clipper mission has recently been promoted from concept to development, associated with this promotion, the name changed from Clipper to 'Europa Multiple Flyby Mission'. In this report the name Clipper will be used to refer to the Europa Multiple Flyby Mission, to be consistent with other reports regarding Clipper. Flybys instead of direct orbit of Europa are chosen because of the extreme radiation environment near Europa. The flyby altitude will range from 2700 kilometres to as low as 25 kilometres achieving near global coverage. The Clipper mission mostly focusses on remote sensing to explore Europa. The main three science requirements: characterize the icy shell and subsurface water, understand the habitability of Europa's ocean through composition and chemistry and understanding the formation of surface features. The main reconnaissance goal is characterizing any scientific compelling sites to analyse them for the possibility of future landers, which is composed of the two objectives site safety and scientific value.

Since in the last report the design concept is fixed to be a piggyback orbiter/lander where the orbiter will mainly function as a relay satellite and the penetrator will do actual in situ experiments. In this report the design takes shape. The concept description is done in Chapter 2 where all system requirements are discussed. Chapter 3 gives the design considerations containing the mission functions, the resource allocations and the system hardware and software diagrams. After this all subsystem chapters will follow having the same chapter build-up, starting with description then function flow diagram, function breakdown structure, performance analysis, verification and validation and ends with a compliance matrix. The astrodynamics characteristics and calculations are done in Chapter 4. After this in Chapter 5 the guidance, navigation and control subsystem is discussed. The propulsion subsystem is discussed in Chapter 6. Chapter 7 gives the scientific instrumentation of the orbiter and the penetrator. The power subsystem is discussed in Chapter 8. In Chapter The telecommunication is discussed in detail in Chapter 9. The thermal control system is discussed in Chapter 10. Chapters 12 and 11 give the radiation shielding strategy and the structure respectively. Risk analysis and mitigation is discussed in Chapter 13. After discussing the system performance in Chapter 14, Chapter 15 discusses the development operations and contains the manufacturing plan, operations logistics, RAMS characteristics, sustainable development and market analysis and return on investment. The project design development logistic, Gantt chart and the cost breakdown are found in Chapter 16. Then Chapter 17 gives the conclusion and Chapter 18 gives recommendations for future mission investigations. Finally in Appendix A the work distribution can be found.

2. Concept Description & Top Level Requirements

In this chapter the mission concept as decided upon during the midterm review is discussed in Section 2.1. Furthermore, the system requirements to which the mission should adhere are stated in Section 2.2.

2.1 Concept Description

The Moonraker mission will be a piggyback mission attached to the Europa Clipper. Moonraker will detach from the Clipper before Jupiter orbit insertion and will therefore have limited influence on the design of the Clipper mission. The main purpose of the 'piggyback' concept is to share the same launcher and therefore reduce the mission cost. This because a market analysis showed that ESA would not support a large class mission until 2030. The mission will after detachment from Clipper first perform a Jovian tour of a year to reduce the required ΔV for Jupiter orbit insertion. During this tour the orbiter will make flybys of the other Jovian moons, namely Callisto and Ganymede. During these flybys the orbiter will make images of these moons and will be able to transmit these images towards Earth. After the Jovian tour the orbiter will perform a polar Europa orbit insertion. The orbiter will then deploy a penetrator and will then mainly function as a relay satellite. Because the data-rate for the orbiter is limited, the orbiter is not able to transmit the large amount of instrument data.

The penetrator will have a polar landing site, since this will give more contact opportunities with the orbiter. This results in a higher data rate. The science performed by the penetrator will address a large number of scientific requirements. Those are investigating the surface composition, the ocean and the ice shell, the geology as well as some geophysical features.

The total combination will be attached to the Clipper mission and will therefore have a volumetric and mass constraint as can be found in the requirements in Section 2.2.

2.2 Top Level Requirements

The top level requirements to which the mission should adhere are presented in this section. They are mainly derived from the midterm report, but some additional requirements are added for the specific mission concept. The science requirements are discussed together with the scientific instruments in Chapter 7. The remaining requirements are discussed in this section. The requirements are divided into performance, safety & reliability requirements, sustainability requirements and cost. The other requirements are not included in this report since a market analysis has already been performed and incorporated in the mission.

2.2.1 Performance Requirements

Number	Requirement
SYS-PERF-01O	The measurement duration shall be 36 days for the orbiter.
SYS-PERF-01P	The measurement duration shall be 14 days for the penetrator.
SYS-PERF-02	Launch date shall be no later than November 2022 together with Clipper
SYS-PERF-03	The total mission mass shall not exceed 350 kg including margins.
SYS-PERF-04	The maximum volume in stowed condition shall not exceed 1 m x 1 m x 3 m.
SYS-PERF-05	The spacecraft shall include and operate the science payload.
SYS-PERF-06	All equipment used shall be at minimum of TRL 6 by 2017.
SYS-PERF-07	The system shall be able to send and receive information with the use of NASA's deep space network.
SYS-PERF-08	All spacecraft systems shall be able compatible to be launched with the Atlas V launcher.
SYS-PERF-09	The system shall be compatible with the interplanetary VEEGA transfer when attached to Clipper.
SYS-PERF-10	The system shall be designed for a maximum lifetime of 8.5 years.

Most of the performance requirements remained the same with respect to the midterm review [DSE Group 10 et al., 2015]. However **SYS-PERF-01** is now split in two requirements, one for the orbiter and one for the lander. The mission duration for the orbiter has reduced from three to one month since a small orbiter is less resistant to Europa's demanding environment. **SYS-PERF-02** has changed to the launch date of the Clipper, which is now scheduled for November 2022 [Niebur et al., 2013]. **SYS-PERF-03** refers to the new total mass of the piggyback mission as was given by the client. The volume of the spacecraft in stowed condition as specified in **SYS-PERF-04** is retrieved from the fairing size of the Atlas V launcher and the size of Clipper, this volume, however, is subject to modification if NASA decides that less volume is available. For **SYS-PERF-06** the year at which TRL 6 has to be achieved for all equipment has changed to 2017 as the launch is three years earlier than initially planned. **SYS-PERF-09** refers to the VEEGA orbit which Clipper uses to reach Jupiter. This orbit takes approximately 6.5 years [Campagnola et al., 2014a] and therefore has a significant influence on the design. Furthermore, the VEEGA trajectory also passes Venus which poses a strict requirement on the thermal control of the spacecraft. Finally, **SYS-PERF-10** relates to the long duration of the VEEGA trajectory and the Jovian tour combined before the orbiter finally comes into an orbit around Europa. This lifetime affect the design of the mission since all systems degrade during this long tour which is no part of the actual measurement part of the mission.

2.2.2 Safety & Reliability Requirements

Number	Requirement
SYS-SR-01	Any exposure to hazardous materials stated by the PHMSA [Pipeline and Hazardous Materials Safety Administration, 2015] shall be avoided for all personnel involved.
SYS-SR-02	Mission success shall be larger than 95 % (excluding launch failure).

The safety requirements remained similar with respect to the midterm review report and are stated again for completeness.

2.2.3 Sustainability Requirements

Number	Requirement
SYS-SUS-01	The probability of contamination of Europa shall be less than 10^{-4} .
SYS-SUS-02	The end-of-life strategy of the mission shall adhere to the COSPAR regulations.
SYS-SUS-03	The orbiter shall adhere to COSPAR III regulations.
SYS-SUS-04	The penetrator shall adhere to COSPAR IV regulations.

The sustainability requirements remained similar with respect to the midterm review report and are stated again for completeness. However, **SYS-SUS-04** the verb lander is replaced with penetrator.

2.2.4 Cost Requirements

Number	Requirement
SYS-CST-01	The mission cost shall not exceed 700 M EUR.

The **SYS-CST-01** has changed since the mission is changed from a high class 2.5 billion Euro mission to a medium class mission of 700 million Euro. This because the market analysis showed that ESA would not support a large class mission before 2030.

3. Design Considerations

3.1 Mission Functions

The functional flow of the mission is presented in Figures 3.1 and 3.3 as a block diagram. For every mission phase a function is allocated and subdivided in functions per mission phase. In Figure 3.3 a Work breakdown structure is presented, the mission is divided in four packages, the orbiter, penetrator, time attached to Clipper and end of life package.

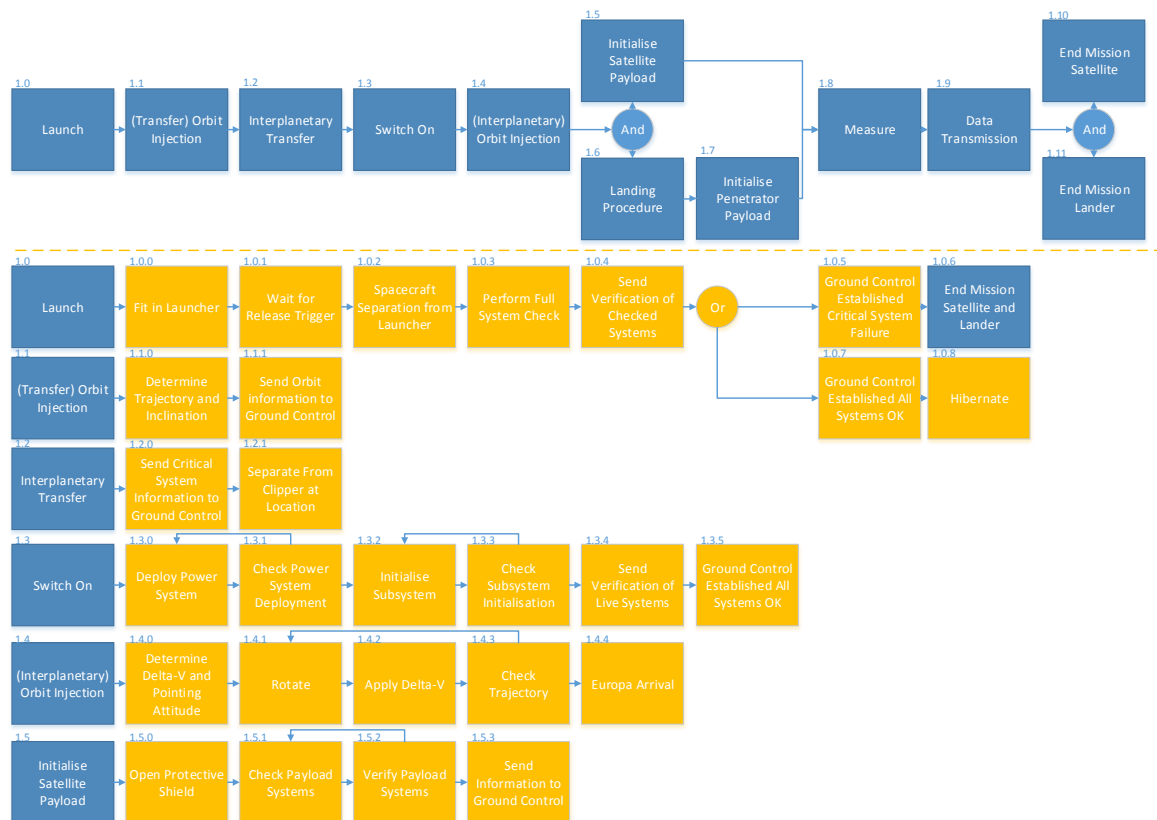


Figure 3.1: Functional Flow Block Diagram - General System (Part 1)

3.2 Resource Allocation and Budget Breakdown

In this section the technical resources mass and electrical power is given. Normally these resources drive the cost of the product and grow during the project development. Therefore, it is important to keep good track of these resources and establish a maximum value at the beginning of the project including a reserve or contingency. This section will discuss the mass, power and data budget.

Mass Budget

The design of this mission includes a penetrator and a relay orbiter to transmit the penetrator data towards Earth. However, during the design process it was found that a penetrator and orbiter within 350 kg were infeasible. Therefore the focus was laid to design an orbiter within 350 kg with an additional penetrator option, for which the mass is added to the 350 kg. From detachment from Clipper to Europa orbit insertion a Jovian tour will be used as proposed for the Europa Orbiter [Campagnola et al., 2014a]. This tour will cost in total 1.55 km/s, applying the ESA margin for ΔV [ESA, 2014] of 5 % the design ΔV will be 1.63 km/s. Assuming a specific impulse of 310 s for a bi propellant engine [Brown, 2002] a dry

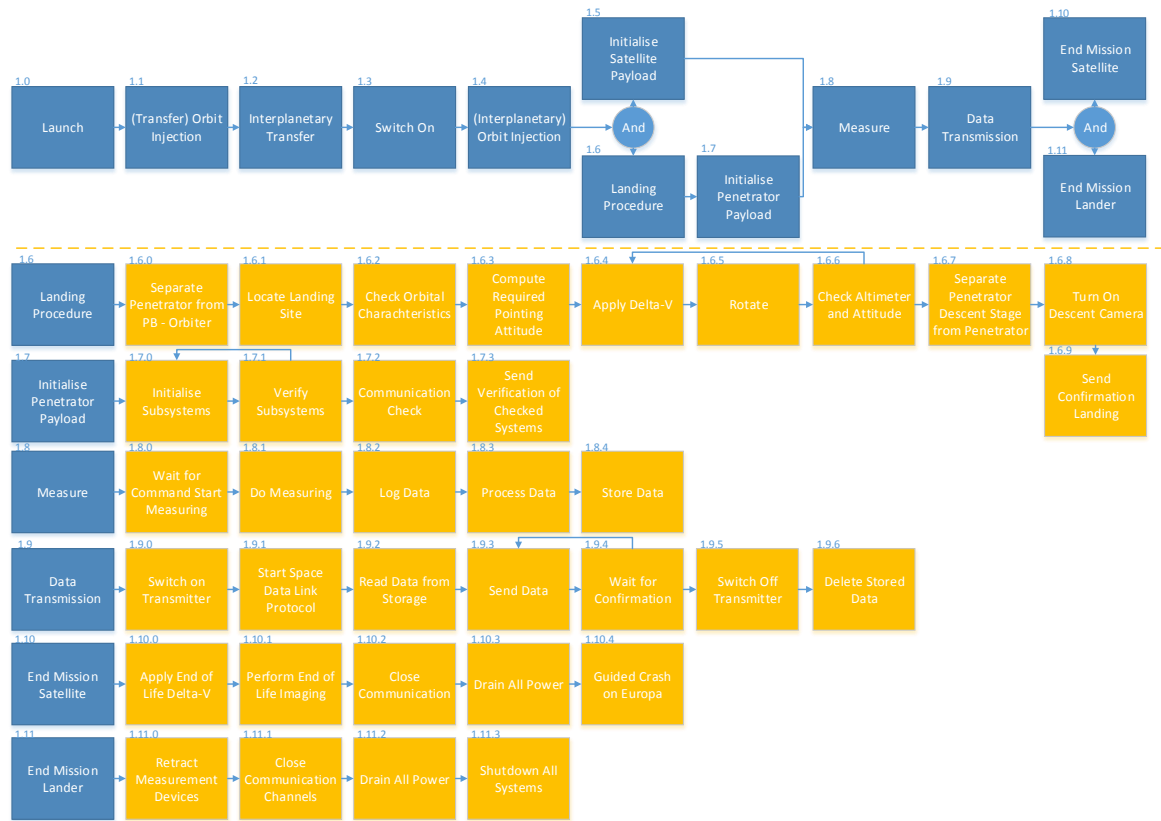


Figure 3.2: Functional Flow Block Diagram - General System (Part 2)

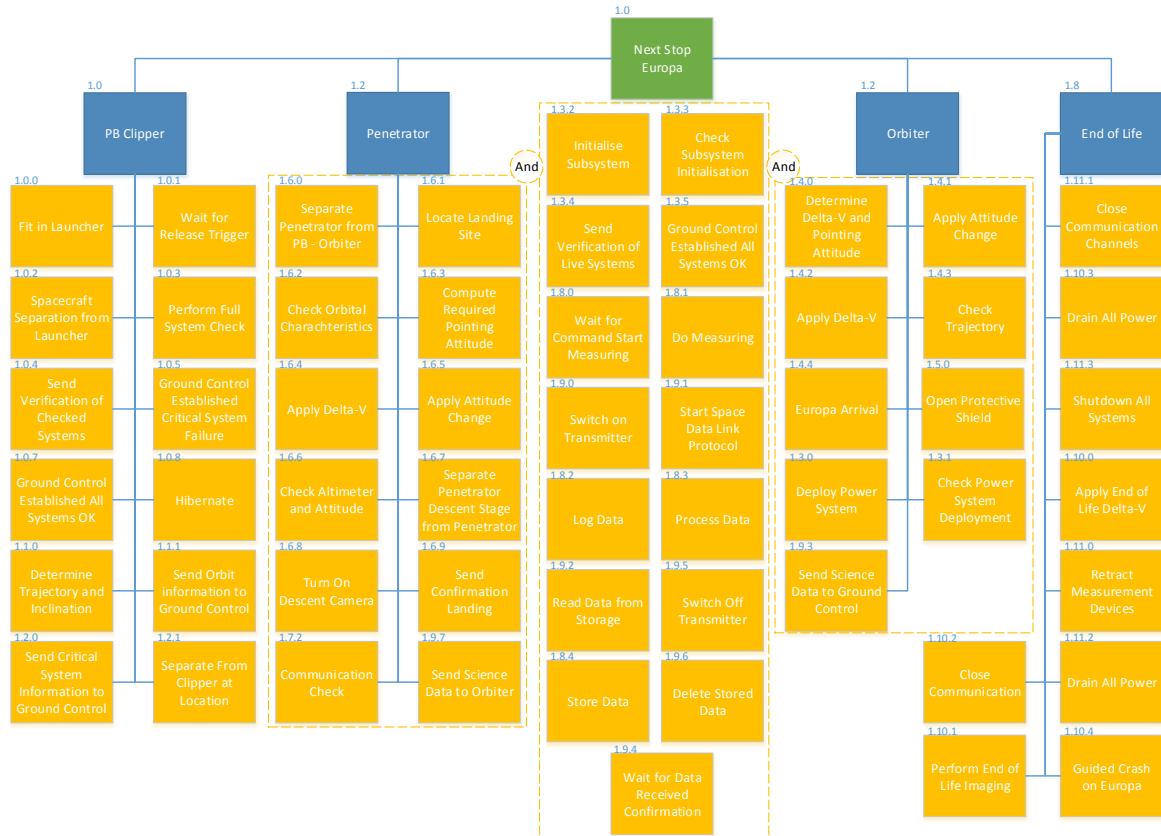


Figure 3.3: Work Breakdown Structure - General System

mass of 205 kg can be found. Using statistics, the mass per subsystem including a 20 % margin [ESA, 2014] can be found in Table 3.1.

Table 3.1: Mass budget and allocation for the orbiter [Wertz et al., 2011]

Subsystem	Percentage [%]	Mass [kg]	Design Mass (incl margin) [kg]
Payload	15	31	26
Structures	25	51	43
Thermal	6	12	10
Power	21	43	36
TT & C	7	14	12
C & DH	4	8	7
GNC	6	12	10
Propulsion	13	27	22
Other (radiation)	4	8	7
Total Dry Mass	100	205	173
Propellant Mass	70	145	
Total Wet Mass	170	350	

Power Budget

The power budget for this mission was initially based on the payload power, however, since the orbiter is now a full relay orbiter the telecommunications module can be considered as a payload. The telecommunications system is relatively power consuming for a Jovian micro-sat since the transmission distance is very large. The total power for this mission can be based on other Jovian orbiters, the relation can be found in Table 3.2.

Table 3.2: Begin of life power with respect to total dry mass for Jovian orbiters

	Dry Mass [kg]	BOL Power [W]	Ratio [-]
Juno ¹	1593	400	0.25
JUICE ²	1900	700	0.37
Clipper ³	2072	391	0.19
Average	1855	497	0.27

So for a dry mass of 205 kg, this relation yields a total mission power of 55.35 W. Applying an ESA power margin of 30 % [ESA, 2014] to this number the total design power for this mission is 72 W. This power is then divided over the subsystem using statistics, these values already include margins. This division can be found in Table 3.3.

Table 3.3: Power budget and allocation for the orbiter [Wertz et al., 2011]

Subsystem	Percentage [%]	Power [W]	Design Power (incl margin) [W]
Payload	22	16	12
Structures	1	1	1
Thermal	15	11	8
Power	10	7	6
TT & C	18	13	10
C & DH	11	8	6
GNC	12	9	7
Propulsion	13	9	7
Total Power		72	56

¹http://www.jpl.nasa.gov/news/press_kits/JunoLaunch.pdf[Retrieved: June 18, 2015]

²http://congrexprojects.com/docs/12c25_2510/05cerd_juicemission.pdf?sfvrsn=2[Retrieved: June 18, 2015]

³<https://solarsystem.nasa.gov/europa/docs/Europa%20Clipper%20Info%20Sheet%2020130903.pdf>[Retrieved: June 18, 2015]

4. Astrodynamical Characteristics

The astrodynamical characteristics of the mission analysed and detailed. First, the interplanetary transfer of Clipper is analysed and documented in Section 4.1. Second, the chosen Jovian tour that will lead the spacecraft to its final Europa orbit is documented in Section 4.2. Furthermore, the final Europa orbit is studied with respect to its groundtrack, perturbations and trajectory. This is presented in Section 4.3. Finally, the ΔV budget of the mission is compiled and presented in Section 4.5.

4.1 Interplanetary Transfer

The outcome of the trade-off previously performed [DSE Group 10 et al., 2015], greatly affected the choice of interplanetary transfer. Since the piggyback orbiter-lander mission profile won the trade, the decision of sharing Clipper’s interplanetary transfer became trivial. The baseline of Clipper is a Venus-Earth-Earth Gravity Assist (VEE-GA) on board an Atlas V rocket [Niebur et al., 2013]. In Section 4.1.1, the advantages of gravity assist trajectory, Clipper’s trajectory and its time line are described. Furthermore, other important aspects of the trajectory are given such as the transfer duration, flyby altitudes and detachment strategy.

Interplanetary trajectory are costly manoeuvres with respect to the amount of ΔV needed to achieve direct transfer. This implies that careful considerations should be made when deciding on a specific trajectory to take. In the case of an interplanetary transfer to Jupiter, there is a substantial difference in ΔV budget when comparing a direct transfer and a gravity assist transfer, with the gravity assist transfer being much cheaper (numerical values to follow). The reason for this is that when performing gravity assist manoeuvres, the spacecraft is swung by the planets motion in its orbit, which cause rotation and an increase in magnitude of the spacecraft’s V_∞ vector [Petropoulos et al., 2000]. Ultimately, the reduction in ΔV budget facilitated by a gravity assist transfer has flight time drawbacks, however, the ΔV budget is of more importance since it can dictate whether a mission is feasible or not.

4.1.1 VEE-GA transfer

The baseline chosen for the interplanetary transfer for the Clipper mission is a VEE-GA with launch date on the 21st of November 2021 on board an Atlas V rocket [Niebur et al., 2013]. It should be noted that this date is not fully fixed by NASA yet and that the date might slightly shift by a few hours, which would result in a launch date on the 22nd of November 2021. Indifferent of the choice of launching on the 21st or 22nd, the same arrival date at the Jovian system will take place. Table 4.1 assumes the latest launch date of 22nd of November and provides details of the flyby altitudes at Venus and Earth [Campagnola et al., 2014b]. The transfer begins with launch from Earth surface followed by escaping Earth influence. This is done at an altitude of 200 km above the surface of Earth. The first flyby Clipper will perform is at Venus on the date of 14th of May 2022. Furthermore, Clipper will flyby Earth twice, on the 24th of October 2023 and 24th of October 2025. Excluding the ΔV required to reach the altitude of 200 km above Earth surface, the transfer requires a mere ΔV of **3.852 km/s** to reach the Jovian system. This is a great decrease compared to a direct transfer, which would require 6.4 km/s [DSE Group 10 et al., 2015]. The interplanetary transfer is plotted in 3D and is displayed in Figure 4.1. The coordinates are centred at Jupiter’s centre (0,0,0).

Table 4.1: Flybys performed during the interplanetary assist.

Event	Date (ET calendar)	Manoeuvre ΔV [km/s]	V_∞ [km/s]	Altitude [km]
Earth escape	22 Nov 2021 00:01:13	3.852	3.77	200
Venus flyby	14 May 2022 09:30:43	-	6.62	300
Earth flyby	24 Oct 2023 22:41:49	-	12.07	11761
Earth flyby	24 Oct 2025 09:06:48	-	12.05	3330

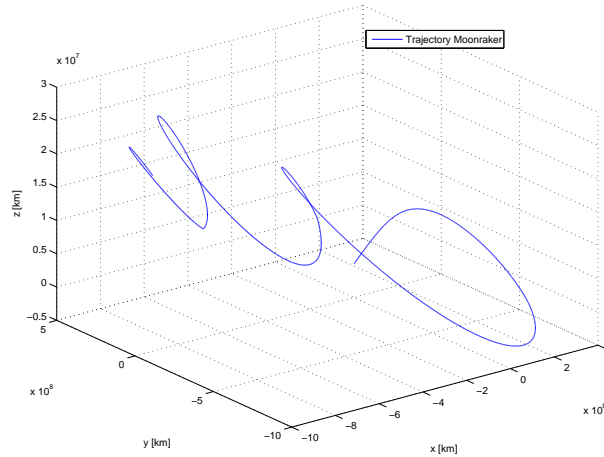


Figure 4.1: Interplanetary VEE-GA transfer trajectory.

Following the last Earth flyby, Clipper will be catapulted towards the Jovian system. The spacecraft will arrive at the Jovian system on the **3rd of April 2028**, making the transfer last **6.37 years**.

4.2 Jovian Tour

Following the interplanetary transfer, the spacecraft needs to detach from Clipper and insert itself into a Europa orbit. This can be done with two different methods; direct Jupiter orbit insertion (JOI) followed by raising of orbit to intersect Europa's orbit and then Europa orbit insertion (EOI), or following a series of flybys to lower the energy of the system using the gravitational forces of the bodies used to fly by. The latter option is considerably cheaper in terms of ΔV budget and facilitates the feasibility of the mission [Campagnola et al., 2014b]. A numerical comparison will be presented below. Considering the large decrease in fuel weight that such an option can provide, the spacecraft's Jovian tour is based on the findings of Stefano Campagnola et al. [Campagnola et al., 2014b], which describes a Jovian tour that ends with a Europa orbit at 100 km altitude and an inclination of 95 degrees. Furthermore, the tour is designed for low total ionising dose (TID); an important aspect for missions in the Jovian system. For the current mission, however, the end orbit of the designed tour will not be feasible with respect to communication, hence the tour is slightly modified to accommodate the current mission. The last manoeuvre of the tour, EOI, is recalculated such that the spacecraft will be captured in a polar orbit at an altitude of 244 km. Below, the full tour is described.

Upon arriving at the Jovian system, the orbiter-lander module will detach from Clipper prior to Clipper's first flyby of Ganymede performed on the 3rd of April 2028 at 11:58:34. Due to this early detachment, the spacecraft can be considered independent from Clipper post-arriving at the Jovian system. Following the detachment from Clipper, the spacecraft will follow a series of 15 flybys to dissipate its energy and finally insert itself into a Europa orbit. The purpose of the flybys is to use the gravitational force of Ganymede, Callisto and Europa to lower the required ΔV for EOI [Campagnola et al., 2014b]. Table 4.2 contains the time line of the flybys the spacecraft will take preceding Europa orbit insertion [Campagnola et al., 2014b]. The tour is initialised by a 500 km-altitude Ganymede flyby, followed by a JOI-manoeuve, capturing the spacecraft in a 230-day capture orbit. The spacecraft continues along this orbit until the first apojove, where a Perijove Raise manoeuvre (PJR) is applied, raising the perijove to approximately 15 Jupiter radii. The following four flybys are performed to decrease the energy of the spacecraft and its inclination. A orbit trim manoeuvre (OTM) is performed between the first and second Ganymede flybys. Flyby Ganymede 4 is purposed to target the next flyby, Callisto 5. This flyby in turn will pump up the perijove and set the spacecraft on a trajectory targeting Ganymede 6 flyby. The next four Ganymede flybys, 6 though 9 will further reduce the orbit period and prepare the spacecraft for Callisto 10 flyby. This will pump up the perijove further and beyond Ganymede orbit. Starting with Callisto 10 flyby, the spacecraft would enter its final phase before EOI. This phase contains Ganymede flybys 11 through 13, preparing the spacecraft for two Europa high-altitude flybys and two Tisserand-leveraging manoeuvres (TLM). It should be noted that TLM further reduce the needed ΔV budget with respect to V_∞ - leveraging [Campagnola et al., 2014b]. Finally, the spacecraft exerts EOI manoeuvre that will place it in an orbit of **244.29 km** with an inclination of **90 degrees**. The value for EOI of 0.566 km/s was calculated as follow:

- The final orbit was raised from 100 km to 244.3 km, hence lowering the required ΔV for the breaking

by 28.6 m/s from the original value of 477 m/s.

- The manoeuvre of EOI was combined with an inclination change of 5 degrees, requiring ΔV of 117.1 m/s.
- The values of ΔV were summed, resulting in a EOI requiring a ΔV of 0.566 km/s

Table 4.2: Flybys performed during the Jovian tour.

Event	Date (ET calendar)	Manoeuvre ΔV [km/s]	V_∞ [km/s]	Altitude [km]
Ganymede 0	03 Apr 2028 11:53:40	-	7.99	500
JOI	03 Apr 2028 22:53:35	0.812	-	-
PJR	14 Jul 2028 13:40:14	0.122	-	-
Ganymede 1	18 Nov 2028 20:22:49	-	5.61	629
OTM	28 Dec 2028 04:45:07	0.005	-	-
Ganymede 2	05 Feb 2029 12:34:23	-	5.68	100
Ganymede 3	03 Apr 2029 17:20:35	-	5.80	3370
Ganymede 4	09 May 2029 11:45:33	-	5.79	643
Callisto 5	17 Jun 2029 12:40:13	-	5.48	221
Ganymede 6	21 Jul 2029 13:57:07	-	3.87	6645
Ganymede 7	02 Sep 2029 10:32:53	-	3.79	268
Ganymede 8	23 Sep 2029 21:08:34	-	3.77	2009
Ganymede 9	08 Oct 2029 04:05:01	-	3.76	2730
Callisto 10	23 Oct 2029 05:10:28	-	1.77	2124
Ganymede 11	27 Oct 2029 09:33:56	-	-	23667
Ganymede 12	17 Nov 2029 22:51:09	-	-	4900
Ganymede 13	24 Nov 2029 20:15:57	-	1.19	1185
Europa 14	27 Nov 2029 08:10:12	-	-	6681
TLM	09 Dec 2029 15:08:29	0.054	-	-
Europa 15	11 Dec 2029 17:16:32	-	-	6563
TLM	27 Dec 2029 01:25:06	0.097	-	-
EOI	03 Jan 2030 21:29:49	0.566	-	244

The total ΔV for the tour is summed up to be **1.656 km/s**. Comparing this value with the ΔV value of 11.08 km/s (6.4 km/s for escaping Earth and the transfer, 4.5 km/s for capturing at Jupiter and 0.18 km/s to raise the orbit and capture at Europa) [DSE Group 10 et al., 2015] for direct capture, it can be justified why such a tour is implemented. The Jovian tour trajectory is plotted in 3D and shown in Figure 4.2. The coordinates are given with respect to Jupiter's centre.

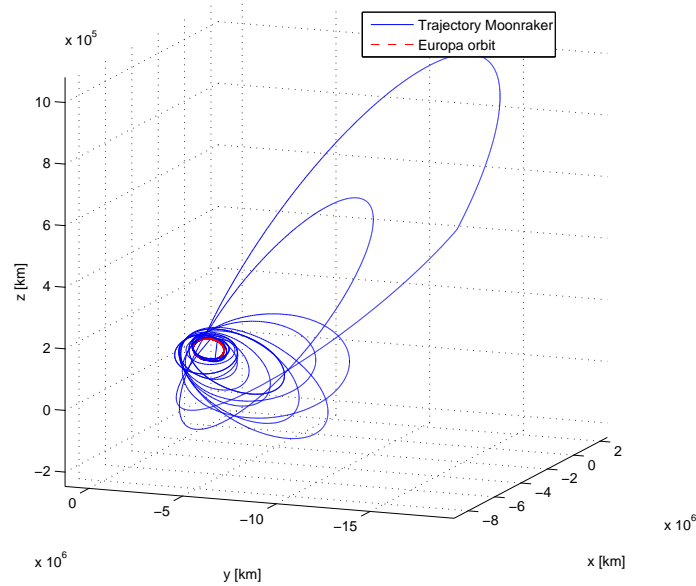


Figure 4.2: Jovian tour trajectory.

4.3 Europa Orbit

The orbit assumed by the spacecraft at Europa will dictate the science the mission can accomplish as well as the limitations of the spacecraft with respect to communication capabilities, power generation, coverage and visiting frequency. Furthermore, the orbit is analysed for its orbital decay. The ground track of the orbit is computed and presented.

The initial strategy for finding an appropriate orbit was to research literature for already defined orbits about Europa. This enabled the finding of orbits with specific science abilities or limitations. It was found that polar orbits at Europa can remain frozen for up to 300 days [dos Santos Carvalho et al., 2013]. Considering polar orbits, it is trivial that they would offer the maximised coverage and communication with a lander at either one of the poles. Furthermore, at the correct right ascension of the ascending node it would provide minimum eclipse duration. Therefore, it was chosen for a polar orbit for which the groundtrack repeat and coverage, decay and trajectory would be analysed and iterated upon to satisfy all mission requirements. These are presented in Section 4.3.1, 4.3.2 and 4.3.3 respectively.

4.3.1 Groundtrack

This section will treat the groundtrack of the orbit. First, the model used is stated and verified. Second, the visiting frequency of the orbit is computed and verified by plotting its groundtrack and comparing it to groundtracks from literature. Finally, the coverage and communications abilities of the orbit are assessed from its groundtrack.

Model

The model presented by Michael Bettner in [Bettner, 1995] is fully implemented in this study. The model implements a two-body problem solved in time using the Kepler equation. Furthermore, transformations are applied from a right hand system in the orbital plane to a planetocentric coordinate system. Finally, planetocentric coordinates are transformed to latitude and longitude values. The following assumptions apply for the model:

1. Constant orbital parameters; semi-major axis (a), inclination (i), mean motion (n), eccentricity (e), argument of periapsis (ω), right ascension of ascending node (Ω), angular momentum (H)
2. The only force acting on the satellite is gravitation force of Europa
3. The main body is a uniform sphere
4. J2 effects are accounted for separately
5. The main body is modelled as an ellipsoid

Governing Equations

$$\ddot{\vec{r}} + \left(\frac{\mu}{r^3}\right)\vec{r} = 0 \quad (4.1) \quad M_i = M + n\Delta T \quad (4.6)$$

$$r = \frac{a(1 - e^2)}{(1 + e\cos(\nu))} = \frac{p}{(1 + e\cos(\nu))} \quad (4.2) \quad \cos(\nu_i) = \frac{e - \cos(E_i)}{e\cos(E_i) - 1} \quad (4.7)$$

$$\cos(E) = \frac{e + \cos(\nu)}{1 + e\cos(\nu)} \quad (4.3) \quad \vec{r} = r\cos(\nu)\vec{P} + r\sin(\nu)\vec{Q} \quad (4.8)$$

$$M = E - e\sin(E) \quad (4.4) \quad \dot{\Omega}_{J_2} = -1.5nJ_2\left(\frac{R_e}{a}\right)^2\cos(i)(1 - e^2)^{-2} \quad (4.9)$$

$$n = \sqrt{\frac{\mu}{a^3}} \quad (4.5) \quad \dot{\omega}_{J_2} = 0.75nJ_2\left(\frac{R_e}{a}\right)^2(4 - 5\sin^2(i))(1 - e^2)^{-2} \quad (4.10)$$

Equation 4.1 is the differential equation of motion describing the spacecraft's motion. A solution for Equation 4.1 is given by Equation 4.2. Furthermore, the initial eccentric anomaly (E), is obtained using Equation 4.3 and the initial mean anomaly (M) is obtained using Equation 4.4. The simulation can then be started and related to time using Equation 4.6. At each time step a mean anomaly is found and then the eccentric anomaly is calculated using Equation 4.4. It should be noted that E_i can not be computed explicitly and therefore an iterative method should be implemented to solve for E at each time step. The Newton-Raphson iteration method is used to solve Equation 4.4 with an initial guess $E_i = M_i$. Finally, the effects of J2 are taken into account using Equations 4.9 and 4.10.

Coordinate Systems

Two coordinate systems were used in the model; a planetocentric coordinate system and a right hand coordinate system in the orbital plane. The planetocentric coordinate system at Europa is defined as following:

- xy-plane - central-body mean equator plane at reference epoch
- x-axis - out along the ascending node of the central-body mean equator plane on the reference plane at the reference epoch
- z-axis - along the central-body mean north pole at the reference epoch

Furthermore, x, y and z axis are defined by unit vectors I, J and K respectively. The coordinate system in the orbital plane is assumed to have axes P, Q and W oriented as follow:

- P - in the direction of periapsis from the centre of the main body
- Q - in the orbital plane 90 degrees from P in the direction of satellite motion
- W - perpendicular to the orbital plane

Figure 4.3, illustrates the two coordinate systems for Earth. Due to the lack of illustrations of the defined coordinate systems at Europa, these are not shown here, but they are analogous to the Earth coordinate systems.

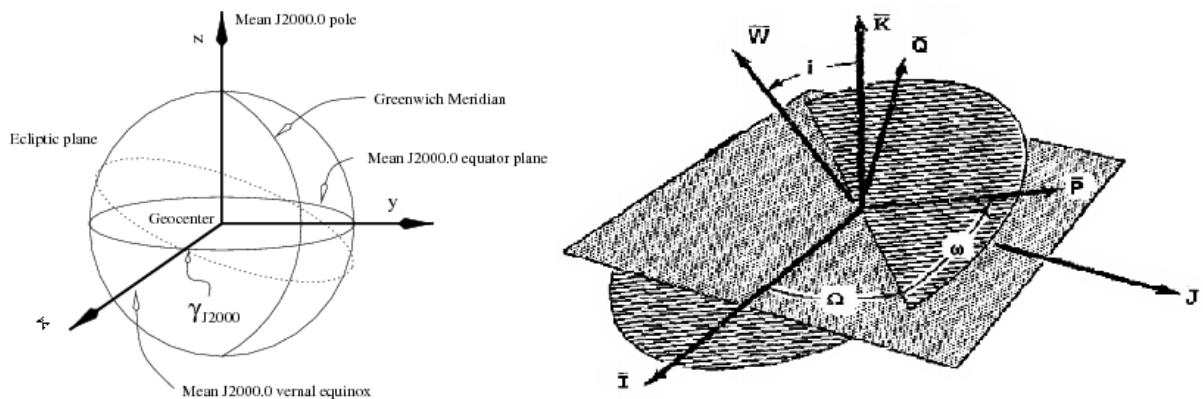


Figure 4.3: Coordinate systems used for Earth.

Transformations

First, the calculations of the motion is carried in the orbital plane and then transformed to the PQW-coordinate system using Equation 4.8. Second, the PQW components of the position vector are transformed to the IJK-frame using the relation shown by Equation 4.11.

$$\begin{bmatrix} r_I \\ r_J \\ r_K \end{bmatrix} = \begin{bmatrix} 1 & 0 & 0 \\ 0 & \cos(-\Omega) & \sin(-\Omega) \\ 0 & -\sin(-\Omega) & \cos(-\Omega) \end{bmatrix} \begin{bmatrix} \cos(-i) & \sin(-i) & 0 \\ -\sin(-i) & \cos(-i) & 0 \\ 0 & 0 & 1 \end{bmatrix} \begin{bmatrix} 1 & 0 & 0 \\ 0 & \cos(-\omega) & \sin(-\omega) \\ 0 & -\sin(-\omega) & \cos(-\omega) \end{bmatrix} \begin{bmatrix} r_P \\ r_Q \\ r_W \end{bmatrix} \quad (4.11)$$

Furthermore, the IJK coordinates need to be transformed to latitude and longitude coordinates. The longitude is considered first. Equations 4.12 through 4.18 will be used for this. The procedure used is as follow:

1. The planet is assumed to be an ellipsoid described by Equation 4.12.
2. The IJK coordinates are used to calculate magnitudes X_0 and Z_0 , using Equation 4.13.
3. A point (X,Z) on the planet ellipsoid is found such that the slope of the line from (X_0, Z_0) to (X,Z) is the same as the slope of the line normal to the ellipse at (X,Z) . The normal to the slope of the ellipse is given by Equation 4.14 and the slope of the line from a point on the ellipse to the satellite is given by Equation 4.15.
4. The two slopes are set equal to each other and X is extracted explicitly. This is shown in Equation 4.16.
5. The explicit expression for X is substituted back in the ellipsoid's equation; shown in Equation 4.17. This equation is then solved numerically for a value of Z . The found value of Z is used to compute a value of X .
6. Finally, the latitude is given by Equation 4.18.

$$\frac{X^2}{A_e^2} + \frac{Z^2}{B_e^2} = 1 \quad (4.12) \quad X = -\frac{X_0 A_e^2 Z^2}{(B_e^2 - A_e^2)Z - Z_0 B_e^2} \quad (4.16)$$

$$X_0 = \sqrt{r_I^2 + r_J^2}; Z_0 = r_K \quad (4.13) \quad \frac{X_0^2 A_e^2 Z^2}{((B_e^2 - A_e^2)Z - Z_0 B_e^2)^2} + \frac{Z^2}{B_e^2} = 1 \quad (4.17)$$

$$-\frac{dX}{dZ} = \frac{A_e^2 Z}{B_e^2 X} \quad (4.14) \quad \delta = \tan^{-1}\left(\frac{Z - Z_0}{X - X_0}\right) \quad (4.18)$$

$$m = \frac{Z - Z_0}{X - X_0} \quad (4.15) \quad \theta = \theta_0 + \vec{\omega}_{planet}(t - t_0) + \lambda \quad (4.19)$$

In addition, the longitude (λ) can be computed from Equation 4.19. One, however, should define the location of the meridian at the initial time of the simulation (θ_0) and the angular rate of the planet ($\vec{\omega}_{planet}$).

Verification and Validation

The software written based on the model described about is validated by means of comparing output groundtrack of a predefined orbit gathered from literature. Figure 4.4 shows the groundtrack of the LAGEOS-1 mission [Capderou, 2005] and Figure 4.5 shows the simulated groundtrack for the same orbit. Furthermore, the software constants used are as follow: time of simulation = 12 hours, $\mu_{Earth} = 396600.4 \frac{km^3}{s^2}$, $\vec{\omega}_{Earth} = 7.29E-05$ rad/s, $A_e = 6378.14$ km, $B_e = 6356.8$ km.

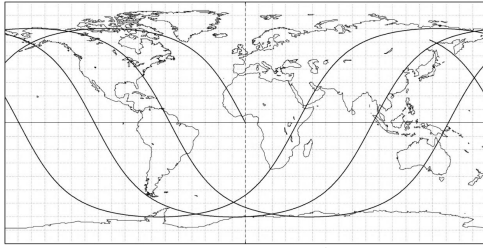


Figure 4.4: Ground track of the LAGEOS-1 mission. $h = 5891.9$ km, $i = 109.81$ degrees, $e = 0$, $\Omega = 0$, $\omega = 0$

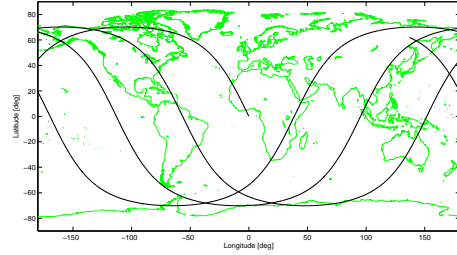


Figure 4.5: Simulated Ground track of the LAGEOS-1 mission. $h = 5891.9$ km, $i = 109.81$ degrees, $e = 0$, $\Omega = 0$, $\omega = 0$.

The software was implemented for an Earth orbit for the purposes of validation. Since the validation was successful, the planetary parameters are changed to be equal to Europa parameters and the sizing of the groundtrack of an Europa orbit is performed. The parameters used in the groundtrack software for Europa are: time of simulation = 35.5 days, $\mu_{Europa} = 3203.3 \frac{km^3}{s^2}$, $\vec{\omega}_{Europa} = 2.05E-05$ rad/s, $A_e = 1565$ km, $B_e = 1560.8$ km.

Visiting frequency

The visiting frequency is chosen such that the orbiter passes the lander enough times per each Europa sidereal day, i.e. the time it takes Europa to complete an orbit about Jupiter. It is then implied that the period of the spacecraft shall be a multiple of Europa's sidereal day and therefore the ground repeat is a function of orbit height, rotation rate of Europa and inclination of orbit. Furthermore, from the study of frozen polar orbits [Santos et al.,], only orbits with height between 100 and 290 km are considered. Taking into account telecommunications the optimum height in this range is chosen to be 244.29 km. This means that the spacecraft will revolve about Europa 36 times for every Europa sidereal day; i.e. the ground track repeats every 36 orbits.

4.3.2 Orbital Perturbations

The orbital perturbations are analysed using the Lagrange planetary equation and a disturbing potential presented in [Santos et al.,]. The model is presented and validated using data from [dos Santos Carvalho et al., 2013].

Model

The model is governed by the Lagrange planetary equation shown by Equations 4.20 through 4.25 [Wakker, 2015]. The disturbing potential accounts for Jupiter's gravitational disturbances, for J2 and J3 oblateness effects of Europa; this is shown by Equations 4.26 through 4.34.

$$\frac{da}{dt} = -2\frac{a^2}{\mu} \frac{\partial R}{\partial M} \quad (4.20) \quad A = e^2(\cos(i) + 1)^2 \cos(2\omega + 2\Omega - 2M_j) \quad (4.28)$$

$$\frac{de}{dt} = -\frac{a(1-e^2)}{\mu e} \frac{\partial R}{\partial M} - \frac{1}{e} \sqrt{\frac{1-e^2}{\mu a}} \frac{\partial R}{\partial \omega} \quad (4.21) \quad B = e^2(\cos(i) - 1)^2 \cos(2\omega - 2\Omega - 2M_j) \quad (4.29)$$

$$\frac{di}{dt} = \frac{\cot(i)}{\sqrt{\mu a(1-e^2)}} \frac{\partial R}{\partial \omega} - \frac{1}{\sqrt{\mu a(1-e^2)\sin(i)}} \frac{\partial R}{\partial \Omega} \quad (4.22) \quad C = \frac{6}{5}(\cos(i) - 1)(e^2 + \frac{2}{3})(\cos(i) + 1)\cos(2\Omega - 2M_j) \quad (4.30)$$

$$\frac{d\omega}{dt} = \frac{1}{e} \sqrt{\frac{1-e^2}{\mu a}} \frac{\partial R}{\partial e} - \frac{\cot(i)}{\sqrt{\mu a(1-e^2)}} \frac{\partial R}{\partial i} \quad (4.23) \quad D = (-2e^2(\cos(i))^2 + 2e^2)\cos(2\omega) \quad (4.31)$$

$$\frac{d\Omega}{dt} = \frac{1}{\sqrt{\mu a(1-e^2)\sin(i)}} \frac{\partial R}{\partial i} \quad (4.24) \quad E = \frac{6}{5}(e^2 + \frac{2}{3})(-\frac{1}{3} + (\cos(i))^2) \quad (4.32)$$

$$\frac{dM}{dt} = 2\frac{a^2}{\mu} \frac{\partial R}{\partial a} + \frac{a(1-e^2)}{\mu e} \frac{\partial R}{\partial e} \quad (4.25) \quad R_{J_2} = -\frac{1}{4} \frac{\varepsilon n^2(-2 + 3\sin(i)^2)}{(1-e^2)^{\frac{3}{2}}} \quad (4.33)$$

$$R = R_2 + R_{J_2} + R_{J_3} \quad (4.26) \quad R_{J_3} = -\frac{3}{8} \frac{\varepsilon \varepsilon_1 n^2 \sin(i)(-4 + 5\sin(i)^2)\sin(\omega)}{a(1-e^2)^{\frac{5}{2}}} \quad (4.34)$$

$$R_2 = \frac{15}{32} n_j^2 a^2 \times (A + B - C + D + E) \quad (4.27) \quad \varepsilon = J_2 R_e^2; \varepsilon_1 = J_3 R_e^3 \quad (4.35)$$

Verification and Validation

The simulation is started with the initial values and constants shown in Table 4.3 [dos Santos Carvalho et al., 2013], with the intention to replicate graphs presented in [dos Santos Carvalho et al., 2013] and shown in Figure 4.6. The result of the simulation is presented in Figure 4.7. It can be seen that the curves match each other and thus the software is deemed valid.

Table 4.3: Initial conditions and constants for the simulation with verification purposes.

Parameter	Value	Unit
h	435	km
e	0.005	[-]
Ω	90	degrees
ω	270	degrees
i	90	degrees
T_f	300	days
R_e	1565	km
J_2	4.355E-04	[-]
J_3	1.3784E-04	[-]

Table 4.4: Initial conditions and constants for the simulation of the chosen orbit.

Parameter	Value	Unit
h	244.29	km
e	0.005	[-]
Ω	90	degrees
ω	270	degrees
i	90	degrees
T_f	35.5	days
R_e	1565	km
J_2	4.355E-04	[-]
J_3	1.3784E-04	[-]

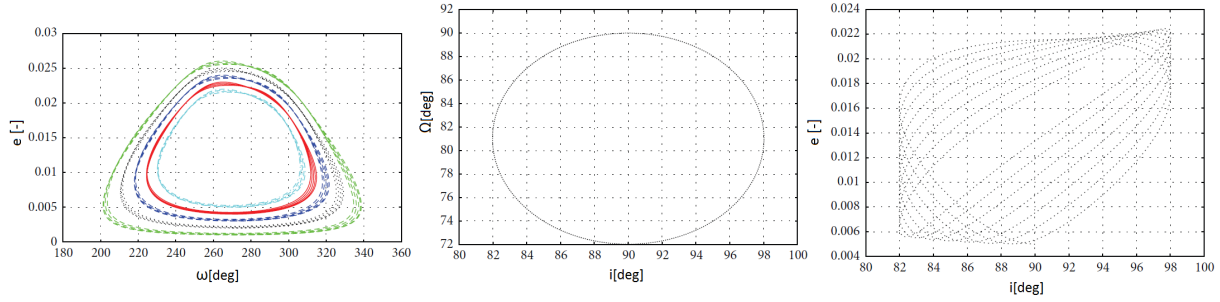


Figure 4.6: Perturbation software validation data.

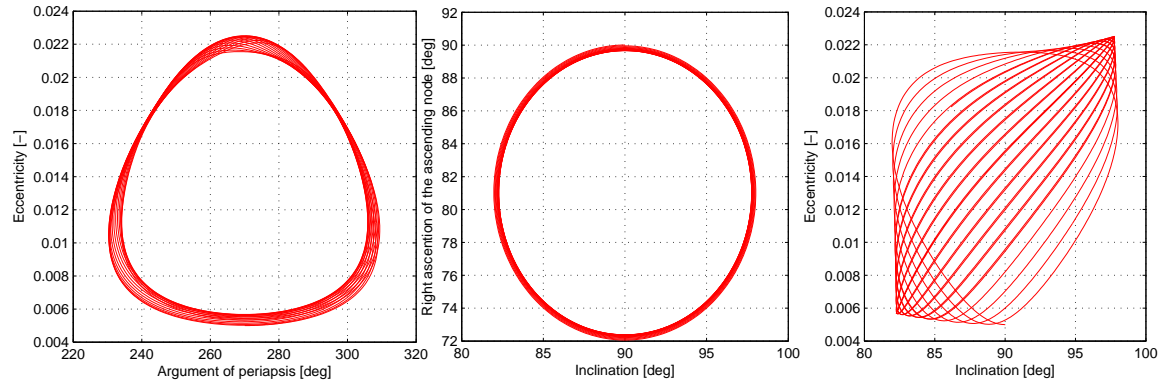


Figure 4.7: Perturbation software simulated validation data.

Results

The results of the simulation for validation purposes show that there exist frozen polar orbits at Europa for long periods of time. However, even though they are frozen, that does not deem them stable. There is still variation of orbital parameters, which oscillate between maxima and minima. Their oscillation period, however, is far greater than the mission duration at Europa, hence the chosen mission orbit is analysed for disturbances in its orbital parameters over a period of 35.5 days, with parameters shown in Table 4.4. The obtained variations are presented in Figure 4.8.

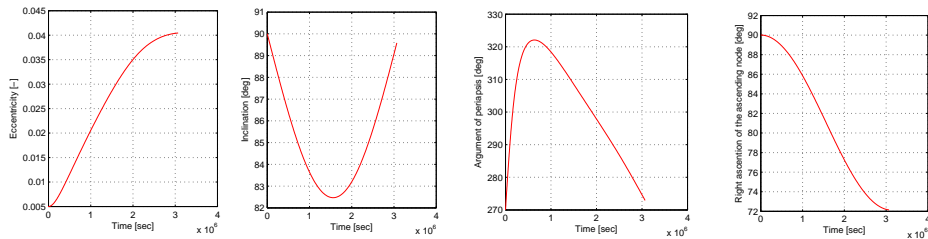


Figure 4.8: Perturbation simulation of the Europa orbit.

As seen on Figure 4.8, the inclination varies from an initial value of 90 degrees to approximately 82 degrees over a period of approximately 5 Europa sidereal days (17.75 days). Following, the inclination increases back to a little under 90 degrees. Since the orbit's main function is to pass over the lander at the South pole, no inclination change is allowed due to loss of communication. In total, the inclination varies over a range of 16 degrees. Equation 4.36 [Wakker, 2015] computes the ΔV value needed to counteract this change and hence provides the ΔV budget for orbit maintenance. It should be noted that the burn shall be performed at $\nu = -\omega, \pi - \omega$, the optimum true anomaly for the most effective burn for inclination changes. Furthermore, to keep the design as light as possible only correction of inclination is considered since any change in inclination will deem the orbiter inefficient with respect to communications with the lander; i.e. the orbiter will be inefficient at its primary purpose.

$$\Delta V \approx |\Delta i| \sqrt{\frac{\mu}{a}} \quad (4.36)$$

4.3.3 Trajectory

The trajectory of the orbit is simulated using the same model used to simulated the groundtrack described in Section 4.3.1. Furthermore, the interplanetary trajectory of Clipper is accessed at ¹. In addition, the chosen Jovian tour trajectory is obtain through personal communication with Stefano Campagnola. The orbit trajectory is presented in Figure 4.9. The simulation for the purpose of displaying the trajectory of the orbit was done only for 5 sidereal Europa day to avoid a cluttered plot.

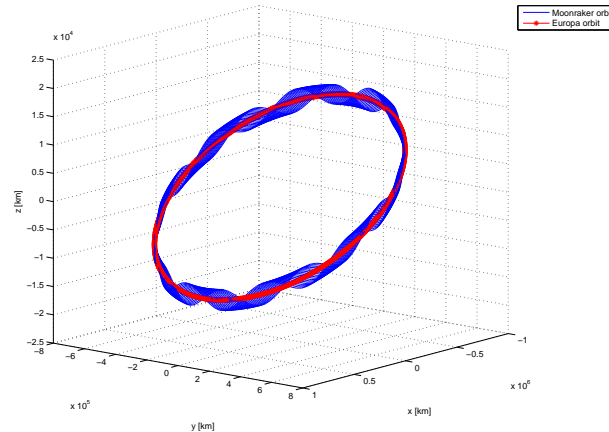


Figure 4.9: Europa orbit trajectory.

4.4 De-orbiting

Using a model based on Hohmann transfer theory [DSE Group 10 et al., 2015] [Wertz et al., 2011], the required ΔV for de-orbiting the spacecraft is computed. The strategy used is that the spacecraft will perform a burn of **100 m/s** lowering the periapsis of the orbit to the surface of Europa. The spacecraft will follow half a period in this orbit and finally crash on the surface of Europa on the **7th February 2030**.

4.5 ΔV Budget

The total ΔV budget is assessed to estimate the amount of fuel the spacecraft needs to take on board. There are three contributions to the ΔV budget; the Jovian tour, orbital maintenance and de-orbiting. The distribution of the ΔV budget is presented in Table 4.5. The final value of the total ΔV budget is **2127 m/s**.

Table 4.5: ΔV budget of the mission

Mission phase	ΔV [m/s]
Jovian tour	1656
Orbit maintenance	371
De-orbiting	100
TOTAL	2127

¹<http://solarsystem.nasa.gov/europa/iceedocs.cfm>[Retrieved May 28, 2015]

5. Guidance, Navigation and Control Subsystem

This chapter describes the design process of the guidance, navigation & control (GNC) subsystem. The GNC subsystem ensures that the spacecraft keeps pointing in the desired direction, makes changes to the attitude and determines when certain ΔV 's need to be carried out. Section 5.1 gives a description of the GNC subsystem. In section 5.2 and section 5.3 the functional flow block diagram and the functional breakdown are described respectively. Section 5.4 describes the performance of the GNC subsystem. Section 5.5 explains how the used code was verified. Furthermore, 5.6 describes the compliance matrix.

5.1 Subsystem Description

Functional Requirements

Number	Requirement	Orbiter	Lander
ACFR-01	The GNC shall be able to determine the distance w.r.t a Europa-centered inertial reference frame with a \mathbf{X} [m] accuracy.	1	n/a
ACFR-02	The GNC shall be able to determine the velocity w.r.t a Europa-centered inertial reference frame with a \mathbf{X} [m/s] accuracy.	$0.1 \cdot 10^{-3}$	n/a

Performance Requirements

Number	Requirement	Orbiter	Lander
ACPR-01	The mass of the GNC shall be no more than \mathbf{X} [kg].	6	5
ACPR-02	The GNC shall have a maximum power usage of \mathbf{X} [W].	21	12
ACPR-03	The absolute pointing error of the thrust vector during orbital manoeuvres shall not exceed \mathbf{X} deg.	0.25	0.25
ACPR-04	The GNC components shall stay within its \mathbf{X} volume [cm^3].	3	0.08
ACPR-05	The GNC components shall not exceed a cost of \mathbf{X} [EUR].	15M	15M
ACPR-06	The GNC shall withstand accelerations of \mathbf{X} g-loads [-].	6	6
ACPR-07	The startracker shall withstand radiation levels of \mathbf{X} [krad].	100	n/a
ACPR-08	The IMU shall withstand radiation levels of \mathbf{X} [krad].	300	300
ACPR-09	The startracker shall be able to operate in temperatures between \mathbf{X} [deg. C].	-20/+50	n/a
ACPR-10	The IMU shall be able to operate in temperatures between \mathbf{X} [deg. C].	-54/+71	-54/+71
ACPR-11	The GNC shall provide a slew rate of \mathbf{X} [deg/s].	0.05	1.5
ACPR-12	The GNC shall be able to point at a desired position with an accuracy of \mathbf{X} [deg].	0.25	20

Verification Requirements

Number	Requirement	Orbiter	Lander
ACVR-001	The GNC shall be tested while taking into account operational safety regulations.	OK	OK
ACVR-002	The GNC shall be designed, built and tested before \mathbf{X} [month/year].	01/2022	01/2022

The GNC subsystem should be able to adjust the attitude of the spacecraft and keep it pointing in a desired direction. The different methods for doing this are shown in Table 5.1 [Wertz et al., 2011]. Because the spacecraft needs pointing in 3 axes with an accuracy of 0.25 deg according to requirement ACPR-12, all gravity-gradient, magnetic and rate-damping methods drop. Spin stabilization could provide a high enough accuracy, but would be problematic when the attitude alternates between nadir pointing and

Earth pointing as the solar panels need to point to the sun as well. Thrusters, reaction wheels or control moment gyroscopes (CMG's) remain the only option. As CMG's may require high redundancy [Wertz et al., 2011] and therefore more mass, this is not the most suitable option for this piggyback mission.

Table 5.1: Possible attitude control systems [Wertz et al., 2011]

Type	Pointing Options	Typical Accuracy
Gravity-Gradient	Earth local vertical only	± 5 deg (2 axes)
Gravity-Gradient + Momentum Bias	Earth local vertical only	± 5 deg (3 axes)
Passive Magnetic	North/South only	± 5 deg (2 axes)
Rate-Damping + Target Vector Acquisition	Usually Sun (Power) or Earth (Communciation)	$\pm 5 - 15$ deg (2 axes)
Pure Spin Stabilization	Inertially fixed any direction	± 0.1 deg to ± 1 deg in 2 axes (proportional to spin rate)
Dual-Spin Stabilization	Limited only by articulation on despun platform	same as for spun direction. Despun dictated by payload reference and pointing
Bias Momentum (1 wheel)	Local vertical pointing or inertial targets	± 0.1 deg to ± 1 deg
Active Magnetic with Filtering	Any, but may drift over short periods	± 1 deg to ± 5 deg (depends on sensors)
Zero Momentum (Thrusters only)	No constraints	± 0.1 deg to ± 5 deg
Zero Momentum (3 wheels)	No constraints	± 0.0001 deg to ± 1 deg
Zero Momentum (CMG)	No constraints short CMG life may require high redundancy	± 0.001 deg to ± 1 deg

The two remaining options are listed in a trade off in Table 5.2. The mass for the reaction wheels is slightly higher than the thruster option. 12 thrusters are needed to control the attitude which have a mass of 2.4 kg and fuel that has to be added for attitude control has a mass of 9.8 kg in a worst case scenario where the it has to rotate around the axis with the highest moment of inertia. The reaction wheels will have a weight of 7.8 kg. This is the case for 3 reaction wheels so there is no redundancy. The thrusters are graded a 10 for mass as they have the best mass performance. The reaction wheels are graded a 7 as they are slightly heavier than required mass for the thrusters. The mass criterion has a weight of 30 because the mass of the orbiter and penetrator must be as low as possible.

The power that is required to control the thrusters is negligible as they only use a slight amount of power for a short time. The required power by the reaction wheels is estimated to range between 15-30 W during manoeuvring ¹ and even can use up to 30 W when fully loaded and not being used. This is why the thrusters are graded a 10 and the reaction wheels a 3. Chapter 8 describes the mass for power and it can be seen that the mass increases aggressively when more is power required. That is the reason why power has a high weight in this trade off.

There was also a look at the accuracies of the two different attitude systems. Both seemed to fit the requirement of 0.25 deg accuracy so it was taken out of the trade off.

The risk for the two systems is also compared and is weighted with 15 because it is not as important as the power and the mass. The thrusters have the lowest risk as their lifetime is determined by the amount of fuel and the lifetime of the reaction wheels is determined by the bearings of the reaction wheels [Wertz et al., 2011]. As the thruster fuel can easily be upgraded and the reaction wheels are harder to be designed for longer mission durations, the thrusters are again scored a 10 and the reactions wheels an 8.

As can be seen, according to the trade off, the thrusters are the best option as it scored a 10. These will be used in both the lander and the orbiter.

For the attitude determination system, less options exist compared to the control system. Ideally, only a low mass inertial measurement unit would be used, but since this unit needs to be calibrated once in a while, other ways of determining the attitude need to be used. Star trackers are very commonly used for deep space missions, as gps systems do not (yet) work for deep space satellites. The problem

¹<http://www.sst-us.com/shop/satellite-subsystems/attitude-and-orbit-control-systems/100sp-o-small-satellite-microwheel-3-unit-package> [Retrieved June 17, 2015]

Table 5.2: Trade off for attitude control systems

	Weight	Thrusters	Reaction wheel + unloading thrusters
Mass	30	10	7
Power	40	10	3
Risk	15	10	8
Total	100	10	6.3

of optical devices is that the harsh radiation environment can easily damage the instruments. Therefore the instruments need to be radiation resistant and shielded well. Table 5.3 presents typical options for attitude determination. Considering the required accuracy of at least 0.25 deg, the magnetometer is already eliminated. Gyroscopes and inertial measurement or reference units are very reliable, and can typically be used in harsh radiation environments. Sun sensors can be used as safe mode function, and some do not require power. Star sensors are useful to determine the location and attitude of the spacecraft, and can be used to recalibrate gyroscopes.

Table 5.3: Possible Attitude Determination Systems [Wertz et al., 2011]

Sensor	Typical Performance Range
Gyroscopes	Drift Rate = 0.003 deg/hr to 1 deg/hr
Sun Sensors	0.005 deg to 3 deg
Star Sensors	0.05 deg to 1 deg
Magnetometer	0.5 deg to 3 deg

For the attitude determination system of the orbiter, it has been decided to use an IRU and star trackers to calibrate the IRU after a certain period of time, and sun sensors for safe mode and easy sun point acquisition.

The selected IRU for the orbiter is based on the Scalable SIRU from Northrop Grumman [Grumman, 2014]. This device is radiation hardened up to 300 krad. Its power usage and mass is currently too high; 43 W and 7.1 kg respectively. For this mission, the SIRU will have to be scaled down by a factor of four. Assuming the accuracy also decreases by four, this still provides a high enough accuracy for the mission.

The star tracker is based on the ST-200 star tracker by Berlin Space Technologies [Technologies, 2013]. This is a very lightweight star tracker which is accurate enough for the mission requirements. Mission budget has to be invested, to make it radiation resistant for up to 100 krad. Next to that, a radiation shielding system has to be designed. The star tracker will only be exposed to radiation if the SIRU needs to be recalibrated. Two star trackers will be used for redundancy purposes.

Concerning the sun sensor, sensors weighing about 0.03 kg are used with an accuracy of approximately 0.3 degrees. This accuracy is enough for sun pointing only.

An overview of the estimated performance characteristics of both the attitude control and attitude determination devices can be found in Table 5.4. The reason for this design choice for these thrusters is given in Section 5.4.1.

Table 5.4: Estimated characteristics of the ADC system

Subpart	Mass [kg]	Power [W]	Performance	Number
Thrusters	0.2	0	0.2 [N]	12
Star Tracker	0.05	0.22	30 arcsecond	2
SIRU	1.8	10.8	Bias: 0.006 [deg/hr]	1
Sun Sensor	0.2	0	0.3 [deg]	6
Total	5.6	11.2	[-]	21

Following the bias of the SIRU, the star trackers would have to be used approximately once every 40 hours for calibration. These can be shielded in the remainder of the time. Concerning the penetrator, the same thrusters and SIRU is used. This results in a required power of 11 W and a mass of 4.2 kg for the attitude determination and control system of the lander.

5.2 Functional Flow Block Diagram

The functions the GNC system has to carry out are ordered in a functional flow block diagram (FFBD) in Figure 5.1. As can be seen in the diagram, the main branch is given on top and starts with starting the GNC subsystem (3.0). After the subsystem has been started, the GNC prioritizes all incoming requests

for changing attitudes (3.1). When the most important GNC request has been chosen the GNC system controls its attitude (3.2) and/or determines its location (3.3). Now the GNC chooses whether it wants to guide its trajectory (3.4) or starts the loop again and prioritizes its requests again (3.1). If it continued to guide its trajectory it has the option to continue to shut down the subsystem (3.5) or loops back to prioritizing the requests again (3.1).

Controlling the attitude (3.2) is described more in detail below the main branch in the diagram. As can be seen in the diagram, first the sensors are switched on (3.2.1), after which the sensors are read-out (3.2.2). These signals are processed (3.2.3) and next the attitude can be determined w.r.t. the reference frame (3.2.4). With this the attitude change manoeuvre can be determined (3.2.5). From this the GNC system determines if it wants to check its attitude again starting with reading out the sensors (3.2.2) or continues on to the next blocks (3.1 or 3.4).

Determining the location of the spacecraft is described in further detail in the branch beneath the attitude control branch. First, the sensors are turned on (3.3.1) and read-out (3.3.2). These are processed (3.3.3) and with this the location w.r.t. the reference system can be determined (3.3.4). With this knowledge the location can be changed to a desired position (3.3.5). From this the GNC system can decide whether to do the location determination again by reading out the sensors again (3.3.2) or turn off the sensors and go further to the next blocks (3.1 or 3.4).

On the bottom of the diagram the trajectory guidance is explained in detail. First, the attitude and current location are processed in parallel (3.4.1 and 3.4.2). With this, the current trajectory can be determined (3.4.3). Next, the desired location is processed (3.4.4) and desired trajectory that belongs to this (3.4.5). From this the required ΔV is determined (3.4.6) and the thrust is applied to get the desired trajectory (3.4.7). From this, the system goes further to the next blocks (3.1) or 3.5).

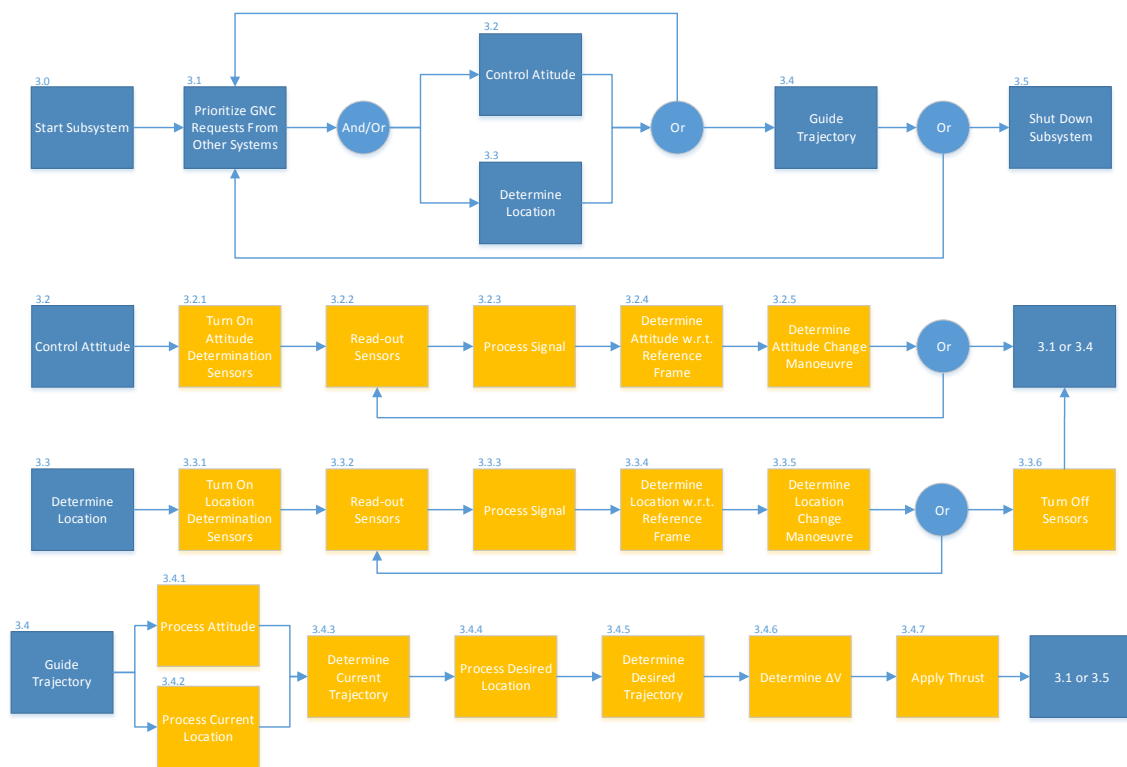


Figure 5.1: Functional flow block diagram of the GNC subsystem

5.3 Functional Breakdown Structure

The functions the GNC subsystem has to carry out are listed in the functional breakdown structure (FB) in Figure 5.8. As can be seen in the diagram, the functions have been split up in 3 branches. These branches are Guidance (sub-5.1), navigation (sub-5.2) and attitude control (sub-5.3). The functions under these branches are numbered in the same way as in the FFBD and are also explained in the section about the FFBD.

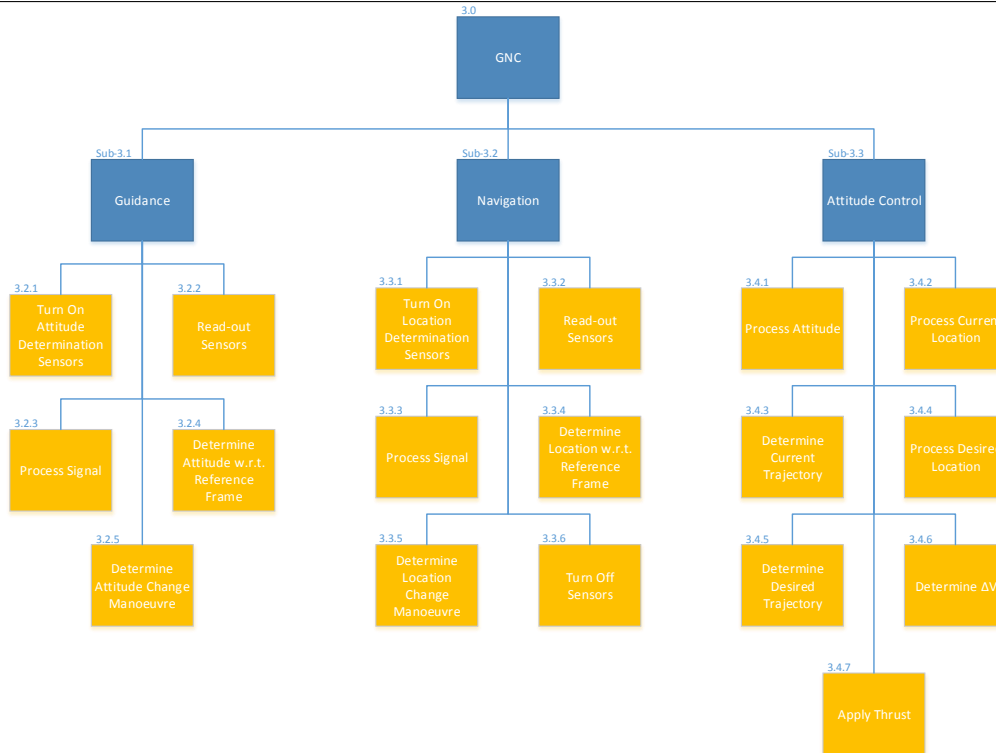


Figure 5.2: Functional Breakdown of the GNC Subsystem

5.4 Performance Analysis

A crucial aspect for GNC is to know what disturbance torques play a role in the environment of the spacecraft and what manoeuvres have to be performed. Subsection 5.4.1 discusses the disturbance torques acting on the orbiter during its one year trajectory and the 36 day orbit. In Subsection 5.4.2 the controlled descent and the stability of the penetrator are discussed.

5.4.1 Orbiter Torques & Momentum

Four main external disturbances generally apply to satellites: solar disturbance, atmospheric drag, magnetic torque, and gravity perturbations. Considering the atmospheric pressure around Europa is only $0.1 \mu\text{Pa}$, it is assumed that the atmospheric drag disturbance can be neglected. The other disturbances, however, are accounted for. A division is made between the two year Jovian tour and the actual orbiting mission around Europa for the calculation of the torques and momentum. For all calculations a worst case scenario is assumed.

The solar radiation pressure is caused by the pressure the sunlight exerts on an object if it absorbs or reflects the light. The solar pressure can be computed using Equation 5.1 [Wertz et al., 2011]. Here, T_s is the produced torque, Φ is the solar constant w.r.t. to the location of the spacecraft from the sun and which is assumed to be $51 \frac{\text{W}}{\text{m}^2}$, where c is the speed of light, A_s is the sunlit surface area which is 13.5 m^2 , q is the unitless reflectance factor that is set at 2 assuming worst case, ϕ is the angle of incidence of the Sun which is assumed to be 90 deg , and cp_s and cm are the centres of solar radiation pressure and mass, 4.5 m and 0 m respectively.

$$T_s = \frac{\Phi}{c} A_s (1 + q) (cp_s - cm) \cos(\phi) \quad (5.1)$$

It should be noted that for both the Jovian tour, and the actual Europa orbit, the solar radiation pressure is assumed to be constant due to the low magnitude and relative small deviations in distance from the sun.

The magnetic torque is caused by the magnetic field and can be calculated using Equation 5.2 [Wertz et al., 2011].

$$T_m = D \left(\frac{M}{R^3} \lambda \right) \quad (5.2)$$

In Equation 5.2, R is the distance between the spacecraft and the center of Jupiter, 676938 km, and λ is a unitless factor ranging from 1 to 2 and thus assumed to be 2 for worst case. M is the magnetic moment of Jupiter multiplied by the magnetic constant, which was found to be $1.55 \cdot 10^{20}$ Tesla. Dipole moment D can only be obtained accurately by testing the spacecraft [Wertz et al., 2011]. Reference spacecraft of similar dimensions showed a dipole between 0.5-1 Am². Adding a safety factor because of the uncertainty of 2, and assuming a worst case scenario results in dipole moment of 2 Am². For the arrival trajectory, at every time step the magnetic torque is evaluated using the distance between Jupiter and the spacecraft. Magnetic disturbances from other celestial bodies, as well as the induced magnetic field at Europa are neglected as they are small compared to the other disturbances. For the orbit around Europa a constant magnetic torque is assumed.

Gravity-gradient torques happen when the center of gravity of a spacecraft is not aligned with its center of mass w.r.t. the local vertical. Equation 5.3 shows how it is calculated for this mission [Wertz et al., 2011].

$$T_g = \frac{3\mu}{2R^3} |I_z - I_y| \sin(2\theta) \quad (5.3)$$

The gravity disturbances from Jupiter, Europa, Callisto, Io, Ganymede and the Sun are included during the Jovian tour and are evaluated at every time step. During the Europa orbit, only disturbance from Jupiter, Europa and the Sun are included. In Equation 5.3, μ is the gravitational constant of the celestial body, and R is the distance from the center of the orbit w.r.t. the spacecraft. I_z is the moment of inertia about the minimum principal axis Z and I_y is the moment of inertia about y-axis in kg·m². The moments of inertia about the x, y, z axis are assumed to be 103, 665 and 718 kg·m² respectively for the trajectory, and 48, 626 and 665 kg·m² respectively for the Europa orbit. These are computed by CATIA software, for the Europa orbit the propellant tanks are almost empty, compared to the full tanks assumed during the Jovian tour. That is why there is a difference in the moments of inertia in the two cases

The total momentum which is build up over time can be calculated by multiplying the torque by the time. For the trajectory, the torque at every time step is evaluated and multiplied by the time step. Then all is toques are summed to get to the total torque the s/c is subjected to.

To correct the disturbance torques, the system should be able to change attitude and point in an arbitrary direction.

$$T = \frac{4\theta I}{t^2} \quad (5.4)$$

Equation 5.4 calculates the torque that is needed to perform a certain slew. θ is the required slew angle in radians, t is the amount of time for the manoeuvre in seconds which equals 300 s, and I is the moment of inertia of the spin axis in kg·m². This results in a required slew torque of 0.1 Nm for the highest moment of Inertia. With two thruster and an arm of 0.33, this would require thrusters of 0.15 N.

From the propulsion subsystem, Chapter 6, it was found that thrusters smaller than 0.5 N are not easily available on the market. Therefore thrusters of 0.5 N have been selected. This obviously is a higher thrust than required. To know what the new slew rate would be, Equation 5.4 had to be rewritten to Equation 5.5. A moment arm of 0.33 m and a thrust of 0.5 N (1 N for two thrusters) result in a torque of 0.33 Nm for two thrusters combined. Equation 5.5 gives a slew time of only 159 s, which satisfies the needs of the other subsystems.

$$t = \sqrt{\frac{4\theta I}{T}} \quad (5.5)$$

The total momentum change that the thrusters need to supply can be calculated using Equation 5.6. T is the applied torque, which is 0.5 N from the thrusters, and t is the slew time which is 159 sec. Filling al value gives a momentum of 6302 Nms.

$$h = T \cdot t \quad (5.6)$$

The total momentum can also be computed using Equation 5.6. For the trajectory, the torque at every time step is multiplied by the time step. Summing all values results in the total momentum that is caused by disturbances and needs to be corrected. Table 5.5 shows all results.

As can be seen in Table 5.5, the gravity gradient is the dominating disturbance when in the Europa orbit. The total momentum from the trajectory and orbit together is $7.27 \cdot 10^3$ Nms. The total propellant

Table 5.5: Computed torques and momentum changes

Attitude Control	Torque _{Traj} [Nm]	Momentum _{Traj} [Nms]	Torque _{Orb} [Nm]	Momentum _{Orb} [Nms]
Solar pressure	$1.47 \cdot 10^{-5}$	814.58	$1.47 \cdot 10^{-5}$	44.52
Magnetic field	Mean: $1.46 \cdot 10^{-7}$	7.76	$2.00 \cdot 10^{-6}$	6.04
Gravity gradient	$2.46 \cdot 10^{-4}$	2.17	$5.04 \cdot 10^{-4}$	269.45
Slew	n/a	n/a	0.33	$6.3 \cdot 10^3$
Total	$2.46 \cdot 10^{-4}$	824.51	0.33	$6.46 \cdot 10^3$

mass that is required to stabilize the spacecraft from disturbances and provide slew control during the complete mission, can be computed using Equation 5.7.

$$m_{prop} = \frac{h}{r_{prop} \cdot I_{sp} \cdot g} \quad (5.7)$$

In this equation, h is the total momentum in Nms, r_{prop} is the propellant arm of 0.33 m, specific impulse I_{sp} equals 230 s, and g is the gravitational constant on Earth. Using this equation, a result 9.79 kg propellant mass for worst case torques and slew on the highest inertia axis.

5.4.2 Penetrator Descent, Control & Stability

As mentioned in Section 5.1, the descent stage of the penetrator will contain the same thrusters and SIRU as found in Table 5.4.

The trajectory of the penetrator and orbiter have been analysed using an iterative software script which uses a backward Euler method to calculate each next position in time. The basic Newton formula's have been used to calculate the forces acting on and motion of the s/c. The code that iteratively calculates the trajectory of the orbit was improved by using the book Moving Stars Around [Hut et al., 2003]. Furthermore, it was taken into account that the thrust was distributed along the path and that the penetrator loses mass as it burns its fuel. To have an optimal trajectory, the penetrator first rotates 180 deg and then burns at maximum throttle in retrograde direction until it has cancelled all its velocity. After that, the penetrator will redirect about 100 deg, so it points at Europa and the descent stage will decouple from the penetrator while letting itself drop from an altitude of about 35 km, reaching the surface with a speed of about 300 m/s. First, it is iteratively determined what thrust is required to cancel the velocity at a height of about 35 km as from this point it will reach the desired speed of lower than or equal to 300 m/s. After that, the accuracy's of the engine thrust, which is ± 1 N, and the thrust pointing, which is 0.25 deg, will be taken into account. This influences, the height from which the penetrator will drop and thus, which speed it impacts the ground and the distance the penetrator will have from the desired impact zone.

To ensure a stable descent during the 35 km free fall when detached from the controlled descent stage. The lander is given a spin which provides gyroscopic stability. Gyroscopic stability can passively provide resistance to external torques. The spin rate depends on the moments of inertia, total torque and maximum allowed precession angle. Equation 5.8 is used to compute the required spin rate.

$$\omega_{spin} = \sqrt{\frac{TI}{(I - I_z)\theta I_z}} \quad (5.8)$$

In this equation, the penetrator is assumed to be axisymmetric about the Z-axis, therefore $I_x = I_y = I = 0.09 \text{ kgm}^2$ and $I_z = 0.027 \text{ kgm}^2$. These values are obtained from CATIA design. A constant torque is assumed as well. T is the total disturbance orbit torque from Table 5.5, and the allowed precession angle θ is 0.35 rad. The minimum spin speed is found to be 0.28 rad/s

Using Equation 5.6, the momentum which the thrusters need to provide is calculated to be 0.43 Nms.

Results

The penetrator will be released during the fourth orbit after circularization exactly half an orbit before the penetrator start burning. Figure 5.3 show the trajectory of the orbiter and penetrator since the start of the fifth orbit. When a half orbit is used for checking the penetrator systems, the penetrator will start

burning in retrograde direction. It will keep doing so until it reaches a height about $32 \text{ km} \pm 0.25 \text{ km}$ where its velocity w.r.t. the ground has been cancelled. From there on it will accelerate until it impacts the ground with 0 horizontal velocity and a vertical velocity of about $285 \text{ m/s} \pm 1 \text{ m/s}$. The details of the descent phase can be found in Figure 5.4. The location of impact is $0 \text{ m} \pm 120 \text{ m}$ from the pole. The distributions from 50 simulations of, the freefall height of the penetrator, the impact speed of the penetrator and the distance of the penetrator from the pole can be found in Figures 5.5, 5.6 and 5.7 respectively.

For the required slew of 180 degrees, a time of 5.5 s is required and for the 100 degree turn 4.1 s is required. This results in a momentum of 1.4 Nms by multiplying the torque by the time. Combining the momentum from the spin and the slew, and inserting this value in Equation 5.7, results in a required propellant of 0.0055 kg for the penetrator.

The angular velocity the penetrator needs to have stability during the 35 km freefall is 0.28 rad/s.

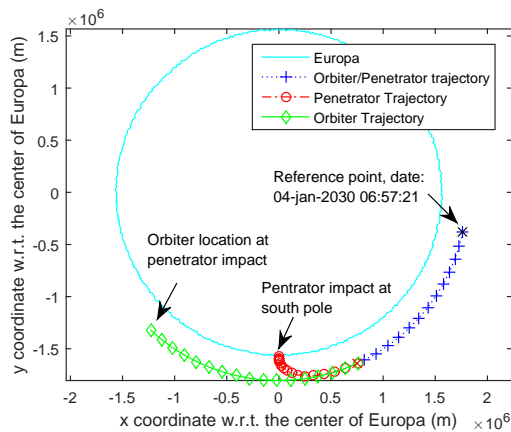


Figure 5.3: Trajectory of the orbiter and penetrator before and during the descent of the penetrator

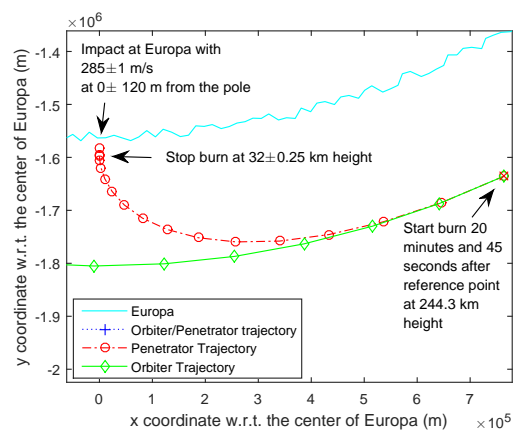


Figure 5.4: Zoomed in trajectory of the orbiter and penetrator during the descent of the penetrator

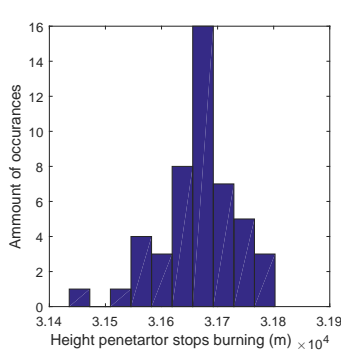


Figure 5.5: Freefall height of the penetrator

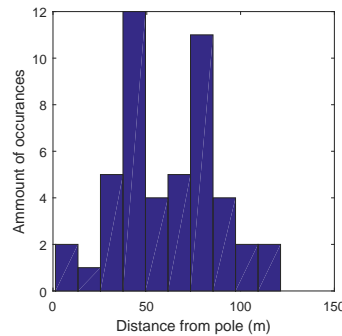


Figure 5.6: Impact distance of penetrator from the pole distribution

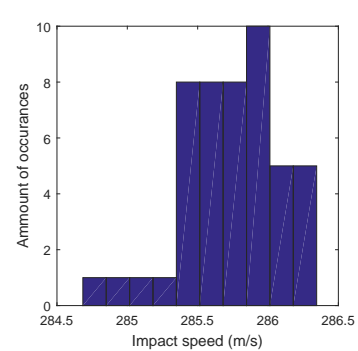


Figure 5.7: Penetrator impact speed distribution

5.4.3 Orbiter End-of-Life

For the end of life solution of the orbiter, two main options exist: escaping Europa or crashing into Europa. Favourably, crashing into Europa is avoided as it increases the risk of contamination and requires additional sterilization procedures to be applied to the spacecraft. Unfortunately, however, escaping Europa was found to cost too much propellant [DSE Group 10 et al., 2015]. A controlled crash is the safest option left.

To ensure that the orbiter will not crash onto a random place on the surface of Europa, a crash site has been selected. The main reason is to avoid damaging possible future research sites. The best location is thought to be the north pole. Figure 5.8 shows the path the orbiter will follow. At the location indicated in the figure the thrusters will burn with a force of 1 N, continuously decreasing the velocity of the spacecraft. After 7 hours, 27 minutes and 52 seconds the orbiter impacts the north pole of Europa at a velocity of 1.4335 km/s. The regulations and requirements to prevent contamination are discussed

in Section 15.3.

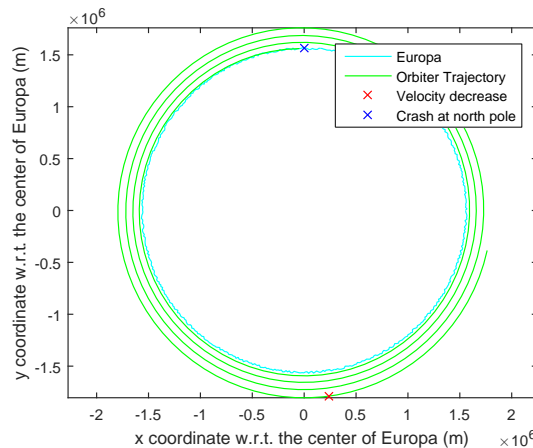


Figure 5.8: Controlled crash of the orbiter as end-of-life solution

5.4.4 Cost

The thrusters are estimated to cost 50000 EUR per thruster². As there are 24 thrusters in total required for the penetrator and orbiter, the total thruster cost is approximately 1.2 M EUR. The sun sensors are estimated to cost 5000 EUR each³. As there are six sun sensors, the total sun sensor cost is only 30000 EUR. The standard star tracker costs are estimated at 400000 EUR each, resulting in a total of 800000 EUR. The estimated SIRU costs 9 M EUR for two, which is exactly the number of units required⁴. Currently the total cost is 11.27 M EUR. The SIRU and star trackers require further development for scaling and radiation hardness. The costs for these developments are currently unknown.

5.5 Code Verification

In this section the verification of the code for the GNC subsystem is explained.

Solar Torque

For the verification of the solar pressure, an example calculation from SMAD [Wertz et al., 2011] has been used. For Equation 5.1, the following input values have been used: $\Phi = 1367 \frac{W}{m^2}$, $c = 299792458.458 \frac{m}{s}$, $A_s = 3 m^2$, $q = 0.6$, $cp_s = 0.3 m$, $cm = 0$ and $\phi = 90$ deg. The expected value from SMAD is $T_s = 6.6 \cdot 10^{-6} N \cdot m$ and is also the outcome of the code, so it is working properly.

Magnetic Field Torque

For the verification of the magnetic field torque, an example calculation from SMAD [Wertz et al., 2011] has been used. For Equation 5.2, the following input values have been used: $D = 0.5 A \cdot m$, $R = 7078000 m$, $M = 7.8 \cdot 10^{15} T \cdot m^3$ and $\gamma = 1.9$. The expected value from SMAD is $T_s = 2.1 \cdot 10^{-5} N \cdot m$ and this is also the output of the code so the code is working properly.

Gravity Gradient Verification

For the verification of the gravity gradient, an example calculation from SMAD [Wertz et al., 2011] has been used. For Equation 5.3, the following input values have been used: $\mu = 3.986 \cdot 10^{14}$, $R = 7078 km$, $I_z = 25 kg \cdot m^2$, $I_y = 50 kg \cdot m^2$, $\theta = 1$ deg. The reference value from SMAD is $T_{gref} = 1.5 \cdot 10^{-6} Nm$, and the obtained value from the code, rounding to the same significant digit, is $T_g = 1.5 \cdot 10^{-6} Nm$. These values match perfectly. This means the code is working as expected.

Slew Torque, Time and Momentum

For the slew torque, Equation 5.4, the following parameters from SMAD have been used: $\theta = 30$ deg, $I = 50 kg \cdot m^2$, $t = 600$ sec. The reference value from SMAD is $T = 2.9 \cdot 10^{-4}$, and the calculated value,

²<http://www.lr.tudelft.nl/nl/organisatie/afdelingen/space-engineering/space-systems-engineering/expertise-areas/space-propulsion/design-of-elements/cost/> [Retrieved June 22, 2015]

³http://www.cubesatshop.com/index.php?page=shop.product_details&flypage=flypage.tpl&product_id=98&category_id=7&option=com_virtuemart&Itemid=69 [Retrieved June 22, 2015]

⁴<http://investor.northropgrumman.com/phoenix.zhtml?c=112386&p=irol-newsArticle&ID=1938605> [Retrieved June 22, 2015]

rounding to the same significant digit, is $2.9 \cdot 10^{-4}$. These values match, and thus this equation is verified.

For the slew time the following values are used: $\theta = 6$ rad, $I = 10$ kg·m² and $T = 0.5$ N. The code results in $t = 21.9$ s. Performing this calculation by hand results in the same result of $t = 21.9$ s.

Using $T = 0.5$ N and $t = 5$ sec, the code computes a momentum of $h = 2.5$ Nms. Filling in the same inputs and calculating it by hand gives 2.5 Nms. The difference between the values is 0%. Therefore this formula is considered to be verified.

Propellant Mass

The propellant mass from Equation 5.7 is verified using the following values: $h = 10$ Nms, $r_{prop} = 2$ m, $I_{isp} = 230$ s, $g = 9.81$ m/s². The code calculates a propellant mass of 0.0022 kg, the hand calculation results in the same value of $m = 0.0022$ kg.

Descent Penetrator

The descent of the penetrator was modelled using the fundamental Newton equations. Output was generated for 4 cases. The first one has exactly the speed for a circular orbit at that height, so it is expected that the result of the circular. The second one has a slightly reduced speed so it should have a lowered perigee close to Europa. The third one has a slightly increased speed so its apogee should have been increased. The last one has no speed so should drop straight to the surface of Europa. Figure 5.9 shows the results 4 different cases. As can be seen the orbits do exactly as one would expect. This means the code is functioning properly.

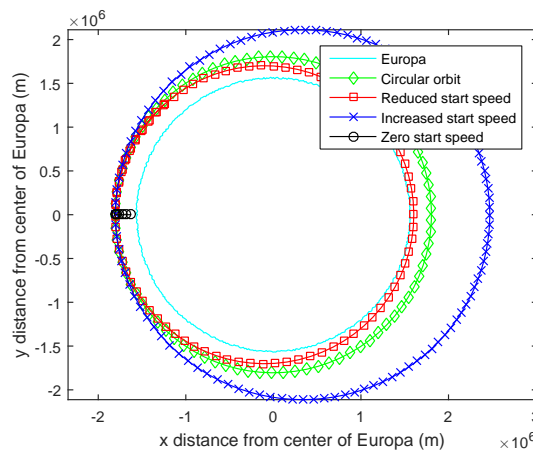


Figure 5.9: Verification of backward Euler orbit calculator

Spin Rate Penetrator

Regarding the spin rate of the penetrator, Equation 5.8, the following inputs have been used for verification: $I = 10$ kg·m², $I_z = 5$ kg·m², $\theta = 0.0175$ rad, and $T = 0.01$. The code results in a spin rate of 0.479 rad/s, and the hand calculation results in 0.478 rad/s. This is a difference of 0.2%, which is acceptable.

5.6 Compliance Matrix

Table 5.6 shows whether each of the requirements in Section 5.1 have been satisfied. It turned out that all of these requirements are met. For the penetrator some of the requirements have an n/a, because the penetrator doesn't have these components.

Number	Requirement	Orbiter	Lander
ACFR-01	The GNC shall be able to determine the distance w.r.t a Europa-centered inertial reference frame with a X [m] accuracy.	✓	n/a
ACFR-02	The GNC shall be able to determine the velocity w.r.t a Europa-centered inertial reference frame with a X [m/s] accuracy.	✓	n/a
ACPR-01	The mass of the GNC shall be no more than X [kg].	✓	✓
ACPR-02	The GNC shall have a maximum power usage of X [W].	✓	✓
ACPR-03	The absolute pointing error of the thrust vector during orbital manoeuvres shall not exceed X deg.	✓	✓
ACPR-04	The GNC components shall stay within its X volume [cm^3].	✓	✓
ACPR-05	The GNC components shall not exceed X cost [EUR].	✓	✓
ACPR-06	The GNC shall withstand accelerations of X g-loads [-].	✓	✓
ACPR-07	The startracker shall withstand radiation levels of X [krad].	✓	n/a
ACPR-08	The IMU shall withstand radiation levels of X [krad].	✓	✓
ACPR-09	The startracker shall be able to operate in temperatures between X [deg. C].	✓	n/a
ACPR-10	The IMU shall be able to operate in temperatures between X [deg. C].	✓	✓
ACPR-11	The GNC shall provide a slew rate of X [deg/s].	✓	✓
ACPR-12	The GNC shall be able to point at a desired position with an accuracy of X deg.	✓	✓
ACVR-01	The GNC shall be tested while taking into account operational safety regulations.	✓	✓
ACVR-02	The GNC shall be designed, built and tested before X [month/year].	✓	✓

6. Propulsion Subsystem

The propulsion system is responsible for getting the spacecraft where it wants to end up at. The propulsion subsystem chapter starts with stating the functions of the system in Section 6.1 and 6.2. The performance of the whole system is analysed in Section 6.3. After this analysis, the used code is verified in Section 6.4. The requirements are checked for compliance in Section 6.5.

6.1 Functional Breakdown Structure

The functions of the propulsion system are found by making a functional breakdown structure. This FBS is shown in Figure 6.1. The propulsion system follows commands from the GNC. Therefore, a standby mode is needed when the system is inactive. The main function of the propulsion system is the performing of all of the ΔV 's. These include orbit insertion, orbit raise and inclination changes and counteracting disturbance torques. The transportation of the fuel to the engines is done by a series of valves, and it is regulated by the pressure transducers which measure the pressure. The lander phase, in specific, is highly depended on the propulsion. The main engine and the reaction control thrusters need to be activated and deactivated to control the descent.

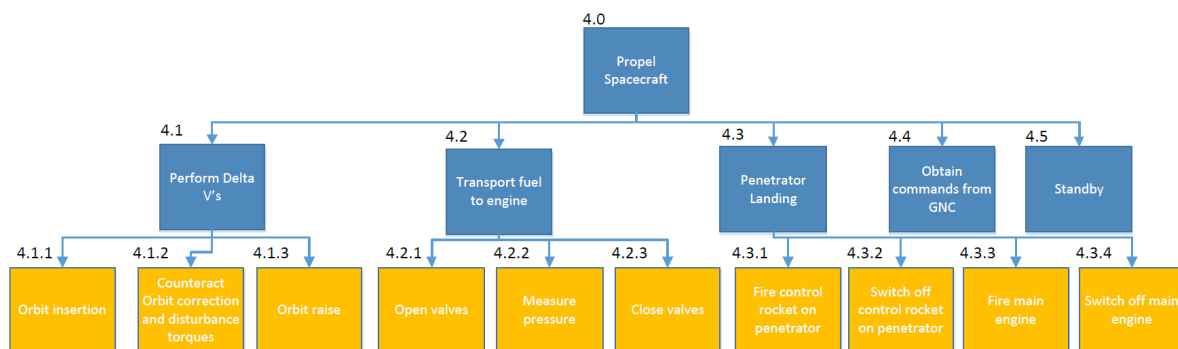


Figure 6.1: Functional Breakdown Structure of the Propulsion System.

6.2 Functional Flow Block Diagram

The functional flow block diagram of the propulsion system is shown Figure 6.2. The numbering of the FBS is continued in the FFBD. The first function that needs to be performed are the manoeuvres. This is an iteration of obtaining commands from GNC to open or close the valves. Pressure measurements are done while burning to monitor the performance. Before the decoupling, the reaction control thrusters are deactivated. After the decoupling of the penetrator, the reaction control thrusters of the orbiter and the penetrator are used. The landing of the penetrator is highly dependant on the propulsion system. This function is therefore highlighted. The propulsion system needs to control thirteen engines simultaneously on command of the GNC subsystem.

6.3 Performance

In this section, all performance characteristics of the propulsion system are shown. The performance analysis will focus on the chosen propellant, engines, regulating system and the fuel tanks.

6.3.1 Propellant

From the midterm report [DSE Group 10 et al., 2015], it was concluded that a bi-propellant liquid propellant will be used. This conclusion is still valid and in this section, the exact propellant type is determined and the regulating system is chosen and sized.



Figure 6.2: Functional Flow Block Diagram of the Propulsion System.

Main Engine

The selection of the propellant is mainly based upon the performance, mixture ratio, operating temperature and the availability of engines with the selected propellant. By looking at the operating temperature, several oxidisers can be omitted from this trade-off. Liquid oxygen and liquid fluorine need to be kept below -183.0 and -188.1 degrees Celsius respectively ¹. It is not feasible to keep the oxidiser at this temperature. As for the remaining oxidisers, NTO (Nitrogen Tetroxide) is the only remaining used oxidiser. The specific impulse and density impulse achieved by this oxidiser is one of the highest, after liquid oxygen and liquid fluorine. Other oxidisers like Nitric acid have been completely replaced by NTO in the late 1950's ². The only variation present in oxidisers is done by adding a percentage of nitric oxide to the NTO, resulting in oxidisers like MON-3 (3% of nitric oxide). This is done to reduce the freezing point and corrosiveness of the liquid, at the cost of decreasing the oxidation potential and increasing the cost. The next step is determining the fuel used. The most commonly used fuels with NTO for spacecraft missions are Hydrazine, MMH (Mono-methyl Hydrazine) and UDMH (Unsymmetrical Di-methyl hydrazine). In Table 6.1, the relevant performance characteristics are shown. These performance characteristics are calculated with a chamber pressure of 68.9 bar and an atmospheric pressure of 1.01 bar.

Table 6.1: Performance characteristics of different fuel types

	Fuel	Mixture ratio	Specific impulse [s]	Density Impulse [kg s/L]	Melting point [Deg Celsius]	Usable as Mono-propellant?
NTO	Hydrazine	1.08	286	342	1.4	Yes
	MMH	1.73	280	325	-52.4	No
	UDMH	2.1	277	316	-58	No

Hydrazine tops out at the specific impulse and the density impulse, which makes it the best option from a performance perspective. The drawback it has, is that it has to be kept at a relatively high temperature to stop it from freezing. But since the freezing temperature of NTO is -9.3 degrees Celsius, the thermal control is already to be maintained at this relatively high temperature. Another big advantage of hydrazine is that it can be used as a mono-propellant. This enables the ability to use a dual-mode system. After this comparison, it was chosen to go for a NTO as an oxidiser together with hydrazine.

¹<http://www.braeunig.us/space/propel.htm>

²<http://www.astronautix.com/props/nitrosene.htm>

Orbit control

The orbital control thrusters used for attitude control use mono-propellant, since this is a relatively simple type of propellant with a good performance. The amount of thrusters needed makes the system too complicated and too heavy to use bi-propellant thrusters. The best mono-propellant is hydrazine with a specific impulse of around 230 seconds in vacuum [Brown, 2002]. Hydrazine is the most used mono-propellant by far since the second best option is hydrogen test peroxide with an specific impulse of 150 seconds [Zandbergen, 2010]. The same hydrazine fuel tanks used for the main stage will also be used for the orbit control thrusters to reduce weight. The combination of these two types of thrusters results in a so-called dual-mode system.

Propellant Mass Budget

The propulsion budget is obtained from the ΔV 's from the astrodynamics section and the propellant masses needed for GNC. The propellant mass is calculated using the Tsiolkovsky rocket equation for the astrodynamics manoeuvres. The propellant mass needed for GNC includes the disturbance torques and the pointing manoeuvres. The calculations for these propellant masses are done in Chapter 5 and summarized in this section. The breakdown of the propulsion mass given in Table 6.2. Three stages are separated, the orbiter + penetrator stage, the orbiter stage and the penetrator stage. A summary of every stage is given in bolt face. A margin of 5% is taken on the ΔV 's. A margin of 2% is taken on the propellant mass and 20% on the dry mass. The table includes the specific impulse for every manoeuvre, in this way, it can be seen which thrusters are used.

Table 6.2: Mass breakdown for all manoeuvres

Manoeuvre	Delta V [m/s]	Propellant mass needed [kg]	Total mass before burn [kg]	Total mass after burn [kg]	I.sp [s]
1. Orbiter + Penetrator stage	1738.3	326.0	753.4	427.4	N/A
1.1 JOI	852.6	181.9	753.4	571.5	320
1.2 Other manoeuvres	291.9	51.7	571.5	519.8	320
1.3 EOI	470.8	73.6	519.8	446.2	320
1.4 Inclination and orbit raise	123.0	17.5	446.2	428.7	320
1.5 Disturbance torques	N/A	1.3	428.7	427.4	227
2. Orbiter stage	390.0	74.0	336.8	262.8	N/A
2.1 Perturbations	390.0	54.9	336.8	281.8	227
2.2 Pointing manoeuvres	N/A	6.1	281.8	275.7	227
2.3 EOL	105	12.9	275.7	262.8	227
Orbiter dry mass	N/A	N/A	N/A	262.8	N/A
3. Lander stage	2264.4	46.6	90.6	44.0	N/A
3.1 Landing	2264.4	46.6	90.6	44.0	320
Lander dry mass	N/A	N/A	N/A	44.0	N/A

The total amount of bi-propellant needed for the orbiter and the penetrator are 303.6 kg and 47.7 kg respectively. The amount of mono-propellant for the orbiter is equal to 42.1 kg. The mono-propellant for the penetrator is neglected since it is insignificant compared to the bi-propellant mass. The mono-propellant mass for the penetrator is in the order of tens of grams.

6.3.2 Engines

Two types of engines are included in this design. One main engine is responsible for all big translational manoeuvres. The orbit control thrusters perform all positioning manoeuvres, momentum corrections and orbit maintenance.

Main Engine

One main engine is used for all big ΔV manoeuvres. The main engine is located on the penetrator and this is secured to the orbiter. Having one engine reduces the mass and volume added to the system. After penetrator detachment, the mono-propellant hydrazine thrusters will do the remaining manoeuvres. The sizing of the main engine is based upon the time needed to perform the ΔV manoeuvres summarized in

Table 6.2. The three big manoeuvres that need to be performed are the JOI, EOI and the descent of the lander. The most critical manoeuvre is the descent of the lander, needing almost 2.3 km/s of ΔV . The thrust needed to null the horizontal velocity of the orbit and impact with a speed of 300 m/s is 96 Newton. The method of this computation is described in Chapter 5. With this thrust, engines are found and scaled to 102 N, with the use of several equations and a software tool called Rocket Propulsion Analysis (RPA) ³.

Inputs

To calculate this thrust, several inputs are needed. The inputs are summarized in Table 6.3.

Table 6.3: Inputs of the performance analysis for the rocket engine

Chamber pressure [bar]	Atmospheric pressure [bar]	Expansion Ratio [-]	Exit Diameter [m]
9.6	0	300	0.144
Chamber Temperature [K]	Specific heat ratio [-]	Molecular Mass [g/mol]	Mixture ratio [-]
3012	1.231	19.56	1.1

The chamber pressure is taken by looking at reference hydrazine/NTO engines. The aerojet HiPAT 445N engine and the R-42DM 890N engine have a chamber pressure of 9.6 bar ⁴. The atmospheric pressure is equal to 0 bar, because vacuum is assumed in all manoeuvres. This results in a higher thrust and specific impulse compared to the atmospheric conditions shown in Table 6.1. The expansion ratio is assumed to be equal to 300 by comparison of the 24 N DST-11H engine from Moog ⁵ and the aerojet HiPAT 445N engine and the R-42DM 890N. The mixture ratio is determined by first looking at the reference engines mentioned above. The mixture ratios of these engines range from 0.85 to 1.1. These mixture ratios are analysed with the Rocket Propulsion Analysis (RPA) tool to obtain the best specific impulse with the given mixture ratio. Results of this analysis are shown in Table 6.4. From this analysis, the mixture ratio is determined to be 1.1, this number is not exceeded because the deviation from reference engines is trying to be minimised which results in sticking between the 0.85 and 1.1 ratios found in reference engines.

Table 6.4: Determination of the mixture ratio

Mixture ratio [-]	0.85	0.9	0.95	1	1.05	1.1
Specific impulse with RPA tool [s]	322.9	325.9	328.5	330.8	332.9	334.8

The specific heat, molecular mass and chamber temperature are found by analysis from the RPA tool. These three numbers are not given in the engine data sheets and calculation by hand requires too many assumptions, which results in inaccurate values. These three parameters depend on the reaction process of Hydrazine and NTO. This reaction results into 4 different exhaust molecules, namely: H₂, H₂O, N₂ and NH₃ with respective mass fractions of 0.0265, 0.362, 0.608 and 0.00255. The reaction process is a combination of several reactions. This combined reaction results in a chamber temperature of 3013 K, a specific heat ratio of 1.231 and an combined molecular mass of 19.56 g/mol. The final input in the calculations is the exit diameter, this diameter is iterated to obtain the required thrust of 96 N. The resulting diameter is equal to 0.144 m.

Performance Calculations

The required outputs of the calculation are the mass flow, specific impulse and thrust of the resized engine. The calculation starts by calculating the Vandekerckhove function shown in Equation 6.1. This function is used in the calculation of the mass flow and the thrust. The throat area is calculated by Equation 6.2.

$$\Gamma = \sqrt{\gamma \left(\frac{1+\gamma}{2} \right)^{\frac{1+\gamma}{1-\gamma}}} = 0.6545 \quad (6.1)$$

$$A_t = \frac{\pi \left(\frac{D_e}{2} \right)^2}{\epsilon} = 5.43 \cdot 10^{-5} m^2 \quad (6.2)$$

The exit pressure is numerically solved from Equation 6.3, resulting in an exit pressure of 135 pascals. The ideal specific impulse is calculated by Equation 6.4. From the RPA tool, two efficiencies are added to this to estimate the delivered performance. A reaction efficiency of 0.9632 and an nozzle efficiency of 0.9779 resulting in a overall efficiency of 0.942. Therefore, the estimated specific impulse equals 319.5

³<http://www.propulsion-analysis.com/>

⁴<https://www.rocket.com/propulsion-systems/bipropellant-rockets>

⁵<http://www.moog.com/products/thrusters/bipropellant-thrusters/>

seconds. The mass flow is calculated by Equation 6.5. The thrust is calculated by Equation 6.6. The universal gas constant is 8314 J/(K kmol).

$$\epsilon = \frac{\Gamma}{\sqrt{\frac{2\gamma}{\gamma-1} \left(\frac{P_e}{P_c}\right)^{0.5\gamma} \left(1 - \left(\frac{P_e}{P_c}\right)^{\frac{\gamma-1}{\gamma}}\right)}} \quad (6.3)$$

$$I_{sp} = \frac{\sqrt{\frac{2\gamma}{\gamma-1} \frac{R_A T_c}{M_W} \left(1 - \left(\frac{P_e}{P_c}\right)^{\frac{\gamma-1}{\gamma}}\right)}}{g} = 339.2s \quad (6.4)$$

$$\dot{m} = \frac{p_c A_t \Gamma}{\sqrt{\frac{R_A}{M_W T_c}}} = 0.0301 \quad (6.5)$$

$$F = \dot{m} I_{sp} + (p_e - p_a) A_e = 96.6N \quad (6.6)$$

Mass and Dimensions

The thruster mass is approximated by a linear regression line found by plotting the seven bi-propellant thrusters shown in Table 6.5. The relation between thrust mass and the thrust is shown in Equation 6.7.

Table 6.5: Mass and dimensions estimation data ⁶

Engine	R-6D	R-1E	R-4D	HiPAT	R-42	R-42DM	AMBR	Design
Thrust [N]	22	111	490	445	890	890	623	75
Mass [kg]	0.454	2	4.31	5.2	4.53	7.3	5.4	1.728
Nozzle diameter/ engine length [-]	0.296	0.357	0.512	0.518	0.495	0.536	0.499	0.46

$$\text{Thruster mass} = (1.293 + 0.0058 \cdot F) = 1.844\text{kg} \quad (6.7)$$

The nozzle diameter is determined to be 0.144 meters from calculations in Section 6.3.2. The length of the engine is approximated by establishing an average relation between nozzle diameter and length of the engine. This ratio is equal to 0.46 and the length of the engine is therefore 0.31 meters.

Reaction Control Thrusters

The reaction control thrusters are sized in Chapter 5. This results in a very low required thrust. Currently the smallest thrusters on the market are 0.5 N. Resizing these to a smaller size will result in a higher cost and risk. Since there is no reference of lower thrusters, it is difficult to estimate the performance characteristics of these engines. Therefore, a set of off-the-shelf thrusters is chosen. The resulting thrusters provide 0.5 N at an specific impulse of 227.3 seconds ⁷. To have 3-axis control, 12 thrusters are needed. 3-Axis control is needed in the orbiter stage and in the penetrator stage. A total of 24 hydrazine thrusters are implemented in the design. Each thruster has a length of 113 mm, a nozzle diameter of 4.8 mm and a mass of 195 g. The mass of this system is included in the GNC mass allocation. These engines can also be used for torque vectoring on the orbiter and penetrator. This is done by the thrusters in z-direction, these are located tangential to the main engine.

6.3.3 Regulating System

The propellant stored inside the tanks needs to be transported to the combustion chamber. This can be done by either a blow-down system or a regulated system. The blow down system includes a pressurant inside the tank. This requires a membrane in-between the pressurant and the propellant. In a regulated system, the pressurant is stored in a separate tank. This tank pressure is usually kept on a constant pressure of about 20-30 bar with the use of a regulator. The advantages and disadvantages are shown in Table 6.6 [Zandbergen, 2010].

From this table, the design choice of a pressurized system is made. It can be seen that a regulated system performs better by having a stable mass flow and mixture ratio. This is important in this mission since the total amount of impulse needed for this mission is very high (800,000 Ns). This due to the high ΔV needed. It will reduce the amount of propellant mass and increase the component mass. Judging

⁵<https://www.rocket.com/propulsion-systems/bipropellant-rockets>

⁶<https://www.rocket.com/propulsion-systems/bipropellant-rockets>

⁷<http://cs.astrium.eads.net/sp/spacecraft-propulsion/hydrazine-thrusters/heritage-thrusters.html>

Table 6.6: Summary overview of the advantages and disadvantages of a blow down and a regulated system [Zandbergen, 2010]

Parameter	Blow down	Regulated
Performance	Mass flow and mixture ratio varies during operation	Stable mass flow and mixture ratio
Mass	High tank mass, limited component mass	Limited tank mass, high component mass
Volume	Large	Limited due to high pressure storage of pressurant
Reliability	High	Low

from the high amount of ΔV , reference missions and expert opinion from B.T.C. Zandbergen, the total mass of a regularised system will be lower. The volume constraint of this mission highlights the design choice of a pressurised system even more. Risk will be negatively affected, but extra redundancy can be implemented in this system when needed by inserting extra cross links in the system. This prevents the whole system from malfunctioning when only one valve is blocked.

6.3.4 Mass Estimation

The weight of the whole system is estimated by an empirical relation from SMAD [Wertz et al., 2011]. The mass is estimated by Equation 6.8, where the volume is in litres. The total volume is 424 L resulting in 30.3 kg. Where 5.7 kg is allocated to the penetrator since it has a volume of 42.8 litres. the remaining 24.6 kg is assigned to the orbiter.

$$m_{components} = 2.36 \cdot 10^{-7} \cdot V_{total}^3 - 2.32 \cdot 10^{-4} \cdot V_{total}^2 + 0.131 \cdot V_{total} + 0.264 \quad (6.8)$$

6.3.5 Fuel Tanks

The loaded fuel tanks are the heaviest parts of the orbiter and the penetrator. It is essential that the centre of mass is located in the centre of the spacecraft, so that the thrust vector intersects the centre of mass. This will then give a pure force and no undesired moment. For this reason, the oxidiser and fuel tank of the penetrator are located in the centre and the oxidiser and fuel tanks of the orbiter are located around the central cylinder. The penetrator has one fuel tank and one oxidiser tank and the orbiter has two of each. With the propellant mass calculated in Section 6.3.1, the tank volumes are determined. The density of hydrazine is equal to 1004 kg/m³ and 1450 kg/m³ for NTO [Zandbergen, 2010]. A 10% margin on the volume is taken. The tanks in the orbiter are made spherical to fit within the volume constraints. The feed pressure of the tanks is specified by the reference engines. The tank pressure is equal to 21.4 bar. The material of all of the tanks is titanium, since this results in the lowest tank mass. A comparison between 7025 aluminium and titanium was made. The density of the titanium is 4428 kg/m³ and the yield stress is equal to 965 Mpa. The thickness of the shell is determined by Equations 6.9 and 6.10.

$$t_{sphere} = \frac{Pr}{(2\sigma)} \quad (6.9) \quad t_{cylinder} = \frac{Pr}{(\sigma)} \quad (6.10)$$

A summary of the fuel tank dimensions and masses is located in Table 6.7.

Table 6.7: Summary of fuel tank mass and dimensions

	Oxidiser Penetrator	Fuel Penetrator	Oxidiser Orbiter	Fuel Orbiter
Number of tanks	1	1	2	2
Spherical or Cylindrical	Spherical	Spherical	Cylindrical	Cylindrical
Wall thickness [mm]	0.184	0.202	0.428	0.428
Length of tank [m]	0.332	0.364	0.644	1
Radius of tank [m]	0.164	0.180	0.217	0.217
Volume per tank [L]	18.5	24.3	64.5	125
Mass of tank shell	0.285	0.375	0.594	1.41
Mass of tank fuel	25.5	23.2	93.0	79.4

The thickness of these calculations are only based on the pressure of the tanks. The resulting thickness's are not able to be manufactured, therefore all the wall thickness's will be 1 mm.

Pressurant

The regulated system needs one pressurant tank for the fuel and one for the oxidiser. The fuel and oxidiser tanks on the orbiter are linked together, so only two pressurant tanks are needed on the orbiter. The mass of the pressurant is calculated by Equation 6.11 [Wertz et al., 2011].

$$M_{pres} = \frac{P_{fuel} * V_t}{R_{pres} * T_{pres} - \frac{P_{end}}{\rho_{pres}}} \quad (6.11)$$

The pressure in the pressurant tanks needs to be twice the pressure in the fuel tanks. The pressure in these tanks is therefore 42.8 bar. The volume of the fuel tanks of the orbiter and penetrator is 252 L and 24.3 L. The temperature of the pressurant is assumed to be 323 Kelvin. The pressurants helium and nitrogen are analysed. The density of helium and nitrogen are 44.79 kg/m³ and 301.4 kg/m³. The specific gas constant of helium and nitrogen are 2077 J/kg.K and 296.8 J/kg.K. The mass of the helium tank is seven times lighter than the nitrogen tank and the volume is slightly smaller for the helium tank. Therefore, helium is chosen as a pressurant. With Equation 6.9, the thickness of the pressurant tanks are calculated. Two equally sized helium tanks are located in the orbiter and two equally sized helium tanks are located in the penetrator. A summary of the mass, volume and thickness of each tanks are located in Table 6.8.

Table 6.8: Summary of results for the helium pressurised tanks

	Orbiter	Penetrator
Nnumber of helium tanks	2	2
Wall thickness [m]	0.000215	0.000107
Radius of pressurant tank [m]	0.0968	0.0484
Volume per pressurant tank [m³]	0.00380	0.000474
Mass of tank [kg]	0.112	0.014
Mass of pressurant [kg]	0.170	0.021
Total mass [kg]	1.129	0.141
Volume Fuel tank [L]	252	24.3

6.4 Verification

The energetic properties of the reaction process were assumed from the RPA model. These were initially compared with hand calculations. When a single reaction is assumed, the reaction will result in the reaction given by Equation 6.12.



The calculated molar mass results in 22.3 g/mol, which is significantly different to the 19.44 g/mol. This shows the inaccuracy of the simple approximation. The values given from the RPA tool are already validated and verified⁸, but they are checked with values found on the TUDelft website⁹. The RPA tool and the TUDelft website are compared with an mixture ratio of 1.15 and an chamber pressure of 10 bar. Results are shown in Table 6.9.

Table 6.9: Verification of energetic properties

	Chamber Temp. [K]	Specific heat ratio [-]	Molecular Mass [g/mol]
RPA	3040	1.235	19.66
TUDelft	3059	1.229	19.7
Relative difference	-0.00621118	0.004882018	-0.002030457

The differences are small and the inaccuracies are mainly due to the more detailed analysis done by the RPA tool. The engine calculations are verified by the AE 2230-II lecture slides [Cervone, 2014]. A summary of the results is shown in Table 6.10.

⁸<http://www.propulsion-analysis.com/verification.htm>

⁹<http://www.lr.tudelft.nl/?id=26264&L=1>

Table 6.10: Verification of engine performance calculations

	Exit pressure	Thrust	Exit Mach number	Exit Temperature	mass flow	Isp
Lecture slides	6021.5	401491	5.06	702	132.9	308
Result	5999.84	414059.25	5.06	701.59	133.05	308.09
Relative difference [-]	0.00361	-0.0304	-0.00073	0.00058	-0.00116	-0.00029

The differences seen in Table 6.10 is mainly due to the more accurate iterations done by the software tool.

6.5 Compliance Matrix

From the functions described in Section 6.1, several subsystem requirements are set up. These have been split up into functional, performance and verification requirements. The subsystem is designed to meet these requirements. The requirements are summarised below.

Number	Requirement orbiter (lander)	Met?	Value orbiter (lander)
PPFR-006	The propulsion system shall be able to exert at least 95 [N] of propulsive force.	✓	95 N (95 N)
PPFR-007	The propulsion system shall perform all manouvres which will require a total of 4200 [m/s].	✓	N/A
PPFR-010	The propulsion system shall provide an maximum acceleration of 4 g.	✓	0.02 g
PPFR-012	The propulsion system shall include 7.4 kg of mono-propellant to perform orbit control.	✓	7.4 kg
PPFR-022	The propulsion system shall have a maximum dry mass of 22 [kg].	✗	24.6 (5.7) kg
PPVR-002	All margins specified by ESA shall be taken into account.	✓	N/A
PPVR-015	The propulsion system shall be designed, built and tested before September 2018.	✓	N/A

7. Scientific Instrumentation

The main mission goal is to serve a scientific purpose, in this case determining whether extraterrestrial life is possible in our solar system. When investigating potentially habitable bodies, three things are searched for, the three "so called" pillars of life: liquid water, organic materials and exchange of chemical energy. The Moonraker mission with penetrator will be able to investigate Europa and determine whether the right conditions are present. The carefully selected science instruments will be able to look for the signs pointing to these conditions.

7.1 Orbiter & Lander Instrumentation Performance

In this section the instrumentation specifics of the orbiter presented in table 7.1 and discussed briefly. The same numbering as given in section 7.1.1 is also used in table 7.1 and 7.2. Furthermore, the accuracy, units and specifics are given. The camera will operate while in the Jovian tour for short periods of time, taking valuable pictures when performing flybys while being fed by the battery. During the Europa orbit phase, the transmission of the penetrator data will have priority over imaging, so that the camera will only be operating when no data from the penetrator is being transmitted.

7.1.1 Orbiter Instrumentation

Achieving the science objectives in the best way possible is the main goal of the mission. Generating high resolution pictures of Europa is a valuable addition to the mission. To this extend the SILAT camera is selected for imaging.

O1. Stereo Imager (SI)

To image at a high resolution a state of the art camera is required. Therefore, the SILAT [Moon et al., 2009] [Kraft,] camera and laser altimeter is selected. The HRC (high resolution camera) contains a 2048x2048 pixel camera, which will be used for high resolution imaging and a 1024x1024 pixel camera oriented at 27deg, which can be used for stereoscopic imaging.

O2. Laser Altimeter (LAT)

The LAT is a state of the art Photon-Counting laser altimeter which can function in both day and night conditions and will be able to determine the altitude with a vertical resolution of 0.15m. In terms of data rate, this altimeter is more than 100 times more efficient compared to conventional altimeters.

Table 7.1: Orbiter Instrumentation Specifics

Instrument Specifics	Accuracy	Unit
O1. Stereo Imager (SI) ¹		
FOV (High resolution)	3.3	deg
Resolution	7	m/pixel
Amount of pictures	N.A.	-
Bits	8	per pixel
Data compression ratio of 1.5		
-	-	-
FOV (Stereo imaging)	2.7	deg
Resolution	7	m/pixel
Bits	8	per pixel
-	-	-
O2. Laser Altimeter (LAT)	-	-
Pulse rep.	10	kHz
-	-	-
SILAT Total		
Average power	12	W
Weigth	5	kg
Dimensions	0.3x0.3x0.3	m

7.2 Penetrator Instruments:

Landing on Europa offers great opportunities in terms of science and therefore, maximum advantage has to be taken. This steers the payload science instrumentation in to a direction of taking and processing samples, but also taking seismic measurements for the duration of the entire mission. A total of 60 samples will be processed over the lifetime of the microbiology part of the penetrator, which will be between 12 and 24 hours. The drill will penetrate about 0.2-1 meter into the ice, depending on the composition. After acquiring the 60 samples, the primary payload bay will be switched off and only the communication part and the seismometer will stay active, until all the data is transmitted and the batteries have run out.

P1. Seismometer

Characterize the subsurface the subsurface ocean, interior body structure and measure and map the seismic activity levels. A single 3-axis seismometer could determine both the upper ice shell thickness and the depth of the subsurface ocean with an accuracy of 1-10 km (in combination with other data).

P2. Descent camera

The micro size camera will take several pictures, starting right after detachment up until impact. As the penetrator nears Europa, the image rate will go up, as will the resolution of the images. The camera will be destroyed upon impact.

P3. Sampling drill

This device uses a combination of heating and drilling to drill its way through the ice, the drill contains heating elements and rotating drill heats which will grind away at the ice. The pieces of ice that have been separated by the drilling bit can be transferred back to the penetrator with the use of a valve in the drill head and a suction system to transfer the samples to the Microbiology camera and the geochemistry package.

P4. Geochemistry package

Including a mass spectrometer and experiments that measure the pH, conductivity, redox and temperature. This package is compiled in such a way that it is able to determine whether the conditions for potential life are present on Europa.

P5 Microbiology camera

This is a strong complement to the geochemistry package and will be able to analyse the samples and also the grain size distribution of the ice and non-ice grains, shape and colour.

P6 Magnetometer

Ocean thickness, bulk salinity and depth of local water layers using multi-frequence electromagnetic sounding.

7.3 Objectives, Requirements and Instruments

This section will make the link between the instrumentation chosen for this mission and the previously defined objectives and requirements clear. First, in Table 7.3 it is illustrated how the instrumentation will fulfil the science requirements. Secondly, which instruments match which objectives is shown in Table 7.4. As can be seen from the tables all objectives and lander science requirements are fulfilled using the instrumentation selected. The orbiter instrument will mainly act as an extra and will not have major contributions to the scientific yield since the transmission rate will be very limiting, especially when the orbiter is sending the penetrator data. Only the laser altimeter will take measurements at set times during the mission lifetime. The camera will, as mentioned before, only be used when the link budget allows for it.

¹ [Moon et al., 2009], [Kraft,]

² [Gowen et al., 2007], [Gowen et al., 2011]

³ [Gao et al., 2008]

⁴ [Weiss et al., 2011]

⁵ [Thomas et al., 2003], [Luthi et al., 2004]

⁶ [Gowen et al., 2007], [Gowen et al., 2011]

⁷ [Gowen et al., 2007], [Gowen et al., 2011]

⁸The dimensions, data rate and power usage of the magnetometer are assumed to be so small that they are neglected in the further calculations

⁹The telecommunication system is able to map the gravity field using doppler measurements & Telecom.

Table 7.2: Instrumentation Specifics Lander

		Unit
P1. Seismometer (3-axis) ²	-	
Mass	0.3	kg
Volume	2.0E-4	m ³
Data aq. Rate	720	bits/s
Related to/taken from	ExoMars	
Power	112	mW
-	-	-
P2. Descent Camera ³		
Mass	0.01	kg
Volume	3.0E-6	m ³
Data aq. Rate	2000000	bit
Related to/taken from	beagle 2, ExoMars	-
Power	160	mW
-	-	-
P3. Sampling drill ⁴		
Mass	0.75	kg
Volume	1.92E-4	m ³
Data aq. Rate	N.A.	
Related to/taken from	Heated sampling drill paper	-
Power	1000	mW
-	-	-
P4. Microbiology/Astrobiology Camera ⁵	six micron resolution	
Mass	0.2	kg
Volume	1.27E-4	m ³
Data aq. Rate	10	bit
Related to/taken from	beagle 2	-
Power	1500	mW
-	-	-
P5. Geochemistry package (incl. Mass spec.) ⁶		
Mass	0.26	kg
Volume	1.6E-4	m ³
Data aq. Rate	50000	bit
Related to/taken from	beagle 2 XRS	-
Power	4000	mW
-	-	-
P6. Magnetometer ^{7 8}		
Mass	0.06	kg
Volume	-	-
Data aq. Rate	500	bits/s
Related to/taken from	various missions	-
Power	150	-

7.4 Choosing a Landing Site

In choosing a landing site, not only the scientific knowledge is taken into account, also the risk of landing at that site and the data that can be transmitted during the mission life are taken into account. After discussion with a Europa specialist, H. M.(Hermes) Jara Orue, different scientifically interesting sites were identified, where the most interesting site for a lander is assumed to be Tera Macula located at 50° Z 180° W. A polar orbit is chosen for global coverage of Europa, landing at one of the poles allows for much more contact time (+/-31 times). Landing at Tera Macula will give a contact time of 36 seconds every 3.5 days while landing at the South Pole will give that same contact time but with a repetition of 2.3 hours. When comparing pro's and con's of the different landing sites with the data found in Table 7.5, it can be seen that although Tera Macula is potentially more interesting for a lander to visit, landing there will allow transmission for only 9% of the gathered data. It was decided that 9 % of the data is unacceptable, therefore, the South Pole is chosen as landing site. Note that the South Pole is potentially even more interesting, since the forces acting on the surface of Europa are largest in the pole regions.

Table 7.3: Science Requirements and Instrumentation Links

Requirements	Description	Instruments
SYS-SCI-01	The ice thickness shall be established with an accuracy of 3-5 km	P1. P6.
SYS-SCI-02	The temperature and the rigidity of the ice shall be investigated	P3. P4. P5.
SYS-SCI-03	The depth of the sub-surface ocean shall be established with an accuracy of 5-10 km	P1. P6.
SYS-SCI-04	It shall be established whether lateral variations in ice dynamics are present with less than 1 meter vertical resolution ⁹	
SYS-SCI-05	The thickness of the (metal) moon core shall be established	P1. P6.
SYS-SCI-06	The state of the (metal) core shall be established	P1. P6.
SYS-SCI-07	The composition and chemistry of the subsurface ocean as expressed on the surface shall be analysed	P2. P3. P4. P5.
SYS-SCI-08	The system shall determine the salinity of the sub-surface ocean	P6.

Table 7.4: Lander Objectives and Instruments

Category	Objectives	Instrument(s)
Composition	Characterize surface and subsurface chemistry, analysing both endogenic, and exogenic processes that affect the composition.	P2. P3. P4. P5.
Ocean and Ice shell	Determine the thickness and salinity of Europa's ocean.	P6.
	Determine the thickness of Europa's ice layer and any water within it.	P1.
	Locate the regions of heterogeneity.	P3. P4. P5. P6.
	Establish seismic activity and its variation over the tidal cycle.	P1. P6.
Geology	Identify processes that exchange material between the surface and sub-surface.	P1. P3. P4. P5. P6.
	Identify the processes and rates by which the surface forms and evolves.	P1. P6.
	Characterize the physical environment of the near-surface and sub-surface regions.	P1.
Geophysics	Determine the internal structure of Europa and its dynamics.	P1. P6.

The current state of imaging is of such poor quality, therefore it is unknown what will be found. As can be seen in Table 7.5 landing at the poles will give three times more contact time than strictly needed, so more science can be done, yielding a larger scientific return.

7.5 Payload Bay Layout

In Figure 7.1 the payload bay of the penetrator is shown. The penetrator has 2 payload bays, a short life and a long life bay. The first will contain the most instruments, namely: the drill, the micro imager and the geology package. The drill is in a separate compartment so that when the drilling starts the rest of the instruments will not suffer from the cold. The drill tip is hollow and connected to a tube that feeds back the samples to the microbiology package and the micro imager then after 60 samples the first bay is shut down completely. The second bay will contain the power supply, data handling and storage and but also the seismometer and the magnetometer. The instruments have to be fitted and secured in such a way that the high impact loads will not cause system failure.

Table 7.5: Landing Site Comparison

Landing site	Science potential	Data over lifetime (bits)	DATA (as % of total data gathered)
Tera macula	high	1171200	9
Polar	unknown (potentially high)	41686780	320

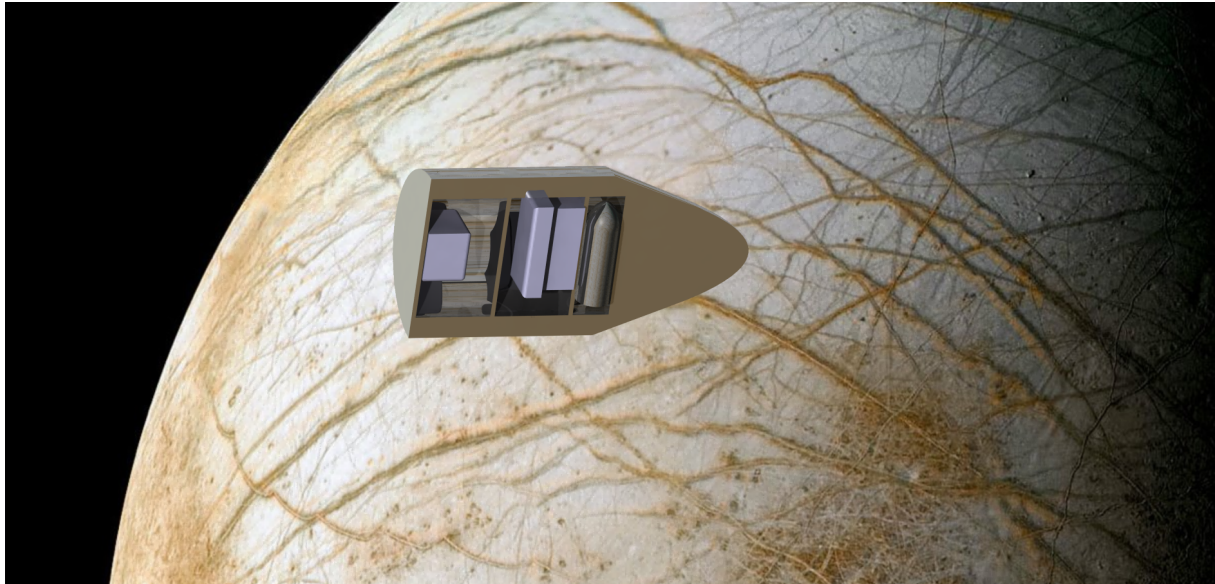


Figure 7.1: Penetrator payload bays

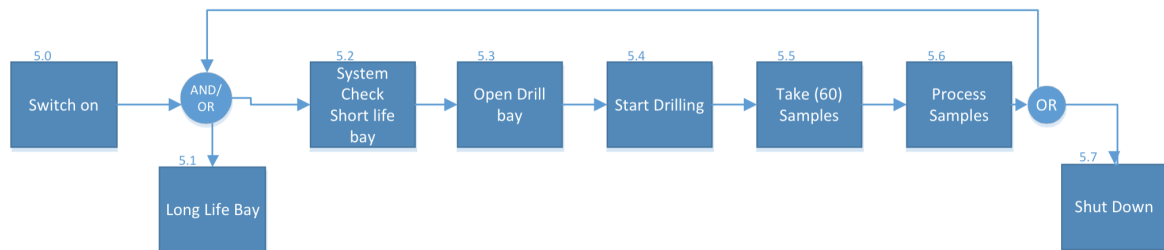


Figure 7.2: First bay function flow

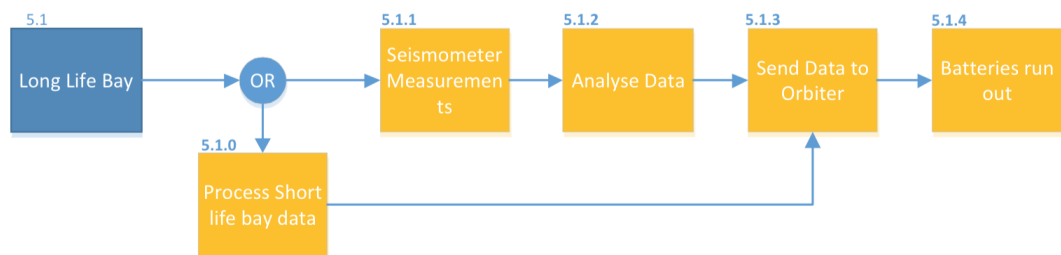


Figure 7.3: Second bay function flow

8. Power Subsystem

In this chapter the power system design will be described in detail. This chapter starts with a brief function description of the power system in Section 8.1. The functional flow and breakdown structures are discussed in Section 8.2 and 8.3 respectively. The actual design is discussed in Section 8.4. A summarizing electrical block diagram is presented in Section 8.3. A sanity check is performed in Section 8.5. This chapter is concluded with a compliance matrix in Section 8.6 to check whether the power system is designed in the right manner.

8.1 Subsystem Description

The main function of the power system is to generate, store and distribute power to the other spacecraft systems. The generation and storage of power can be done in multiple ways. The power normally goes from the source to a power conditioning unit (PCU) after which it is distributed to the other systems by a power distribution unit (PDU). For solar panels, during eclipse, power is provided by the batteries, which have been charged during daylight time. The charge and discharge of the batteries is controlled by a battery charge/discharge regulator (BCDR). The requirements used during the design can be found in Section 8.6.

8.2 Functional Flow Diagram

In this section the functional flow of the power subsystem is presented. The functional flow block diagram for the power subsystem can be found in Figure 8.1. As can be seen the power subsystem consists of eight main functions, of which five of them consist of several sub functions. The or-block in the main tree makes a division between eclipse time (where the orbiter runs on battery power) and daylight time (where the orbiter runs on solar power and charges the batteries). As can be seen from the power generation branch (6.2) the solar panels are actively pointed towards the sun to improve the overall efficiency. A maximum power point tracker (MPPT) is used to determine the maximum power point of the solar cells, providing the array power regulator (APR) with a certain impedance. This results in maximum power available for the spacecraft. The battery charge and discharge regulator (BCDR) ensures the battery is charged and discharged in the right manner (functions 6.3.2 and 6.4.1). The bus voltage is regulated by a mean error amplifier (MEA) in function 6.4.3. The power system is then monitored by the command and monitoring module (CM), which monitors the solar cell performance as well as the battery charge and discharge cycles. It also acquires telemetry regarding the power subsystem and sends this to the on board data handling system. Finally the power is transported to the different loads by the power distribution unit (function 6.4.4). The spacecraft has to shut down at the end of the mission which is represented by function 6.7.

8.3 Functional Breakdown

In this section the functional breakdown structure is described. The functional breakdown structure is presented in Figure 8.2. As can be seen in the diagram the power subsystem consists of six main components which each consist of one or more sub-functions. Comparing the functional breakdown to the functional flow, all the functions present in the breakdown are present in the flow as well. However, the functions are arranged in a different manner to clarify the functions of the different components of the power subsystem. The solar array deployments and drive mechanism (6.1) consists of the functions solar array deployment (6.1.1), checking of deployment (6.1.2), solar array pointing (6.1.3) and checking of the right pointing (6.1.4). The array power regulator (6.2) consists of the functions tracking of maximum power (6.2.1) and checking of the output power (6.2.2). Next, the battery charge/discharge regulator (6.3) performs the functions regulation of charging (6.3.1) and discharging (6.3.2). The power system amplifier (6.4) only performs the function regulation of bus voltage (6.4.1). The power command and monitoring unit (6.5) performs the the monitoring of the solar array (6.5.1) and the battery (6.5.2) and acquires and transmits power telemetry (6.5.3). Finally the power distribution unit (6.6) distributes the power among the different spacecraft loads (6.6.1).

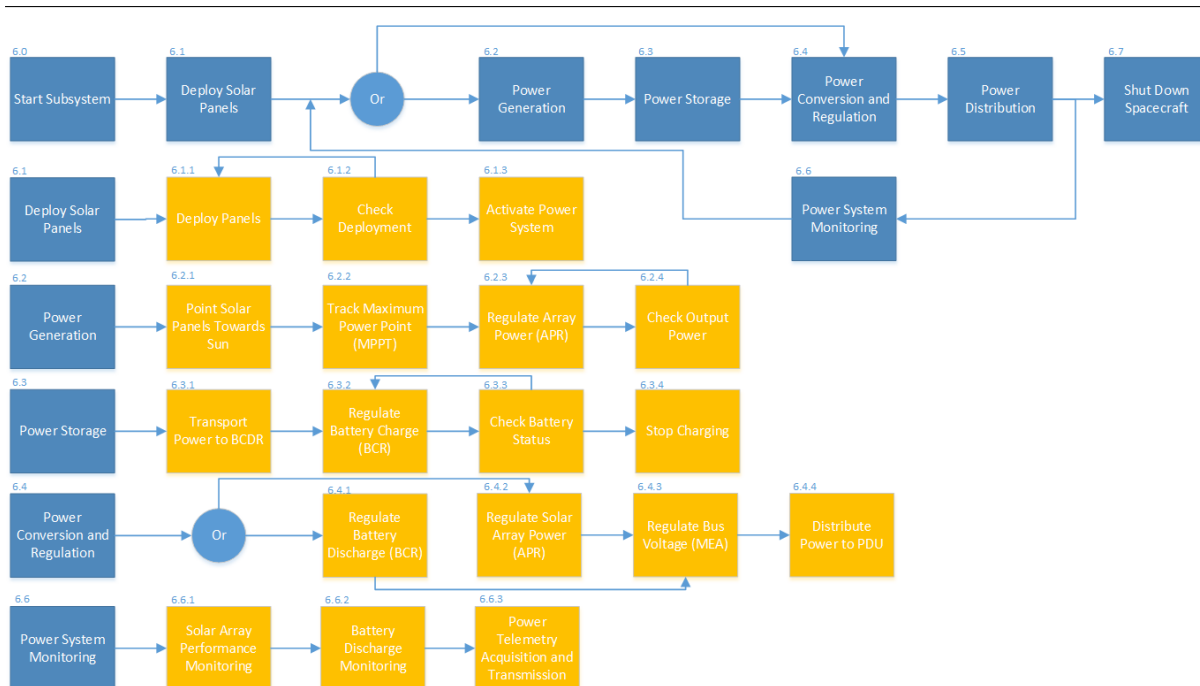


Figure 8.1: Functional flow block diagram for the power subsystem

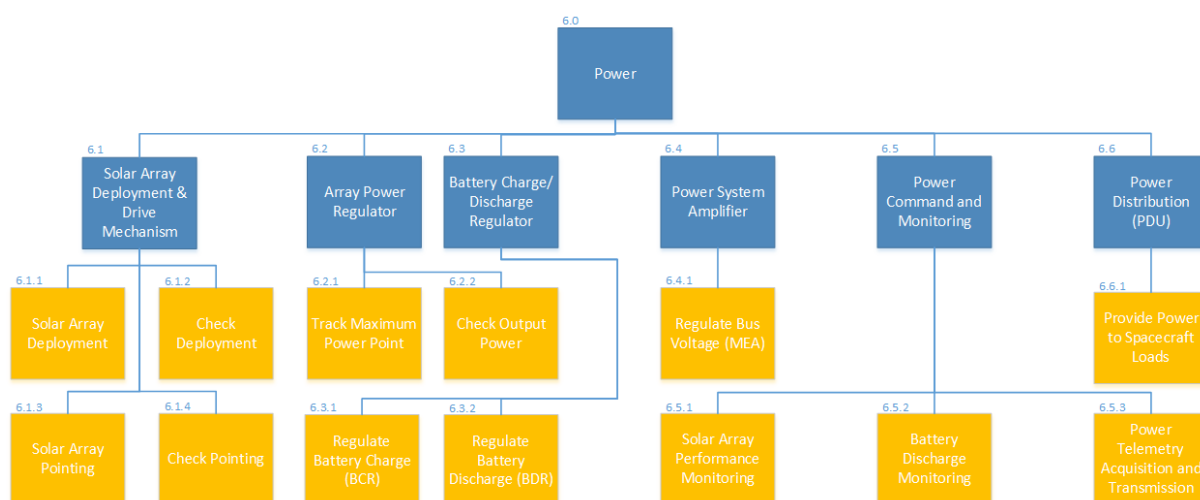


Figure 8.2: Functional breakdown block diagram for the power subsystem

8.4 Performance Analysis

The generation of power can be done in multiple ways, the best method is chosen after a trade-off which is discussed first. The design of the photovoltaic-battery system starts with the sizing of the solar arrays, then, the batteries are designed, and finally, the power conditioning and distribution system is designed.

8.4.1 Design Concept

For the power system four different technologies were investigated. These include the photovoltaic-battery system, a primary battery, a fuel cell and a radioisotope thermal generator (RTG). The main characteristics of these systems are summarized in Table 8.1.

Table 8.1: Trade-off for different power concepts

Concept	Mass	Estimated [kg]	Feasibility	Remarks
Photovoltaic-battery	-	90	+	Heavy/large due to low solar constant, proven flight ready (Juno, Rosetta 6.5 W/m^2 ¹)
Primary battery	-	140	-	Already 140 kg for very high energy density Lithium-air battery ²
Fuel cell	+	65	-	Not feasible, storage of cryogenic reactant impossible ³
RTG	++	20	-	Only 20 kg for 140 W ASRG, not feasible since run-out of Pu-238 ⁴

It can be seen that in terms of mass, the RTG would be the favourable option. However this option is infeasible since no Pu-238 will be available for an ESA mission. The only feasible option remaining is the photovoltaic-battery system with a relatively high mass.

8.4.2 Solar Array Design

The IMM4J CIC solar cells from SolaAero Technologies were chosen for the solar array. These cells are quadruple-junction Gallium Arsenide (GaAs), with a minimum average efficiency of 33 %. The cells are also 42 % less heavy than traditional multi-junction solar cells⁵. The solar intensity at Jupiter as a function of the solar intensity on Earth can be calculated with Equation 8.1 [Brown, 2002]. In this equation R is the distance between the Sun and Jupiter which is equal to 778 million km. I_{sc} is the solar constant at Earth and is equal to 1367 W/m^2 . This equation gives a solar constant of 50.6 W/m^2 at Jupiter. Multiplying this value with a number of loss factors which are summarized in Table 8.2 gives the amount of power which can be actually generated by the solar cells at end-of-life.

$$I_{planet} = \left(\frac{149.6}{R_{planet}} \right)^2 I_{sc} \quad (8.1)$$

Table 8.2: Solar array loss factors

	η_{UV}	η_{cy}	η_m	η_l	η_{con}	η_{PCU}	η_{rad}	\bar{L}_p
Efficiency [-]	0.98	0.99	0.975	0.98	0.99	0.95	0.71	0.996

The value for the radiation performance will be discussed later in this section. After multiplication of the solar constant with the loss factors a power of 10.3 W/m^2 remains which is actually generated by the solar cells. From Section 3.2 the required power equals 71.9 W for daylight time and 51.2 W for eclipse time. Applying the ESA power margin of 30 % [ESA, 2014] the design power becomes 93.4 W for daylight time and 66.5 W for eclipse time. Taking into account the losses during charging and discharging which are $X_d = 0.96$ and $X_e = 0.94$ respectively for the used power conditioning unit (PCU). Taking into account the worst case in orbit around Europa (very short cycles), the power which has to be generated by the solar array can be calculated using Equation 8.2. In this equation P_e and P_d are the power required during eclipse and daylight respectively. T_d and T_e are the length of the daylight and eclipse phase of the orbit respectively and are 5680 s and 1985 s respectively for a Europa orbit. X_d and X_e are the losses occurring in the system during daylight and eclipse respectively. Their values can be found above.

$$P_d = \frac{\frac{P_e T_e}{X_e} \frac{P_d T_d}{X_d}}{T_d} \quad (8.2)$$

This gives a design power of 122 W, which gives a solar array size of 13.5 m^2 , using a packing factor of 0.88 [Brown, 2002]. The structure of the array is based on a aluminium honeycomb structure. The

¹ [Fiebrich et al., 2004]

² [Girishkumar et al., 2010]

³ [Patel, 2004]

⁴ [Richardson and Chan, 2007]

⁵ <http://solaerotech.com/wp-content/uploads/2015/04/IMM4J-CIC-Datasheet.pdf> [Retrieved: June 17, 2015]

materials used and their respective thickness for the array structure can be found in Table 8.3. The total thickness equals 13.36 mm at a mass of 2.56 kg/m².

Table 8.3: Panel cross section with honeycomb substrate [Patel, 2004]

Components from top to bottom	Typical thickness [mm]	Density [g/cm ³]	Mass [kg/m ²]
Fused silica coverglass	0.15	2.32	0.35
Coverglass adhesive (DC93-500)	0.1	1.08	0.11
GaAs IMM4J CIC cell	–	–	0.49
Cell adhesive (RTV-566)	0.1	1.15	0.12
Kapton insulation	0.05	1.42	0.07
Adhesive (GRP-33A)	0.005	1.15	0.01
Face skin (aluminium)	0.1	2.70	0.27
Adhesive (FM-300)	0.1	0.88	0.09
Honeycomb (aluminium)	12.5	0.05	0.66
Adhesive (FM-300)	0.1	0.88	0.09
Face skin (aluminium)	0.1	2.70	0.27
Back paint (Z-305)	0.05	0.95	0.05
Total	13.36		2.56

The mass of the solar array can now be found equal 34.5 kg. During launch and the VEEGA tour, when the orbiter is attached to Clipper, the solar arrays need to be stowed, and these need to be unfolded after detachment. The deployment mechanism has a mass of 15 kg per array [Brown, 2002], and uses springs and thermal knives for deployment. This mechanism is also capable of pointing the solar arrays to the Sun within an angle of 5 ° referring to L_p in Table 8.2. Furthermore, the attachment of the array to the bus has a mass of 15 % of the total array mass [Brown, 2002] and equals 10 kg for both panels. This gives a total solar array mass of 74.2 kg.

The thickness of the fused silica cover glass was established at 150 μm. This was the optimal thickness in terms of cover glass thickness and solar array degradation as can be seen in Table 8.4. This computation is based on the different EOL/BOL efficiencies as a function of different 1 MeV equivalent electron fluences. The solar cell degradation was modelled by an ESA tool (SPENVIS) for a Europa orbit around Jupiter.

Table 8.4: Coverglass thickness versus array mass

Thickness [μm]	Eq Fluence [cm ⁻²]	η_{rad} [%]	Mass Coverglass [kg]	Mass Cell [kg]	Mass Array [kg]
100	1.00 E+16	56	4.0	8.4	41.8
150	3.00 E+15	71	2.3	6.6	34.5
500	1.00 E+15	81	13.7	5.8	39.8

The size of one array is 6.7 m², however, the actual dimensions are determined by the deployment mechanism. The bus allows for a panel width of 0.9 m, which makes the height of each array 1.87 m, when a four times folded array is used. Therefore the array dimensions are 1.87 x 3.6 m when deployed. A strut of 0.45 m is used to attach the array to the bus, which can be deployed as well and prevents the array from bus shadow.

8.4.3 Battery Design

Orbiter

To provide the orbiter with power during eclipse, batteries are required. The size of the battery is determined by the required voltage and capacity. The required power during eclipse is 66.5 W including a 30 % ESA margin [ESA, 2014]. The longest eclipse time the orbiter will encounter is the Jovian eclipse, which will have a duration of 2.83 hr, based on simple Kepler equations. The required energy storage for the battery is then 188 Wh. Since the number of charge and discharge cycles is limited to around 500 cycles due to limited eclipse encounters, a depth of discharge (DOD) of 0.6 is assumed [Peterson et al., 2010]. Given the standard spacecraft bus voltage of 28 V [Patel, 2004] the required capacity is 6.7

Ah. Given the battery efficiency of 80 %, the design capacity is 392 Ah. The Sony 18650 HC cell has a capacity of 1.5 Ah at a voltage of 3.7 V and has a mass of 42 g ⁶. 8 Cells in series are required to get to the bus voltage of 28 V. This means a total of 10 cells parallel and 8 cells in series are required to obtain the battery requirements. However, if two batteries of 7 cells in parallel and 8 in series are used, the spacecraft is still able to survive full eclipse on one battery which is then used at a higher DOD of 0.9. This influences the battery life, but as the spacecraft does not encounter that many cycles. this would not pose a problem. This implies a total battery mass of 4.70 kg. The size of one cell is 18 mm in diameter by 65 mm in length. This gives a battery size of 126 x 144 x 65 mm. and a mass of 2.35 kg per battery. One battery can provide 188.3 Wh at 80 % efficiency and 0.9 DOD which is exactly the required storage as can be seen above.

Penetrator

The penetrator will have a relatively short lifetime and can therefore run on primary batteries. The penetrator is divided into two sections. The penetrator itself and the penetrator descent stage. The penetrator itself requires a total energy of 370 Wh. The penetrator uses state-of-the-art Lithium/Carbon Monofluoride cells with a specific power of 514 Wh/kg ⁷. These batteries have a self discharge rate of 0.5 % per year and provide 16 Ah at a voltage of 2.6 V at a mass of 81 g. Using a power margin of 30 % and the self discharge rate for 10 years the battery mass is estimated at 810 g. The battery providing a voltage of 12.5 V consists of 2 cells in parallel and 5 in series, so in total 10 cells, resulting in a total energy of 400 Wh. The mass of the power regulation unit will be approximately 83 g ⁸. Which will give a total mass of 0.9 kg for the actual penetrator. The delivery system only requires 23 Wh caused by the its very short life time, thereby only requiring two cells in series at a voltage of 5.2 V and a mass of 162 g. Using the same power conditioning unit the total mass for the descent equals 0.25 kg.

8.4.4 Power Conditioning and Distribution Design

Electrical Block Diagram

The power conditioning and distribution unit controls the power system. The system is summarized in the electrical block diagram to clarify the design. The diagram can be found in Figure 8.3. The diagram actually represents both the power conditioning unit (PCU) and the power distribution unit (PDU). The equipment, heater and thermal distributors/actuators belong to the PDU where the other units belong to the PCU. When read in colour the orange lines and blocks represent command and control data flow, the blue lines represent power lines and the yellow lines represent the output from the mean error amplifier (MEA).

Power Conditioning and Distribution Design

For the current design, mainly of-the-self components have been used. These components are also used for the Rosetta, Mars Express and Venus Express missions. Each of the solar panels is controlled by two array power regulators (APR), which makes this function dual hot redundant. The APR consists of a maximum power point tracker (MPPT). The MPPT finds the maximum power point by oscillating the APR input impedance around the load point, thereby providing maximum power [Jensen and Laursen, 2002]. This is necessary since in the large operating temperature of the solar arrays the maximum power point changes drastically. The MPPT then controls then the APR, which then determines the load impedance to provide maximum power at a voltage of 28 V. The battery charge and discharge control is regulated by the battery charge/discharge regulator (BCDR). The APR and BCDR functions are all regulated by a main error amplifier (MEA). Furthermore, the command and monitoring (CM) module executes the commands send to the power control system and acquires and transmit unit telemetry [Jensen and Laursen, 2002].

The distribution of the power is regulated by six different distribution units. Two units distribute the equipment power to all the instruments. The heater distribution unit distributes the power to the spacecraft heater system and finally the thermal knife actuator regulates the thermal knives required for solar array deployment. The total mass of the power conditioning and distribution unit is 10.6 kg including the backplane. The dimensions of the PCU are 235 x 156 x 354 mm. The power conditioning system will dissipate a total of 20 W which has been taken into account for the power subsystem design.

⁶<http://sci.esa.int/science-e/www/object/doc.cfm?fobjectid=36580>[Retrieved: June 20, 2015]

⁷<http://www.eaglepicher.com/technologies/battery-power/lithium-carbon-monofluoride>[Retrieved: June 21, 2015]

⁸<http://www.clyde-space.com/documents/1819>[Retrieved: June 21, 2015]

8.4.5 Cost Estimation

At this phase of the design, a cost estimation is very difficult since the unit price for the components is not publicly made available. When the design is actually proposed offers can be made to different companies, after which a first real cost estimation can be performed. The estimated solar array price will be 617 \$/W for GEO orbit [Wertz et al., 2011]. However this price tag is based on the solar constant at 1 AU, therefore this value has to be scaled to the solar constant at 5.2 AU. Then this value increases to 16700 \$/W. Since power generated by the solar array is 122 W, the total cost for the solar arrays can be estimated at 1.9 million EUR for the solar arrays only. The power of the rest of the system cannot be estimated at this point, so the cost analysis as presented in Section 16.2, which estimates the total power system cost at 18.3 million EUR, will be used for the cost budget at this point.

8.5 Sanity Check

For the power system no complex code which has to be verified has been used. However, to check if the design is feasible and realistic, a sanity check is performed. This can be done by comparing the power system to the power systems of other existing, orbiters operating in similar solar conditions such as Rosetta and Juno (both at 5.2 AU), the result of this sanity check can be found in Table 8.5.

Table 8.5: Sanity check with other orbiters operating at 5.2 AU

Mission	Power [W]	Cells used	Mass [kg]	Density [W/kg]	Size [m^2]	Density [W/m^2]
Rosetta ⁹	400	Silicon Hi-ETA (17.3 % ¹⁰)	260	1.54	61.5	6.50
Juno ¹¹	486	GaAs	340	1.43	60.4	8.05
Proposed mission	122	MJ GaAs (33 %)	88	1.38	13.5	9.04
Error				6.8		24.2

The error for the density is relatively low, however the error for the density per square meter the error is relatively high (24.2 %). This can be explained by the fact that Rosetta used Silicon cells with a lower efficiency than the efficiency of the GaAs cells used for the proposed mission. The density per square meter is highest for the proposed orbiter as expected since state-of-the-art solar cells with a very high efficiency and low mass are used. That the mass density is relatively low for the proposed mission is due to the heavy deployment mechanism and the relatively high mass for the power conditioning unit which does not scale down accordingly with the size of the solar arrays.

8.6 Compliance Matrix

To check whether the power system is designed within the right constraints, a compliance matrix is formulated. PRPT requirements refer to the penetrator, however the other requirements with a ✓ in the last column are also applicable to the penetrator.

⁹ [Fiebrich et al., 2004]

¹⁰ [Strobl et al., 2000]

¹¹ http://www.nasa-usa.de/mission_pages/juno/launch/Juno_solarpower.html [Retrieved: June 21, 2015]

Number	Requirement	Compliant	Value	Lander?
PRFR-001	The power system shall be able to regulate voltage and current on the spacecraft.	✓		✓
PRFR-002	The power system shall be able to distribute the generated power to the relevant components.	✓		✓
PRFR-003	The power system shall be able to store 392 [Wh].	✓	392 [Wh]	✗
PRFR-004	The power system shall have the capability of restarting automatically after power loss.	✓		✓
PRFR-005	The solar cell array shall be sized with 30 % margin for the worst case power situation and provide power up to the end of mission.	✓	30 [%]	✓
PRPR-001	The system shall generate a minimum of 120 [W] at end-of-life.	✓	122 [W]	✗
PRPR-002	The system shall generate a minimum of 170 [W] at begin-of-life.	✓	172 [W]	✗
PRPR-003	The system shall be provided with power by Clipper during the VEEGA transfer.	✓		✓
PRPR-004	The amount of power generated may not degrade more than 30 [%] due to radiation.	✓	29 [%]	✗
PRPR-005	Solar array temperature must stay between -175 and 120 [° C].	✓		✗
PRPR-006	Power control temperature must stay between -25 and 60 [° C].	✓		✓
PRPR-007	Battery temperature must stay between 0 and 25 [° C].	✓		✓
PRPR-008	The power system shall have a maximum mass of 36 [kg].	✗	89.5 [kg]	✗
PRPR-009	The system shall generate a peak power of 72 [W].	✓	72 [W]	✗
PRPR-010	The system shall generate power for at least 700 [Days].	✓	703 [Days]	✗
PRVR-001	Testing of the power system may not conflict with power generation safety regulations.	✓		✓
PRPT-001	The penetrator shall be able to store 370 [Wh].	✓	400 [Wh]	
PRPT-002	The penetrator delivery system shall be able to store a minimum of 23 [Wh].	✓	83 [Wh]	
PRPT-003	The penetrator power system shall have a maximum mass of 1.7 [kg].	✓	1.15 [kg]	
PRPT-004	The penetrator power system shall generate power for 26 [days].	✓	26 [days]	

As can be seen, only **PRPR-008** has been violated. This is mainly because the mass of very low solar intensity at Jupiter which makes the power subsystem quite heavy. The mass of the power system can be reduced significantly when using an advanced Stirling radioisotope generator (ASRG) which generates 140 W at 20 kg [Richardson and Chan, 2007]. The development of the ASRT has been cancelled, however, if NASA decides to continue on the development of the ASRT, the mass of the orbiter could be reduced significantly and the requirement can be met. Furthermore the mass of the radiation system is also quite heavy because of the harsh radiation environment around Europa.

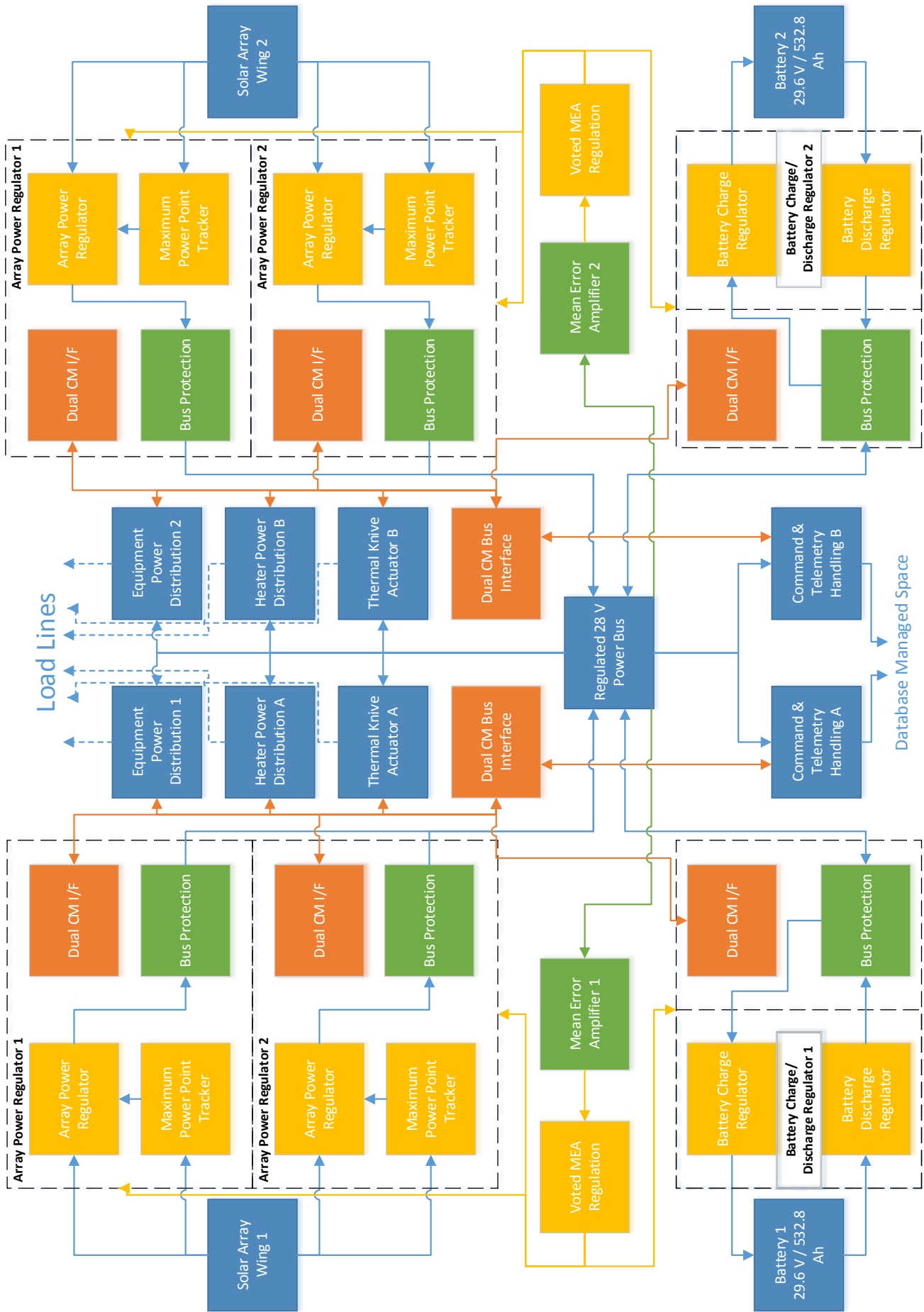


Figure 8-3: Electrical block diagram for the power subsystem

9. Telecommunication, Command & Data Handling Subsystem

The Telecommunication, Command & Data Handling subsystem (TC&DH) on the spacecraft is responsible for establishing communication links between Earth and other spacecraft, as well as handling all the on-board data processing and flow. This chapter describes how the TC&DH was designed. In Section 9.1, a description of the subsystem is given. Section 9.2 and 9.3 give an overview of the functions of the system shown in respectively a functional flow block diagram and a functional breakdown structure. Section 9.4 describes the performance of the subsystem. A hardware block diagram of the whole system is shown in Section 9.5. Code verification and the compliance of the subsystem are shown in Sections 9.6 and 9.7.

9.1 Subsystem Description

The TC&DH subsystem provides a spacecraft with an uplink (or forward link) for commands, and a downlink (or return link) for mission data. It also provides radiometric links for Doppler shift measurements and ranging signals which allow for tracking its velocity and distance relative to the ground station. The set-up of this mission is such that the orbiter will serve as a communication relay for the penetrator. To accomplish a reliable data relay that also works together with all other subsystems, the TC&DH has to comply to various requirements. With the requirements in mind, Section 9.7, the telecommunications system is designed.

9.2 Functional Flow Block Diagram

The functional flow block diagram, Figure 9.1, displays the flow of steps that the TC&DH system goes through during the mission. This flow of system functionalities is important in understanding the inner workings of the system, and in which order they follow each other up. On the top level, blocks 7.0 through 7.7, the main functions that the system handles are stated. It mainly consists out of receiving commands, and transmitting engineering and science data. Also all of this information has to be processed, and that happens in between. Next to that, the system is also responsible for providing the ground station with ranging and Doppler measurements. Because this measurement is not always combined with downlinking science/engineering data, this is behind an AND/OR block.

Returning Doppler and ranging signals normally happens by using the uplink signal as a reference signal, and then multiplying the frequency of that signal with a predetermined turn-around ratio. When an uplink reference signal is not provided, the Ultra Stable Oscillator (USO) provides the reference downlink frequency.

Receiving a signal from the ground station (7.2) happens by first locking on to the phase of the signal by using a phase lock loop (PLL). The signal is then filtered to eliminate frequencies the system does not have to listen to. Low noise amplification (LNA) is done to make sure the received signal does not decrease too much during processing. The signal is then down-converted from the receiving band to the band the system works with, after which it is demodulated and demultiplexed. In other words, it is separated from its carrier wave and then cut into pieces of useful information. The data is then handed over to the data handling via the data interface (Data I/F).

Processing, and distribution, of commands (7.3/7.4) is done by decoding and decrypting the information. An important step is to authenticate the commands that enter the system. A check is performed to see if a command actually is a command. This is important to eliminate random word combinations to trigger events. The commands are then queued and stored for distribution. Usually, this is a time activated sequence of the commands. The commands are then identified per subsystem and executed when their time triggers. The response of the given command is logged for feedback.

A different function of the TC&DH is data handling. All science that is gathered should be saved in a certain format, digitally. Also, the data handling unit is responsible for distributing time and gathering the systems' overall status, health and performance. In sub-flow 7.5, therefore, the data is converted to

the digital format, compressed, encoded, and stored. This adds redundancy on the data and produces smaller files for storage and transmission.

Transmission of data to Earth is done by pulling the data from the storage via the data interface, and multiplexing the data. A signal is created by modulating it onto a carrier wave. Thereafter the signal is converted to the transmitting frequency, and amplified by the solid state power amplifier. A last filter is applied to filter any noise outside of the wanted bandwidth for transmission.

9.3 Functional Breakdown Structure

Another way of representing the functions of a system, is by representing them in a functional breakdown structure, Figure 9.2. Rather than displaying the blocks as a function of time, they are grouped according to their shared purpose in the system. For the TC&DH subsystem there are four functions. Processing signals, processing commands, providing Doppler/ranging measurements, and data handling. The numbers given to the blocks correspond to the numbering in the FFBD.

9.4 Performance Analysis

The TC&DH subsystem is meant to provide a stable connection between nodes in the network. Therefore, certain data rates need to be achieved. In this particular case, two systems have to be designed. One for the orbiter, and one for the penetrator. Subsection 9.4.1 discusses the design choices for the orbiter, while Subsection 9.4.2 describes those for the penetrator.

9.4.1 Orbiter Link Analysis

The design of the telecommunications subsystem is mainly based on two factors, the input power of the system, and the separation distance from the receiver. For internals, the input power of the system is of most importance. Choice of antennas is based upon the separation distance of spacecraft and receiver. For relaying data from the penetrator, two links are to be maintained. Because the penetrator generates 13 Mbit of data in its lifetime, this data has to go through the orbiter as well.

Gravitational Measurements

The purpose of the orbiter is not only to relay data from the penetrator. By using Doppler measurements, which are accurate up to 0.1 mm/s [Europa Study Team, 2012], gravitational data about Europa can become further constrained. The amplitude and phase of tidal deformations can give information about the internals of Europa. Because the orbiter, contrary to Clipper, orbits Europa at a constant height, it can make higher degree accurate measurements. For Clipper it is estimated that it will produce a degree two to three accurate model of the spherical harmonics [Mazarico et al., 2015]. For a dedicated orbiter about Europa, the degree of accuracy that can be recovered is degree and order 15. In combination with a laser altimeter (SILAT, Subsection 7.1.1), the static topography field can be obtained with an accuracy of 1 m [Wahr et al., 2006]. This is one of the large benefits of having a dedicated orbiter over the flyby trajectory that Clipper follows. Over the course of a month, global gravitational Europa data can accurately be gathered.

Earth Communication (X-Band)

By analysing the minimum data rates needed during the mission, the performance of the system is found. According to the Europa study 2012 report [Europa Study Team, 2012] and the Juno mission [Mukai et al., 2012], the minimum data rates are 7.8 bit/s for commanding and 10 bit/s for telemetry. Therefore the system has to be able to, as a minimum, receive at least 10 bit/s at all time. For returning telemetry data, 2 kbit/s is used.

For communication to Earth, the X-band transceiver module is chosen, since that can provide for enough data rate. Also it is less dependent on weather conditions on Earth compared to a Ka-band transceiver [Shambayati, 2009]. This results in a more reliable link. The antenna chosen is a parabolic dish with a diameter of 1.3 meters, similar to the one used on the Odyssey mission to Mars. This is the maximum dish size that fits in the packaging for a piggyback with NASA's Clipper. It is a fixed-body antenna, meaning that the whole spacecraft has to move to point the antenna. This antenna is chosen because of the high focus of the signal, the high gain. This high gain antenna (HGA), however, does not provide reception of signals when it is not pointed at Earth. To assure uplink to the orbiter at all times, two more low-gain antennas (LGAs) are mounted on the spacecraft as well. One is mounted on the HGA assembly as well, and provides a forward view. The other one is mounted on the opposite side of the spacecraft and provides an aft view. Because of the large beam-width of the LGAs (± 80 degrees), the

spacecraft can always be contacted. To finalize the design, a medium-gain horn antenna is also added to the HGA assembly, and has the same boresight as the HGA.

Transmission can only be done via the MGA and the HGA. The MGA is chosen over the HGA in case not much data has to be transmitted. It requires less power. The HGA is able to transmit and receive, also at the same time. The MGA is only capable of transmitting, and the LGAs can only receive. This is the most efficient set-up.

Considering the use of this set-up, the input power determines the speed of the data link. By setting the RF output power to 3 W, the data rate for the orbiter caps off at a convenient 2943 bit/s, using a 50% margin over the required 2 kbit/s for telemetry. Table 9.1 gives an overview on the link budget made for the direct to Earth (DTE) link of the orbiter. Table 9.2 summarizes the communication design choices.

Table 9.1: Orbiter Link Budget

Quantity		Value	Unit
P	Transmitter power	+4.77	[dBW]
L_t	Loss factor transmitter	-0.46	[dB]
G_t	Transmitting antenna gain	+39.06	[dB]
L_a	Transmission path loss	-0.20	[dB]
G_r	Receiving antenna gain	+68.26	[dB]
EIRP	Equi. isotropic power	+73.10	[dBm]
L_s	Space loss	-288.85	[dB]
L_{pr}	Antenna pointing loss	-0.26	[dB]
L_r	Loss factor receiver	-0.97	[dB]
$1/k$	Boltzmann constant	+228.60	[dB]
$1/T_s$	System noise temperature	-12.55	[dB]
E_b/N_0	Received SNR	+3.10	[dB]
E_b/N_0_{req}	Required SNR	+0.10	[dB]
	Margin	+3.00	[dB]
Data Rate		2943	[bit/s]

Penetrator Communication (UHF-Band)

To receive and relay data coming from the penetrator, the orbiter communicates with the penetrator via its UHF-antenna. This helical shaped antenna is fixed on the orbiter pointing towards nadir, the same direction as the SILAT instruments points. During contact time with the penetrator, the orbiter must thus be nadir pointed, as well as for taking altimeter measurements. The UHF transceiver must be capable of receiving 8 kbit/s. Its wide beamwidth (± 80 degrees) allows for having the penetrator in view during pass over. Both the UHF system and the X-band system are coupled via the command and data handling system for processing of the data. Hardware concerning both systems is shown in Figure 9.5.

9.4.2 Penetrator Link Analysis

The penetrator relies on a UHF-band based system for transmission of its gathered data to the orbiter. This system is based on the Mars 96 penetrators and the Huygens probe [Ball et al., 2007]. They both rely on the UHF band for transmission for its excellent close range performance. Data rates for these systems are 8000 bit/s for transmission. Most important for the penetrator is to uplink its data. The limiting factor in this is the landing site situation. Because the penetrator has to send from a hole, the effective beamwidth angle of its antenna is limited to the width of the hole. Figure 9.3 displays the situation of the penetrator while sending. Its contact window equals ± 37 seconds while the orbiter is flying over. This is assuming a depth of impact of 1 meter. By dividing the total data gathered by the penetrator, 13 Mbits, by the data rate, 8000 bit/s, the total contact time can be calculated. This total time equals 28 minutes, or 0.5 hours. Taking the flyby contact time of 37 seconds into account, the total amount of flybys needed to

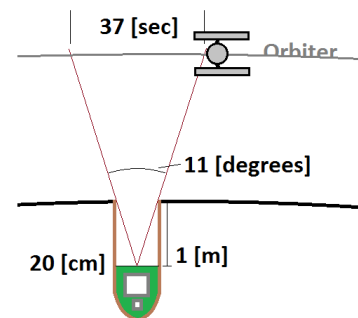


Figure 9.3: Contact window

transmit all this data is 46.

Table 9.2: Communication design choices summary

Orbiter	
Part	Details
HGA	Parabolic Dish, 1.3m diameter
MGA	Horn Antenna, beamwidth ± 30 degrees
LGA	Full coverage, beamwidth ± 80 degrees
Transceiver #1	X-Band, 8GHz
Data Rate Earth	2943 bit/s
Minimum Data Rate	10 bit/s
Transceiver #2	UHF-Band, 400MHz
LGA UHF	Helix, beamwidth ± 80 degrees
Data Rate Penetrator	8 kbit/s
Penetrator	
Antenna	Spiral UHF, beamwidth ± 11 degrees limited
Data Rate	8000 bit/s

9.4.3 Command and Data Handling

"The C&DH system maintains timing, interprets commands from Earth, collects, processes, and formats the telemetry data to be returned to Earth, and manages high-level fault protection and safing routines"¹. The communication system heavily relies on the command and data handling subsystem. For this reason, they are often combined into one subsystem. As for the internals of the C&DH subsystem, Figure 9.4 displays them. This figure has been adapted from a study for a nano-satellite formation, to suit our needs. Because also that mission mostly copes with the attitude determination, and therefore does not require that much computing power.

To carry out all the assigned tasks, the 1750A processor is chosen. It does not have the most computing power, but it is used in the Cassini-Huygens and the Rosetta missions, which both also have a relay function. On top of that, the processor offers very high levels of radiation protection.

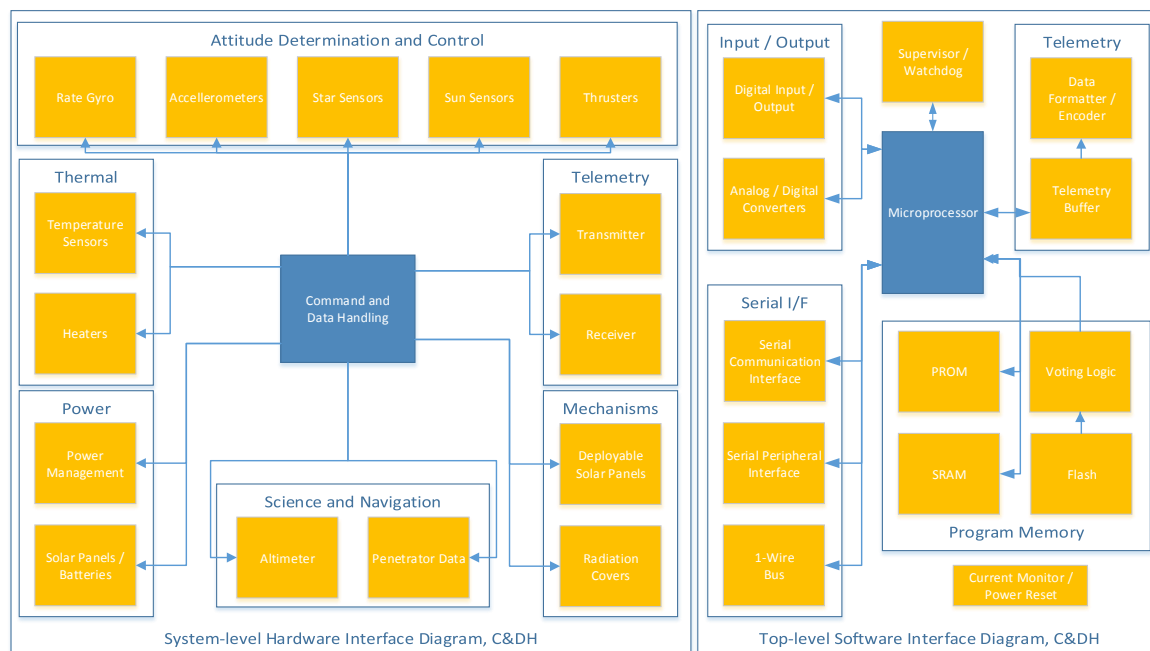


Figure 9.4: Hardware and Software block diagram of the C&DH Subsystem [Jensen, 2000]

¹<http://www2.jpl.nasa.gov/basics/bsf11-1.php#data>[Retrieved: June 9, 2015]

9.5 Hardware Block Diagram

The systems analysis is based upon the Mars Odyssey mission [Makovsky et al., 2002] and the Juno communications system [Mukai et al., 2012]. Also, a Europa study by ESA has been used as a reference [Europa Study Team, 2012]. The hardware of the Odyssey mission is adapted to suit our mission, and its power usage, 70W, is scaled down to 20W to get a good overview of the spacecraft's internals. Juno is used as a reference for the link budget calculations, and the Europa orbiter study was used to get an idea on minimum data rates.

Parts considered in the design of the communications subsystem are shown in Figure 9.5. This hardware block diagram shows the interaction between the different modules of the system. Also, it shows how the system has been made redundant to provide no single point of failure. The hardware diagram is split up between the X-band system on the left side, and the UHF-band system on the right side.

There are numerous parts involved in getting a signal ready for transmission. The small deep space transponders (SDSTs) are responsible for modulating the data onto a carrier wave. The coupler then routes the signal to either solid state power amplifiers (SSPAs). A band pass filter (BPF) is then applied before the wave-guide transfer switch routes the signal to either the MGA or the HGA. Similarly, when a signal arrives, the diplexer separates the arriving signal from the transmitting signal. The coaxial transfer switch (CTS) then sends the signal to one of the SDSTs after applying a noise filter (NF). The SDSTs then demodulate the signal again and communicate with the C&DH interface. By making use of the WTS and the CTS, as well as by cross linking the SDSTs and the C&DH interface, system redundancy is applied. There is no single point of failure in this system.

For the UHF side of the system, also an interface with the C&DH is found. The ultra stable oscillators (USOs) provide a reference for the systems frequency. The transceivers then fabricate a signal which is separated from the incoming signal by the diplexer. The WTS then couples both side 'A' and 'B' to the antenna. There is a full backup system running alongside the 'A' side. In case one of those components fails, the other side can take over. Also the UHF system has therefore no single point of failure.

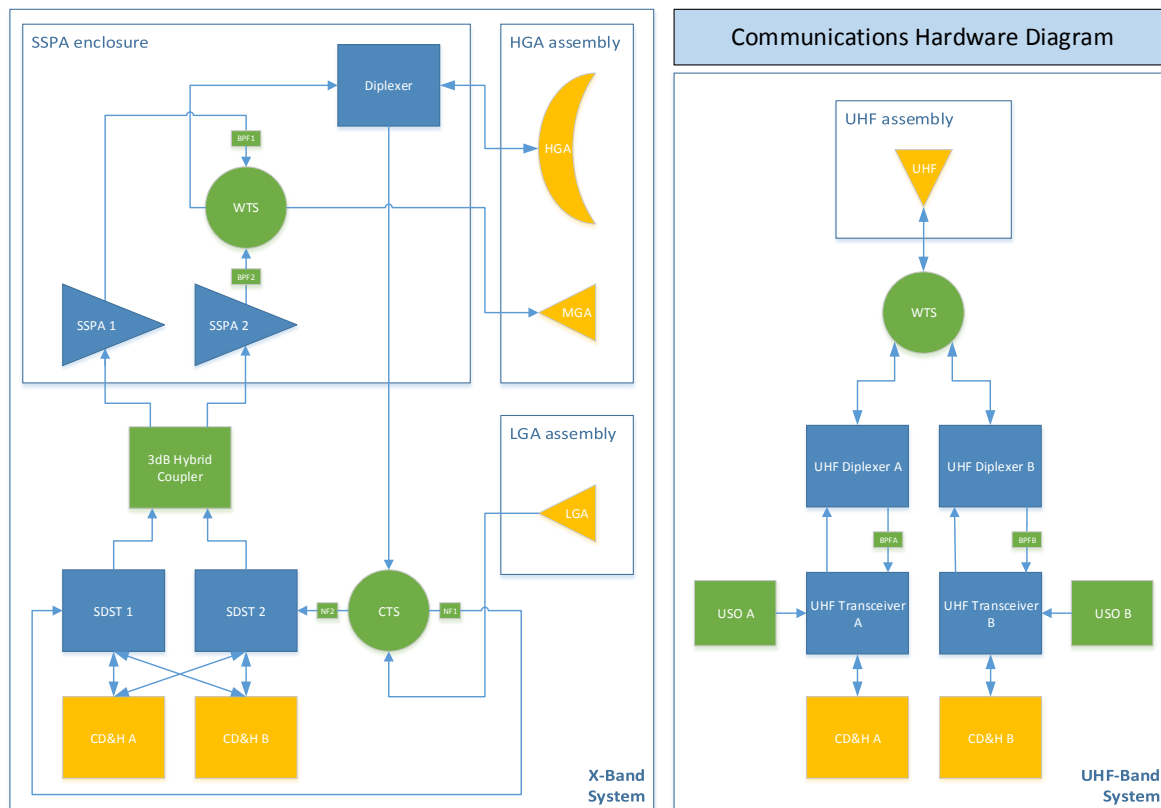


Figure 9.5: Hardware block diagram of the TC&DH Subsystem [Makovsky et al., 2002]

9.6 Code Verification

The code used for determination of the link budget, Table 9.1, has been done by using the Juno mission as a reference. Also it is designed alongside an example link budget from the course Aerospace Design & Systems Engineering (AE2111-II), part of the TU Delft Aerospace Engineering bachelor. For both cases of the Juno mission the code worked properly. Therefore, it can be used to determine the link budget for this relay orbiter.

Code used for determination of the contact time for the penetrator has been verified with the model from the astrodynamical calculations. They produced the same results. This piece was then integrated into the link budget to have a complete overview of both penetrator and orbiter in one place.

9.7 Compliance Matrix

They are divided into functional requirements, performance requirements and verification requirements. All of these are stated below.

Number	Requirement	Orbiter	Met	Lander	Met
TRFR-001	The TCDS shall be able to transmit data to Earth.	OK	✓	OK	✓
TRFR-002	The TCDS shall be able to receive data from Earth.	OK	✓	OK	✓
TRFR-003	The TCDS shall transmit data following the X protocol.	Deep-Space Transport Protocol	✓	Proximity-1	✓
TRPR-001	The downlink rate should be at least X [bit/s].	2000	✓	8000	✓
TRPR-002	The uplink rate shall be at least X [bit/s].	10	✓	10	✓
TRPR-003	The TCDS shall use X band transceiver.	X-band	✓	UHF-band	✓
TRPR-004	The TCDS operation temperature must stay between X [deg K].	100-400	✓	150-250	✓
TRPR-005	TCDS power consumption must not exceed X [W].	21	✓	2	✓
TRPR-006	The time in view of ground system (deep space network) is at least X [hours] per day.	8	✓	N/A	-
TRPR-007	The TCDS mass shall be less than X [kg].	20	✓	5	✓
TRPR-008	The TCDS shall stay within its allocated cost envelope [EUR].	6M	✓	TBD	✗
TRVR-001	Cable losses shall be taken into account during the design and verification.	OK	✓	OK	✓
TRVR-002	The TCDS shall be tested using a X space signal simulator.	TBD	✗	TBD	✗

All requirements for the TC&DH subsystem have been met, except for a few. The cost for the penetrator is hard to determine because it can only be based on a few designs. This can be further investigated to come up with a proper estimate. Furthermore, the subsystem shall be tested in real life before applying it to the spacecraft. This can be done in a space simulator, but the exact location and simulator still has to be determined. Lastly, time in view of the ground station only applies to the orbiter, which is 8 hours per day, but does not for the penetrator. Time in view of the penetrator, as seen from the orbiter, should be sufficient. This is the case since it was a design driving requirement for the trajectory that the orbiter follows. Therefore, all important requirements have been met.

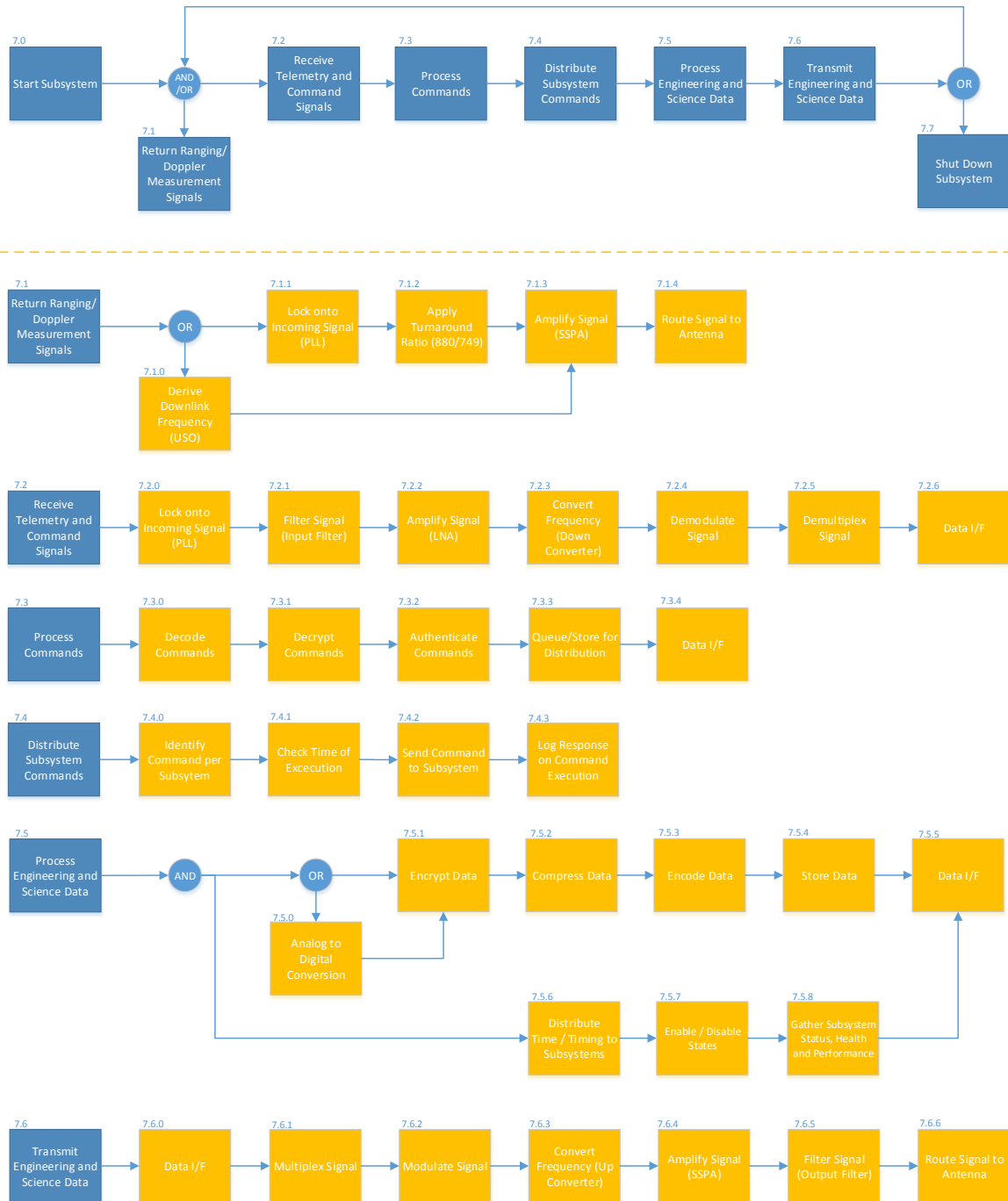


Figure 9.1: Functional flow block diagram of the TC&DH Subsystem

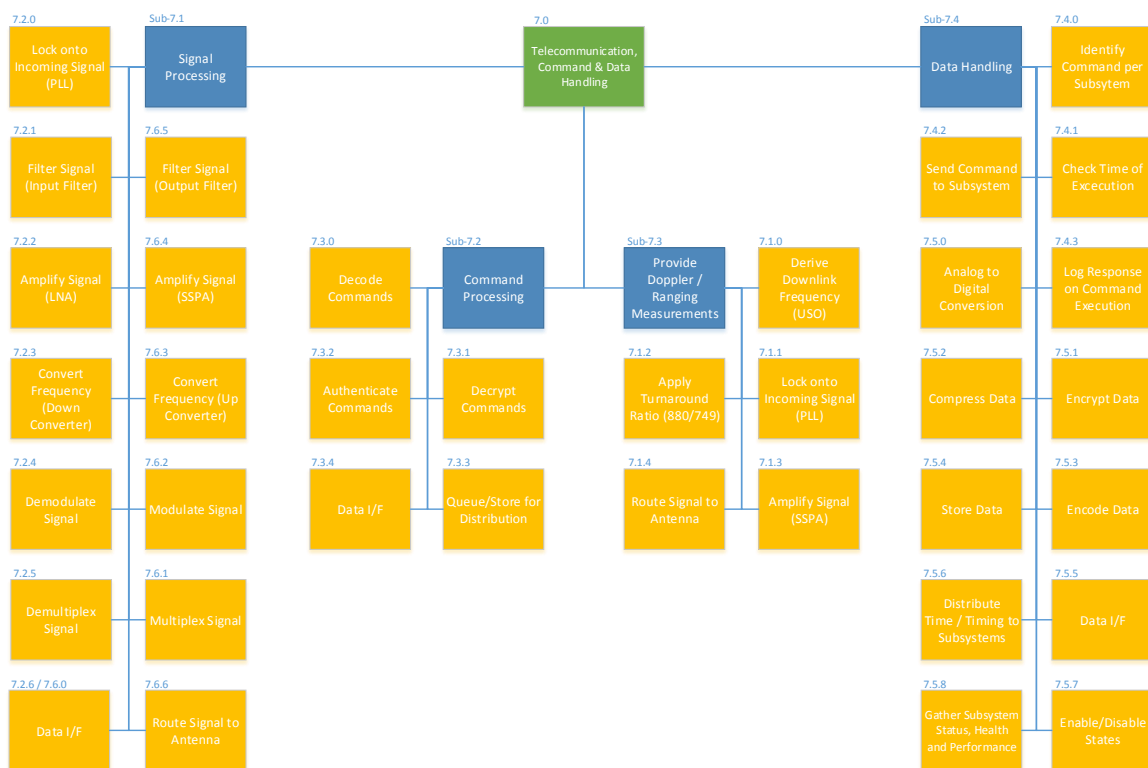


Figure 9.2: Functional breakdown structure of the TC&DH Subsystem

10. Thermal Control Subsystem

This chapter presents the functions, requirements and design of the thermal control system (TCS). In Section 10.1, the system is described. Section 10.2 presents a functional flow block diagram of the TCS, followed by a function breakdown structure in Section 10.3. Thermal model code verification is explained in Section 10.5. The chapter concludes with a requirements compliance matrix in Section 10.6.

Definitions

The following definitions are used in this chapter:

- Temperature Reference Point (TRP)* A point located in/on the unit and shall be selected so it is representative of the unit temperature.
- System Interface Temperature (STP)* A point representative of the temperature of the structural interface to the unit.

10.1 Thermal Control System Description

The TCS ensures that all components stay within their required temperature range. The space environment has a strongly varying influence throughout the mission, because of changing energy flux into the system. Therefore a system is designed that is able to keep all S/C components at the right temperature in all different mission phases. The requirements that were set for the system can be found in Section 10.6.

10.2 Functional Flow Block Diagram

The TCS functionality is not limited to heating or cooling components, as can be seen in the FFBD in Figure 10.1. Once the system has been switched on (8.1), it communicates with the TC&DH system to receive commands (8.2). These can be updates on temperature set-points (lower branch) or commands to switch off (8.7). When the system is active, it uses closed loop feedback control to guarantee temperature ranges. It registers the temperatures at TRP and STP points (8.3), which can be send for interpretation to the TC&DH system (8.4). This is done to ensure that the spacecraft health data is stored and can be transmitted to Earth. The temperature error is determined by comparing the required TRP and STP temperatures with the actual temperatures (8.5). When the temperature error is larger than a predefined value, the spacecraft energy balance is changed (8.6). How this can be done is explained in Section 10.3. With an altered energy balance, the temperatures are measured again (back to 8.3). In any case, the system keeps processing commands from TC&DH (back to 8.2). This loop is followed until the mission ends or the system is shut down.

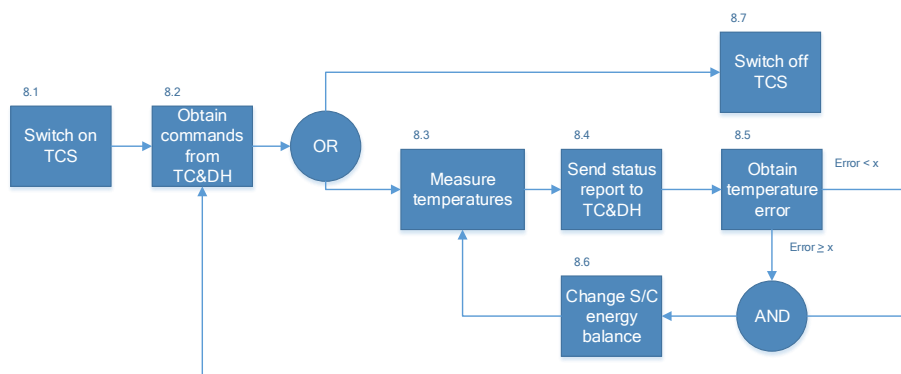


Figure 10.1: Functional Flow Block Diagram of the TCS.

10.3 Function Breakdown Structure

To ensure the design of the TCS fulfils all necessary functions, a FBS was made. The functions mentioned in Section 10.2 can be seen as part of two overarching functions: obtain S/C temperature (8A) and adapt S/C temperature (8B), both originating from the main goal of controlling the S/C temperature (8.0). Functions 8.3 to 8.6, mentioned before at the FFBD, are third-level functions, directly following from 8A and 8B. On the lowest level shown, nine distinct functions can be seen. It should be noted however, that functions 8.3.1 to 8.4.2 and 8.5.1 could also be performed by the same on-board processing hardware as the TC&DH uses. Therefore, the functions below 8.3 and 8.4 are not elaborated on in detail. The functions below 8.5 are also not specific for this mission design. Obtaining temperatures and calculating an error requires less tailored designing procedures than the major function of the system: change S/C energy balance (8.6). Because of its specific requirements, this chapter focuses on executing function 8.6 specifically for the Europa mission.

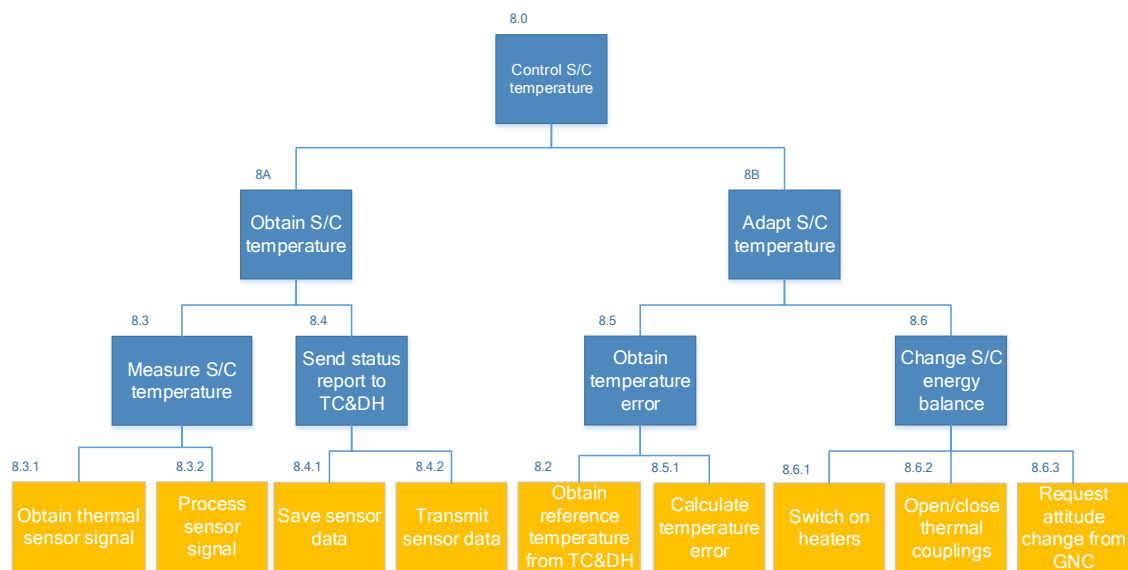


Figure 10.2: Function Breakdown Structure of the TCS.

10.4 Performance Analysis

To ensure the temperatures of the orbiter and penetrator stay within the ranges mentioned in Requirements TCFR-004, a thermal mathematical model (TMM) was developed following the procedures from Chapter 11 of Spacecraft Systems Engineering [Fortescue et al., 2011]. The goal of this model is to show the variation in temperatures of the eight nodes and to ensure that the modelled temperatures fall within the temperature range between T_{min} and T_{max} mentioned in Table 10.2. The governing equations of this model are given below, together with the parameters of the nodes. Three extreme space environments encountered by the S/C are listed, and finally a design is presented of both the orbiter and penetrator TCS.

Governing Equations

The TMM was created using the governing equations for heat transfer and conduction. It assumes the spacecraft consists of a set of nodes that can receive and emit energy, have a specific mass and area. The S/C receives energy from sunlight, light reflecting on celestial bodies (albedo) and planetary thermal radiation [Fortescue et al., 2011]. The power per area received from sunlight is given in Equation 10.1.

$$J_{sun} = \frac{P_{sun}}{4\pi s_{sun}^2} \quad (10.1)$$

with $P_s = 3.856 \cdot 10^{26}$ [W] and s_{sun} depending on the mission phase. The power received from planetary albedo is given by Equation 10.2.

$$J_{alb} = J_{sun} F_{alb} a_{surf} \quad (10.2)$$

where F_{alb} can be estimated via Figure 11.2 in [Fortescue et al., 2011], under the assumption that the numbers in this figure hold for Europa. The albedo a_{surf} differs per celestial body. Thermal radiation from celestial bodies is calculated via Equation 10.3.

$$J_{rad} = \sigma T_{bb}^4 \frac{r_{planet}}{r_{planet} + h_{orbit}} \quad (10.3)$$

The total incoming energy on a thermal node is given by Equation 10.4.

$$P_{in,i} = \alpha_i (J_{sun} A_{i,sun} + J_{alb} A_{i,alb}) + \varepsilon_i J_{rad} A_{i,rad} \quad (10.4)$$

Power is emitted by thermal radiation from a node i into space following Equation 10.5. Thermal emission between nodes is calculated via Equation 10.6. Power conducted by physical contact from node i to j is given by Equation 10.7. The total outgoing power in a node is therefore given by Equation 10.8.

$$P_{emit,space} = \sigma \varepsilon_i A_{space} T_i^4 \quad (10.5)$$

$$P_{emit,node} = \sigma \varepsilon_{i,j} F_{i,j} A_{i,emit} (T_i - T_j)^4 \quad (10.6)$$

$$P_{cond} = h(T_i - T_j) \quad (10.7)$$

$$P_{out} = P_{emit,space} + P_{emit,node} + P_{cond} \quad (10.8)$$

Furthermore, a node can have internal heat dissipation Q_i . Combining the above relations, and knowing the nodal temperature T_0 at $t = 0$, the temperature of the nodes can be approximated numerically via Equation 10.9.

$$T_{i,1} = T_{i,0} + \frac{Q_i + P_{in,i} - P_{out,i}}{m_i C_i} \Delta t \quad (10.9)$$

Nodal Parameters

Eight nodes were used to model the orbiter with the penetrator attached, see Figure 10.3. To limit modelling time, it was decided to only create separate nodes when large different temperature requirements were given between components. The entire structure and stored penetrator are modelled as one central cylindrical structure. Furthermore, the four propellant tanks are modelled as one tank, and of the two symmetrically mounted solar panels, only one is included. The entire outer heat shield is modelled as one node as well. All systems in the payload vault have comparable temperature range requirements (273 to 293 [K]), therefore it was decided to group these in one node as well.

Interaction between any nodes i and j is determined by visibility factor $F_{i,j}$, relative emissivity $\varepsilon_{i,j}$ and conductivity $h_{i,j}$. The latter is shown schematically in Figure 10.3. All numbers were determined with guidelines from literature [Fortescue et al., 2011, ECSS Requirements and Standards Division, 2011, Karam, 1998] and by consultation with TNO. Relative emissivity is calculated using the approximation in Equation 10.10).

$$\varepsilon_{i,j} = \frac{\varepsilon_i \varepsilon_j}{\varepsilon_i + \varepsilon_j - \varepsilon_i \varepsilon_j} \quad (10.10)$$

Where ε for each node can be found in Table 10.1. This table also shows the mass, specific heat capacity, absorptivity, emissivity and total heat emitting area per node.

Extreme Environments

With the developed and verified TMM, four cases were selected that show extreme temperature and heat flows during the Europa mission. For all cases, the combined albedo and thermal radiation of Jupiter were found to add less than 1% to the total energy influx, therefore Jupiter's effects on the TCS were ignored. The blackbody radiation of Europa is taken as 130 [K] [Mills and Brown, 2000].

1. Europa Orbit (Orb.)

During this phase, the S/C is orbiting Europa at 244 [km] altitude. During this orbit, it is in the shadow of Europa for 23% of the orbit, which is 1960 [s] per 8520 [s]. Furthermore, once per Europa day of 85.2 [hrs], it is in the shadow of Jupiter for 2.8 [hrs]. The albedo of Europa it is 0.67¹. When on the day side of Europa, energy influx is $J_{sun} = 46.6$ [W/m²], $J_{alb} = 4.7$ and $J_{rad} = 12.1$ [W/m²]. On the night side of Europa, $J_{sun} = J_{alb} = 0$.

¹<http://nssdc.gsfc.nasa.gov/planetary/factsheet/joviansatfact.html>, [Retrieved: June 4, 2015]

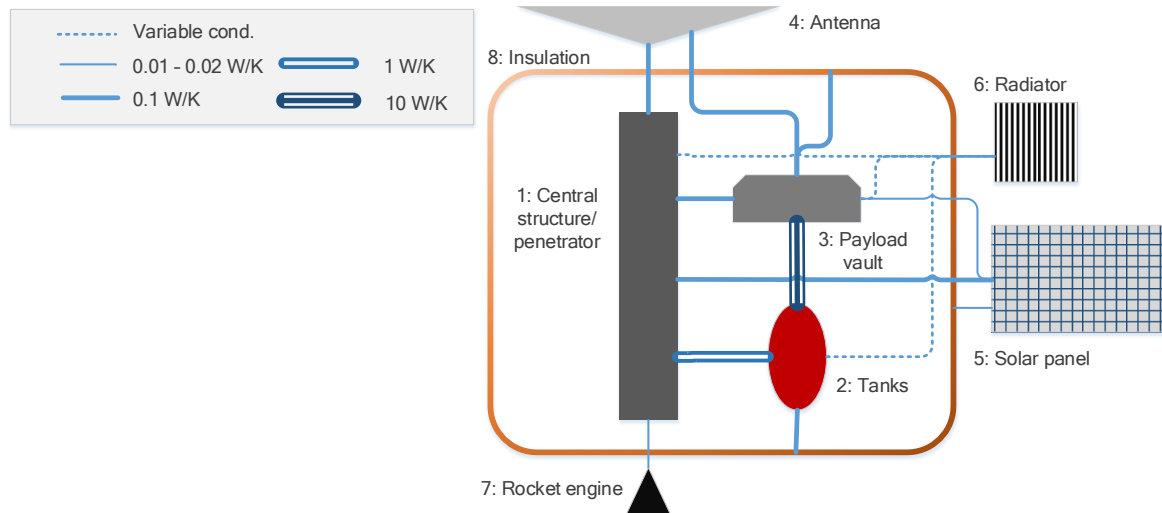


Figure 10.3: Schematic overview of the orbiter, represented by the eight nodes. Conductivities are represented as lines.

Table 10.1: Major parameters for the eight nodes used in the TMM. A_{emit} is the entire heat emitting area, so both to space and other nodes. α and ε are based on Table 11.3 from Space Systems Engineering [Fortescue et al., 2011]

Node	no.	Outer Material	Mass [kg]	C [J/ kg · K]	α	ε	A_{emit} [m ²]
Structure	1	Aluminium	160	921 ^a	0.24	0.08	1.0
Tanks	2	Titanium	270	544 ^a	0.6	0.6	4.51
Vault	3	Aluminium	80	921 ^a	0.1	0.01	3.90
Antenna	4	Alum. Kapton (top) Black paint (back)	15	921 ^a	0.14 0.95	0.05 0.85	1.3 1.7
Sol. panel	5	GaAs (top) Black paint (back)	50	350 ^b	0.14 0.95	0.05 0.85	8.0 8.0
Radiator	6	Black paint	1	921 ^a	0.95	0.85	0.70
Rocket Eng.	7	Titanium	3	544 ^a	0.6	0.6	0.15
Insulation	8	Gold. Kapton	6.7	1090 ^c	0.25	0.014	13.4

a: www.engineersedge.com b: www.janis.com c: www.dupont.com

2. Europa Orbit + Engine On (Orb. En.)

This case is equal to the Europa Orbit case, with the single difference that node 7 (rocket engine) is ignited, and therefore obtains a constant temperature of 1430 [K]². This will occur during the mission, when orbit manoeuvres are performed.

3. Minimum Distance to Sun (MDS)

During the interplanetary transfer, the S/C attains a minimum distance of 0.65 AU to the Sun. In this case, $J_{sun} = 3245$ [W/m²], but $J_{alb} = J_{rad} = 0$. Furthermore, a 300 km altitude Venus flyby at 0.72 AU was considered, but it was found that this was no extreme case in terms of energy influx, because the S/C will pass on the shadow side of Venus.

TCS Orbiter Design

Using the three environmental cases described above, together with the estimated parameters from Tables 10.1 and the conduction and visibility factors between nodes, the temperatures of the nodes were calculated. In practice, this came down to iteratively changing structural properties and surface coating properties. A passive TCS (using no power) was aimed for, instead of an active TCS. This would reduce power consumption, mass and cost [Brown, 2002]. From the TMM, no design solution was found where all conductances could have a constant value for all three extreme mission environments. Therefore, it was decided to keep the conductance from nodes 1, 2 and 3 to node 6 (radiator) variable throughout the

²<http://cs.astrium.eads.net/sp/spacecraft-propulsion/bipropellant-thrusters/220n-atv-thrusters.html>, [Retrieved: June 19, 2015]

mission by using variable conductance heat pipes (VCHP). Besides that, in the MDS case, the parabolic antenna on the orbiter should act as a heat shield: the S/C should point this large diameter top-mounted antenna towards the sun, providing shadow to the entire body of the S/C. The TCS is able to keep all temperatures within the required ranges using the system components below.

- **Side-mounted radiator and antenna-mounted radiator**

On one side of the orbiter, a 0.3 m² radiator is placed. This radiator is used to emit heat coming from the central structure, payload and tanks. To keep the S/C at the right temperature in the MDS case, it was also found that using the high-gain antenna as heat shield is a very low-weight solution, also used e.g. the Juno S/C [NASA, 2011]. To prevent overheating of the antenna in this case, its back is painted black to allow high thermal emission. Furthermore, a 0.4 m² radiator is placed on the back of the antenna, mounted such that heat is emitted most effectively into space. The radiators are passive components, made of a 1 mm thick aluminium plate and painted with black epoxy paint. The total mass of both radiators combined is 1.9 kg. Material cost is insignificant compared to the cost for testing and validating the radiators, which will have to prove that its surface finish does not degrade under the ionizing radiation around Jupiter.

- **Variable conductance heat pipes**

To protect the payload, structure and propellant tanks from overheating during the MDS and Orb. En. case, it was found that conduction paths from 0.1 W/K up to 10 W/K are needed. As found in Karam [1998], this rate can be achieved in a very mass efficient manner by using variable conductance heat pipes (VCHP). These aluminium pipes use ammonia as working fluid. This evaporates at the warm end of the pipe (in this case the payload, structure and four tanks) and condensates at the cold end (the radiator). Capillary forces then drive the liquid ammonia back to the warm end, creating an effective and still passive system. In total, 3.9 m of heat pipe is needed, with a diameter varying from 1 cm to 3 cm [Enertron Inc, 2001]. The total mass of the heat pipes is 2.5 kg. The cost is low, as heat pipes are almost off-the-shelf products which are widely used in space industry³. However, radiation protection testing should still be performed on these components.

- **Heaters**

When the spacecraft is not using the TC&DH system and GNC, the power dissipated in the payload vault is too low to keep the temperature above 273 K. Therefore, it was found that a redundant 20 W patch heater is needed inside the vault. This is a resistance placed in Kapton[®] with a size of only 2.1 cm². Its mass is a few grams, and development cost is low. Examples of manufacturers are NPH Heaters⁴ and Tayco Engineering⁵.

- **Multi-layer insulation blankets**

The low solar intensity and low thermal radiation from Europa cause a low energy influx when the S/C is in Europa orbit. Heat emission can be made low by covering the orbiter in Multi-layer insulation blankets (MLI). A high ratio is needed to make most effective use of the scarce sunlight falling on the spacecraft [Fortescue et al., 2011], therefore 25-layer blanket, that uses layers of goldized kapton and a mesh of Dacron[®], will be used [Poinas, 2004]. According to TNO, this MLI has a ratio $\alpha/\varepsilon = 0.25/0.014$. The radiation environment makes detailed investigation necessary, as it is known that e.g. Beta cloth, used as protective MLI outer layer, can degrade by ionisation [Finckenor and Dooling, 1999]. The cost of the MLI will therefore be largely determined by testing and manufacturing. The mass density, according to TNO, is 1 kg/m². This gives 6.7 kg MLI mass in total.

- **Temperature sensors**

Temperature sensors are connected to the TC&DH system to provide feedback on the S/C temperature at least once per 10 seconds. Examples of locations for these sensors are on the TRP and STP of batteries, instrumentation, solar panels and processors. An example of space qualified thermistor sensors is the 44900 Thermistor series from Measurement Specialities^{®6}. These have a mass in the order of grams. Radiation protection, however, is not included in the design. This may lead to cost and mass increase.

³<http://www.thermacore.com/applications/satellite-thermal-control.aspx>, Retrieved: June 19, 2015

⁴http://www.nphheaters.com/products/kapton_flexible_heaters.htm, Retrieved: June 18, 2015

⁵<http://www.taycoeng.com/proa.htm>, Retrieved: June 18, 2015

⁶<http://www.meas-spec.com/product/temperature/44900.aspx>, Retrieved: June 19, 2015

The total mass of the above system is 11.1 kg. By using the above component parameters as input for the TMM, it was verified that requirements TCFR-004 can be fulfilled in all extreme mission environments. The results are shown in Table 10.2. Some nodes are colder in the MDS and Orb. En. case than in the Orb. case. This is caused by the increased conduction to the radiator.

Table 10.2: Temperatures in [K] of the eight nodes as modelled by the TMM in three extreme cases. By using the described design, all temperature requirements are met. For the Orb. case, temperatures vary during orbit, therefore max. and min. temperatures are provided. Some nodes are colder in the MDS and Orb. En. case than in the Orb. case. This is caused by increased conduction to the radiator.

Temperatures of nodes [K]	T_{min} allowed	T_{max} allowed	T Orb. (max)	T Orb. (min)	T Orb. En.	T MDS	Within range
1: Structure	252	323	264	262	263	281	Yes
2: Tanks	274	293	280	280	277	281	Yes
3: Vault	273	293	283	281	279	279	Yes
4: Antenna	103	394	150	150	149	303	Yes
5: Sol. panel	98	393	190	170	190	133	Yes
6: Radiator	100	368	146	146	164	277	Yes
7: Rocket Eng.	100	3500	249	233	430	243	Yes
8: Insulation	200	374	251	229	249	239	Yes

TCS Penetrator Design

The penetrator thermal requirements are less extensive than those of the orbiter. All instrumentation and electronic devices should be kept between 273 K and 293 K when landed, except for the drill that takes a surface sample. The penetrator will land on the South Pole of Europa, where surface temperatures are expected to be 50 K [McFadden et al., 2007]. From a simplified model, taking into account conduction between the cylindrical penetrator and the surrounding ice, it was found that a single-walled penetrator would need hundreds of Watts to maintain a temperature difference of 223 K with the surroundings. To reduce conduction, a design based on a vacuum flask has been developed. In this design, the instrumentation is placed in a single ‘warm’ compartment. This closed compartment is mounted with an offset to the outer shell by six titanium supports with a length of 2 to 5 cm and a cross-section of around 0.6 cm². Full-scale impact tests were successfully performed with this kind of structure by ESA [Vijendran et al., 2014]. Goldized kapton is used as insulator on the wall of the compartment. This technique greatly reduces the heat loss from the payload compartment to 17 W. Around 6 W is dissipated by internal penetrator equipment, leading to 11 W shortage of heat generated. By reducing conduction from the internal equipment to the wall of the payload compartment, e.g. with aerogel, it is expected that the power loss can be reduced to a few Watts. This and other techniques to reduce heat loss on penetrators have been more thoroughly described in [Nouvellon et al.,]. The total TCS mass is around 0.2 kg. The design of the penetrator thermal control system will require more detailed research and validation, leading to significant cost increase. The actual manufacturing and material cost is expected to be low.

Design Cost

The budget for the TCS is 2.2M EUR, see Chapter 16 for more information on system cost. TCS cost for both the orbiter and lander remain unclear, although it is expected that the radiation robustness and penetrator impact testing phase will cost in or above the order of 1M EUR. Therefore, the 2.2M EUR cost budget can become a restrictive factor in the next phase of the design.

10.5 Code Verification

During the design of the TCS, use was made of the NASA Guidelines for Thermal Analysis of Spacecraft Hardware [NASA, 1999], which provide a framework for the TCS design procedure. The equations from Section 10.4 were implemented in a script using Matlab, after which the model was verified. Firstly, unit tests were performed on the input values. These were compared with literature values. Secondly, the results of the TMM were compared to those of the example on page 364 in Space Systems Engineering [Fortescue et al., 2011]. The S/C was assumed to be spherical and divided into eight equal nodes, representing the spherical orbiter from the example. It was shown that the equilibrium temperature of the eight connected S/C nodes reached 292.41 K, whereas the example obtained 292.45 K. This difference is lower than 0.1%. Therefore, the TMM is considered verified.

The TCS itself can be verified by simulating orbital fluxes, preferably in vacuum, and comparing the S/C temperature with the outputs predicted in Table 10.2. Typical verification tests for the different components (batteries, solar panels, instrumentation, etc.) are described in Chapter 7 from Karam [1998]. These serve as guideline for the TCS testing phase.

10.6 Compliance Matrix

The TCS certainly complies with 8 of the 10 requirements listed in Table 10.3. However, to ensure the fulfilment of TCPR-004 and TCPR-005, more specific research is needed. These requirements dictate that the TCS performs well under the magnetic fields and radiation environment encountered, but no clear research results were found that could verify this is the case for the materials and components in the current design. It is known that the MLI and coatings on the S/C may show different thermo-optical properties after radiation exposure, but the exact changes remain unknown. Therefore, additional testing and analysis is required in the next design phase.

Table 10.3: Compliance matrix for the TCS. TCPR-004 and TCPR-005 could not be verified in this design stage.

Number	Requirement orbiter (lander)	Met?	Value orbiter (lander)
TCFR-001	The TCS (Thermal Control System) shall monitor TRP and STP temperatures.	✓	
TCFR-002	The TCS shall be able to send TRP and STP temperature data to the TCDS once per 10 [s].	✓	10 [s]
TCFR-003	The TCS shall control the TRP and STP temperatures for all phases of the mission.	✓	
TCFR-004	The TCS shall keep all components within their required temperature range	✓	See Table 10.2
TCPR-001	The mass of the total TCS shall be below 15 (0.5) [kg]	✓	11.1 (0.2) [kg]
TCPR-002	All parts belonging to the TCS shall not use more than 22 (10) [W] in total.	✓	20 (<10) [W]
TCPR-003	The TCS shall be capable of operating during the entire mission duration.	✓	
TCPR-004	The TCS functionality shall not suffer from ionizing radiation.	N/A	
TCPR-005	The TCS functionality shall not suffer from magnetic fields of $1.05 \cdot 10^{-6}$ ($9.99 \cdot 10^{-7}$ [T])	N/A	N/A
TCVR-001	The TCS heat transfer shall be verified using a Thermal Mathematical Model (TMM)	✓	

11. Structural Subsystem

The structure is an important part of the spacecraft, it has to carry all the loads during the life time of the mission. Especially during the launch the encountered loads will be large. This chapter will start with a system description, next the functional flow block diagram and functional break down diagram are shown. In Section 11.4.1 the design loads and fairing constraints will be described, in Section 11.4.2 a material selection is made. The structure configuration and sizing is shown in Section 11.4.3 and the separation mechanism is shown in Section 11.4.5. The chapter will conclude with a verification and validation section and a compliance matrix.

11.1 Subsystem Description

The structure must fulfil the requirements listed in section 11.6. The structure serves as a central frame of the spacecraft, it provides mechanical support for all subsystems and payload. Further description of the structure subsystem can be found in Section 11.4.1.

11.2 Functional Flow Block Diagram

All the functions the structure subsystem has to fulfil are listed in a diagram shown in Figure 11.1. During assembly of the spacecraft, other loads can be encountered by the structure than during the mission lifetime, these have to be taken into consideration when designing the structure of the spacecraft. During launch the structure has to withstand all the loads encountered during the launch, for example the massive longitudinal launch loads. During the transfer to the Jovian system the spacecraft will also encounter loads, for example, the engine vibration loads during engine burns. When the spacecraft is deployed, the structure will encounter shock loads caused by the deployment system. Arrived at the Europa orbit the structure will encounter, amongst other, loads caused by attitude changes. Once deployed the penetrator structure will encounter high shocks during impact. All these loads have to be taken into consideration when designing the structure subsystem, an elaboration on the loads encountered during the above mission phases can be found in Figure 11.1.

11.3 Functional Breakdown Structure

A work breakdown diagram for the structure is shown in Figure 11.2. This diagram shows the main functions of the structure. If every sub-package is completed the preliminary design of the structure is complete. This is an iterative diagram and is subject to changes during the design process. Therefore, it can be seen as a preliminary approach to designing the structure subsystem.

11.4 Performance Analysis

This section will start with the investigation of the design loads and fairing constraints. Next a material selection is performed and a structure configuration is presented. The last subsection will size the structure.

11.4.1 Design Loads and Fairing Constraints

The structure shall be divided in two parts, the primary structure and the secondary structure, the primary structure shall carry the main loads encountered by the spacecraft. The largest loads encountered by the spacecraft are at launch, the Clipper mission will be launched by either the Atlas V551 or the NASA SLS. The Atlas V551 will be the worst case in terms of fairing dimensions and lift capabilities. The loads during launch will be critical for the spacecraft structure. The design loads for the Atlas 5 launcher are $-2g$ to $6g$ in axial direction and $-2g$ to $2g$ in lateral direction [United Launch Alliance, 2010]. Also the natural frequency of the structure is an important design parameter, the Atlas launcher manual states that the minimum frequencies in lateral direction are 8 Hz and in longitudinal directions 15 Hz. However, this design being a piggyback, the interaction of natural frequencies between Clipper and PB will also be of influence. The natural frequency of Clipper will be (at least) twice as high as the stated

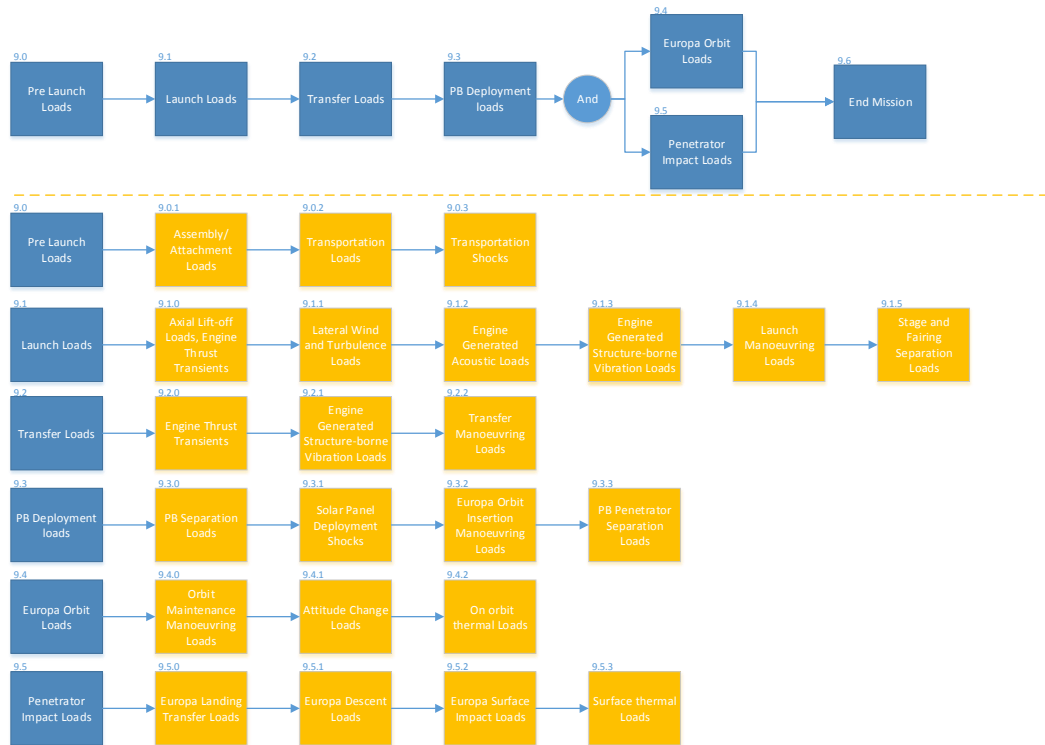


Figure 11.1: Functional Flow Block Diagram - Structure subsystem

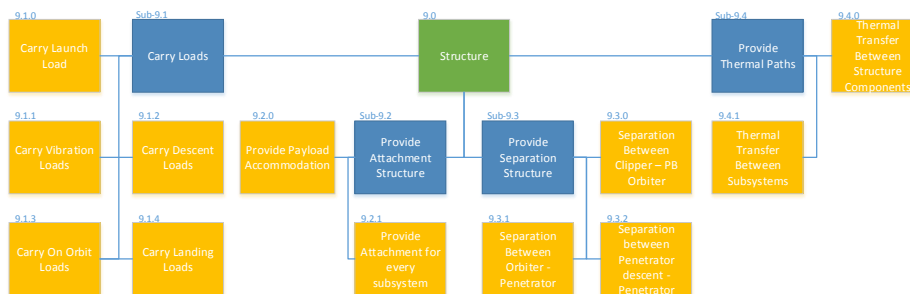


Figure 11.2: Functional Breakdown Diagram - Structure subsystem

minimum (safety factor of two). The natural frequency of the PB may not interfere with Clipper's, so the natural frequency of the PB should be higher than that of Clipper. For the PB again a safety factor of two is taken, resulting in a minimum natural frequencies of 60 Hz in longitudinal direction and 32 Hz in lateral direction. The secondary structure consist of the outer structure of the spacecraft and subsystem attachments, this study will focus primarily on the primary structure of the spacecraft. The fairing size of the Atlas launcher will be critical in terms of volume, for the Clipper mission the short payload fairing is selected, this fairing is shown in Figure 11.3. The estimated dimension of Clipper are given in Figure 11.4. Because it is not allowed to change the configuration of Clipper, the only option for an attached PB is on the side of Clipper, which will have a large influence on the center of gravity of the Clipper. This can be limited if the center of gravity of the PB is located as close as possible to the attachment to Clipper. Furthermore, the PB will induce extra loads on the structure of Clipper. The change in center of gravity and induced loads by the PB need to be taken into account by the Clipper design team. The PB will be attached at the location indicated in Figure 11.4, at this location the outer dimensions of the PB can be 1 by 1 by 3 meters (WxDxH).

11.4.2 Material Selection

The materials will be selected based on the properties in the list below. For this preliminary design the use of composites is not considered. However, the optimisation of the proposed structure, in a later stage of the design, could conclude that a composite material is favourable. The material descriptions in this

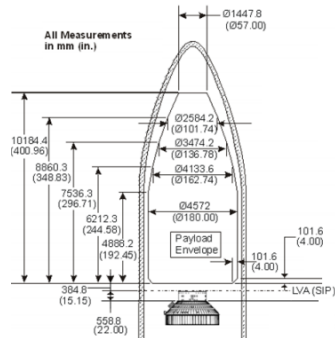


Figure 11.3: Atlas 5 launcher short payload fairing

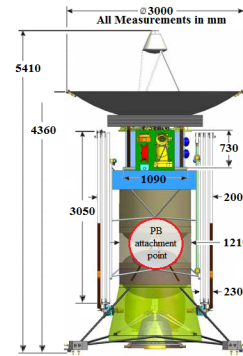


Figure 11.4: Clipper dimensions

section are based on [Fraser et al., 1990]. The thermal characteristics are important because, two different materials can have different thermal expansion coefficients, which may cause large thermal stresses in the spacecraft structure. The structure is also commonly used for thermal conduction or insulation, which can be a secondary function of the structure of a spacecraft. If a material has a high fracture and fatigue resistance, the safety factor of a structure can be reduced, this can result in a more efficient structure. Cracks in a structure will grow if the stresses in the material are high enough, it must be made sure that the cracks will not grow to a critical length during the life time of the spacecraft. The ease of manufacturing is another important aspect when designing spacecraft structures, some materials, like composite materials, may be expensive to manufacture. Materials like beryllium can present toxic or dangerous conditions during manufacturing.

- Specific Strength
- Specific Stiffness
- Thermal Characteristics
- Fracture and Fatigue
- Ease of Manufacturing
- Cost

Steel Alloys

Steels are unfavourable because of their magnetic properties. However, austenitic stainless steels are non-magnetic. Unfortunately, the stiffness to density ratios for these steels are lower compared to those of aluminium alloys. The high strength of steel may still be used in some instances where titanium is not desirable or available.

Aluminium Alloys

Aluminium represents the majority of spacecraft structural materials. A combination of high stiffness to density ratio, non magnetism, high corrosion-resistance, moderate cost, excellent workability and availability, makes it a choice worth considering for many cases. The disadvantage of aluminium is the low yield strength.

Magnesium Alloys

Magnesium has a stiffness to density ratio that is comparable to aluminium. However, it is prone to brittle fracture. The barely higher yield strength of this material compared to aluminium makes it not applicable for many cases.

Titanium Alloys

Titanium is used in many applications where aluminium does not possess the required strength. The material has a substantially greater yield strength, a higher stiffness to density ratio, compared to aluminium and is suitable for low-temperature applications. However, manufacturing of titanium components is far more complex than the manufacturing of aluminium components.

Beryllium Alloys

With a density approximately 60% of aluminium and a stiffness to weight ratio six times better than aluminium or titanium, this material has many potential applications. Being stiffer than other materials, it can be useful in avoiding resonant frequencies that may occur between a satellite and its booster during launch. Furthermore, the material is non-magnetic and has a high yield strength. Using Beryllium instead of aluminium can reduce the weight of the spacecraft structure significantly. However, the materials dust is very toxic, thus special facilities and tools are needed. This makes the material very expensive.

Table 11.1: Materials Trade-off

	Weight	Steel	Aluminium	Magnesium	Titanium	Beryllium
Specific Strength	20	3	3	1	5	4
Specific Stiffness	20	1	1	1	1	5
Fracture and Fatigue	15	3	2	2	4	2
Ease of Manufacturing	15	4	5	3	2	1
Cost	30	4	5	3	2	2
Total	100	3,05	3,35	2,05	2,7	2,85

In Table 11.1 a trade-off is made between the above mentioned materials. As can be seen Aluminium is the best option for this mission. Because the spacecraft is relatively lightweight, the lower strength of aluminium gives no problems. The aluminium is also favourable in terms of costs. As can be seen in table 11.2, aluminium can be used in the temperatures given in the requirements.

Table 11.2: Aluminium 6061 T6 Material properties for different temperatures [Sciver and W.,]

Temperature	0 K	80 K	300 K
σ_y [MPa]	345	332	282
σ_u [MPa]	580	422	312
Young's modulus [GPa]	78	77	70

Honeycomb Sandwich Structure

The facing skin of a sandwich panel can be compared to the flanges of an I-beam, as they carry the bending stresses to which the beam/panel is subject to. One face skin in compression and the other in tension. The core of a sandwich panel can be compared to a web of an I-beam. The core resist the shear loads and increases the stiffness. Sandwich panels are commonly used in spacecraft structures. The design of such panels can be a tedious process as a panel can comprise an unlimited variety of materials and panel configurations. The panels used for this design are selected on the required stiffness and strength. Further optimization of these panels can be done to optimize the structure design.

11.4.3 Structure Configuration

The selected configuration for the main structure of the orbiter is based on a central thrust cylinder [Wertz et al., 2011]. The cylinder has to carry the orbiter and penetrator, excluding the main propellant tanks, which will be carried by a separate structure. The spacecraft is divided into two parts, the lower part, including, a central cylinder, the lower support structure, propellant tanks and solar panel attachment structure, and the top part, including but not limited to, a central cylinder, antenna support structure and payload accommodation.

Orbiter - Lower Structure

The lower cylinder radius is set by the accommodation requirement of the penetrator descent stage. The descent stage of the penetrator will be located inside the lower central cylinder. The central cylinder will be supported by one honeycomb beam [Composites, 2000](Center beam). The four propellant tanks will be supported by two honeycomb beams(Outer beams), see Figure 11.5. This configuration is chosen because, there is no need to guide the loads to a central Launch Vehicle Adapter (LVA), instead, the loads need to be transferred to Clipper. The top support for the main tanks is shown in Figure 11.6, the tanks are free to move in longitudinal direction and are supported in lateral direction only. This way no thermal and deflection strains can form in the support structures.

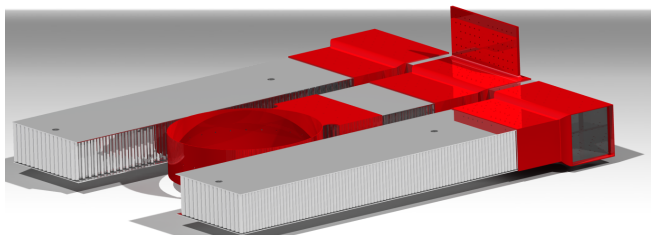


Figure 11.5: Lower piggyback support structure

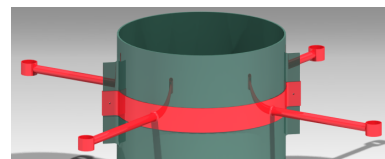


Figure 11.6: PB Orbiter - Top main tank support structure

The lower support structure in Figure 11.5 will be carried by a vertical plate, which is attached to Clipper by a separation ring, see Subsection 11.4.5, located at the circular section of the plate, see Figure 11.7. The base of the lower support structure will press against Clipper, preventing a large bending moment in the separation ring. This structure is comparable to the structure used in the Philae lander (Horizontal base panel with vertical attachment structure). This structure is reinforced with struts, this may also be favourable for this case, however, this study is limited to the vertical panel shown.

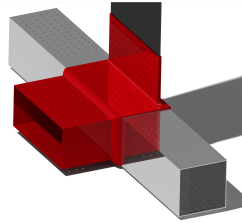


Figure 11.7: PB Orbiter - Clipper attachment structure



Figure 11.8: Top view - Cylinder joint

Orbiter - Top Structure

The top cylinder has a smaller radius and is connected to the lower cylinder with the joint shown in Figure 11.8. Attached to the joint a separation ring, see Section 11.4.5, is placed for deployment of the penetrator. The penetrator payload will be located in the top cylinder. A honeycomb base panel is attached over the joint to accommodate the subsystems and payload. Around the base panel a cover is constructed with dimension of 600x600x600 mm.

Penetrator - Structure

The penetrator structure is based on the structure shown in [Gowen et al., 2011] for an Europa penetrator. As the penetrator is attached to the PB orbiter at the top of the penetrator descent stage, the descent stage structure must be able to carry all the loads introduced by the main engine. During Launch the structure will be in tension and during engine burns in compression. The penetrator itself will be made from titanium with a thick wall, the exact thickness of this wall has not yet been established for this study. The payload bays inside the penetrator will be supported by a minimum set of brackets that reduce the shocks encountered by the payload bays and reduce the heat flow between the outer shell and payload bays.

11.4.4 Structure Sizing

In this subsection the preliminary sizing methods and results will be presented per component. Note that the joining methods between components are not investigated for this preliminary design.

Central Cylinder

The cylinder has a uniform thickness and no ring or longitudinal stiffeners. For the analysis of this component a method from SMAD [Wertz et al., 2011] is used. The input and output values from the analysis are shown in Table 11.3. Different thicknesses for the cylinder were calculated based on the list below, if the required thickness was lower than 1 mm, a minimum thickness of 1 mm was assumed. The lower cylinder is constraint by the lateral natural frequency requirement and the top cylinder by the minimum thickness requirement of 1 mm. The Safety Factors are based on the factors mentioned in the requirements documentation of the Rosetta Mission [Gardini et al., 1999].

- Meeting the natural frequency requirements, Axial (Equation 11.1) and Lateral (Equation 11.3).
- Applied and equivalent stress (Equations 11.5 and 11.8)
- Tensile strength (Solve Equation 11.8 for t with stress equal to the yield strength)
- Compressive strength (Equations 11.9, 11.10, 11.11 and 11.12)
- Margin of Safety (MS) (Equation 11.13)

$$f_{nat_{axial}} = 0.25 \sqrt{\frac{AE}{m_b L}} \quad (11.1)$$

$$A = 2\pi R t \quad (11.2)$$

With A equal to the expression given in Equation 11.2.

$$f_{nat_{lateral}} = 0.56\sqrt{\frac{EI}{m_b L^3}} \quad (11.3) \quad I = \pi R^3 t \quad (11.4)$$

With I equal to the expression given in Equation 11.4.

$$P_{eq} = P_{axial} + \frac{2M}{R} \quad (11.5) \quad P_{axial} = m_b g_{ax} \quad (11.6) \quad M = m_b g_{lat} L \quad (11.7)$$

With axial load equal to Equation 11.6 and the moment equal to Equation 11.7.

$$\sigma = \frac{P}{A} \quad (11.8)$$

$$\phi = \frac{1}{16}\sqrt{\frac{R}{t}} \quad (11.9) \quad \gamma = 1 - 0.901(1 - e^{-\phi}) \quad (11.10) \quad \sigma_{cr} = 0.6\gamma\frac{Et}{R} \quad (11.11)$$

$$P_{cr} = A\sigma_{cr} \quad (11.12) \quad MS = \frac{P_{allowed}}{P_{design}} - 1 \quad (11.13)$$

Table 11.3: Preliminary sizing central cylinder

Input	Lower Cyl.	Top Cyl.	Unit	Output	Lower Cyl.	Top Cyl.	Unit
R	0.19	0.11	m	$P_{eq_{UL}}$	11.5	9.55	kN
L	1.0	0.60	m	$P_{eq_{YI}}$	10.3	8.53	kN
m_b	355	265	kg	$P_{eq_{BU}}$	11.5	9.55	kN
g_{ax}	6	6	-	$t_{f_{ax}}$	0.2	0.181	mm
g_{lat}	2	2	-	$t_{f_{lat}}$	1.2	0.612	mm
Ultimate SF	1.4	1.4	-	$t_{\sigma_{UL}}$	0.4	0.446	mm
Yield SF	1.25	1.25	-	$t_{\sigma_{YI}}$	0.4	0.447	mm
Buckling SF	1.4	1.4	-	ϕ	0.722	0.656	-
E	$68.9 \cdot 10^9$	$68.9 \cdot 10^9$	Pa	γ	0.537	0.567	-
ρ	2700	2700	kg/m ³	σ_{crit}	$166 \cdot 10^6$	$268 \cdot 10^6$	Pa
F _{tu}	$310 \cdot 10^6$	$310 \cdot 10^6$	Pa	P_{cr}	200.79	147.22	kN
F _{ty}	$276 \cdot 10^6$	$276 \cdot 10^6$	Pa	MS	0	0.16	-
-	-	-	-	Mass	3.58	1.12	kg

Honeycomb beams and base panel

The preliminary sizing of the honeycomb beams is based on a report of HexWeb, Honeycomb Sandwich Design Technology [Composites, 2000]. For this analysis a cantilever beam with a load on one end is assumed. The material properties can be found in the appendix of the HexWeb report. Setting the facing thickness to a fixed value, Equations 11.14 and 11.15 are used to come up with a core thickness. Equations 11.16 (Bending stiffness), 11.17 (Shear stiffness) and 11.18 (Deflection) are used to estimated the deflection per beam. The input and outputs are given in Table 11.4. For the Tank beam, only one is calculated, the other is mirrored and assumed to carry the same loads. The honeycomb base panel proposed in Subsection 11.4.3, for support of the subsystems and payload, located in the top section of the spacecraft, is calculated in a same manner, but with panel theory instead of beam theory. See [Composites, 2000] for more details.

$$\sigma_f = \frac{M}{ht_f b} \quad (11.14) \quad \tau_c = \frac{P}{hb} \quad (11.15)$$

$$D = \frac{E_f t_f h^2 b}{2} \quad (11.16) \quad S = bhG_c \quad (11.17)$$

$$\delta = \frac{k_b PL^3}{D} + \frac{k_s PL}{S} \quad (11.18)$$

Other Structure Components

Other components of the structure are sized in a similar manner. The tank top structure is sized for bending, buckling and yielding. The base plate for the subsystems is sized for bending and yielding.

Table 11.4: Preliminary sizing Honeycomb beams

Input	Central	Tank	Unit	Output	Central	Tank	Unit
L	0.226	0.70	m	S	$1.839 \cdot 10^4$	$1.288 \cdot 10^4$	Pa
w	0.14	0.14	m	M	$4.157 \cdot 10^4$	$4.97 \cdot 10^4$	Nm
m_b	355	200	kg	t_f	2	2	mm
g_{ax}	6	6	-	t_c	60	50	mm
g_{lat}	2	2	-	τ	$2.124 \cdot 10^6$	$1.24 \cdot 10^6$	Pa
ρ_f	2700	2700	kg/m ³	MS	0.364	0.210	-
ρ_c	127	72	kg/m ³	δ	2.56	16.45	mm
k_s	1	1	-	Cell Size	6	3	mm
k_b	0.33	0.33	-	Facing mat.	AL 6061 T6	Carbon Steel 1017	-
SF	1.25	1.25	-	Core mat.	AL 5052	AL 5052	-
-	-	-	-	Mass	0.583	1.31	kg

The vertical plate that attaches the PB to Clipper is sized for yield only. The need for shear panels between, for example, the vertical attachment plate and the central cylinder has not been investigated. An overview of the structure components can be seen in Table 11.5.

Table 11.5: Structure Component Overview

Component	Dimensions [m]	Material	Weight [kg]
Lower Central Cylinder	(RxL)(0.19 x 1)	AL 6061 T6	4.19
Top Central Cylinder	(RxL)(0.11 x 0.6)	AL 6061 T6	1.12
Tank Support Beam (2x)	(Lxb)(0.7 x 0.14)	AL 6061 T6/ Carbon Steel 1017	2.62
Cylinder Support Beam	(Lxb)(0.26 x 0.14)	AL 6061 T6/AL 5052	0.62
Clipper Attachment Structure	n/a	AL 6061 T6	0.61
Base panel	(Lxb)(0.6 x 0.6)	AL 6061 T6	1.5
Top Tank Support (4x)	(RxL)(0.05 x 0.22)	AL 6061 T6	0.76
Joints	TBD	TBD	4.4
Total	-	-	16.54

Natural Frequency

The natural frequency of the entire PB is hard to estimate. A Simple approximation can be given with the PB modelled as a cantilever beam (connected to Clipper) with an end mass(PB) [Pope,]. This is done in Equation 11.19, with k the stiffness of the attachment beam, M the mass of the PB and m the mass of the attachment beam. The stiffness of the attachment beam is given in Equation 11.20. With I the moment of inertia of the lower supports beams, filling in the values gives an approximate natural frequency of 80 Hz in longitudinal direction and 50 in lateral direction. This is above the required minimum frequency.

$$w_n = \sqrt{\frac{k}{M + 0.23m}} \quad (11.19) \quad k = \frac{3EI}{L^3} \quad (11.20)$$

11.4.5 Separation Mechanism

The PB should, at some point, be separated from Clipper. This section will give a short overview of how this will be done. In its turn, the penetrator must be separated from the PB orbiter as well, the system used for this will be similar to the one used to separate the PB from Clipper.

Clipper - PB Separation

The PB will be attached to Clipper by a Lightband [Planetary Systems Corporation, 2014] space vehicle separation system, being Commercial Off-The-Shelf technology it is highly reliable. The separation system will be integrated horizontally to the adjoining vehicles (Clipper and PB). This means the the longitudinal launch loads will give a lateral force on the separation system. Furthermore, the weight of the PB cannot be used to compress the separation springs, so the system has to provide for the capability to compress the springs. Because the PB is attached to Clipper with the center of mass of the PB above the attachment(in longitudinal direction), the spring loaded separation system may give a rotation to the PB at separation. This may also be the case, to a lesser extent compared to the longitudinal case, on

the lateral axis of the PB. The offset of the separation system to the center of mass of the PB will cause a rotation of the PB at separation. This can be avoided by placing the springs of the separation system in a configuration such that the spring loads acts in line of the center of mass.

PB Orbiter - PB Penetrator Separation

The penetrator is located inside the central thrust cylinder, and is attached by the same system as mentioned in Section 11.4.5. However, the system will be integrated vertically to the adjoining vehicles (PB orbiter and PB penetrator). The weight of the penetrator deployment structure will pull on the separation ring during launch, meaning attention has to be paid to compress the springs in the separation system during longitudinal loads encountered during the launch. If the PB is deployed, the thrusting engine will push the penetrator against the separation system, however, these loads are small compared to the loads encountered during launch. The center of gravity of the penetrator will be at the center of the separation ring, meaning no special attention has to be given to the placements of individual springs.

Penetrator Descent - Penetrator Separation

The loads between the penetrator descent stage and penetrator will be small compared to the loads in the rest of the spacecraft, as the system only has to carry the penetrator payload. A complex separation system is therefore, not needed.

11.5 Verification & Validation Structure Subsystem

The equations used in the preliminary sizing of the structure are straightforward and verified by simple hand calculations. Analysing the model even further with the help of a finite element model was not possible in the given time constraint. Therefore, the structure mass is compared to other spacecraft missions instead. The percentage of the primary structure mass compared to the launch mass of the PB is quite low, because, the secondary structure and attachment structure masses are accounted for by each individual subsystem. The primary structure of the PB is 4.28 % of the total PB mass. The MAVEN spacecraft, has a primary structure of 5.09 % of the entire spacecraft mass ¹. This validates the obtained mass for the structure.

11.6 Compliance Matrix

The subsystem requirements seen in the table below have all been met with the proposed design. However, the natural frequencies need further investigating and the secondary structure is not checked to be decoupled from any major frequencies of the spacecraft.

Number	Requirement	Met?	Value
SRPR-001	The eigenfrequencies in lateral direction of the payload structure shall be above 32 [Hz].	✓	50 Hz
SRPR-002	All structural components that make contact with Europa adhere to COSPAR category IV.	✓	
SRPR-003	The structure shall not release any part during the mission.	✓	
SRPR-004	Secondary structure shall be designed to be decoupled from any of the major frequency of the S/C.	✗	
SRPR-005	The structure shall be able to withstand all the loads induced by the launch of the spacecraft.	✓	
SRPR-006	The structure shall be able to carry 760 [kg].	✓	760 kg
SRPR-007	The yield strength and Young's modulus shall remain above the stated values at 300K in a temperature range of 253K to 300K encountered during the mission.	✓	
SRPR-008	Material deformations in main support component(s) shall be below 30 [mm/m] during the entire mission.	✓	25.4 mm/m
SRPR-009	The structure shall stay within its allocated volume [3 m ³].	✓	2 m ³
SRPR-010	The structure shall not exceed TBD cost [EUR].	✓	
SRPR-011	The eigenfrequencies in longitudinal direction of the payload structure shall be above 60 [Hz].	✓	80 Hz

¹<http://www.spaceflight101.com/maven-spacecraft-information.html> [Retrieved June 22, 2015]

12. Radiation

Radiation poses a unique technical challenge for any mission to Europa due to the flight system spending a significant time in the harsh Jovian radiation belts. Like Earth, the presence of a magnetosphere has led to the formation of belts of trapped radiation. Due to the fact that Jupiter is much larger than Earth, Jupiter's equatorial radius is $R_J=71500$ km and Earth's radius is 6380 km, the radiation belts are much more extensive than Earth's Van Allen belts. In comparison to Earth (GEO), Europa energies are higher by two orders of magnitude, integral fluxes are higher by one order of magnitude for electrons and three orders for protons.

Section 12.1 shows the applied design approach, followed by the effects of radiation in Section 12.2. Next, the Jovian radiation environment is briefly described, also discussing the model used to estimate the radiation environment. The used radiation transport codes, the reference radiation design point and the shielding distribution for both the relay satellite and the penetrator are given in section 12.4. The radiation monitoring subsystem (RMS) is discussed and recommendations are given in respectively Sections 12.5 and 12.6.

12.1 Design Approach

The Moonraker mission design follows the conventional engineering practice of multiplying the estimated total ionising dose (TID) level by a radiation design factor (RDF) of 2 due to intrinsic uncertainties within the radiation environment models. The resultant environment is used for the selection of parts, materials, detectors and sensors, resulting in a mission design that should function well beyond its intended design environment and mission lifetime. For example, Galileo's mission was extended three times with the spacecraft accumulating about eight times its design level. Because of the sheer amount of radiation in the Jovian environment, a clear system engineering approach has been followed, prioritizing the radiation protection subsystem from the start and throughout the design. Working as a team, radiation, configuration and trajectory designers, can achieve the optimum shield effect at the spacecraft system level by strategic placements of the shielding enclosures and following a trajectory that minimizes the accumulated ionizing dose. This approach will result in the optimum system in terms of mass, lifetime and costs.

The first step in designing the radiation protection shield is to analyze the Jovian radiation environment, followed by selecting the optimum trajectory. Next, radiation transport codes are utilized to obtain the required radiation design point and required thicknesses for different materials and parts. Lastly, strategic placement of other spacecraft parts will reduce the required mass and lengthen the mission life time.

12.2 Radiation Effects

Successful operation of space systems in the Jovian radiation environment cannot be ensured without careful consideration of the effects of radiation. The predominant effects that pose a threat to the system are; Total Ionizing Dose (TID), Displacement Damage Dose (DDD) and Single-Event Effects (SEEs).

12.2.1 Total Ionizing Dose

Photons or charged particles knock an electron loose from an atom, yielding an excited state. TID degradation in microelectronics results from the build up of charge in insulating layers, and has a cumulative effect on electronics, resulting in loss of performance and eventual failure. Furthermore, TID affects optical components such as cover glasses, fibre optics and passive materials such as plastics, polymers, lubricants, thermal control paints, ceramics, wiring and cabling. TID can increase the temperature and accumulate charging in dielectrics and semiconductors resulting from mission electrons and protons. Protons will deposit all of their ionizing dose within the first millimeter, electrons will deposit all their ionizing dose within the first few centimeters. TID is defined as the amount of energy deposited by ionisation or excitation in a material per unit mass of material. The dose is dependent on the target material, where silicon is most generally used in space engineering, and is therefore expressed in rad(Si), where 1 rad (radiation absorbed dose) is equal to $1 \text{ cGy} = 0.01 \text{ J/kg}$.

12.2.2 Displacement Damage

Displacement damage is a cumulative radiation damage effect which results from an atom being knocked out of its position in a crystal lattice, resulting in a vacancy and an atom, or pair of atoms, (the interstitial) displaced to another location. Interstitials and vacancies are mobile and can cluster together or react with impurities, causing numerous component parameter degradation effects. Its primary effects are damage to semiconductor devices, density and refractive index change, discoloration in glasses, decrease in tensile and yield strength in some metals and possibly damage to permanent magnets and ceramics. DDD is also referred to as non-ionising dose damage, as it arises from particles losing energy, not by ionisation, but by elastic/inelastic collisions with nuclei in the target material. Displacement dose in the Jupiter environment results from exposure to trapped electrons (<0.5 MeV) and protons. DDD is commonly expressed as the non-ionising energy loss (NIEL) dose; the energy deposition in a material per unit mass by radiation through displacements.

12.2.3 Single Event Effects

Energetic ions passing through integrated circuits semiconductors produce a trail of ionisation which induces a variety of physical phenomena known as single event effects (SEE). SEEs can also arise from the interaction of protons and neutrons with semiconductors by means of nuclear reactions, causing either destructive, potentially destructive or transient effects. Examples of SEE include:

- Destructive
 - Single event latch-up (SEL) in CMOS circuits - the passage of a charged particle through a semi-conductor creates a parasitic transistor. A large current can flow if the device is powered up, and the heating produced will destroy the device.
 - Single event gate rupture (SEGR) - formation of a single conducting path triggered by a single ionising particle.
- Non-destructive
 - Single event upset (SEU) in memory and registers - passage of a particle through a digital component alters the state of that component. A bit is 'flipped', from '0' to '1' or vice versa. If the bit is in a computer instruction, the effect may be profound and impossible to predict.
 - Single event transients (SET) in linear circuits - a current transient which can be falsely interpreted as a signal.

For detailed descriptions on all single event effects, please refer to ECSS-E-HB-10-12A.

12.2.4 Spacecraft Charging

Spacecraft charging can arise from energetic electrons (tens of MeV), which penetrate the spacecraft and collect in insulators, leading to deep dielectric charging. The discharges can couple into spacecraft systems, leading to damage of the system. Charging of the spacecraft can lead to phantom commands from electrostatic discharge.

12.3 Jovian Radiation Environment

The Jovian trapped belts are far more intense and extensive than the Earth's radiation belts, primarily because Jupiter has a magnetic field that is about 20 times higher than the Earth. Rapid rotation, together with interior mass loading by Io, stretches the magnetosphere into a disk-like shape.

The mission is subject to three major radiation sources; solar energetic particles during the interplanetary cruise, galactic cosmic rays (protons and heavy ions) during the interplanetary cruise and trapped particles (electrons, protons and heavy ions) in the Jovian magnetosphere during the Jovian tour and Europa orbit phase. Among the three radiation sources, the high-energy trapped electrons and protons at Jupiter are the dominating contributors to the TID and DDD effects. Correctly defining and characterizing the radiation environment results in an optimal trajectory, constraining the radiation level to an acceptable level.

The radiation environment at Europa's distance from Jupiter, around $\sim 9.39 R_J$ (here $R_J = 71,492$ km), is substantial and hostile. However, the moon itself provides a great deal of shielding to any orbiting spacecraft. This is caused by energetic electrons traveling with high velocity along magnetic field lines (in the north/south direction at Europa) and very slowly in the perpendicular directions. Therefore, electrons spiraling up and down the field lines hit Europa as soon as the field lines come into contact with

it. Energetic electrons are therefore heavily lost near the equatorial trailing hemisphere, leaving flux tubes depleted of electrons, over about half of Europa's surface. Hundreds of keV to tens of MeV electrons are absorbed by the moon due to their short bounce times. For example, electrons between 0.1 and 50 MeV do not have direct access to more than 50% at 100 km Europa altitude. The result is that Moonraker, with a circular 244 km polar orbit, would spend about half its time in Europa's 'shadow', therefore, experiencing significantly less radiation. The approximate amount of obscuration due to the presence of Europa would be approximately 33% at 100 km, 27% at 200 km and 17% at 500 km. [Paranicas et al., 2007]

12.3.1 Jovian Radiation Environment Models

Storm-like and other disruptive events have been observed to occur over time at Jupiter. Storms can be caused by changes at the sun and throughout the heliosphere, which can perturb Jupiters magnetosphere. However, Galileo data has shown that these effects do not affect the overall fluence significantly, therefore, the total dose and radiation environment in the inner regions of Jupiter is predictable. [JPL, 2008]

The Divine and Garrett model from 1983 (DG83) is to date the standard model used to model Jupiter's radiation environment. DG83 is a quantitative model of the distribution of charged particles between 1 eV and several MeV in the Jovian magnetosphere. The model is primarily based on in situ data returned by experiments on the Pioneer and Voyager spacecraft, supplemented by Earth-based observations and theoretical considerations where needed. DG83 models the magnetic field, based on the upper cutoff field strength derived from the O4 model [Smith et al., 1976], resulting in estimates for the trapped electrons and protons in Jupiters radiation belt. The model is applicable to particle energies larger than 0.06 MeV, the range of applicability of the energetic electron model extends to the Jovian magnetopause (118 R_J), while that of the protons extends out to $R_J=12$. The electron model includes a pitch angle dependence within $R_J=16$ but is considered isotropic beyond that point, the proton model includes a pitch angle dependence within $R_J=12$. From in situ data and the modeled magnetic field, the intensity can be described. Integrating the intensity I (in units of $\text{cm}^{-2}\text{s}^{-1}\text{sr}^{-1}$) over the pitch angle α results in the omnidirectional fluxes, integrating again over time provides the fluence estimates. Furthermore, several ion species (H^+ , O^{++} , S^+ , S^{++} , S^{+++} and Na^+), electrons and protons are modeled as Kappa distributions for an estimation on the thermal plasma. Within each plasma region, the models results are compared with observed spectra, showing that the model represents the data typically to within a factor of $2^{\pm 1}$. Unfortunately, these models do not take the shielding of Europa into account, therefore resulting in an overestimation of the radiation environment. It is, however, standard practice to neglect the shielding effect of Europa in preliminary phases of the design.

To validate the usage of the DG83 model, the differential fluence for the Clipper mission [Brinza, 2014] is compared to the fluence outcome of the DG83 model, incorporated in SPENVIS [Heynderickx et al., 1998], for the specific trajectory of Clipper, see figure 12.1. The trajectory of clipper is based on SPICE files originating from JPL, utilizing a Jupiter-centric ecliptic J2000 reference frame with a time step size of 3.07 hours.

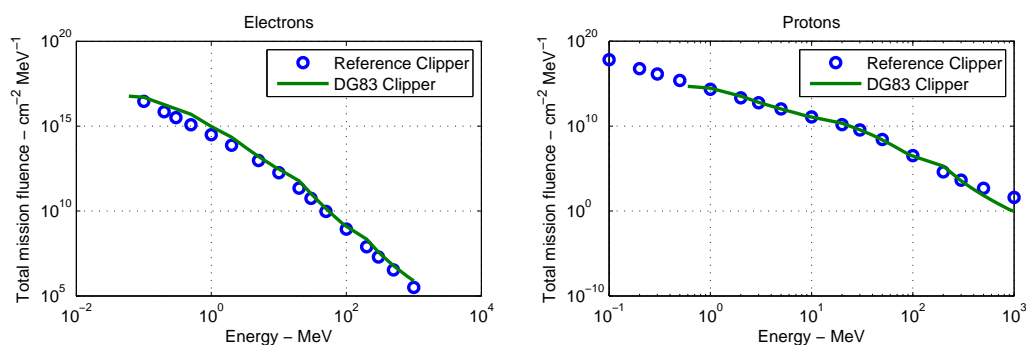


Figure 12.1: Comparison between reference Clipper differential fluence data and the DG83 model differential fluence estimate for the Clipper trajectory.

Moonrakers Jovian tour 1103 coordinates and dates were acquired from a SPICE file generated by JPL. MATLAB, with the added MICE package to read the SPICE files, was used to generate the coordinates for the Europa orbit phase and to connect the two phases. Please refer to Chapter 4 for more details. The resulting trajectory is used to model the radiation environment with the DG83 model, resulting in differential and integral fluxes and fluences as shown in Figure 12.2.

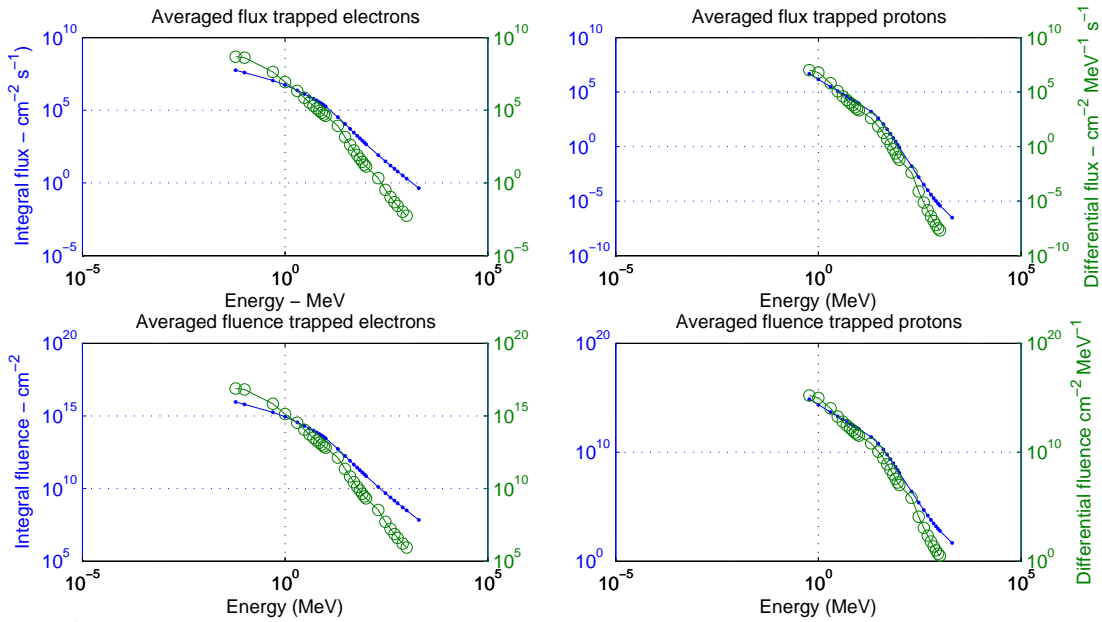


Figure 12.2: Average flux and fluence estimates from the DG83 model for the Moonraker mission. Dotted line represent integral with y-axis on the left hand side, circles represent differential with y-axis on the right hand side.

12.4 Shielding

Preventing the damaging radiation effect, as discussed in Section 12.2, requires the reduction of the external radiation. Three basic methods can be used to reduce the external radiation hazard, namely, time, distance and shielding. The duration of the Europa orbit phase has been limited as much as possible, the Jovian tour trajectory is designed to obtain the highest distance possible from the harshest radiation belts and otherwise minimising the exposure duration. The remainder is shielding, which will be discussed in this section.

12.4.1 Radiation Transport Processes

The transport of radiation through materials is a highly random process, scattering particles in all directions. Some preliminary knowledge about radiation transport processes are discussed in this section.

Electrons

Electrons interact with material mainly at the atomic level, producing excitation and ionisation, losing energy and being scattered in the process. Electron acceleration in the strong electric field of the atomic nucleus results in the generation of energetic photons known as bremsstrahlung or braking radiation.

For a particle with speed v , charge z , energy E , traveling a distance x into a target material and mean excitation potential I , the required stopping power for electrons, protons and heavy ions can be calculated by the Bethe-Bloch equation:

$$-\frac{dE}{dx} = \frac{4\pi}{m_e c^2} \cdot \frac{N_A \cdot Z \cdot \rho}{A \cdot M_u} \cdot \frac{z^2}{\beta^2} \cdot \left(\frac{e^2}{4\pi\epsilon_0} \right)^2 \cdot \left[\ln \left(\frac{2m_e c^2 \beta^2}{I \cdot (1 - \beta^2)} \right) - \beta^2 \right] \quad (12.1)$$

Where c is the speed of light, ϵ_e the vacuum permittivity, $\beta = \frac{v}{c}$, e the electron charge and m_e the rest mass. ρ is the density of the material, Z its atomic number, A its relative atomic mass, N_A the Avogadro number and M_u the Molar mass constant. Typically, the Z/A factor dominates for the collision stopping power of electrons. Therefore, since there are fewer target electrons per unit mass in high- Z material, these high- Z materials tend to provide the most mass-efficient electron shielding design.

Protons and Other Heavy Particles

Inelastic collisions with atomic electrons is the main mechanism of energy dissipation for protons and heavy ions. Since protons and ions are heavier than electrons, they are not subject to the same level of scattering as experienced by electrons, their paths through materials are therefore easier to compute. Due to the smaller scattering of heavy particles, the Z/A term in the Bethe-Bloch equation always means that low- Z materials provide more mass-efficient shields.

Electromagnetic Radiation - Bremsstrahlung

As electrons slow down in a target material, they generate bremsstrahlung, photons with a distribution of photon energies and directions. These photons subsequently interact, resulting in the production of electrons or positrons that can induce further ionisation and/or bremsstrahlung. Bremsstrahlung is the main concern from a space radiation perspective, since this allows energetic electrons to deposit energy significantly beyond the range of electrons itself due to the longer average ranges of photons. The fraction of energy loss by bremsstrahlung is highly dependent on the material, increasing with the square of the atomic number Z . Therefore, low- Z materials are the most mass-efficient in preventing the buildup of bremsstrahlung.

Material Selection

As previously described, higher- Z materials are more effective at shielding out electrons, however, bremsstrahlung photon production increases with Z Number. Lower- Z number materials are the most mass-efficient in shielding from protons and heavy ions, therefore, an optimum shield employs a combination of low- Z and high- Z materials. Either by first employing a low- Z material, such as aluminium, followed by a high- Z material, such as tantalum, or a combination of both materials by means of an alloy. The shielding material selection cannot be optimized without a careful application of radiation transport simulation codes.

Radiation Transport Simulation Code

A full treatment of the transport of radiation implies the solution to the seven dimensional stochastic coupled set of Boltzmann transport equations (BTE), please refer to [Brunner, 2005] for more details. Most often, geometries are simulated using Monte Carlo solutions of the BTE, where execution speed is the main limiting factor of such codes. Shielding codes such as SHIELDOSE and SHIELDOSE-2Q [Seltzer, 1979] are more generally used for ionising dose predictions. These tools employ pre-calculated data from Monte Carlo simulations to determine the dose behind 1-D finite-slab, semi-infinite and spherical shields of varying thicknesses. [ECSS, 2010] Where SHIELDOSE was only capable of determining the dose-depth-curve for aluminium shields, SHIELDOSE-2Q can determine it for 6 different materials; aluminium ($Z=13$, most used material for Earth based mission), titanium ($Z=22$, used on JUNO), iron ($Z=26$), tantalum ($Z=73$), CW80 (20% copper, $Z=29$ and 80% tungsten, $Z=74$) and a 1 mm thick aluminium layer plus a, in thickness varying, tantalum layer.

SHIELDOSE-2Q was used to determine the depth-dose-curve for the aforementioned materials for the fluxes and fluences as shown in Figure 12.2. Use is made of a semi-infinite slab shielding geometry, which is generally used to quantify radiation dose to components near to the surface of a spacecraft, where the source provides isotropically incident electrons and protons over 2π steradians. This assumption is valid since the majority of the spacecraft provides, effectively, an infinite shield over 2π steradians. The simulations result in a very demanding reference radiation design point of 1.63 Mrad behind a 100 mils (1 mils=2.54 mm) Al layer of shielding. The resulting depth-dose-curves can be seen in Figure 12.3(a)-(d), note that low Z materials perform better in terms of bremsstrahlung and proton shielding, however, since the electrons are dominating, these materials perform worst overall. The most mass-efficient material is the combination of a higher- Z and lower- Z material, namely CW80, an alloy containing 20% copper and 80% tungsten, closely followed by the Al-Ta bi-layer. Figure 12.3(e) shows the effect of duration on the Moonraker mission, the dose-dept-curves for the most mass-efficient material for different durations are plotted. The results have shown that CW80 is the most mass-efficient material for only the Jovian tour, Jovian tour plus 5 Europa days (1 Europa day = ± 35 Earth days) in orbit around Europa and the Jovian tour plus 10 Europa days in orbit, the Al-Ta bi-layer turned out to be most efficient for the Jovian tour plus 20 Europa days of orbiting. Tungsten has more favorable properties, no other metal can compare with tungsten when it comes to heat resistance. Tungsten has the highest melting point of all metals and is therefore also suitable for very high-temperature applications. It is also characterized by a uniquely low coefficient of thermal expansion and a very high level of dimensional stability.

Validation efforts of the SHIELDOSE-2Q model have shown that the models result show a similar level of agreement as other, more sophisticated, models. However, at greater depths (>13 mm eqv Al) the model starts deviating, with a maximum deviation of $\sim 50\%$ at a depth of 20 mm eqv Al [Truscott et al., 2010]. Again, these deviations lead to the usage of a RDF of 2.

12.4.2 Relay Satellite

Parts have been selected to be capable of receiving a total ionising dose of 300 krad whenever possible. Utilising a RDF of 2, this leads to a shielding distribution so that the instruments effectively receive 150 krad (the design dose line in figure 12.3. The required thickness for CW80 is then 427.6 Al equivalent

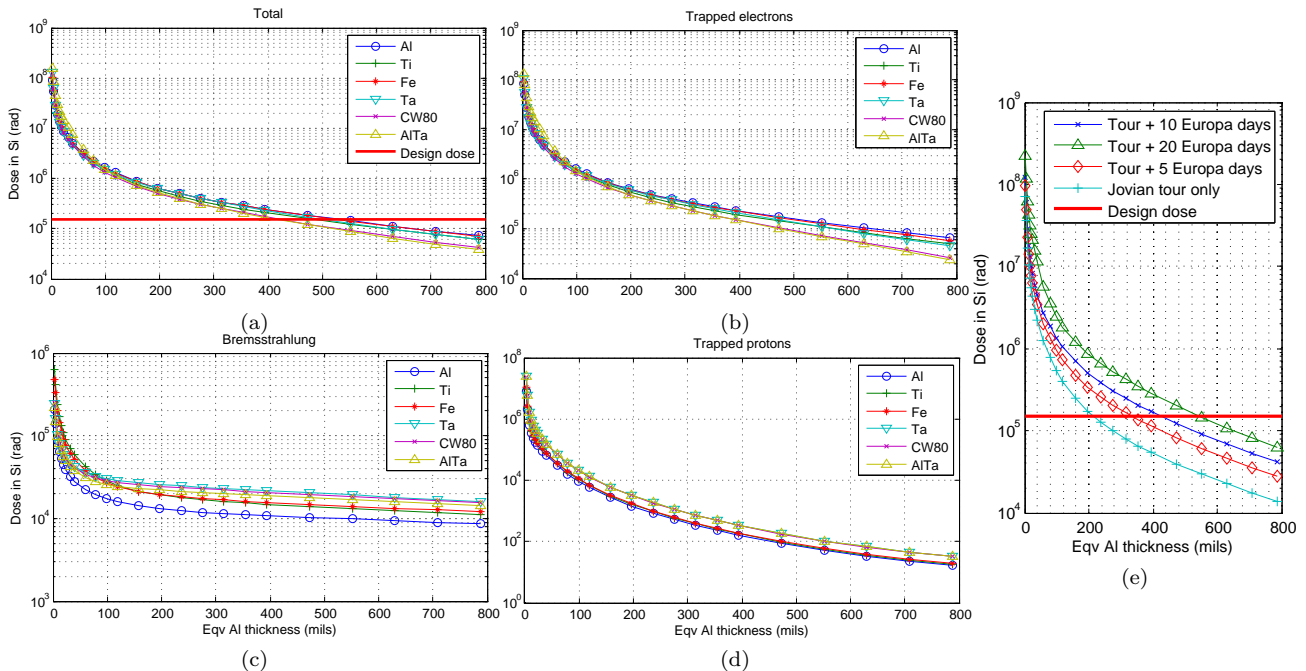


Figure 12.3: Horizontal axis shows the dose in rad(Si), vertical axis the equivalent aluminium thickness in mils. (a)-(d) Resulting dose-depth-curves from SHIELDOSE-2Q in aluminium equivalent mils for the Moonraker mission. (e) Effect of duration on TID for the optimal material.

mils, or 1.882 mm actual thickness. Shielding the entire satellite would require an exorbitant 181.5 kg, assuming all components have a TID capability of 300 krad. Shielding everything down to the lowest common denominator (75 krad) would require a shielding mass of 349.5 kg. The selected approach for the Moonraker mission makes use of a dedicated chassis, integrated as far as possible to the center of the spacecraft, providing it with shielding by other subsystems. The chassis is sized for standard 6U PCB cards, and will contain the power distribution unit (PDU), power conditioning unit (PCU), avionics, a CPU, the memory and the radiation monitoring subsystem electronics. The chassis provides the most light-weight solution for different parts radiation capabilities, since the center of the chassis is further shielded by the outer compartments and allows for additional PCB spot shielding. Please refer to Figure 12.5 for a 3-D render and an isometric technical drawing of the chassis. The total weight of the chassis adds up to 12.2 kg, excluding PCB cards. Furthermore, use is made of enclosure type shielding, which is applied to components too big to fit in the chassis or that have to be located on a specific location, for instance, the parts originating from the telecommunications subsystems that require shielding, should be placed on the back of the high-gain antenna (HGA) to limit cable losses. The star trackers are shielded by a movable slab of CW80, only opening when the star tracker is operated and closing immediately after. The total estimated shielding mass using CW80 is then 35.9 kg, over 22% mass saving and over 5 times volume saving over aluminium. Please refer to Table 12.1 for the radiation shielding mass distribution for all parts requiring shielding. Please note that dedicated radiation wire insulation is not required and is therefore not accounted for in the shielding mass budget, the regular used Teflon PTFE or FEP may survive high doses with no damage. [Willis, 2006] The Europa Study Report [2012] estimates a total cost of 9 M\$FY15 for the radiation shielding, scaling for Moonrakers shielding mass results in a cost estimate of 2.67M\$FY15.

12.4.3 Penetrator

The penetrator consists of two parts, namely, the penetrator itself and its descent stage. Neglecting the natural shielding effect of Europa and the shielding of the icy layer around the penetrator, utilising a RDF of 2 and a parts TID design capability of 300 krad, would require a shielding thickness of 7.41 mm of titanium. Since the penetrator wall is significantly thicker to survive impact loads, dedicated radiation shielding is not required. During the Jovian tour, the penetrator, and its accompanying descent stage, are located inside the central thrust cylinder, constructed out of titanium with a thickness of 1.2 mm. This cylinder will shield the descent stage from radiation, however, not enough. To this extent, a CW80 enclosure type shielding is used for the CPU, memory and the five transducers of the propulsion system, resulting in a total shielding mass of 1.7 kg for Drax.

Table 12.1: Radiation shielding mass distribution and type for the various subsystems.

Subsystem / Description	TID design capability (krad)	Shield type	Shielding mass per assembly (kg)	Comments
GNC			1.452	
Star tracker	100	Enc	0.726	x2
Propulsion			4.416	
Transducers	75	Enc	0.276	x16
Telecom			17.876	
SDST & USO	300	Enc	5.387	
WTS	300	Enc	1.199	x2, on back of HGA
CTS	300	Enc	0.303	on back of HGA
Multiplier	300	Enc	0.091	x2, on back of HGA
LNA	300	Enc	1.976	x2, on back of HGA
SSPA	300	Enc	2.827	x2, on back of HGA
Chassis			12.189	
C&DH			-	
Avionics	300	Chassis	-	
Memory	1000	Chassis	-	
CPU	1000	Chassis	-	
Power			-	
PDU	300	Chassis	-	6x 6U cards
PCU	300	Chassis	-	8x 6U cards
Total Moonraker Shielding Mass				35.933 kg

12.5 Radiation Monitoring Subsystem

Much of the Jovian radiation environment is still unknown or uncertain, which explains the seemingly excessive radiation design margin of 2. To this extent, a radiation monitoring subsystem (RMS) will be flown on board of Moonraker. The main function of the RMS is to continuously monitor the real-time radiation and surface charging environment, consisting of two sensors and multiple electronics. One sensor will be placed inside of the 6U chassis and consists of an Internal Electrostatic Discharge (IESD) sensor, a SEU detector and three TID dosimeters distributed so as to measure the TID behind and within various shielding locations. The other sensor will be placed on the star tracker, it contains the same sensors and detectors as the 6U chassis sensor, with the addition of a surface potential monitor to measure surface charging. Figure 12.4 shows the the aforementioned components comprising the RMS in a hardware block diagram. Furthermore, the RMS will provide real-time information of the performance of the radiation shielding, especially towards the effect on the star tracker. If it is found that the radiation is effecting the star tracker too much, proactive measures can be performed in terms of opening the star tracker less often or rotating the spacecraft away from the harshest radiation environment. The RMS is an adaptation of the RMS designed for NASA’s JEO concept mission [JPL, 2008], which is estimated at a mass of 8 kg and 4 W power consumption. Since Moonrakers RMS requires less sensors, the current best mass estimate of the RMS is 4 kg and is expected to use more or less the same power, since it is being dominated by the electronics. The estimated cost from the JEO concept study for the RMS entailed 5.9 M\$FY09, and is assumed to be equal to Moonrakers cost. The RMS complies to all its requirements, as can be seen in the following compliance matrix:

Number	Requirement	Compliant?	Value
RMSFR-001	The RMS shall be able to measure the radiation and surface charging environment.	✓	-
RMSFR-002	The RMS shall collect data to determine the effectiveness of the shielding design.	✓	-
RMSFR-003	The RMS shall collect data to understand anomalies in the computer system due to IESD and SEUs.	✓	-
RMSPR-003	The RMS shall collect data continuously and uninterrupted.	✓	-
RMSPR-003	The RMS shall not use more than 5 W average power.	✓	4 W
RMSPR-003	The RMS shall have a maximum mass of 6 kg.	✓	4 kg

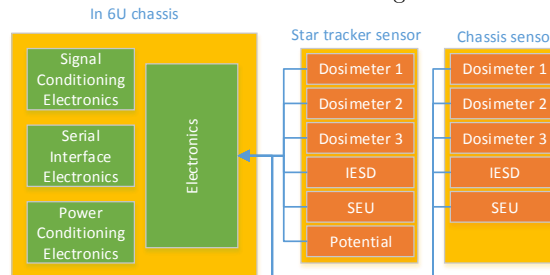


Figure 12.4: Hardware block diagram of the radiation monitoring subsystem.

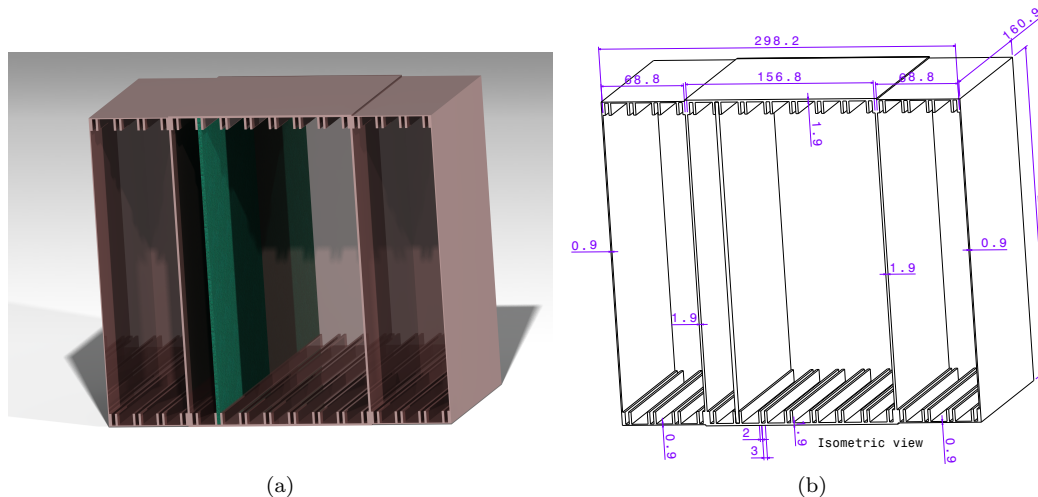


Figure 12.5: (a) 3-D render of the inside of the 6U chassis, showing one PCB card for illustrative purposes. (b) Isometric technical drawing of 6U chassis including one PCB card, dimensions are in mm.

12.6 Compliance & Recommendations

To check whether the radiation shielding is designed within the right constraints, a compliance matrix is developed:

Number	Requirement	Compliant?	Value
RADI-001	The spacecraft shall be designed to withstand the effects of the varying flux of high energy particles encountered in its mission.	✓	-
RADI-002	Electronic components applied in the spacecraft shall either be resistant to the expected radiation levels, to SEU and Latch-Up, or suitable provisions shall be made.	Partly	-
RADI-003	A radiation design factor of 2 shall be applied.	✓	2
RADI-004	The radiation shielding mass shall not exceed 8 kg.	✗	37.6 kg

It has been shown that the initial allocated mass budget for radiation shielding of 8 kg was highly optimistic, several iterations have provided an optimal mass of 37.6 kg for the combination of Moonraker and Drax. At the current maturity of the design, RADI-002 has only partly been met. This is caused by the fact that SEE and DDD have not yet been analysed in detail. Following are recommendations on how to improve on the current status of the radiation shielding design.

The conservative design approach, utilising a RDF of 2, has shown to lead to excessive over design in terms of mission lifetime, resulting in a, higher than necessary, mass. The margins have a compounding effect caused by the application of worst-case assumptions at every level: from parts selection to system design and engineering. More rigorous analysis and modeling needs to be performed to allow for a decrease in RDF, examples are to make use of the model PLANETOCOSMICS-J to take the natural shielding of Europa into account, utilising, and perhaps updating, more sophisticated models than DG83 to model the radiation environment, examples are GIRE, GRID2, etc. Full 3-D ray tracing and Monte Carlo simulations will have to be performed on the specific geometry of the spacecraft to determine more accurate dose-depth-curves, the effect of SEEs and DDD. Use can be made of models such as the commercially available FASTRAD, NOVICE or GEANT4. Single event effects are important, but the environment for Europa is not that different from other deep space missions with regards to SEE. The risk of some SEEs, such as SEU latch-up, can be mitigated by making use of software and dedicated circuitry, on which R&D should start as soon as possible. At the current state of the design, annealing of shielding materials has not been taken into account. Annealing is known to have a reversing effect on TID and DDD, however, currently there are no techniques or models available to predict the effect of annealing for outer space missions. Rigorous test should be performed to design appropriate models, which might allow significant mass savings. Typical tests include Enhanced Low Dose Rate Sensitivity for susceptible parts, typically performed at dose rates between 5 and 10 mrad/s. At these rates, tests for the Moonraker mission would take longer than a year and would require a significant part of the total cost budget. It is therefore essential that parts, components and materials testing starts as soon as possible.

13. Technical Risk Assessment

Mission risk is the product of probability of failure and the consequence of failure. For this mission, requirement SYS-SR-02 dictates a lower limit 95% mission success. Therefore, the probability of having a catastrophic failure, or critical failures, should be below 5 %. In this chapter, the risks that are associated with the different subsystems are considered. The risk elements are shown in Section 13.1. Per risk, a mitigation plan is provided. The risk maps and discussion for mitigated and unmitigated risks are shown in Sections 13.2 and 13.3.

13.1 Risk Elements

In this section, all of the risks are listed. The risks from the midterm report [DSE Group 10 et al., 2015] are adjusted and updated, as was done before in the midterm report. The relevant performance risks are given for astrodynamics, for each subsystem and for planetary protection. For all these, the risks are listed. The probability and consequence of the risk is shown, followed by possible and mitigation solutions.

13.1.1 Astrodynamic Characteristics

From launch at Earth until landing at Europa, many specific manoeuvres should be performed. These can all fail, although the risk differs per manoeuvre. Firstly, the launcher may fail: failed detachment of the spacecraft from the rocket payload bay would give problems with orbit insertion. The risk of this happening is low, but the consequences would be catastrophic. Mitigation is not performed easily, as risk mitigation in rocket launchers is already done for years (and with success). The consequence would always be catastrophic.

Secondly, collisions can occur with different objects in the Solar System: during the flybys with Venus and Earth, surface collision or space debris collision can occur. The probability of this happening is very low. The consequence will always be catastrophic. On the other hand, flybys can be performed imperfectly, leading to extra orbit corrections needed and hence more ΔV . This has a low probability and a moderate consequence.

Thirdly, the orbit insertion at Europa may not be performed in the allocated time slot. This can happen when, during the interplanetary trajectory, the velocity was slightly off. The Europa Orbit Insertion phase may therefore be performed late, leading to a different orbit than intended.

Finally, detachment from Clipper may not succeed or not at the right moment, also leading to extra ΔV needed. This has a low probability and a critical consequence.

All risks described above can be mitigated by verifying the trajectory calculations properly, and by frequently analysing the S/C position and velocity status during its journey. When potential trajectory problems arise, solutions should be found in close cooperation with the GNC and propulsion system.

Number	Risk	Consequence	Probability
A-1	Launcher failure	Catastrophic	Low
A-2	Collision with planet/debris	Catastrophic	Low
A-3	Europa orbit insertion failure	Critical	Moderate
A-4	Failed detachment from Clipper	Critical	Low

13.1.2 GNC

The risks of the the sensors are mostly low. The SIRU is designed for the harsh environments, and has a reliability of 0.997 [Grumman, 2014]. The performance consequence in case of a failure would be marginal, as the star and sun sensors could, temporarily, take over. If the SIRU in the descent stage fails, no trajectory data can be obtained, this could be catastrophic. The sun sensor is also able to withstand the high radiation environment¹. Having six sun sensors reduces the performance consequence to marginal. The star tracker is a high risk. It is highly sensitive and needs to be shielded from the radiation. Even with shielding, it has a higher probability of failure. As two star trackers would be taken

¹http://www.cubesatshop.com/index.php?page=shop.product_details&flypage=flypage.tpl&product_id=98&category_id=7&option=com_virtuemart&Itemid=69 [Retrieved June 21, 2015]

into the spacecraft, a failure consequence would be moderate, but a second failure would be critical as it becomes more difficult to calibrate the SIRU. The thrusters are proven reliable and have a low probability of failure.

Failure of detachment from penetrator and orbiter, or penetrator and descent stage, can be catastrophic for the complete mission. If the penetrator stays attached to the orbiter, slewing the orbiter might be problematic. A risk for the complete system, is that the torques and momentums are much higher than accounted for in the worst case scenarios used for the calculated torques. Using safety factors in the calculations can mitigate this risk to have a lower probability.

Possibly the highest risk of the entire mission originates from the lack of detail on the roughness of the European surface. The penetrator only survives impacts within certain degrees of impact angle with the surface (at least up to 25° was successfully tested [Gowen et al., 2011]). As the surface of Europa is expected to be very rough, the chances of having a neat, near-vertical impact are very low. The consequences of a non-vertical impact are catastrophic for communication with the orbiter. In more extreme cases, the penetrator shell may not stay intact. In that case, consequences are catastrophic. This risk can be mitigated by testing the penetrator design through impacting tests in the expected range of impact angles.

Number	Risk	Consequence	Probability
G-1	The malfunctioning of the SIRU	Marginal	Low
G-2	The malfunctioning of the SIRU during descent	Catastrophic	Low
G-3	Detachment failure of penetrator	Catastrophic	Low
G-4	Higher torques encountered	Moderate	Moderate
G-5	Penetrator angle of impact too high	High	Catastrophic

13.1.3 Propulsion

The propulsion systems main function is to transport the fuel into the engines resulting in performing manoeuvres. A malfunctioning of a small valve may result in not being able to give any thrust. The pressure transducers are used to measure the mass flow of the system to determine the fuel remaining and thrust delivered. This is important for the system, because it needs this data to perform accurate manoeuvres. Both of these risks need to be mitigated. This is done through adding extra redundancy by adding extra valves, pressure transducers and cross-links in-between the system fuel lines. This reduces the probability of both risks to very low. The main engine of the spacecraft is a new design based upon a larger engine. A risk accompanied by this design choice is schedule and cost. The TRL of the engine may not yet equal to 7 in 2017 as the requirement states. This can have a moderate consequence to the whole design, since a lot of extra money has to be allocated to meet this requirement. The probability of this risk is moderate.

Number	Risk	Consequence	Probability
P-1	The malfunctioning of a valve.	Catastrophic	Low
P-2	The malfunctioning of a pressure transducer.	Critical	Moderate
P-3	Design of the main engine does not meet the schedule and/ or cost	Moderate	Moderate

13.1.4 Scientific Instrumentation

The risk for the orbiter instrumentation is low, since it will not take as great impact loads as, for example, the penetrator instrumentation. It will be shielded well to protect it against radiation. Due to the highly integrated lay-out of the SILAT instrument, the consequence of one of the sensors failing can have large consequences for the other sensors. So, for the orbiter instrumentation, the risk of failure will be low. However, the consequences for mapping will be catastrophic, although it is not a primary mission objective. So, for the mission goal, failure of the SILAT instrument will not be catastrophic, but marginal.

The risk for the penetrator instrumentation will be high, since it will be able to survive the impact loads, which can be more than 20,000g. The testing phases for the instrumentation and the impact of the penetrator will be extensive, and within the budget there is room for several tests. The consequence of failure of the instruments will be critical: with every instrument that fails, a part of the science objectives can not be fulfilled. The only two partly redundant instruments are the geology package and the micro imager, because they are complimentary to each other. On the other hand, if, for example, the drill fails, all particle instruments become useless. So, the probability of failure is moderate to high and the consequence is severe to catastrophic for the whole mission.

Number	Risk	Consequence	Probability
I-1	Orbiter instrumentation failure.	Marginal	Low
I-2	Penetrator instrumentation failure.	Catastrophic	Moderate

13.1.5 Power

The power subsystem involves no new technologies and therefore has a higher reliability. However, still some events can occur, which can have a catastrophic impact on the nominal mission.

The first risk is that the solar arrays could not deploy due to a dis-functional thermal knife. The probability is low for this failure, since the spacecraft uses a proven technology. However, the impact of a deployment failure is catastrophic, as the required power cannot be delivered. This risk can be mitigated by adding two thermal knives (which makes the system redundant).

Next, the solar arrays can be hit by micrometeorites. The probability for this is moderate. Since the solar array is designed with a margin of 30 %, some loss of array can be tolerated which makes the consequence marginal. However, if critical lines are hit, the consequence may be critical since too much power can be lost. This risk can be mitigated by protecting the critical lines of the spacecraft and thereby reducing the consequence of a micrometeorite encounter to marginal.

Furthermore, the power conditioning unit could fail. The probability of this is low, since the power conditioning unit used on Rosetta, where the proposed power conditioning is based on, has a reliability of more than 98 % for 11 years ². However the consequence of such a failure is catastrophic as the power generated would never reach the equipment. This risk can be mitigated by application of more redundancy. The failure of individual components would then have a marginal impact.

Finally, the radiation damage could be over the design limit. The probability of this is high, since the solar cells are not tested within a similar environment. The consequence is moderate. Since less power is available at end of life, the mission might have to be shortened. This risk can be mitigated by applying a larger safety factor, or by using a more accurate model. For example, the model used do model Juno's solar arrays.

Number	Risk	Consequence	Probability
PR-1	Fail to deploy solar panels.	Catastrophic	Low
PR-2	Micrometeorite impact.	Critical	Moderate
PR-3	Failure of the power conditioning unit.	Catastrophic	Low
PR-4	Radiation damage over the design limit.	Moderate	High

13.1.6 Telecommunications, Command & Data Handling

The TCDH subsystem involves proven in-flight technology. All antennas have been used before, and so have all internals. Possible risks during flight are therefore on a base level already reduced to a minimum. Other risks that can occur during the mission can, however, still have an impact.

Firstly, pointing accuracy might not be as accurate as required due to a GNC failure. This means the link budget, although accounted for a 3dB loss, can throughput less data than currently anticipated. This has a low probability and may compromise gravitational measurements or scientific downlink. Therefore, consequences are moderate. The best way to mitigate this risk is by testing the system in a simulation on Earth.

Next, due to unforeseen environmental characteristics (e.g. radiation), the loss of the signal may be higher because of more noise. This has a moderate probability and may reduce mission lifetime. This has moderate consequence. In-flight mitigation can be performed by temporarily increasing the RF transmission power.

Besides this, a software error can occur which creates a malfunctioning computer. Depending on the severity of the bug, consequences may range from negligible to catastrophic. The chances are high that bugs are present, but the chance of a catastrophic software bug is moderate. Mitigating this risk can be done by extensively testing the safe mode, the state it returns to in case of software failure. After this, the other modes should be tested. This can lower the probability for a catastrophic bug to low.

Furthermore, the high-gain antenna can fail. In this case, the medium gain antenna should be used for transmission. This MGA cannot be used to transmit all scientific data and gravitational measurements. Therefore, although probability is low, the consequence is critical. There are little ways to mitigate this risk.

²http://www.terma.com/media/177710/power_conditioning_unit.pdf [Retrieved: June 21, 2015]

Number	Risk	Consequence	Probability
TD-1	High pointing loss	Moderate	Low
TD-2	Higher signal-to-noise	Moderate	moderate
TD-3	Software bug	Catastrophic	Moderate
TD-4	Antenna failure	Critical	Low

13.1.7 Thermal Control

As the TCS of the orbiter contains no actively moving parts, nor newly developed technologies, it has a relatively low risk compared to e.g. the penetrator structural design. The most notable risks for the TCS systems are given here.

Firstly, impact by micrometeorites is considered. This affects the MLI and radiators. This has a moderate probability, and moderate consequence. It cannot easily be mitigated, unless the MLI is over-designed to counteract potential functional loss.

Secondly, a risk is radiation degeneration, which can affect all coatings and heaters. This risk has a high probability and moderate consequence. It can be mitigated by sufficient testing and analysis to reduce the probability to low.

Finally, impact damage on the penetrator can be a problem. This has a moderate probability and a critical consequence, because the extreme g-loads during impact may deform or damage the penetrator such that the thermal analysis done on the design is not valid any more. This risk can be mitigated by full-scale system testing.

Number	Risk	Consequence	Probability
T-1	Impact by micrometeorites.	Moderate	Moderate
T-2	Radiation degeneration.	Critical	Moderate
T-3	Impact damage on the penetrator.	Moderate	High

13.1.8 Radiation

Electronic assemblies are vulnerable to failure when exposed to a high radiation environment for long durations. Many parts stay functional after exposure, however, the parameter degradation may be significantly different from typical parameters shown on specification sheets from vendors when exposed for a long time. The probability of occurrence is high and the consequence is moderate.

The radiation risk can be subdivided in three main categories; (1) effects on parts, materials and sensors, (2) internal charging and (3) instrument development. Taken all individually, these have a low likelihood of creating a moderate consequence, after all, radiation builds up over time and will not cause a sudden-death of the entire system in early to moderately late phases of the mission. However, adding these risks together and realising a lot of the Jovian radiation environment and radiation transport processes is uncertain, they become a significant risk when not properly designed.

(1) Effects on parts, materials and sensors

If radiation effects in parts and materials are more severe than expected, failures may occur, resulting in a loss of science data. Sensors are particularly susceptible to radiation, and could result in degradation of pointing, navigational accuracy and science return. These effects could occur if test techniques over-estimate the component hardness, for instance due to the neglecting of lower dose effects or unpredicted and unforeseen damage effects. The probability of occurrence is moderate and the consequence is moderate. Mitigating this risk requires setting up a proper Approved Parts and Materials List (APML), adequate testing of parts, materials and sensors, improving the understanding of both radiation transport processes and the Jovian radiation environment. Much has been accomplished in these fields over the last few years. For instance, both ESA, with its JUICE mission and NASA, with its Clipper mission, have developed APMLs and have provided updates on multiple models and testing techniques. This will decrease the probability of occurrence to low.

(2) Internal charging

Internal charging causes an electrostatic discharge within the flight system, leading to material damage and electromagnetic pulse damage to electronics. Mitigation requires rigorous design guidelines, such as the specifications on the maximum length of ungrounded wire, specifications on the restriction of ungrounded metal areas, etc. Designers will need to be trained to deal with these specific effects, as these do not happen to such an extent for near-earth based missions.

(3) Instrument development

Instruments are selected on the basis of an announcement of opportunity, specifying the requirements and allowing outside contractors to design and develop the instrument. Instrument developers will have to

be made aware of the radiation effects in a timely fashion by the usage of design guidelines. Taking into account the inexperience of mission, parts, materials and instrument designers for such harsh radiation environments, the likelihood of the radiation risk is high with a critical consequence. However, these risk can be mitigated by the use of proper design guidelines. After taking the mitigation steps, the likelihood of radiation risk is low with a moderate consequence.

Number	Risk	Consequence	Probability
R-1	Parameter degradations shown on specification sheets differ to the actual situation.	Moderate	Moderate
R-2	Radiation effect are more severe than expected.	Moderate	Moderate
R-3	Internal charging occurs.	Critical	Moderate
R-4	The under designing of instruments by outside contractors.	Critical	High

13.1.9 Structural

The separation system described in Section 11.4.5, is a critical part of the structure. If this system fails, the mission fails too. Possible redundancies in the system are a second motor to retract the inner ring of the system, separating the outer ring. The Lightband system is flight proven and has a TRL of 9. Therefore, the probability of failure is low.

Furthermore, there is the risk of a meteorite impact on critical structure elements. However, after launch, the loads encountered by the spacecraft are relatively low. The number of critical structural elements is therefore reduced, once in orbit. Material imperfections can be a catastrophic factor for a spacecraft structure, as usually components have a small thickness. They have a high probability of occurrence and therefore special attention has to be paid to reduce the risk of material imperfections in spacecraft structures. This risk can be mitigated by extensive testing, but takes money from the budget. It will reduce the probability of occurrence to low.

Failures in joints between structure components can also have catastrophic effects on the spacecraft structure. However, joints for materials used in this study have been flight proven many times, the probability of failure in a joint is therefore low.

Number	Risk	Consequence	Probability
S-1	Failure of separating system	Catastrophic	Low
S-2	Meteorite impact.	Critical	Low
S-3	Material imperfections.	Critical	High
S-4	Failure in joints between structure components	Catastrophic	Low

13.1.10 Planetary Protection

The COSPAR requirements state that *Category III and IV Requirements for Europa flybys, orbiters and landers, including bioburden reduction, shall be applied to reduce the probability of inadvertent contamination of an European ocean to less than 1×10^{-4} per mission.* This means that the lander and penetrator need to receive sterilisation before launch. An advantage of the radiation encountered along the way to Europa is another effect on sterilisation. If it is found that sterilisation procedures do not work as intended, they should be re-designed. In that case, the schedule of the mission might be adapted just before launch. This risk has a moderate probability and a critical consequence. Another variant of this risk is that the sterilisation procedure seems to have succeeded, but that in fact Europa is contaminated by the penetrator. The probability of this is low, but the consequences would be catastrophic. Both of these risks can be mitigated by planning, testing and verifying the sterilisation procedures before the actual S/C is sterilised.

Another risk influencing mission success is the location of impact of the penetrator. The impact itself may lead to extreme forces and temperatures for any form of life living within the surface. Therefore, a penetrator might kill organisms in its vicinity. This would destroy evidence of life on Europa. However, as no living organisms are expected just below the surface, the probability of killing these is low. Consequences would be critical. This risk can not be mitigated within the penetrator concept. However, a very soft lander concept could be chosen instead of a penetrator.

Number	Risk	Consequence	Probability
PP-1	Sterilisation procedure found insufficient	Critical	Moderate
PP-2	Europa contaminated with Earthly organisms	Catastrophic	Very Low
PP-3	Europa organisms killed at impact	Critical	Low

13.2 Risk Map

The risks discussed in the above section are presented in a risk map, see Figure 13.1. It may be clear that especially risks S-3, PR-4, S-3, R-4, TD-3, G-5 and I-2 can cause severe problems to mission success, as these have critical or catastrophic consequences and moderate to high probability of occurrence. These risks are linked to failures due to penetrator impact damage, radiation damage, material imperfection damage, under-designed instruments, software bugs, penetrator impact angle and instrument failure, respectively. As can be found in Section 13.1, all these risks have a mitigation plan. The risk mitigation is treated in more detail in the next section.

Probability	Very High				
	High		T-3, PR-4	S-3, R-4	G-5
	Moderate		T-1, G-4, R-1, R-2, P-3, TD-2	A-3, P-2, T-2, PR-2, R-3, PP-1	TD-3, I-2
	Low	G-1	TD-1	A-4, S-2, TD-4, PP-3	A-1, A-2, P-1, I-1, G-2, G-3, PR-1, PR-3, S-1, S-4, PP-2
	Very Low				
	Negligible	Marginal	Moderate	Critical	Catastrophic
	<u>Performance Consequence</u>				

Figure 13.1: Risk map for the unmitigated risks encountered during the mission

13.3 Risk Mitigation Results

Mitigation of the risks is essential to decrease the probability of mission failure to within agreeable bounds. The mitigations, suggested in Section 13.1, all lead to a lower probability of occurrence and/or a lower performance consequence. It can be seen, however, that especially risks I-2 and G-5 cannot be mitigated out of the high-risk zone. Therefore, they are treated in more detail here.

Risk I-2 is associated with penetrator instrument failure at impact deceleration. It is closely related to G-5, which is the risk caused by an imperfect landing on the rough surface of Europa. The main origin of these risks is twofold. Firstly, there is no reference penetrator mission that succeeded to land safely. Secondly, the low-resolution mapping of the surface makes it impossible to select a near-horizontal plain that may act as a landing spot. This combined impact risk could be solved by imaging the South Pole with a high resolution before penetrator deployment. However, it is expected that the roughness of Europa is found up to the scale of meters [Greenberg, 2005], in which case the scale of the landing site still is larger than the scale of the roughness. A way to further mitigate this risk is by designing the penetrator such that it can handle most of the steep slopes encountered during impact, for instance by adjusting the nose sharpness and stiffness. Nevertheless, it will require some luck to land on a sufficiently gentle slope. Finally, an advanced GNC system could be developed that is able to detect a smooth location and precisely land the penetrator there. However, this is not feasible within the given mass and cost budgets.

Ultimately, this risk could be solved by taking multiple penetrators, as this increases the probability that one of them lands on a safe location. This is infeasible for the current mission, as mass and cost

restrictions are too strict.

Probability	Very High					
	High					
	Moderate		PR-2, TD-2	T-1, T-3, P-3	TD-3	I-2, G-5
	Low		G-1, G-2, PR-3	G-4, PR-4, R-2, R-3, R-4,	A-3, T-2, S-2, S-3, TD-4, PP-3	A-1, I-1, G-3, S-4, TD-3
	Very Low			TD-1	A-4, P-2, PP-1	A-2, P-1, PR-1, S-1, PP-2
		Negligible	Marginal	Moderate	Critical	Catastrophic
		<u>Performance Consequence</u>				

z

Figure 13.2: Risk map for the mitigated risks encountered during the mission

13.4 Conclusion of Risk

It was shown that all risks could be mitigated from high risk to moderate or low risk zones, except for two risks associated with surface impact of the penetrator. It follows from the above analysis that there is no clear solution within the selected piggyback orbiter/lander concept to mitigate these risks, without going over the mass or cost budget. Therefore, it is strongly advised to mathematically analyse the different impact scenarios for the penetrator, and accordingly design and execute tests, comparable to those done by ESA [Vijendran et al., 2014]. In this way, it can be found if the mission success of 95 % is still a feasible number. If this is not the case, it should be investigated again if a pure piggyback orbiter or dedicated lander mission could provide sufficient mission success.

14. System Performance

This chapter will discuss the spacecraft performance. In Section 14.1 the spacecraft mass and power budget are discussed. In Section 14.2 the spacecraft configuration is given by CAD drawings and renderings, both showing the interior and exterior design. In Section 14.3 the compliance matrix is formulated, checking if the system requirements have been met. This chapter will end with a sensitivity analysis which is given in Section 14.4.

14.1 Spacecraft Systems Characteristics

In this section the remaining spacecraft performance characteristics mass and power will be discussed. The other spacecraft performance characteristics have already been discussed in their respective section. The mass budget will be discussed in Section 14.1.1 and the power budget will be discussed in Section 14.1.2.

14.1.1 Mass Budget

The mass budget is an important parameter in the design of a spacecraft since it drives the cost to a large extent. The mass budget is much higher than the required 350 kg. This was mainly caused by the high mass of the power subsystem, but also due to the high ΔV budget required for this mission, which translates to a high propellant mass.

The mass budget for the orbiter can be found in Table 14.1. As can be seen the total mass for the piggyback combination which is connected to Clipper equals 704 kg. The margin used in the mass budget is the 20 % ESA margin [ESA, 2014].

Table 14.1: Mass budget for the orbiter

Subsystem	Design Mass [kg]	Margin [kg]	Total Mass [kg]
GNC	6.0	1.2	7.2
Propulsion	17.0	3.4	20.4
Payload	5.0	1.0	6.0
Power	91.5	18.3	109.8
TT & C	18.0	3.6	21.6
Data Handling	10.0	2.0	12.0
Thermal Control	11.1	2.2	13.3
Radiation Protection	44.6	8.9	53.5
Structural	15.0	3.0	18.0
Total Dry Mass	218.2	43.6	261.8
Propellant Mass	289.2	57.8	347.1
Total Wet Mass	507.4	101.5	608.9
Penetrator Mass	79.0	15.8	94.8
Total Mass Added to Clipper	586.4	117.3	703.7

The mass budget for the penetrator is divided into the penetrator itself and the penetrator delivery system. The budgets can be found in Table 14.2 and 14.3 respectively.

Table 14.2: Mass budget for the penetrator

Subsystem	Design Mass [kg]	Margin [kg]	Total Mass [kg]
Payload	1.6	0.3	1.9
Power	1.0	0.2	1.2
TT & C	4	0.8	4.8
Data Handling	1.5	0.3	1.8
Thermal Control	0.5	0.1	0.6
Radiation Protection	0	0.0	0.0
Structural	10.6	2.1	12.7
Penetrator Total	19.2	3.8	23.0

Table 14.3: Mass budget for the penetrator descent stage

Subsystem	Design Mass [kg]	Margin [kg]	Total Mass [kg]
GNC	4.2	0.8	5.0
Propulsion	7.5	1.5	9.0
Power	0.1	0.0	0.1
Data Handling	0.4	0.1	0.5
Thermal Control	0.0	0.0	0.0
Radiation Protection	1.7	0.3	2.0
Structural	5.4	1.1	6.5
Total PDS	19.2	3.8	23.1
Total Penetrator Dry	38.4	7.7	46.1
Total Penetrator Wet	79.0	15.8	94.8

14.1.2 Power Budget

For the power budget of the orbiter, the Telecom phase of Jovian tour is assumed worst case. This because during the manoeuvre phase the propulsion system only uses 36 W for a short period, therefore, this power can be provided by the batteries. The payload uses 0 W in the table, since the time the payload is operational is very short. Therefore it can also use battery power.

Table 14.4: Power budget for the orbiter

Subsystem	Telecom Phase [W]	Maneuver Phase [W]	Eclipse Phase [W]	Jovian Tour [W]	Worst Case Margin [W]	Total Worst Case
GNC	12.0	12.0	12.0	12.0	3.6	15.6
Propulsion	0.0	36.0	0.0	0.0	0.0	0.0
Payload	0.0	0.0	0.0	0.0	0.0	0.0
Power	20.2	20.2	20.2	20.2	6.0	26.2
TT & C	20.7	0.0	0.0	20.7	6.2	26.9
Data Handling	15.0	15.0	15.0	15.0	4.5	19.5
Thermal Control	0.0	0.0	0.0	0.0	0.0	0.0
Radiation Protection	4.0	4.0	4.0	4.0	1.2	5.2
Structural	0.0	0.0	0.0	0.0	0.0	0.0
Total Power	71.9	87.2	51.2	71.9	21.6	93.4

Table 14.5: Power budget for the penetrator (subsystems without power consumption are not displayed)

Subsystem	Power [W]	Duration of Power Consumption [hr]	Energy Required [Wh]
Payload (short)	5.7	12.0	68.4
Payload (long)	0.5	312.0	156.0
TT & C	2.0	0.8	1.6
Data Handling	0.5	288.0	144.0
Thermal Control	1.0	288.0	288.0
Penetrator Total	9.7		658.0

Table 14.6: Power Budget for the penetrator descent stage (subsystems without power consumption are not displayed)

Subsystem	Power [W]	Duration of Power Consumption [hr]	Energy Required [Wh]
GNC	11.0	2.0	22.0
Data Handling	0.5	2.0	1.0
Total descent stage	11.5		23.0

14.2 Spacecraft Configuration

In this section, the internal and external configuration of the orbiter and the penetrator are shown.

14.2.1 Orbiter

The external configuration of the orbiter can be seen in Figure 14.2. The internal configuration of the orbiter can be seen in Figure 14.3. The reaction control thrusters are located on the surface. Two clusters of four and two thrusters are present. Six sun sensors are located in the orbiter. Four of these are located at the four sides of orbiter and two are located at the bottom of the orbiter. The main engine is located below the orbiter to make sure the high temperatures of the engine are not directly transmitted to the rest of the structure. In the bottom box, the fuel tanks and penetrator are located. The helium tanks are stacked on top of the oxidiser tanks which are considerably smaller than the fuel tanks. The top box includes all the payload and the control units. A laser altimeter is included at the nadir pointing side of the spacecraft. The other side includes a radiator for thermal control. The solar arrays are deployable to make the spacecraft fit within the launcher. The solar arrays have a size of 6.7 m^2 and measure $1.87 \times 3.6 \text{ m}$. The panel length is divided in four individual panels with a width of 0.9 m . The strut has a length of 0.45 m such that the folded panel can be stowed to the side of the spacecraft bus. The other spacecraft power components are coloured yellow. The battery is now displayed as a squared box. The battery, however, consists of multiple cylindrical cells and measures $126 \times 144 \times 165 \text{ mm}$. The power conditioning unit is also coloured yellow and measures $235 \times 156 \times 354 \text{ mm}$. The deployment of the solar arrays is visualised schematically in Figure 14.1.

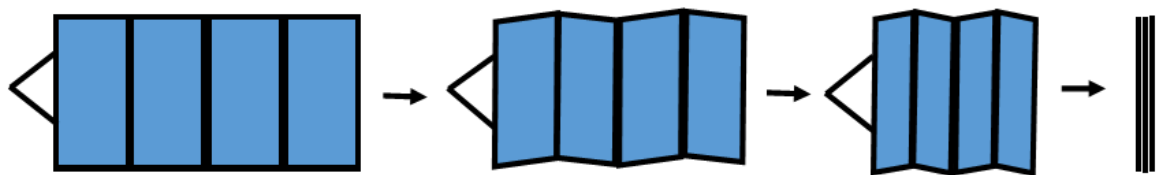


Figure 14.1: Schematic view of the solar array deployment

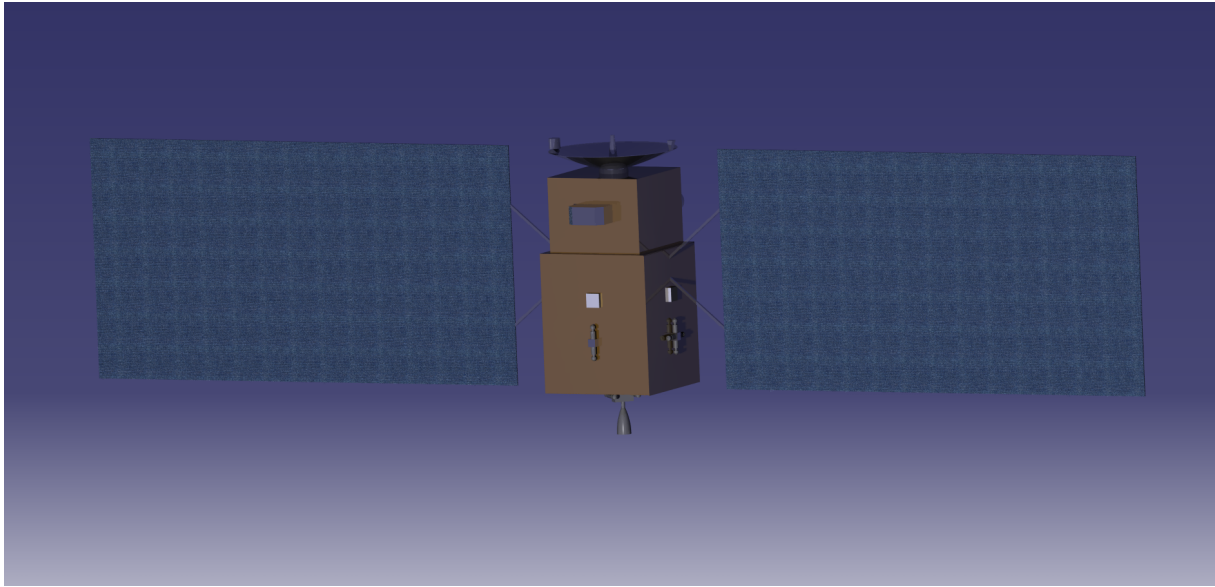


Figure 14.2: External configuration of the orbiter

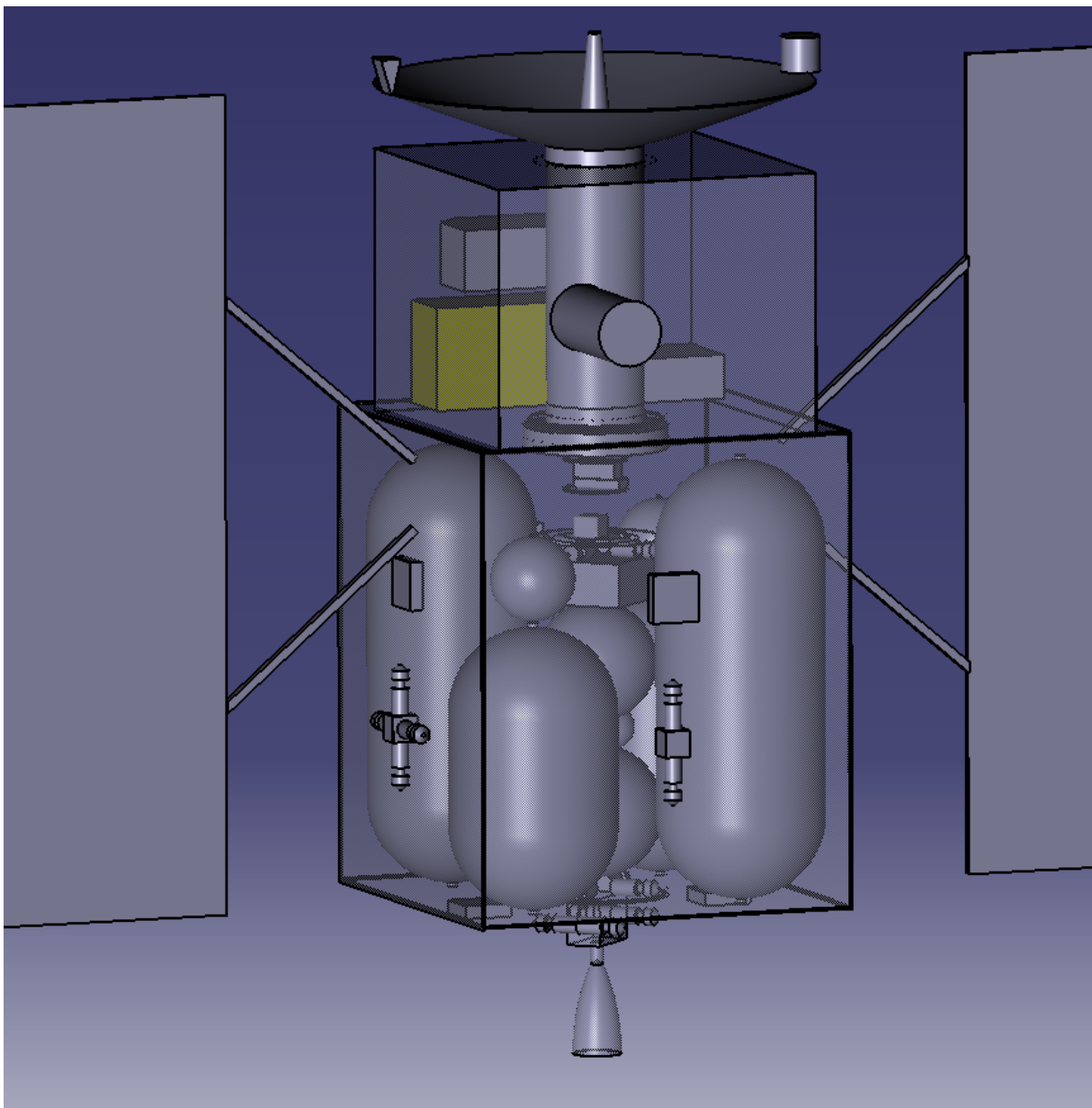


Figure 14.3: Internal configuration of the orbiter

14.2.2 Penetrator

The external configuration of the penetrator can be seen in Figure 14.4. The internal configuration of the penetrator can be seen in Figure 14.5. Four roll control thrusters are located at the back of the penetrator. The yaw and pitch control thrusters are located in front and at the back of the penetrator. The pressurant tanks are located between the oxidiser and fuel tanks to minimize volume. The control unit and batteries of the descent stage are located in the front of the descent stage. Inside the payload bay, all instruments are located. The cold bay is positioned in front, which includes the drill. The middle bay includes the all instruments which do the analysis of the surface samples. The rear bay is the "long life" bay, which includes telemetry, power and seismometer.

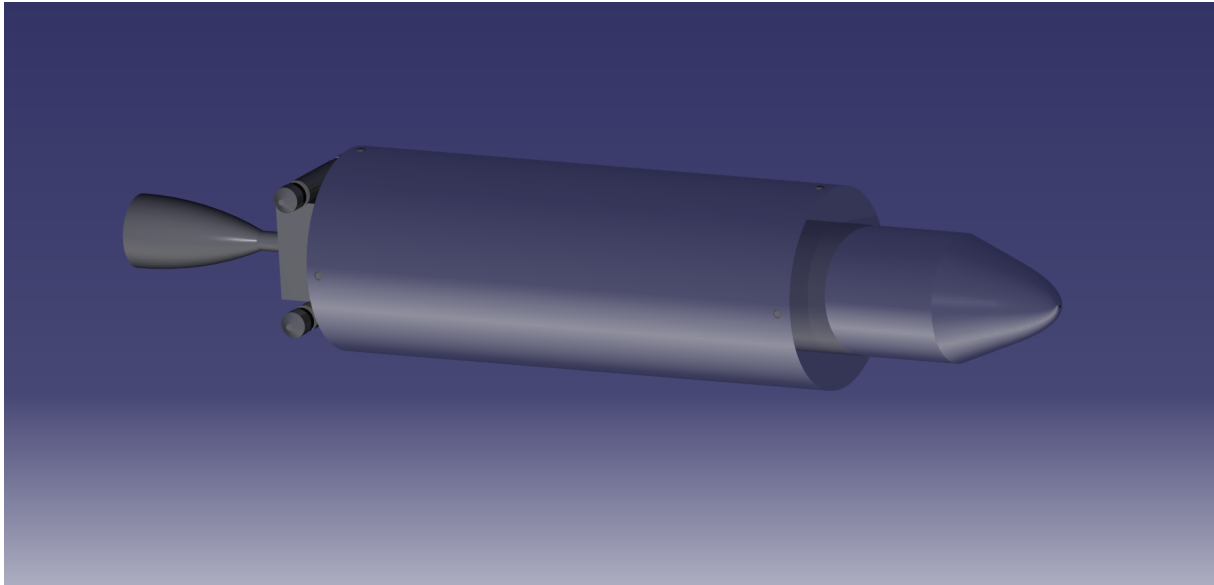


Figure 14.4: External configuration of the penetrator

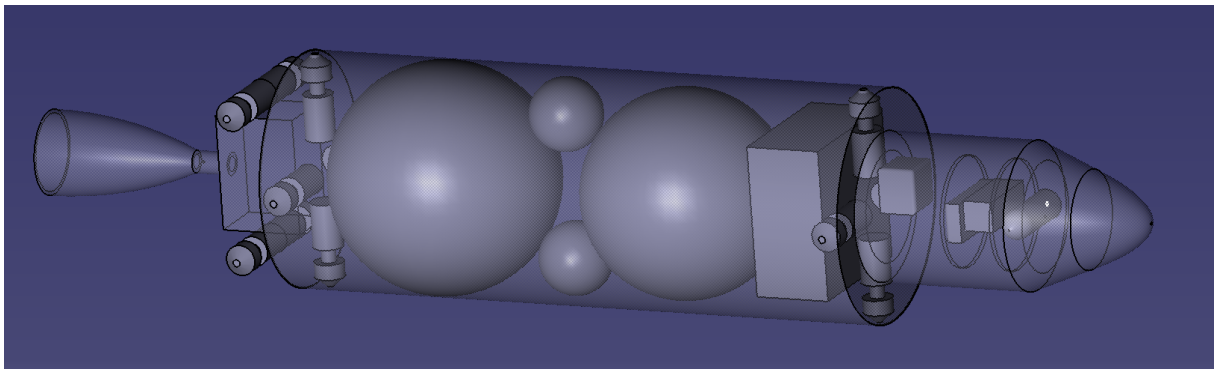


Figure 14.5: Internal configuration of the penetrator

14.3 Compliance Matrix

In this Section it is checked whether the system requirements have been met in the design. This section starts with the actual compliance matrix, after which a feasibility analysis is performed to check which modifications are required to meet the requirements which were not fulfilled initially. Finally, the verification and validation procedures are given. These describe how the proof will be obtained that the system meets the requirements imposed on it.

14.3.1 Compliance Matrix

The compliance matrix for the system requirements can be found below. A ✓ is used that a requirement has been met. The actual value is given as well for the requirements that involve a number.

Number	Requirement	Met?	Value
SYS-PERF-01O	The measurement duration shall be 36 [days] for the orbiter.	✓	36 [days]
SYS-PERF-01P	The measurement duration shall be 14 [days] for the penetrator.	✓	14 [days]
SYS-PERF-02	Launch date shall be no later than November 2022 together with Clipper	✓	
SYS-PERF-03	The total mission mass shall not exceed 350 kg including margins.	✗	704 [kg]
SYS-PERF-04	The maximum volume in stowed condition shall not exceed 1 x 1 x 3 [m].	✓	0.8 x 0.8 x 1.6 [m]
SYS-PERF-05	The spacecraft shall include and operate the science payload.	✓	
SYS-PERF-06	All equipment used shall be at minimum of TRL 6 by 2017.	✓	
SYS-PERF-07	The system shall be able to send and receive information with the use of NASA's deep space network.	✓	
SYS-PERF-08	All spacecraft systems shall be able compatible to be launched with the Atlas V launcher.	✓	
SYS-PERF-09	The system shall be compatible with the interplanetary VEEGA transfer when attached to Clipper.	✓	
SYS-PERF-10	The system shall be designed for a maximum lifetime of 8.5 years.	✓	
SYS-SR-01	Any exposure to hazardous materials stated by the PHMSA [Pipeline and Hazardous Materials Safety Administration, 2015] shall be avoided for all personnel involved.	?	
SYS-SR-02	Mission success shall be larger than 95 % (excluding launch failure).	?	
SYS-SUS-01	The probability of contamination of Europa shall be less than 10^{-4} .	?	
SYS-SUS-02	The end-of-life strategy of the mission shall adhere to the COSPAR regulations.	✓	
SYS-SUS-03	The orbiter shall adhere to COSPAR III regulations.	✓	
SYS-SUS-04	The penetrator shall adhere to COSPAR IV regulations.	✓	
SYS-CST-01	The mission cost shall not exceed 700 [M EUR].	✓	521 [M EUR]

SYS-PERF-02 refers to the launch date which is according to the programmatic possible. **SYS-PERF-06** refers to the minimum TRL 6 level, at this point most subsystems use off-the-shelf space qualified products which are already at TRL 6. Some systems need additional testing but this might still be possible in the coming two years, also given the excess of the cost budget. **SYS-SR-01** is not met at this point as no plan of attack to this requirements has been developed. However, this can be easily performed before the production phase start so this requirement can be met eventually. Requirement **SYS-SR-02** cannot be satisfied yet, since at this point not all information regarding the reliability of the different components is available. This, however, can be done when the mission is continued by contacting the manufacturers of the different components to provide the reliability of the concerning component. Finally the probability of contamination cannot be calculated at this point, however in the next design phase the contamination can be modelled and procedures can be made which ensure that this requirement can be met eventually.

14.3.2 Feasibility Analysis

In this section, the modifications to the system are discussed, which are required to fulfil the failed requirements. As can be seen in the compliance matrix **SYS-PERF-03** is a failed requirement. The

system mass is 703 instead of 350 kg which makes the proposed mission infeasible as a ‘piggyback’ mission. This requirement can be met if the orbiter is dropped and the mission becomes a single ‘piggyback’ mission. A single penetrator can be designed within the 350 kg requirement, however telecommunications would then still pose a challenge. Another modification is that an ASRG should be used instead of a photovoltaic-battery. This reduces the power system mass by more than 60 kg whilst delivering more power. This can only be done if NASA decides to start again with the Pu-238 production. Therefore, the development on the ASRG is not likely to happen before 2022. The mass of the radiation protection can be reduced to lower the total wet mass. This can mainly be done by developing new electronics which are much more radiation tolerant and therefore need less shielding. This however, would mean more development time and could conflict with the early launch date in 2022.

14.3.3 Verification and Validation Procedures

To prove that the proposed system satisfies the requirements imposed on it, verification and validation procedures have to be performed. At this point all the used models have been verified and validated. The next stage in the verification and validation procedures is the planning of the system verification. First the objectives of the verification task have to be established, after which the types of verification activities have to be defined. The potential inputs and outputs have to be determined, and the potential risk associated to (partial) verification failure. Finally, the verification activities need to be planned. The planning is already performed on a top level in Chapter 16. Proof of these requirements can be obtained by either test, analysis, simulation, review of design and similarity.

Telecommunication System Verification Example

The Moonraker mission is a challenging concept, since no other interplanetary ‘piggyback’ mission has ever been designed towards such a demanding environment as around Jupiter. The main problem for this concept concerns the mass budget, which caused some systems to have a significant different design with respect to existing missions operating at the same distance from Earth. For this reason, it is necessary that the compliance of each requirement is proven before the spacecraft is launched. Because of the limited budget extensive testing is not possible, since the mission itself uses already expensive components and systems. Since many subsystems are based on components of existing missions, some requirements can be proven by similarity with existing missions. For example, the orbiter telecommunications subsystem is based on the Mars Odyssey mission. For this reason, a large part of the system is already verified for use in space. However, some specific alterations have been made to make the system comply with the mission specific requirements. Proper analysis and simulation of the new design is also required, to ensure that system alterations are implemented correctly. Mainly the space loss of the telemetry system has to be modelled carefully since the distance to Jupiter is much larger than to Mars, although a Mars mission TC&DH served as a design example.

Power System Verification Example

Secondly, the power system is also based on existing missions. However, the solar array is designed specifically for this mission, using state-of-the-art Gallium Arsenide solar cells which are designed for use in space. Since these cells have not been used on missions in a similar environment, proper review of the design is required to check if the design meets the requirements imposed on it. Furthermore similarity of the design can be checked with existing missions such as Juno and Rosetta, which also use photovoltaic-battery systems. The power conditioning unit of the spacecraft is already space qualified, therefore the requirements imposed on the PCU can be proven by similarity. However, still integration testing is required to check whether the the power system is manufactured in the right manner and if the design is actually capable of delivering the required amount of power.

14.3.4 Verification and Validation Plan

For a good mission, planning of the verification and validation activities is necessary. First the objectives of the verification tasks have to be established. For the Moonraker mission these include the verification of the subsystem and system requirements. Secondly, the type of verification activities needs to be defined. This is already discussed above for two subsystems. Thereafter, the required inputs and outputs have to be determined. This includes the facilities that have to be used as well as the people involved and the money required for the verification activity.

Chosen Verification Strategies for Proposed Mission

For the Moonraker, the facilities will be limited since limited money is available for testing. Most proof of the requirements will be done by either analysis, simulation, or comparing to similar systems (similarity). After determining the required in- and outputs, the potential risks have to be assessed. This refers to what measures need to be taken when verifications fails. For the Moonraker, these risks are very strict, since the development time is limited for launch together with Clipper. Some requirements regarding mass and volume are very strict, as it is a ‘piggyback’ mission. Therefore, activities regarding failed requirements should be planned beforehand for very strict requirements. Another option is to discuss with NASA if slight alterations to Clipper are possible to revise the requirements.

Planning Verification Phase

The next step is to carefully plan the verification activities, which is extra important during this mission, as it has a relatively short design time. The verification activities normally start after the development configuration baseline. Verification in this sense is not limited to qualification, but can also involve development model testing for new technologies which have a lower TRL. For the Moonraker mission, development model testing is minimal since mainly existing systems have been used which are already space qualified. These therefore, by definition, have a high TRL. During the verification process, the production methods and means are also qualified. The verification activities are normally closed by a qualification review [European Cooperation for Space Standardization, 1996]. The final step in the verification plan is the documentation of the plan.

14.4 Sensitivity Analysis

This section gives an overview of the outcome of the sensitivity analysis that was performed. Although a single design has been proposed in this report, there is an uncertainty in the design parameters. When the S/C is developed, several design factors may still change. This is the case, for example, for systems that need verification by testing. Once a system cannot be verified, its design should be adapted. This can lead to a higher mass, cost or require a different operating temperature or power.

In this sensitivity analysis, not all spacecraft parameters are treated. Focus is limited to the most influential design parameters, which are mass, data quantity, cost, power and mission risk. There are close relations between these parameters, but for clarity they are treated separately in the text below.

Mass

Mass is a major parameter for this space mission, driving the design to a great extent. To minimise the S/C mass is a key factor for mission success. This can be done by decreasing the mass of the different subsystems. In general, a lower mass for one subsystem also implies lower mass for the GNC, structure and propulsion subsystems. This, in turn, leads to lower launch cost. The mass can be adapted most significantly by the items listed below.

- **Use of an RTG for power generation**

Currently, the design of the power generation uses solar panels. These have a mass of 74 kg. An RTG could deliver a power of 140 W for a mass of 20.24 kg [Richardson and Chan, 2007], thus saving 54 kg, while providing around 70 W more power than the solar panels. GNC would have a significantly lower moment of inertia to control, leading to less GNC propellant mass or smaller reaction wheels. Finally, the heat coming from an RTG could lower the heat shielding mass with around 4 kg.

- **Propellant with a higher specific impulse**

When new propellant types are developed with a higher specific impulse I_{sp} , the propellant mass can go down. Assuming that the rocket engine mass does not increase, this will lead to a lower propellant tank mass, structural mass and GNC mass. Overall, already when I_{sp} is raised from 320 s to 330 s, propellant mass can go down by around 11 kg. However, if it is dropped from 320 s to 310 s, 11 kg of extra propellant is needed. This most likely causes another mass change of equal order of magnitude by a snowball effect in other subsystems.

- **Different materials for the structure**

Selecting materials with a higher specific strength and/or stiffness would lead to a lower structural mass. For example, titanium alloys or carbon fibre reinforced composites have a higher specific strength than the aluminium currently used. However, manufacturing and processing these materials is more expensive, both in labour cost and equipment cost. As the structure is currently limited

by minimum material thickness, the use of novel materials would highly increase the structure cost, but not directly provide an extremely lightweight solution. On the contrary, in the current design, the mass for the solar panel deployment structure reaches 40 kg. Investing money into researching more lightweight deployment structures might bring significant mass savings.

- **Reduce mission duration** Multiple reasons can be thought of that shorten the mission duration, for example when less scientific data has to be transmitted, or when the period of Europa observation could be shorter. Shortening mission duration would give the penetrator a more lightweight battery. More important, however, would be the mass decrease in radiation protection. Going from a duration of 10 Europa days to 5 Europa days would decrease the radiation shielding thickness from 3 mm to 2.5 mm, saving 10 kg of mass. Also, GNC propellant mass would be less. As this grows nearly linearly with mission duration, the propellant mass could go down by around 2 kg. So, mission duration decrease saves at least 12 kg per 5 Europa days, not even taking into account structural and propellant mass decrease.

It can be seen that many different approaches exist to change mission mass, all leading to a snowball-like effect. This must be taken into account during the coming phases of the design.

Data Quantity

The need for scientific data from Europa is the key driver for mission development. In the ideal case, all interesting parameters and features on Europa would be investigated. In the current design, it was only found feasible to deploy a penetrator with the instrumentation described in Chapter 7. When the mass of the S/C could be increased, two possible strategies can be thought of. Firstly, more scientific instrumentation could be taken, creating more relevant data, and giving the mission a higher scientific data. This would increase the required data rate and/or mission duration, leading to higher mass for both the TC&DH and the propellant, as well as higher power consumption. Secondly, the same instrumentation can be taken, but a higher mass per instrument can be allowed. This would decrease development and radiation shielding cost.

Cost

The effects of a change in mission budget have already briefly been mentioned in the mass and data quantity sensitivity. A decrease in budget would make this orbiter/lander mission infeasible, since even in the current design there is very limited scientific instrumentation mass that can be taken. So, in case of political budget restrictions, either a shorter mission should be developed which only uses an orbiter, or no mission can be developed at all.

When the budget of the mission could increase, for example, if external funding can be found, it is highly suggested to aim for a dedicated orbiter/lander mission to Europa. The current mass of the piggyback design already is too high to be a true piggyback, and a dedicated mission would release the launcher and mass restrictions that are encountered in the piggyback mission. The extra cost could mainly be invested in the development of lightweight radiation protected instrumentation and subsystems, which will eventually give more scientific data for a given mass.

Power Balance

The power balance in the spacecraft is based on the generated and used power. Since the power subsystem has the highest mass of all subsystems, a decrease in required power or increase in power generation efficiency can save mass. The most notable changes that may affect the power balance are given below.

- **Use an RTG for power generation**
See explanation in the mass sensitivity analysis.
- **Development of solar cells with a higher efficiency**
Currently, 33 % efficient solar cells are used in the solar array design. When this would increase to 44 %, the maximum ever achieved in test conditions ¹, the solar panel mass can be decreased from 35 to 25 kg, saving 10 kg of mass on the solar panels. The lower inertia would cause a lower GNC mass too. This technology, however, is currently far from space qualified. To develop space qualified solar cells with a higher efficiency, the mission would likely go over budget.

¹<http://www.ise.fraunhofer.de/en/press-and-media/press-releases/presseinformationen-2013/world-record-solar-cell-with-44.7-efficiency>, [Retrieved: June 19, 2015]

- **Change in the required power**

The major power consumer on-board is the TC&DH subsystem. The required power for this system is $P \cdot \frac{100}{28} + 10$, where P is the transmission power in [W]. Furthermore, the required transmission power increases linearly with bit rate. When an RTG would be used, and 70 W extra is available, the bit rate goes up from 2.9 to 16.7 kbits/s. In practice, part of the extra power should also be used to power an extended package of scientific instruments. When the solar panels do not deliver the amount of power required during the mission, the data rate reduction that follows would make the mission failure risk high, as the 2.9 kbits/s data rate already is just high enough to deliver the required scientific data.

- **Increase in battery energy density**

In the S/C, two batteries of 392 Wh are needed. As described in Chapter 8, the current Li-Ion batteries have a capacity of 116 Wh/kg. However, Li-po batteries are available up to 250 Wh/kg². If these could be space qualified before the S/C qualification test, this would save 3.6 kg.

It can be seen from the above list, that small changes in energy technology may lead to significant mass reductions. However, as many of these technologies have not yet been flight qualified, extensive testing programmes should be set up. This, in turn, would likely make the mission go over budget.

Mission Risk and Margins

The mission is designed to succeed with 95 % chance. Increasing mission risk is equal to lowering this 95 %. Lowering the risk in practice means lowering design safety factors.

- **Reduce structural safety factor**

For the structure, a 1.25 safety factor on yield strength and 1.4 on ultimate were used. Reducing these could save a few kilograms, but an exact number cannot be provided. For the penetrator, the impact forces are difficult to determine, as little is known about the Europa surface. Therefore, the mission risk greatly depends on the safety margin taken for the impact structure. As only one penetrator is deployed, there is no redundancy on impact.

- **Reduce power generation safety factor**

It is also worthwhile to investigate lowering the margins on the power system. A 30% power generation margin was taken for the solar panel design. If this margin were dropped, it would lead to a mass saving in the solar panels of over 10 kg. Furthermore, the support structure of the panels would decrease by around 1.5 kg. Taking the snowball effects into account, a higher risk in power generation would easily save more than 10 kg on total mission mass.

- **Reduce/increase mass margins**

Currently, a wet mass margin of 20 % is taken into account. This would mean that in the ideal case, the ultimate wet mass at launch could be tens of kilograms lower than designed. Therefore, when this margin would be reduced, more dry mass is available for a given wet mass. This dry mass could be used to do more radiation shielding, take more scientific equipment, or reduce launch cost. However, this would come with higher mission risk, as a too optimistic mass estimation can lead to under-designing the GNC, structure, and propulsion systems.

- **Reduce radiation design margin**

In the radiation protection design, safety is guaranteed by a radiation design margin used by ESA and NASA. This factor assumes the dose received by the components is twice as high as calculated. In the extreme case, assuming this margin would be dropped entirely, the shielding would go from 3 mm to 2.2 mm thickness Copper-Tungsten. This would save 17 kg of shielding material, leading to lower GNC and structure mass. Most notably, the propellant mass can decrease by 34 kg. Thus, more than 51 kg can be saved at the cost of taking a higher radiation shielding risk.

As expected, reducing and increasing safety margins has a major effect on spacecraft mass. It is therefore noted here, that a decrease in design safety factor may cause a mass reduction that is so high, that it eventually enables all subsystems to be scaled down and the mission cost reduces. Therefore, lowering the safety factors may increase the probability of failure, but decrease cost and therefore the risk.

²<http://www.amicell.co.il/batteries/rechargeable-batteries/our-extreme-high-energy-density-lithium-polymer-series/>
[Retrieved: June 19, 2015]

Conclusion

From the sensitivity analysis, five main conclusions can be drawn.

Firstly, it is clearly shown that any mass growth in a subsystem causes a snowball effect that can easily bring the piggyback mission in danger. Therefore, if any unexpected dry mass increase of around 10 kg occurs, it is suggested to create a dedicated mission instead of a piggyback one.

Secondly, when more mass and/or budget is available, it was shown that the amount of scientific data can increase. However, this would also give the need for an extended mission duration and a more capable TC&DS system.

Thirdly, it was found that the current design is close to the budgeted cost. Therefore, a cost increase would create a need for increased external funding, which may change the customer requirements. A decrease in cost is not likely to be achieved, as no precedents of the current mission were developed. Therefore, little off-the-shelf technology is available.

Fourthly, the large influence of the power generation system on the design was shown. No RTG is currently used in the design, but this would make the mission feasibility higher, as the mass of the structure, GNC, TCS and power system can be reduced.

Finally, the current design margins and safety factors contribute significantly to a high S/C mass, which leads to a high cost and thus a high risk. Therefore, it may be wise to have a critical look on these safety factors, since the cost reduction that is achieved by lowering them may counteract the increase in mission failure. The effect on risk is therefore not easily estimated.

15. Mission Development & Operations

15.1 Manufacturing, Assembly and Integration Plan

In this section, the manufacturing, assembly, and integration of the subsystems is elaborated on. Subsection 15.1.1 discusses the general manufacturing, assembly and integration plan used for this mission. In Subsection 15.1.2, the components that need to be manufactured and the companies that are selected are discussed. Subsection 15.1.3 elaborates on possible risks for the manufacturing locations of the selected companies. The assembly and integration for this mission is discussed in more detail in Subsection 15.1.4.

15.1.1 General MAI Plan

Controlling the manufacturing, assembly and integration is a vital part for mission success. Figure 15.1 shows the main aspects of this plan. When the spacecraft design is finished, all components have to be manufactured. The specialized companies that can make those advanced space parts are located all over the world. Therefore, after manufacturing, all components need to be shipped to a central assembly location. After assembly, integration and verification needs to be performed. In this phase it is made sure all components behave as expected. Tests are performed in different conditions to see if all requirements are met. Then the spacecraft is handled with great care, and transported to the launch facility.

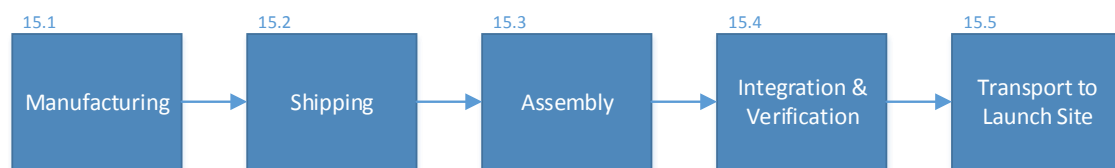


Figure 15.1: Main MAI flow

An elaboration on the manufacturing part is found in Figure 15.2. When all components are identified, a division can be made between off the shelf products and custom made products. For off the shelf products, the manufacturing is taken care off by the company. The products do need to be tested on meeting the requirements. For custom components, first companies that are capable of manufacturing those need to be identified. The manufacturing procedure and requirements of the product need to be discussed with the manufacturing company, and when agreed upon the specifications, the order can be given to the company. After the production, the specifications of the product need to be verified. If all requirements are met, the product can be shipped for assembly.

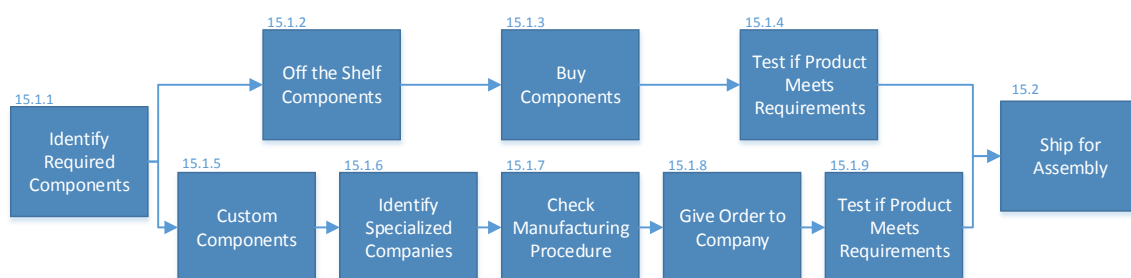


Figure 15.2: General manufacturing flow

15.1.2 Subsystem Manufacturing

GNC Subsystem

Regarding the orbiter, the sun sensors can be bought off the shelf for the GNC system. The star tracker and SIRU have to be developed further, based on an existing design. This can be done by the companies of the base design, Berlin Space Technologies and Northrop Grumman respectively. Numerous other players exist in the market for star trackers so in case the company does not exist any more in the coming years, other companies can take over. For the SIRU, another big player called Honeywell could possibly take over in the event Northrop Grumman goes bankrupt. Therefore, no critical paths exist. For the penetrator the SIRU is identical to the one used in the orbiter.

Propulsion Subsystem

The propulsion system requires fuel lines, a main engine, 12 reaction control thrusters for the orbiter, 12 reaction control thrusters for the penetrator, pressure transducers, joints and valves, filters, one oxidizer tank and one fuel tank for the penetrator, two oxidizer tanks and two fuel tanks for the orbiter, two helium tanks for the orbiter, and two helium tanks for the penetrator. With exception of the reaction control thrusters, all components have to be custom designed to meet the specifications. Three specialised companies have been selected that are capable of delivering the required components; Airbus Defence and Space, Aerojet Rocketdyne, Moog-ISP.

Scientific Instrumentation

The selected instruments of the penetrator are: a micro imager from Physikalisches Institut which is the University of Bern, the SILAT from Cosine Research BV, a drill from the Hong Kong Polytechnic University, a descent camera from the Mullard Space science laboratory, a geology package from the International Research School of Planetary Sciences, and a seismometer and magnetometer from the Mullard Space Science Laboratory. The instruments do not need further development, and can therefore be bought off-the-shelf.

Power Subsystem

The power subsystem contains many parts which have been found to be obtainable off-the-shelf. These components are: array power regulator, battery charge/discharge regulator, telecommunications command & data handling, thermal knife actuator, heater power distributor, equipment power distributor, modular medium power unit. Currently the company Terma is selected to provide these components. For the power generating unit, the solar panel, a custom solution is required. Figure 15.3 presents the logical order in which materials have to be applied in the manufacturing process to get the desired result. The selected company for the solar cells is SolAero, and for the lithium-ion cells is Sony.

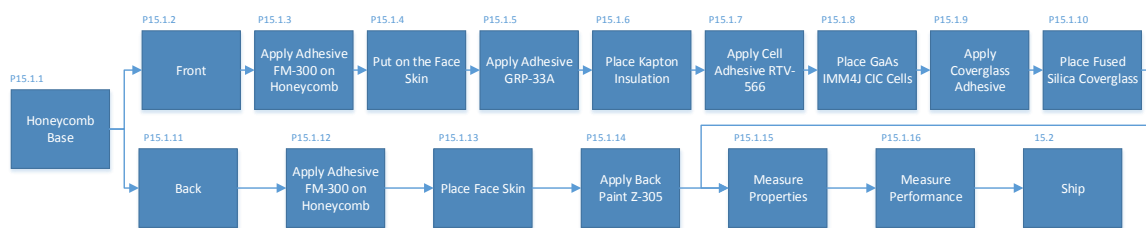


Figure 15.3: Solar panel component order

Telecommunications, Command & Data Subsystem

The components for telecommunications can be divided into three main groups; antennas, signal routers, signal generators. The specific components that need to be manufactured are found in the hardware diagram in Section 9.5. The data handling components will be manufactured by BAE Systems, and the telecommunications components are obtained from NEC.

Thermal Control Subsystem

For thermal control the following components are required: paint & coatings, kapton and aluminium. Aluminium is generally available around the globe, and for kapton Dupont is selected as manufacturer.

Structural Subsystem

The structure subsystem contains mainly custom made components. The required main components

are: penetrator structure, penetrator deployment structure, lower central cylinder, top central cylinder, subsystem base panel, two honeycomb main tank support beams, honeycomb central cylinder support beams, Clipper attachment panel, Clipper piggyback separation structure, upper main tank support, penetrator descent stage. These parts can be manufactured separately. Companies capable of manufacturing these components include Hexcel for the honeycomb structures, Planetary Systems Corporation for the separation system, and RUAG Space and Astro Aerospace for the remaining structures.

Radiation Protection Subsystem

The material CW80 is selected to provide shielding from radiation. This material consists for 20% of copper, and 80% of tungsten. The manufacturing of the alloy is to press the tungsten, sinter the pressed compact at high temperature, and infiltrate with copper ¹. The shielding will consist of boxes and panels. Companies capable of manufacturing these include Eagle Alloys Corporation and NAECO Materials Technology Solutions.

15.1.3 Shipping Separate Components

Most components are made at different locations around the globe, and need to be transported from the manufacturer to the assembly facility. Some locations might not be safe due to political reasons. To see if any critical problems could arise, the locations of the manufacturers are investigated. The two main manufacturers for GNC are Northrop Grumman, facilities in the USA and UK, and Berlin Space Technologies, which is unsurprisingly located in Berlin. For the propulsion subsystem, Airbus Space and Defence has facilities all over most of western Europe. Aerojet Rocketdyne is placed in the USA, and Moog-ISP has got the headquarters in the USA as well. The scientific instruments come from Swiss, the Netherlands, Hong Kong, Italy and the UK. The power subsystem components come from Denmark, the USA and Japan. The telecommunications and data handling components are manufactured in the US and in the UK. For the thermal subsystem multiple manufacturers are capable of delivering the product in Europa and outside of Europe. Concerning the structures components, RUAG Space is placed in Switzerland, Astro Aerospace in the USA Planetary systems Corporation in the USA, and Hexcel can distribute from Belgium. The current selected companies for radiation shielding are located in the USA.

No problems should arise regarding the location of companies. All are placed in steady areas of the world. No critical manufacturing path exists for this mission.

15.1.4 Assembly & Integration

After all manufactured components are shipped to one location, they can be assembled. First only the subsystems are assembled. The sequence is shown in Figure 15.4. After every successful assembly of a subsystem, already testing can be performed. The structure is assembled first, together with radiation protection as all other subsystems will be attached to these components. Then the propulsion subsystem is assembled. The propulsion components are assembled first because the methods used to attach them to the structure are not compatible with electronic components [Wertz et al., 2011]. Then the power subsystem with the heavy deployable panels is installed. Next the thermal subsystem is put into place. Then the command and data handling subsystem is put into place and connected to the power and thermal subsystem. After that the GNC sensors and actuators are positioned and aligned. Last the telecommunications components are placed. The sequence is the same for the orbiter and the penetrator.

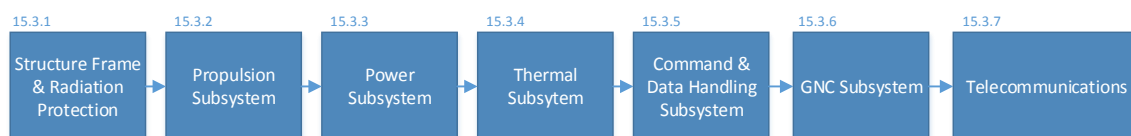


Figure 15.4: Outline of spacecraft subsystem assembly sequence

The outline of the integration sequence is shown in Figure 15.5. Bus level integration is when the assembly of the subsystems is completed. A functional test of the complete system is performed. If this succeeds, the payload is integrated, and testing is repeated.

¹<http://www.eaglealloys.com/copper-tungsten-alloys/> [Retrieved June 21, 2015]

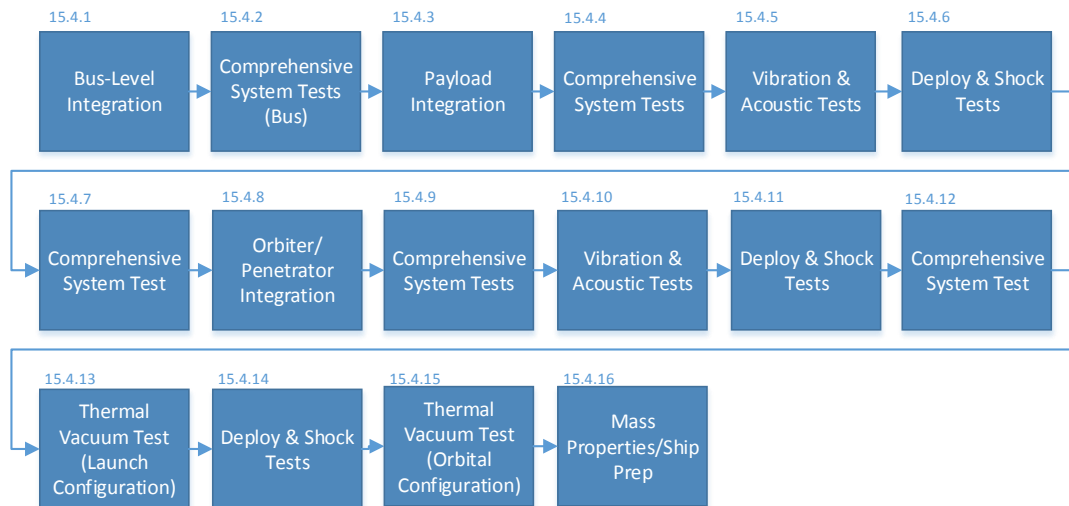


Figure 15.5: Outline of spacecraft integration and verification sequence

The comprehensive system tests are meant to functionally test the installed units and subsystem. Antenna testing, which consists of pattern tests and closed-loop tracking, and attitude control tests which verify attitude control responses and mode transition behaviors are part of the system tests. At block 15.4.5, low frequency sine wave sweep testing and acoustic testing is performed. At block 15.4.6 the release devices are fired and the first motion is verified. Also the re-stowage of the deployables is performed. If every test is successful, the mass properties are determined in block 15.4.16, and the spacecraft is prepared for shipment to the launch facility.

15.2 Operations and Logistic Concept Description

A complex space mission like a mission to Europa is a large operation and involves a large number of logistical operations. To allow for a smooth mission, an operations and logistic concept is described here. At first, the components that have been designed needs to be tested and is described in Section 15.2.1. The production phase concern mainly about logistics, and the actual mission is more focussed on operations. The production phase is discussed in Subsection 15.2.2 and the operational logistics is discussed in Subsection 15.2.3.

15.2.1 Testing logistics

The testing logistics is displayed on top in Figure 15.6. Testing is of vital importance for this mission as several parts have not been used before in such a high radiation environment. That is why first the parts need to be developed so they are expected to meet the requirements. After that the testing environments need to be developed so the parts can be tested in a similar way they will be used during the mission. Next, the developed parts need to be tested in there created environments and are then recovered. It can be seen now whether they have withstand the testing environments and if they can be used as components during the mission. If not, new designs need to be developed and can be tested again next.

15.2.2 Production logistics

During the production of a spacecraft a lot of logistics is involved. A good way to represent this logistical operation is a flow diagram. This diagram can be found in the middel of Figure 15.6. First of all, the manufacturing of different components must be allocated to different subcontractors. For an ESA mission it is expected that different systems and instruments will be manufactured in different member countries of the ESA. The next step is to allocate resources to achieve the manufacturing process, this will mainly be done on the level of the contractor in this case. Furthermore, the raw materials also have to be allocated and distributed to the different manufacturing sites.

Now the preconditions for manufacturing have been met, the actual production can start. This includes processes as curing, machining and shaping of materials. After which parts are assembled, which thereafter are assembled to subsystems. When the subsystems are finished, they have to be verified and

validated to check whether the requirements have been met. This can be performed for example with hardware-in-the-loop testing.

As the subsystems are produced on multiple locations around Europe, all these systems have to be transported to a lander assembly hall where the lander is assembled. This can be mainly done by road transport because of the limited cost involved, however, special care has to be taken for the transport as the spacecraft is quite vulnerable. For example, the high gain antenna of the Galileo spacecraft did not deploy due to damage during the road transport from the assembly hall to the launch site ².

When all the subsystems have arrived at the assembly station the lander can be assembled. After the assembly, the assembled lander has to be verified and validated to check whether the requirements have been met. When the lander is assembled, it can be transported to the assembly station of the orbiter (Clipper). Because the orbiter is assembled in the United States, as it is a NASA mission, the lander has to be transported across the ocean. This can be done preferably by plane since this would save time.

After the lander has arrived in the orbiter assembly station it has to be integrated with the orbiter. After the integration the complete system (orbiter and lander) has to be verified and validated to check whether the requirements have been met. Then the system should be transported to the launch site, where again special care has to be taken to prevent transport damage.

At the launch site the system (orbiter and lander) has to be integrated on top of the launcher after which again verification and validation has to be performed to check whether the system functions as prescribed. Finally, the launcher has to be transported to the launch pad after which the spacecraft can be launched and the operational phase starts.

15.2.3 Operations

During the operational phase of the mission, logistics is of minor importance. Also maintenance as for aircraft is not applicable to spacecraft. However, maintenance is possible when for example the launch is delayed. The operations block diagram is visualised in a flow diagram which can be found in Figure 15.6. As can be seen in the figure, the operation diagram consists of three segments which include control, ground and space segment.

Space Segment

To start with the space segment all main orbiter systems are connected with the orbiter interface. These are the GNC system of the orbiter and the two antenna's. One for communicating to deep space network in the ground segment and one for communicating to penetrator. The GNC thrusters are connected to the orbiter GNC system as they can be used to control the spacecraft attitude and location in space. The GNC system knows where it is in space by using its sensors who give input to the GNC system. Via the low gain antenna's of the orbiter and penetrator, the two interfaces of the orbiter and penetrator can communicate. The penetrator also has a GNC system during the first phase of its mission when it is descending to Europa's surface and thus also has the GNC thrusters and sensors. It also carries scientific instruments which collect the vital data which is desired by the scientist in the control segment. The high gain antenna of the orbiter connects to the deep space network which is in the ground segment.

Ground Segment

The data sent by the spacecraft antenna is received by NASA's deep space network. The data is then received and processed at spacecraft ground control. Ground control is in charge of the nominal mission and can give direct commands to the spacecraft through the deep space network. Ground control also processes the data received by the spacecraft and sends it to the science team for further processing. Ground control is also in charge of transmitting software updates as coded by the programming team to the spacecraft.

Control Segment

The control segment consists of three main parts. First of all the science team which receives processed data from the spacecraft ground control. The science team then interpreters this data and makes decisions for the rest of the mission. In case of a movable lander this can be the new location of the lander. The programming team then delivers the software to the spacecraft ground control. Then the software is transmitted to the spacecraft by the deep space network and is then installed via the interface.

²<http://www.spaceflightnow.com/galileo/030921galileohistory.html>[Retrieved May 12, 2015]

Mission Alteration

The control system as described in this section makes the spacecraft variable in its performance. For example if the scientific instrumentations do certain measurements which are communicated through the interface to the ground control. In the control segment, then a new mission phase can be designed and programmed which is then again sent to the spacecraft after which the interface installs the new software. In the space and ground segment all the arrows are in both directions which means that all systems can interact with each other. However, the control segment is only one-way, because, the new mission phase has to be checked and programmed in sequence.

The Reliability, Availability, Maintainability and Safety (RAMS), of the spacecraft is performed and presented in this section. The team analysed the possible safety critical functions, established a redundancy philosophy, documented methods for computing the reliability and availability and planned the maintenance of the spacecraft. These characteristics are presented below in Sections 15.2.4, 15.2.5, 15.2.6 and 15.2.7.

15.2.4 Safety Critical Functions

Safety is defined, according to H. Hamman [Hamann et al., 2011], as the freedom from hazards to humans and equipment. The means to achieve safety is called safety engineering. Safety engineering protects the loss of life or injury to human beings, damage to the system being designed or developed, damage to other systems and damage to the environment. With these definitions in mind, the team collects a set of fundamental safety critical functions which the spacecraft shall perform. Following this, the functions are used to derive requirements that will reinforce the reliability of the spacecraft. Table 15.1, displays the derived requirements.

1. Securing the spacecraft in the launcher
2. Perform Earth flybys
3. Detach from Clipper
4. Detach penetrator from the orbiter
5. Offer protection to instruments during the impact on Europa
6. Shield instruments and subsystems from heat and radiations
7. Provide enough power to subsystems
8. Perform a controlled crash on the surface of Europa at EOL

Table 15.1: Derived requirements to achieve the safety critical functions.

Requirement ID	Requirement
SYS-RAM-01	The spacecraft shall be secured in the launcher such that it will not jiggle around during launch, causing damage to the system.
SYS-RAM-02	The spacecraft shall be put on a trajectory such that collisions are avoided with any spacecrafts orbiting Earth while performing the Earth flybys.
SYS-RAM-03	The detachment from Clipper shall be done such that no damage is induced to the structure or subsystems of Clipper.
SYS-RAM-04	The penetrator shall detach from the orbiter such that no damage is caused to the structure or subsystems of the orbiter.
SYS-RAM-05	The penetrator shall protect the instruments on board during the impact.
SYS-RAM-06	The system shall provide shielding from heat and radiation to the instruments and subsystems such that they survive till EOL.
SYS-RAM-07	Needed power levels by the instruments and subsystems shall be available throughout the mission.
SYS-RAM-08	The architecture of the system shall be such that enough redundancy is achieved.
SYS-RAM-09	The orbiter shall perform a controlled crash on the surface of Europa as an EOL strategy.

15.2.5 Redundancy Philosophy

The spacecraft is to survive harsh environments; these range from the warmth of the spacecraft during the Venus flyby to the icy conditions at Europa. Furthermore, the spacecraft will be exposed to high doses of radiation during its mission at the Jovian system. Therefore, proper redundancy measures shall be taken to assure the success of the mission. The redundancy philosophy of each subsystem is considered and described below.

Guidance Navigation and Control

The GNC subsystem is crucial for the success of the mission. It is the subsystem which will point the orbiter in the right direction for relaying data from the lander; the utmost important aspect of the mission. Furthermore, the redundancies implemented by the GNC subsystem are divided in two sections, namely for the orbiter and the lander.

Orbiter

Four redundancy measures have been taken to ensure the GNC subsystem of the orbiter will carry out its tasks successfully for the duration of the mission.

1. A Siru system is used. This is a multi redundant system composed of four gyroscopes and four accelerometers that have a high radiation resistance. Further information about the Siru system can be found in Section 5.1.
2. Two star trackers are taken on board for redundancy. These star trackers will undergo further development in later phases of the project to increase their radiation tolerance.
3. Six Sun sensors will be taken on board for redundancy reasons. Furthermore, these sensor have a high radiation resistance.
4. Twelve thrusters will be implemented to provide pure moments.

Penetrator

Similarly, the penetrator will implement two redundancies.

1. An identical Siru system will be placed on the penetrator.
2. An identical series of twelve thrusters will be implemented on the penetrator.

Power

The power subsystem will implement the following redundancies:

1. 2 solar arrays
2. Dual hot redundancy per array
3. 2 batteries, redundant for the duration of measurements at Europa
4. A charge/discharge regulator per battery
5. 2 command and telemetry handling units
6. 2 mean error amplifier regulating the voltage of the spacecraft's bus
7. 2 equipment power distribution units
8. 2 heater power distribution units
9. 2 thermal power distribution units

Propulsion

The propulsion subsystem will implement the following redundancies:

1. 2 pressure transducers per Helium tank
2. 3 pressure transducers per oxidiser tank
3. 2 pressure transducers per fuel tank
4. cross link between fuel tanks
5. cross link between valves

Telecommunications and Data Handling

With telecommunications subsystem being of high importance for the mission success, a lot of redundancy is applied. Below, a list of all components and their redundancies are presented.

- | | |
|----------------------------------|--------------------------------------|
| 1. 1 high gain antenna | 9. 1 hybrid coupler |
| 2. 1 medium gain antenna | 10. 1 diplexer |
| 3. 2 low gain antennas | 11. 2 UHF diplexer |
| 4. 1 waveguide transfer switch | 12. 2 Ultra Stable oscillator |
| 5. 1 coaxial transfer switch | 13. 2 Sufficiently stable oscillator |
| 6. 2 noise filters | 14. 2 Small deep space transponder |
| 7. 2 band pass filter (X-band) | 15. 2 Solid state power amplifier |
| 8. 2 band pass filter (UHF-band) | 16. 2 UHF transceiver |

Furthermore, cross links are applied between the deep space transponders to increase redundancy. This will prevent the subsystem deeming itself unusable in case of one of the deep space transponders failing.

Thermal

The thermal subsystem will implement two radiators in both, the orbit and penetrator to assure redundancy.

Radiation Shielding

The radiation system is crucial for the success of the mission. However, since the radiation shielding is purely adding additional material thickness to the design to keep harmful radiations from delicate electronic circuits on board the spacecraft, hence no redundancy can be assumed. However, a factor of 2 will be used when sizing the shield. Furthermore, 3 dosimeter will be placed in 3 different locations on the spacecraft to monitor the radiation level thoroughly.

Structures

Similarly to the radiation subsystem, the structures subsystem cannot have redundancies per say since the structure is sized to carry launch loads (highest loads expected for the life of the spacecraft). However, safety factors (SF) are accounted for in the design and are as follow:

1. 1.25 SF for yield strength
2. 1.40 SF for ultimate strength
3. 1.40 SF for buckling

15.2.6 Reliability and Availability

The definition of reliability according to [Wertz et al., 2011] is: "The probability that a device will function without failure over a specified time period or amount of usage" [Wertz et al., 2011]. Distinction can be made between basic reliability and mission reliability. Basic reliability relates to "without failure of any kind" [Wertz et al., 2011], whereas mission reliability relates to "without failure that impairs the mission" [Wertz et al., 2011].

With these definitions in mind, the team documents a model by Alex J. Ruiz Torres presented in [Ruiz-Torres et al., 2010], analyse the redundancy philosophy and deduce the reliability of each subsystem.

Reliability model

The assumptions used in this model [RuizTorres et al., 2010] are as follow:

1. Each subsystem is composed of a number of modules in series.
2. A common level of reliability per component and a common level of redundancy across the modules. Thus all the modules will have the same number of parallel components.
3. All components are independent and identically distributed.
4. All redundant systems are in use simultaneously.

The inputs per subsystem then will be as follow:

1. p_j - Average reliability per component of subsystem j
2. k_j - Basic functional subsystem number of components of subsystem j
3. m_j - Number of critical functions (number of modules) of subsystem j
4. n_j - Redundancy level for subsystem j

Finally, the output per subsystem will be as follow:

1. A_j - Additional components for subsystem j. $= m_j(n_j - 1)$
2. F_j - Expected failures for subsystem j. $= (1 - p_j)/p_j * (A_j + k_j)$
3. R_j - Mission reliability of subsystem j. $= (1 - (1 - p_j)^{n_j})^{m_j}$

Furthermore, it is assumed that the vehicle is composed of flight hardware elements (FHEs) and in turn these are composed of subsystems. In addition, a set Γ is assumed to contain all subsystems in the architecture of the vehicle.

The mission is assumed to have two phases, the first with the option to abort the mission and the second without an option to abort, meaning failure will lead to loss of the vehicle. Each subsystem is

assumed to be critical for one of the two mission phases. Finally, set Γ is split into two subsets. Namely, $\Gamma(a)$; that includes all subsystems that must function properly during the first mission phase and $\Gamma(b)$; that includes all subsystems not in $\Gamma(a)$ where its failure will cause loss of the vehicle. With these definitions and assumptions in mind, the probability of mission success can be computed using Equation 15.1.

$$P_{ms} = \int_{j \in \Gamma(a)} R_j \times \int_{j \in \Gamma(b)} R_j \quad (15.1)$$

The model implements a vast amount of assumptions that stray from the real life case, however, it still manages to capture a realistic "worst case scenario" hence still providing useful insight into the reliability of the system [RuizTorres et al., 2010]. The next step would be to gather data on the components used in each subsystem. This would enable the computation of the reliability of the system.

15.2.7 Maintenance

Maintenance of a system can be split into two categories; namely planned and unplanned maintenance [RuizTorres et al., 2010]. However, it is trivial that for an interplanetary mission no physical maintenance can be done post launch. Therefore, only maintenance on the ground and software maintenance is considered in this analysis.

Ground Phase Maintenance

During the manufacture of the system, maintenance by definition is not carried out since the system is still being built. However, maintenance activities can be carried out post completion of the system. The list below, contains these activities.

1. Maintenance of all subsystems when transporting the spacecraft.
2. In case of launch delay, all systems must undergo regular checks to ensure they are still at nominal state.

Flight Phase Maintenance

Since the mission is bound for the Jovian no physical maintenance will be carried out. However electronic maintenance can still be carried out from the ground stations on Earth. Such activities include:

1. Regular software updates and bug fixes
2. Unloading of momentum
3. Subsystem checks
4. Monitoring of radiation levels

15.3 Sustainable Development Strategy

This section addresses sustainability approach of the complete mission. The mission is placed in category III & IV of the COSPAR regulations. An important requirement stated from COSPAR is that the probability of inadvertent contamination of an european ocean should be less than 1×10^{-4} per mission [COSPAR, 2005]. COSPAR recommends that a report is handed to them containing information on the sustainability approach of the mission. The following aspects are addressed [COSPAR, 2005]:

1. The estimated biological burden at launch, the methods used to obtain the estimate (e.g., assay techniques applied to spacecraft or a proxy), and the statistical uncertainty in the estimate.
2. The probable composition (identification) of the biological burden for Category IV missions, and for Category V restricted Earth return missions.
3. Methods used to control the biological burden, decontaminate and/or sterilize the space flight hardware.
4. The organic inventory of all impacting or landed spacecraft or spacecraft-components, for quantities exceeding 1 kg.
5. Intended minimum distance from the surface of the target body for launched components, for those vehicles not intended to land on the body.

-
6. Approximate orbital parameters, expected or realized, for any vehicle which is intended to be placed in orbit around a solar system body.
 7. For the end-of-mission, the disposition of the spacecraft and all of its major components, either in space or for landed components by position (or estimated position) on a planetary surface.

These points are addressed in this section. In Subsection 15.3.1 the sustainable development is discussed. The design philosophy is explained in Subsection 15.3.2. The launch strategy is discussed in Subsection 15.3.3. The biological burden is elaborated on in Subsection 15.3.4. Subsection 15.3.5 discusses additional cleaning problems arising for the penetrator and orbiter.

15.3.1 Sustainable Development

Sustainability is the quality of not being harmful to the environment or depleting natural resources, and thereby supporting long-term ecological balance³. For Spacecraft Engineering and Mission Design this means a heavy task is at hand. Fully completing a mission to Europa will therefore require a well-defined plan on sustainable engineering. By definition, a mission into space is not associated with a very sustainable image, it is therefore mostly about being as much sustainable as possible in comparison with other (similar) space missions.

Sustainability is an essential part of spacecraft design. It focuses on four main stages. Firstly, a sustainable design philosophy focuses on the resources used during design, testing and production. It will be taking into account the carbon footprint of the product. Secondly, launch strategy aims to launch the spacecraft into space in the most sustainable manner. A third important aspect of the sustainable design is the prevention against contaminating Europa with life from Earth. Finally, the end-of-life (EOL) procedure determines what has to happen with the product after its intended lifespan.

15.3.2 Design Philosophy

Materials and Structures

Lightweight structures and materials are of extreme importance in space systems, because the payload weight sizes the launch vehicles. To design a lightweight structure it is necessary to build the most efficient and optimized structure tailored for a specific application. Furthermore, decreasing the complexity of assembly and joining processes decreases costs, weight, and design and manufacturing time. It is therefore favourable to construct large parts in a single process.

To ensure the protection of the environment encountered during its life, it is necessary to fabricate functional and structural materials capable of maintaining the original properties after a defined time period in an extreme environment. Structures that are developed should be reliable and safe, and these levels of reliability and safety should be maintained throughout the service life of the system [Piascik et al., 2012]. Safety margins are therefore added to account for this.

Manufacturing

Manufacturing products should have a minimised negative environmental and economical impact. The need for transporting different manufactured parts to the assembly location should be made as low as possible and any negative impact on the health and comfort of the employees present at the manufacturing site should be addressed already during the design process.

Of course, toxic materials during production and using them in general is a less desirable option. They introduce health and safety risks to the personnel and may play a role in contaminating the moon. Use of them should therefore be minimized.

Considering using off-the-shelf components rather than developing new ones saves time and money on testing. On the other hand off-the-shelf components can be less optimal. This is a trade-off that has to be made, but surely has to be considered, also from a sustainable point of view. Less testing means less material wasted.

15.3.3 Launch Strategy

Conventional space missions require large, non-reusable rockets, which must be filled with a high-energy density fuel. The fuel may be harmful to the environment and the decoupled stages of the rocket that return to Earth as junk may contaminate ecosystems. To minimise these negative effects, an investigation can be done in both using less toxic fuels and launching using reusable rocket stages. Besides this, the

³<http://dictionary.reference.com/browse/sustainability>[Retrieved April 23, 2015]

latitude of the launch site determines to some extent the amount of fuel needed to reach the required orbit, therefore use should be made of the most optimal site. The orbital parameters are explained in Chapter 4. The most efficient trajectory is selected with multiple gravity assists to lower the required propellant mass as much as possible.

The selected propellant for the thrusters of the spacecraft is hydrazine because of its high specific impulse. Unfortunately this propellant is highly toxic for living matter as we know. To reduce environmental contamination and risk factors for the ground personnel, the manufacturing and loading of the propellant tanks must only be performed by highly experienced and certified companies. Hydrazine is inorganic and poses no problem according to the COSPAR regulations.

15.3.4 Biological Burden

Extremophiles might be able to survive the hostile space conditions and contaminate Europa. To prevent contamination, a clean room of a category close to ISO 1 must be used. Landing on Europa requires extra measures to reduce the bioburden. No organic material may be transmitted from the lander to the environment of Europa in any case. Sterilization procedures include dry heat microbial reduction (DHMR) and vapor phase hydrogen peroxide (VHP)⁴.

Recontamination needs to be prevented as well. The sterilized spacecraft can be packaged in a protective biobarrier to avoid recontamination⁵.

Reliable methods to estimate the bioburden on spacecraft are required to ensure the sterilization methods work. The NASA Standard Assay looks at the cultivable heat-tolerant micro-organisms. This includes sampling of the surface and putting the sample to a heat shock. The Total Adenosine Triphosphate (ATP) assay can also be used. This method measures the abundances of ATP, this substance is used in the metabolism of organisms. A third assay which can be performed is the LAL assay. This approach measures the bacterial abundance by looking at the endotoxins produced by Gram-negative bacteria [U.S. Department of Health and Human Services, 2012]⁶. The organic inventory shall not exceed more than 1 kg if all measures are taken.

15.3.5 Additional Challenges Europa

The regulations for landing or crashing on Europa are a lot harsher than for landing on Mars. As discussed in Section 5, the penetrator, the descent stage, and even the orbiter, will eventually crash into Europa. All must have undergone the same extreme sterilization treatment. The sensitive components for the data handling subsystem and the GNC subsystem need to be sterilized as well, but may not survive the current available treatments. A possible solution could be a new method called plasma sterilization, which is safe in terms of thermal, chemical, or irradiation damage⁷. However, this procedure has not matured yet for spacecraft sterilization, and might therefore not be available before the launch in 2022.

Despite of the availability of new sterilization procedures, fact is that the orbiter and the penetrator have to be made ultra clean. With the help of experts on the field of sterilization, a safe cleaning procedure for both humans and spacecraft has to be set up.

15.4 Market Analysis

After conferring with the client, the original specified budget of EUR 2.5 billion for a Europa mission has proven to be out of scope for ESA in the coming decade. Furthermore, international collaboration for an entire new mission is currently not achievable, this is caused by the fact that NASA is already designing a mission to Europa, requesting help on the lander, but not being interested in collaborating in a complete new mission. The Russian Federal Space Agency, Roscosmos, has published a draft of the federal space program's goals for 2016-2025 on April 23, 2015. It shows the effect of a 35% budget cut instated as the nation faces an economic crisis. A large part of its budget is taken up by the Angara launch vehicle, its joint ExoMars mission with ESA, two new modules for the ISS and multiple other (smaller) missions. However, there is no budget or intention described on visiting Europa⁸. Collaborating with the China National Space Administration (CNSA) is highly unlikely. First of all, it has shown no interest in Europa. Its main goal is to bring people to space and to build its own space station. Secondly, a US law from 2011

⁴<http://planetaryprotection.nasa.gov/methods>[Retrieved May 18, 2015]

⁵<http://planetaryprotection.nasa.gov/methods>[Retrieved May 18, 2015]

⁶<http://planetaryprotection.nasa.gov/methods>[Retrieved May 18, 2015]

⁷<http://www.astrobio.net/news-exclusive/ionized-gas-better-job-sterilizing-spacecraft/>[Retrieved June 22, 2015]

⁸<http://www.spaceflightinsider.com/organizations/roscosmos/russias-new-space-program-search-extraterrestrial-life-amid-b>[Retrieved May 9, 2015]

banned any corporation between CNSA and NASA, also influencing other space agencies. CNSA has become even more controversial since the 2007 Chinese anti-satellite test. The test reinforced concerns about Chinese intentions in outer space by creating a large cloud of orbital space debris, causing concerns about China adhering to COSPAR regulations⁹. The Japanese agency, JAXA, has placed security as top priority for the next decade, with most of the funding going toward building Japan's seven-satellite Quasi-Zenith regional navigation system, a new H-3 rocket, a next-generation data relay satellite, an advanced optical imaging satellite carrying a ballistic missile warning sensor and an effort to develop a new line of multi-purpose satellites¹⁰. JAXA currently has no interest and/or budget allocated to Solar System exploration, however, it has shown expressed a strong desire to collaborate with ESA in magnetospheric research, specifically proposing to provide a Jupiter-orbiting magnetospheric research element. [Clark et al., 2011] The Indian Space Research Organisation (ISRO) has no budget allocated towards Europa, it mainly focuses on its Mars orbiter, Lunar orbiter/lander and a new launcher¹¹.

15.4.1 Europa Clipper NASA/ESA Collaboration

NASA is currently designing the Europa Clipper, which will conduct a detailed reconnaissance of Jupiter's moon Europa and would investigate whether the icy moon could harbour conditions suitable for life. The mission would perform a detailed investigation of Europa using a highly capable spacecraft that would perform repeated close flybys of the icy moon. Europa exploration has consistently been rated as among the highest priority scientific pursuits for NASA, because it addresses the fundamental question of life beyond Earth¹².

Because of this oceans potential suitability for life,
Europa is one of the most important targets in all of planetary science.
(NASA Space Studies Board 2011)

Europa Clipper will address the following science objectives (in priority order):

1. Characterize the extent of the ocean and its relation to the deeper interior.
2. Characterize the ice shell and any subsurface water, including their heterogeneity, and the nature of surface-ice-ocean exchange.
3. Determine global surface compositions and chemistry, especially as related to habitability.
4. Understand the formation of surface features, including sites of recent or current activity, and identify and characterize candidate sites for future in situ exploration.
5. Understand Europas space environment and interaction with Jupiters magnetosphere.

As can be seen, these are almost identical to the initial science objectives for the Moonraker mission. To this end, there is no need for a direct copy, therefore, the current mission should fulfil these goals in a better/more adequate way, or investigate new areas. The most feasible way to achieve this is by adding some lander element to Clipper. NASA has a large interest in a potential lander mission to Europa, and therefore formulated the following extra objective for Europa missions:

- Characterize scientifically compelling sites, and hazards, for a potential future lander mission to Europa.

However, it is highly unlikely that US government will pass a budget request for a landed mission after budgeting the Europa Clipper mission. Furthermore, NASA's Planetary Science Decadal Survey 2013 - 2022, stating NASA's interest for the coming decade, recommend the Mars Astrobiology Explorer-Cacher mission as the top priority, followed by the Europa Clipper, and lastly the Uranus Orbiter and Probe mission. Therefore, a second Europa mission will have to make way for the Uranus Orbiter and Probe first.¹³ To this extent, NASA has proposed a joint Europa mission to ESA, combining NASA en ESA's budgets to add a piggyback addition to the Europa Clipper. NASA's Jet Propulsion Laboratory has

⁹<http://www.fas.org/sgp/crs/row/RS22777.pdf> [Retrieved May 09, 2015]

¹⁰<http://spacenews.com/japan-boosts-space-spending-in-support-of-security-focus/> [Retrieved May 9, 2015]

¹¹<http://spacenews.com/india-allocates-1-2-billion-for-space-activities/> [Retrieved May 9, 2015]

¹²<http://nspires.nasaprs.com/external/viewrepositorydocument/cmdocumentid=425528/solicitationId=%7BD663DD46-1929-9482-24BA-D5BCDBAA10BC%7D/viewSolicitationDocument=1/PEA%200%20Europa.pdf> [Retrieved May 7, 2015]

¹³http://solarsystem.nasa.gov/multimedia/downloads/Vision_and_Voyages-FINAL1.pdf [Retrieved May 9, 2015]

worked on a design that will form the foundation for the mission, it is up to ESA to contribute an orbiter, fly-by mission, lander, probe, penetrator or any other kind of descender.

Because of ESA's budget limitations, it is impossible to develop its own orbiter/lander combination, especially if it has to perform better than the Europa Clipper. ESA's Medium Class missions have a budget of around M€500, Large Class missions happen once every 7-10 years with a budget of around M€900 with the next slot in the late 2030's. Therefore, the option to send a piggy-back addition on-board of the Europa Clipper proves to be the most feasible option. A lander, for instance, will provide new information, information the Europa Clipper cannot find on its own. Some possible tasks of a lander could be:

- Measure organic content (including complex organics) of surface and near-surface materials
- Measure mineralogy and volatile content of surface and near-surface materials
- Image collected samples in the micron range
- Measure seismographic phenomena
- etc.

It is clear that a lander would provide extra valuable information on the exploration and habitability of Europa. The possibility of adding a lander to the Clipper has provided this team with a 100% stakeholder, ESA/ESTEC, for whom an added lander to the Clipper will fall within budget, and provided a way to gain valuable new insight in phenomena that would otherwise stay unexplored for many years to come.

Past NASA/ESA Collaboration

Collaboration between NASA and ESA is nothing new. In the past it has proven to be a fruitful combination, missions such as the Cassini-Huygens to Saturn and its moon Titan have been a great success. The Cassini orbiter was build by NASA, the Huygens probe build by ESA. The Cassini mission was originally proposed in November 1982 by a team of European and American scientists as a collaborative initiative with NASA in response to a regular call for mission ideas by ESA. The Huygens probe itself contains six instruments, each developed by different international teams. Some involved organizations are the Universite de Paris VII, France, Universitat Bonn, Germany, and the Open University, UK.

Future NASA/ESA Collaboration

Solar Orbiter is a future joint ESA-NASA collaboration that will address the central question of heliophysics: how does the Sun create and control the heliosphere? NASA is contributing two instruments to the collaboration, as well as an expandable launch vehicle. ESA is providing the spacecraft, build by Astrium, other European nations will provide the remainder of the ten payload instruments.

In 2013 NASA and ESA announced a new collaboration to send astronauts beyond Earth orbit. It was announced that ESA would provide a service module for the first Orion spacecraft mission. Orion is currently intended to facilitate human exploration of asteroids and Mars, as well as to provide a means of delivering or retrieving crew and supplies from the ISS.

15.4.2 ESA Funding

ESA's activities fall into two categories, mandatory and optional. Programmes carries out under the General Budget and the Science Programme budget are mandatory, these include studies on future projects, technology research, training programmes, etc. All Member States contribute to these programmes on a scale based on their Gross Domestic Product (GDP). The optional programmes are only of interest to some Member States, who are free to decide on their level of involvement. The actual design of any mission to Europa by ESA will be financed by optional contributions, meaning some Member States will pitch in and others will not.

When selecting instruments it is worthwhile to investigate its origin. Member States will be more interested in contributing if it boosts their own local industry. As an example, the Radar for Icy Moon Exploration (RIME), employed on JUICE, is developed and build in Italy, possibly making Italy willing to contribute more to the mission.

The same holds for collected scientific data, having a multinational crew of scientist might, again, influence the willingness of Member States contributing to the mission.

15.4.3 Design Constraints

The market analysis has shown the constraints that have to be taken into account during the design of the Moonraker mission. The three main constraints are the usage of radioactive power generation, the maximum mass for a piggyback addition to Clipper and the expected launch date.

Radioisotope Power Source (RPS)

RPSs have been used successfully on multiple space mission, such as Galileo, New Horizons, the Curiosity rover, Cassini, the Voyager Probes and the Viking landers. RTGs provide electrical power for spacecraft by converting the heat generated by the decay of plutonium-238 fuel into electricity using thermocouples. These RPSs are seen as highly reliable power options, but have their drawbacks, such as the high toxicity. ESA does currently not have their own RTG technology and NASA only has enough plutonium left for two missions, therefore being unlikely to share their technology with ESA, let alone for a piggyback addition. ESA, in collaboration with multiple companies, universities and research labs, is working on their own RTG, utilizing Americium-241. This technology, however, is by no way ready to be implemented.¹⁴ To this end, the constraint on the design of the Moonraker mission is to not use RPSs in any part of the system.

Mass Budget

Personal communication with the client has revealed that a reasonable mass constraint for a piggyback addition to Clipper is 350 kg in terms of total mass. This value is comparable to the from reference missions based estimation of 330 kg, for more details please refer to the Baseline report.

Launch Date & Trajectory

Clipper is planned to launch on 21 November 2021, any addition to this mission will require the same launch date. Therefore, the Moonraker mission should be ready for launch by at last that date. Moonraker will piggyback on Clipper during the interplanetary transfer, which follows a VEEGA trajectory with a duration of around 6.4 years, and should be capable to be launched on the Atlas V-551. Clippers launch vehicle is not yet decided, it is either the Atlav V-551 or the SLS, designing for the worst case scenario is in this case required.

¹⁴<http://www.unoosa.org/pdf/pres/stsc2012/tech-18E.pdf> [Retrieved June 18, 2015]

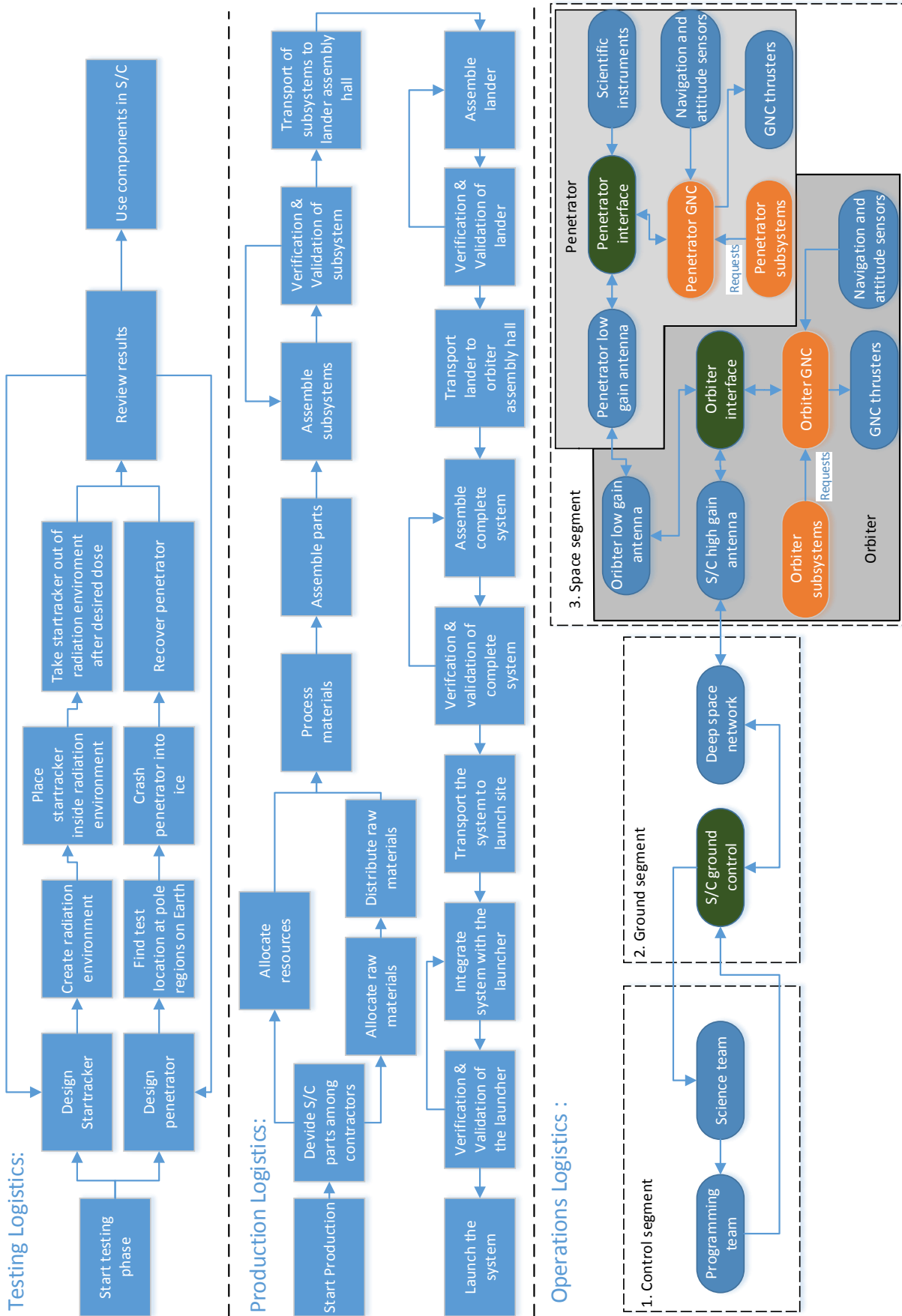


Figure 15.6: Logistics Diagram for Testing, Manufacturing and Operation

16. Programmatic

The programmatic approach is structured to enable effective management and decision taking and effective risk mitigation techniques. The approach outlined here is for the ESA side of the mission -Moonraker and Drax-, and does not discuss NASAs part - Clipper- of the mission. The presented cost estimation only focuses on the piggyback addition, it does not take additional Clipper costs into account.

16.1 Project Design & Development Logic

The design and development can be subdivided in different phases, as specified in 'ECSS-M-30A Space Project Management', these phases, their starting dates, duration and accompanying deliverables are graphically represented in a Gantt chart, see Figure 16.1, and in a functional flow block diagram, see Figure 16.2.

These charts are divided in the following main phases:

- **PHASE O+A: Mission Analysis/Needs Identification/Feasibility** - Phase O concerns the needs identification and the mission analysis. Phase A is the so called feasibility phase and should result in finalising the expression of needs expressed in phase O and proposing solutions meeting the perceived needs. This phase has been finalized in the mid-term report and spanned a total duration of 28 working days.
- **PHASE B: Preliminary Definition** - This phase allows for the selection of technical solutions for the system concept selected in phase A and confirming its feasibility. This report finalizes the first part of phase B, namely phase B1, spanning a total of 23 working days. After further approval and mission adoption, phase B2 is intended to start halfway June 2015 and spans until November 2016. Function numbers 1.x.x relate to this phase.
- **PHASE C: Detailed Definition** - Allows detailed study of the solution retained during the previous phase, as well as the production of representative elements of this solution, leading to a detailed definition of the system and its components. Phase C initiates at the end of phase B2, spanning 2 years, until November 2018. Function numbers 2.x.x relate to this phase.
- **PHASE D: Production/Ground Qualification Testing** - This is the end of the system development and permits a qualified definition of the products, components and the system itself, by completing the ground qualification process, and in particular by the provision of experimental results completing the theoretical elements acquired previously and also during this phase. Phase D will be operational until May 2021. Function numbers 3.x.x relate to this phase.
- **Margin** - Time contingency to allow for catching planning mismanagement, currently specified at just over 6 months.
- **Launch Campaign** - An overall test and commissioning phase of the system, leading up to the launch. Launch is scheduled at the 21st of November 2021. Function numbers 4.x.x relate to this phase.

Each phase contains one or multiple milestones, for a detailed description, please refer to 'ECSS-M-30A Space Project Management'.

KO = kickoff

MDR = Mission Definition Review

PRR = Preliminary Requirements Review

SRR = System Requirements Review

PDR = Preliminary Design Review

CDR = Critical Design Review

QR = Qualification Review

AR = Acceptance Review

ORR = Operational Readiness Review

FRR = Flight Readiness Review

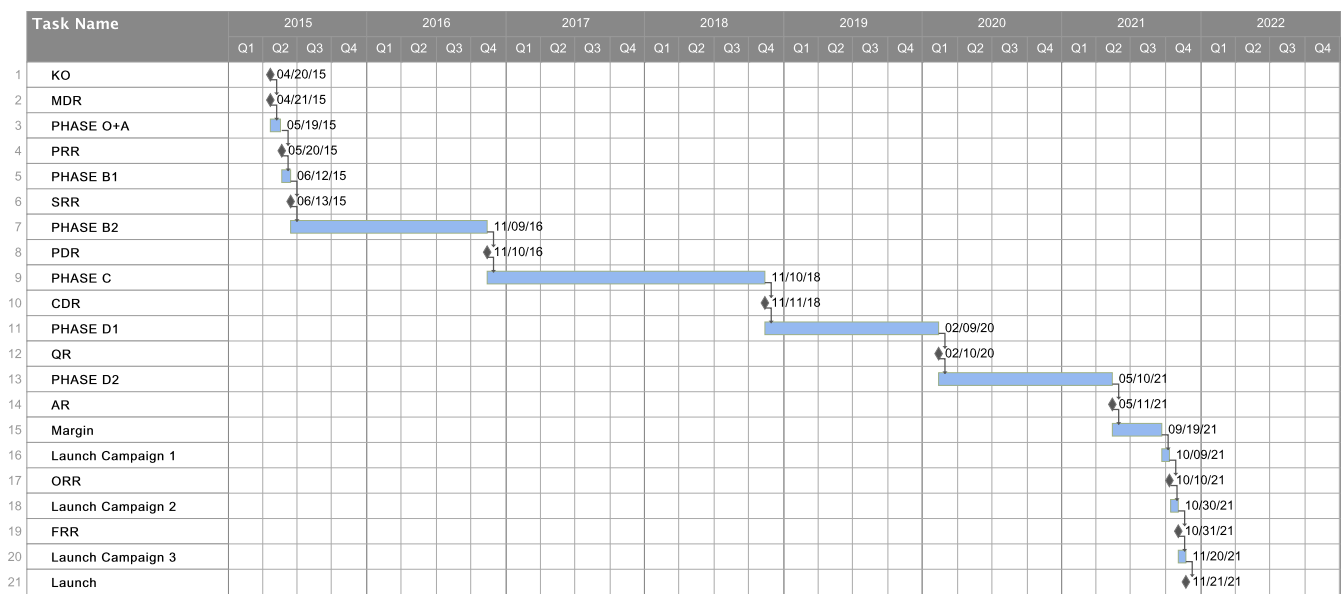


Figure 16.1: Design and Development logic Gantt chart.

After the mission adoption, an Invitation to Tender (ITT) will be issued for the Implementation Phase, from B2 till closure of the project. The scope of the ITT will be to implement all industrial activities leading to a launch and commissioning of Moonraker in the specified timeframe. The successful bidder will be appointed as Prime Contractor in charge, amongst other, of system engineering and management of sub-contractor. Each subsystem will be procured through an open competition, the subsystem contractors will be in charge of the procurement activities at lower levels. The payload will be procured through an Announcement of Opportunity (AO), in which it is up to any prospective contractor to formulate and present design ideas. The AO is planned 2 weeks after the start of phase C, spanning 2 years of total design and development time.

16.2 Cost Break-down Structure

For this piggyback mission, an ESA medium mission budget is available. This budget ranges between 500M and 700M EUR (FY2015), excluding launch costs. To stay within this budget, good estimations on the subsystem and payload costs will have to be made. In this chapter, firstly the instrument costs are calculated using NICM (Nasa Instrumentation Cost Model). After this, using similar mission cost profiles, a cost breakdown is made.

Cost Estimation Instruments

Most of the instruments on the penetrator are deduced from other missions and concept studies. These instruments were developed by universities and research institutes; this means that they will most likely be relatively cheap, compared to normal instruments from industry. Although the instruments are assumed to be very low cost, a part of the budget is set aside for instrumentation. Keep in mind that this strategy of choosing the instrumentation will have a consequence on the risk, as it needs to be tested extensively. The equations used are taken from the NICM manual [Habib-Agahi et al., 2011]. The equations below are all in US\$ FY2004 but in table 16.1 the final values are converted to EUR (FY2015).

NICM:

The different NICM documents give different equations for different systems. In this cost estimation the most applicable equations for the different instruments are selected. Below an overview of the equations used can be found.

General instrumentation equation:

$$Cost = 25.6M \cdot \left(\frac{Power}{61.5}\right)^{0.32} \cdot \left(\frac{Mass}{53.8}\right)^{0.26} \cdot \left(\frac{Data\ rate}{40.4}\right)^{0.11} \quad (16.1)$$

Table 16.1: Instrument cost

Cost per Instrument	
SILAT ¹	4M
Descent camera	0.3M
Seismometer	0.5M
Drill	7M
Micro imager	6.4M
Geology package	8.3M
Magnetometer	0.5M
Shielding per instrument ²	2M
Total instrumentation cost	35M

Particle observation instrumentation:

$$Cost = 13.9M \cdot \left(\frac{P}{10.6}\right)^{0.29} \cdot \left(\frac{\text{Design life}}{4.5}\right)^{0.35} \cdot \left(\frac{\text{Development time}}{49.7}\right)^{0.27} \quad (16.2)$$

Field measurement instrumentation:

$$Cost = 6.3M \cdot \left(\frac{\text{Power}}{10.6}\right)^{0.29} \cdot \left(\frac{\text{Mass}}{12.1}\right)^{0.16} \cdot \left(\frac{\text{Number of detectors}}{4.9}\right)^{0.15} * \left(\frac{\text{Development time}}{56.4}\right)^{0.68} \quad (16.3)$$

The total instrumentation budget is 35M EUR (FY2015). This budget already includes development and impact testing and implementation. Note that the budget needed could be much lower, for previously mentioned reasons. However, if this instrumentation budget is used, the instruments can be intensively tested for impact, radiation and temperature effects.

Total Cost Budget

Since a detailed instrumentation cost budget is available, it can be used to scale all other mission components. In the Table 16.2 three reference missions can be found. All contain a detailed cost breakdown that makes use of the PRICE-H and SEER cost estimation methods. Since most cost estimations are based on reference missions, this is also what is used in this report. The NASA reports [Europa Study Team, 2012] are all detailed studies for missions to Europa. They use different strategies, namely Multiple flyby, Europa Orbiter and Europa Orbiter/Lander, which are all having different budgets. The averages of all segments are given in the fourth column. From this, a scaling factor is made by using the average payload cost and the payload cost for the piggyback mission, calculated in the previous section. Using this scaling factor, all other cost budgets are calculated, after which a sanity check was performed to make sure this method is a good estimation. In the last row of table 16.2, the sanity check can be found. The spacecraft systems budget is taken as a percentage of the total cost, and it can be seen that for all the concepts it is between 25% and 30%. From this, it can be deduced that the method used is good enough to serve as a first estimate. Other sanity checks will be performed it terms of labour cost checks.

Segments Described

In the figure below, the subdivision of the segments from of the different components can be found. The numbering in Figure 16.4 and 16.3 refer to the numbering in table 16.2. Not included in this figure is the spacecraft systems cost breakdown, since this is included in every subsystem chapter separately, and the reserves, which are 20% of the total budget cost. The Figures 16.4 ⁴ and 16.3 ⁵ give a detailed view of what each cost segment contains. The spacecraft systems are composed of the power system, command and data handling, mechanical, radiation shielding, thermal control, propulsion, guidance navigation and control, the harness and the flight system. These form a large part of the content in this report, and their total cost is estimated at about 27% (142.2M EUR (FY2015)) of the total mission cost. Note that this cost estimation will serve as a reasonable preliminary estimate, but since it has been deduced from much

¹SILAT contains 3 instruments so needs trice shielding budget of 2M

²The shielding is only needed for instruments outside of the penetrator and the cost of shielding will be 2M per sensor

³The Spacecraft system cost as a percentage of the total system cost

⁴ [Europa Study Team, 2012]

⁵ [Europa Study Team, 2012]

Table 16.2: Detailed cost break-down based on Europa mission studies. Price in 10⁶ EUR (FY(2015))

Cost Estimation Methodology	Flyby	Orbiter	Orbiter/Lander	Average	Piggyback
1. Project management	52.5	47.3	64.8	54.8	15.2
2. Project systems engineering	43.8	37.6	56.9	46.1	12.7
3. Safety & Msn Assurance	48.1	41.1	62.1	50.5	14
4. Science	62.1	56	77	65	18
5. Payload systems	229.3	65.6	84.9	126.6	35
6. Spacecraft systems	427.9	421.8	693	514.2	142.2
a. Power	59.5	59.5	79.6	66.2	18.3
b. C&DH	23.6	23.6	17.5	21.6	6
c. Telecom	42	47.3	47.3	45.5	12.6
d. Mechanical	38.5	40.3	19.3	32.7	9
i. Radiation shielding	9.6	7.9	5.3	7.6	2.1
ii. Payload radiation shielding	1.8	0.9	0	0.9	0.2
e. Thermal	8.8	8.8	6.1	7.9	2.2
f. Propulsion	47.3	52.5	41.1	46.9	13
g. GNC	49	49	59.5	52.5	14.5
h. Harness	5.3	5.3	5.3	5.3	1.5
i. Spacecraft flight	28.9	29.8	28	28.9	7.9
7. Mission Ops system	149.6	140.9	207.4	165.9	45.9
8. Launch system	N.A.	N.A.	N.A.	N.A.	N.A.
9. Ground data system	34.1	34.1	48.1	38.8	10.7
10. Project system I&T	36.8	37.6	57.8	44	12.2
11. Education and public outreach	10.5	8.8	15.8	11.7	3.2
12. Mission design	21	17.5	25.4	21.3	5.9
13. Reserves (20%)	397.3	324.6	566.1	429.3	118.7
TOTAL	1672.1	1407.9	2304.8	1794.9	521
Sanity check(%) ³	25.6	29.9	30.0	28.6	27.3

larger stand-alone missions, the cost for especially the non-technical segments could turn out higher. Therefore, it is recommended to increase the reserves, because even though in percentage they are equal to the larger missions the actual reserves budget is in total much lower. Also cleanroom product assembly and sterilisation of the the parts to prevent contamination will be expensive and have an effect the costs.

Sanity Check

In this subsection several sanity checks on the estimated cost are preformed. The cost of an engineer per hour is 150 EUR which boils down to a yearly cost of 288k EUR. Then for the mission design (management, analysis, engineering and navigation design) a group of 10 engineers could work on this for 2 years continuously and still stay within the budget. This seems to be a reasonable estimate for non flagship missions in development phase.



Figure 16.2: Design & Development logic functional flow block diagram for the Moonraker mission.

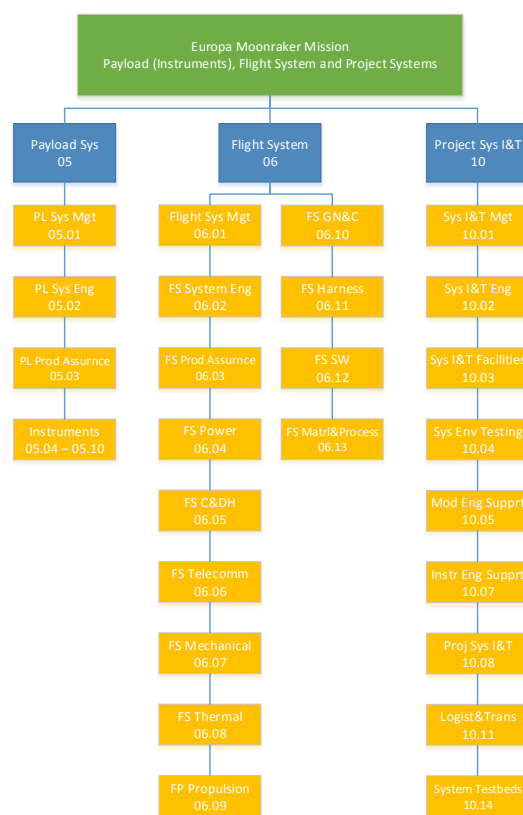


Figure 16.3: Detailed Cost Breakdown Overview

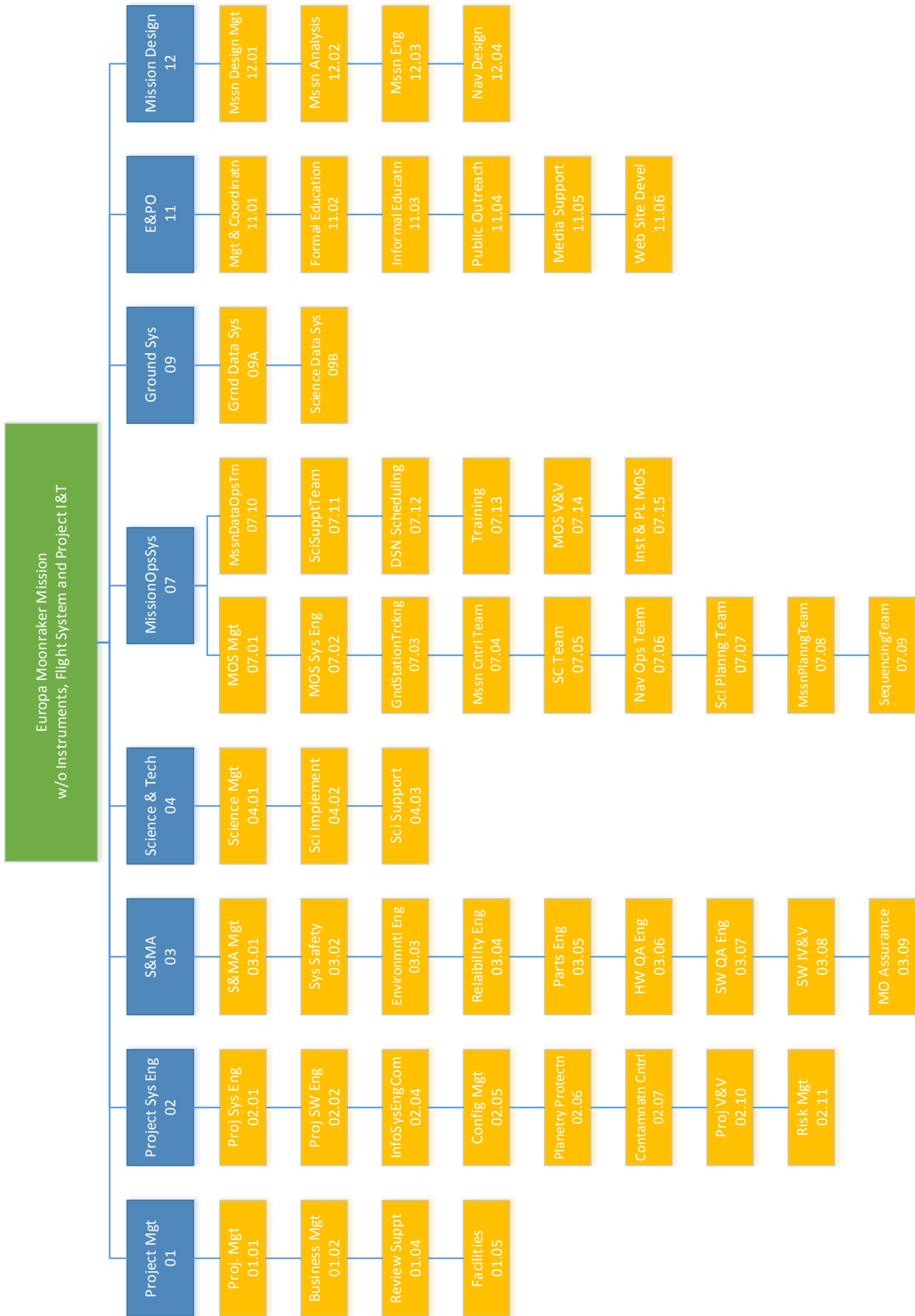


Figure 16.4: Detailed Cost Breakdown Overview continued

17. Conclusion

The main purpose of this final report is to discuss the detailed design of the piggyback orbiter/lander combination, referred to as the Moonraker mission. This concept came out of the trade-off of the midterm report. The Moonraker mission will be attached to the Clipper mission and will be launched in November 2022. Clipper will guide Moonraker on a VEEGA orbit towards Jupiter, when Moonraker will be detached from Clipper just before Jupiter orbit insertion. Moonraker will then perform a Jovian tour of almost two years to reduce the required ΔV for Europa orbit insertion. Moonraker will be finally capture a circular polar orbit around Europa at an altitude of 244 km. After four orbits it will deploy the lander named Drax, which is a hard impact penetrator. The orbiter will mainly function as a relay orbiter for the penetrator. This because the penetrator would not be able to communicate and transfer all acquired data to Clipper, given the large interval of flybys of Clipper.

The design of such a mission posed a lot of challenges on the team, and the mass turned out to be a problem for this mission. The reason is that a small relay orbiter cannot be simply scaled down, as is the case for LEO satellites. The solar constant is only 1/25 of the value of Earth, which means very large solar arrays are required to generate only a limited amount of power. Telecommunications also turned out to be relatively heavy for a small Jovian orbiter. Due to the distance to Earth, a large antenna is required to achieve an acceptable data rate. The radiation shielding turned out to have a relatively high mass, since the environment at Europa is very demanding. Finally because of orbit instabilities, the Δ budget for this mission was also quite high. This, in turn, resulted in a high propellant mass. The total mass for the orbiter and penetrator combined including propellant is established at 704 kg, twice the mass which was designed for. However, looking at other studies currently done for Europa landers, all of them have a very high mass or alter the nominal mission of Clipper significantly. This was chosen not to do for the Moonraker mission.

Because of the high mass, it was decided that the orbiter would service primary as a relay satellite of the penetrator. This was required since this relieved the data rate requirement on the telecommunication system. Therefore, the antenna size could be smaller and also less power could be used for the telecommunication system, therefore also reducing the mass of the power system. However, the orbiter still has a SILAT instrument package that can make images and perform laser altimeter measurements, but this is only done as a secondary mission objective. For example, during the Jovian tour, images of other moons during flybys can be made as the spacecraft would not need communications for penetrator data at that point.

The penetrator will perform a large number of measurements and will perform unique in situ measurements of the surface. These measurements are related to the surface composition, but also to the magnetic field and to the tectonic movements of the icy layer which will be measured by seismometers. The penetrator will consist of two 'bays', one which will live for only 12 hours and perform surface measurements. The other module contains the seismometer package and the telecommunications to relay all the penetrator data of the course of two weeks. A polar landing site is chosen, since this is favourable in terms of contact time between the orbiter and the penetrator. This increases the number of passes of the orbiter over the penetrator.

The design of most subsystems is based on existing systems, therefore most components are already space qualified. However, radiation protection still posed a high challenge. Since some components could not withstand the harsh radiation environment, shielding had to be applied which had a mass of 40 kg. The power system, however, uses state-of-the-art multi-junction Gallium Arsenide cells with a very high efficiency of 33 % to reduce the power system mass. The solar arrays have an area of 13.5 m^2 and a mass of 74.2 kg, while generating 170 W at begin of life and only 122 W at end-of-life, due to radiation degradation. Together with the power conditioning unit, the power system has a mass of 90 kg which makes it the heaviest spacecraft subsystem. The other subsystems are well within or close to their original design mass.

The other large contributor to the high mass is the propellant mass. The largest contributor to the

ΔV budget is the controlled descent of the penetrator, which already requires 2.3 km/s to impact at a velocity of 300 m/s. Furthermore the Jupiter orbit insertion requires 850 m/s which is already optimized by performing the Jovian tour instead of a direct orbit insertion. Perturbations also account for a large part of the ΔV budget, since the orbit around Europa is highly perturbed. The total ΔV budget relates to a total propellant mass of almost 400 kg which is more than half of the mission mass.

The main conclusion of this final report is that a piggyback mission orbiter/lander combination for a mass of 350 kg is not possible. The main reasons for this are the high propellant mass, the low solar constant and the harsh radiation environment. The concept can fit the 350 kg when the design drops the orbiter and focusses on the penetrator. However, the communication problem should then still be solved. This could be done by altering the trajectory of Clipper. The cost is still a primary estimate. It turns out that the mission budget of 700 M EUR is sufficient, and still some money can be invested in testing and development of new technologies. Further recommendations are given in Chapter 18.

18. Recommendations

What was mainly a limiting factor in this piggyback design are the weight, power and dimension restrictions. Increasing the budget for weight, power and dimension restrictions will mainly have a positive effect on the science instruments. The science instrumentation for the orbiter can be changed or added to if the mass and power budget increases, increasing the return on investment. It would be great to take a magnetometer, which can map the magnetic field of Europa globally if the orbiter is in polar orbit. Spectrometers will allow investigation of the possible plumes and particles emitting from Europa, Ion and neutral mass spectrometers but also Raman spectrometers could be considered. A very interesting instrument to take is an ice penetrating radar, which will be able to analyse the ice up to 10 km depth. A Langmuir probe is a plasma instrument that could be used to analyse plasma interaction to derive external magnetic fields. If a larger telecommunications and data processing unit will be available it is of great interest to make a high-resolution global map of Europa using a topographic imager. Such a map will show all interesting sites for future investigation and increase our understanding of Europa greatly. The most ideal case will be to at least locally map with a resolution of 1m/pixel or less to prepare for future landers. These additions will increase the mission lifetime to be optimally, this in turn has a consequences for the radiation shielding. For a dedicated orbiter which will do global mapping will need about 170 kg of radiation shielding and will cost about 1.6 B EUR.

Future missions or increase of the mass budget will make soft landers possible, this will need about 500 kg for landing so a large mass increase will be a consequence. These landers are much less risky and will be able to carry much more multi functional science payload and can even visit multiple interesting sites. Instruments on such a soft lander will be a mass spectrometer to investigate the surface chemistry (organic content) and a Raman spectrometer, which is better for microbiology. Also multiple seismometers are interesting, because multiple seismometers will allow to determine the ice thickness with much higher accuracy. An in situ imaging system, reconnaissance camera and a sampling system are also interesting to include in the payload. Soft landers tend to have bigger communication subsystems, which will allow for larger data rates, so landing at the equator instead of at the poles becomes possible. In the long-term future it would be interesting to completely melt through the icy layer and investigate the subsurface ocean with a submarine like vehicle. Although if the penetrator mission will turn up nothing that points to life future missions to Europa will become much less interesting. A Europa soft lander will however be much more expensive (2.4B EUR) than the piggyback mission considered in this report.

Another restriction was the assumption of not being allowed to affect or alter Clippers mission to a great extent. If, for instance, the trajectory of Clipper could temporarily be altered, there would be no need for a dedicated relay satellite, rendering a stand-alone penetrator a feasible option within the initial assumed mass budget of 350 kg.

Concluding the recommendations it can be said that increasing the budgets will be positive in terms of science but will also greatly affect the cost of the mission. Using an RTG will make small missions more feasible since it is a lightweight solution for powering a Europa mission, since solar panels in the Jovian environment are very inefficient.

Bibliography

- [Ball et al., 2007] Ball, A., Garry, J., and Kerzhanovich, V. (2007). *Planetary Landers and Entry Probes*. Cambridge University Press, Cambridge, UK, first edition.
- [Bettner, 1995] Bettner, M. (1995). Tools for Satellite Ground Track and Coverage Analysis. Technical Report December.
- [Brinza, 2014] Brinza, D. (2014). Europa Clipper Pre-Project 13-F7 Trajectory Trapped Particles Estimated Differential Fluences from Grid2 Model. pages 1–2.
- [Brown, 2002] Brown, C. D. (2002). *Elements of Spacecraft Design*. AIAA, Reston, Virginia, first edition.
- [Brunner, 2005] Brunner, T. a. (2005). Forms of Approximate Radiation Transport. In *5LC*, page 43, Albuquerque, New Mexico. Sandia National Laboratories Albuquerque.
- [Campagnola et al., 2014a] Campagnola, S., Buffington, B. B., and Petropoulos, A. E. (2014a). Jovian tour design for orbiter and lander missions to europa. *Acta Astronautica*, 100:68–81.
- [Campagnola et al., 2014b] Campagnola, S., Buffington, B. B., and Petropoulos, A. E. (2014b). Jovian tour design for orbiter and lander missions to europa. *Acta Astronautica*, 100(0):68 – 81.
- [Capderou, 2005] Capderou, M. (2005). *Satellites: Satellites: Orbits and Missions*. Springer.
- [Cervone, 2014] Cervone, A. (2014). Ae 2230-ii propulsion and power: Rocket propulsion. TUDelft.
- [Clark et al., 2011] Clark, K., Boldt, J., Greeley, R., Hand, K., Jun, I., Lock, R., Pappalardo, R., Houten, T. V., and Yan, T. (2011). Return to europa: Overview of the jupiter europa orbiter mission. *Advances in Space Research*, 48(4):629 – 650. Europa Lander: Science Goals and Implementation.
- [Composites, 2000] Composites, H. (2000). Hexweb honeycomb sandwich design technology.
- [COSPAR, 2005] COSPAR (20 October 2002; Amended 24 March 2005). Cospar planetary protection policy. Retrieved from <http://w.astro.berkeley.edu/~kalas/ethics/documents/environment/COSPAR%20Planetary%20Protection%20Policy.pdf> on 22 april 2015.
- [dos Santos Carvalho et al., 2013] dos Santos Carvalho, J. P., de Moraes, R. V., and de Almeida Prado, A. F. B. (2013). Dynamics of artificial satellites around europa. *Mathematical Problems in Engineering*, 2013:1–7.
- [DSE Group 10 et al., 2015] DSE Group 10, Van den Bercken, V., Burger, S., Dekkers, N., Hoogvliet, J., Kassem, V., Kok, R., Kranen, T., Van Marrewijk, G., Melman, F., and Mulder, B. (2015). Dse next stop:europa - midterm report. Technical report, Faculty of Aerospace Engineering, Delft University of Technology.
- [ECSS, 2010] ECSS (2010). Space engineering: Calculation of radiation and its effects and margin policy handbook. Technical Report December.
- [ECSS Requirements and Standards Division, 2011] ECSS Requirements and Standards Division (2011). *Thermal Design Handbook - Part 1: View factors*. ESA.
- [Enertron Inc, 2001] Enertron Inc (2001). Heat pipe selection. https://www.enertron-inc.com/pdf/thermal_design_guildines/How-to-select-a-heat-pipe.pdf[Retrieved June 16, 2015].
- [ESA, 2014] ESA (2014). Margin philosophy for science assessment studies. Technical Report 2, European Space Agency.
- [Fiebrich et al., 2004] Fiebrich, H., Haines, J., and Tonicello, F. (2004). Power system design of the rosetta spacecraft. In *2nd International Energy Conversion Engineering Conference, AIAA*, volume 5535.
- [Finckenor and Dooling, 1999] Finckenor, M. M. and Dooling, D. (April 1999). *Multilayer insulation material guidelines*. NASA.

-
- [Fortescue et al., 2011] Fortescue, P., Swinerd, G., and Stark, J. (2011). *Spacecraft Systems Engineering*. Wiley, fourth edition.
- [Fraser et al., 1990] Fraser, D., Kleespies, H., and Vasicek, C. (1990). *Spacecraft Subsystems*. Department of Aerospace Engineering and Engineering Mechanics, The University of Texas.
- [Gao et al., 2008] Gao, Y. et al. (2008). Lunar science with affordable small spacecraft technologies: Moonlite and moonraker. *Planetary and Space Science*, 56(-):368–377. MoonLITE and Moonraker.
- [Gardini et al., 1999] Gardini, B. et al. (1999). Rosetta system requirements specification ro-est-rs-2001. Technical report, European Space Agency.
- [Girishkumar et al., 2010] Girishkumar, G., McCloskey, B., Luntz, A., Swanson, S., and Wilcke, W. (2010). Lithium- air battery: promise and challenges. *The Journal of Physical Chemistry Letters*, 1(14):2193–2203.
- [Gowen et al., 2007] Gowen, R. et al. (2007). Kinetic penetrators for exploration of solar system bodies. *International Planetary Probes Workshop (IPPW-5) Bordeaux, France, -(–):-*. ESA Special Publication.
- [Gowen et al., 2011] Gowen, R., Smith, A., Fortes, A., et al. (2011). Penetrators for in situ subsurface investigations of europa. *Advances in Space Research*, 48(4):725 – 742. Europa Lander: Science Goals and Implementation.
- [Greenberg, 2005] Greenberg, R. (2005). *EUROPA: The Ocean Moon*. Praxis Publishing Ltd, Chichester, UK.
- [Grumman, 2014] Grumman, N. (2014). Scalable SIRU Family. Technical report, Northrop Grumman, Woodland Hills, CA 91367 USA.
- [Habib-Agahi et al., 2011] Habib-Agahi, H., Mrozinski, J., and Fox, G. (2011). Nasa instrument cost/schedule model hamid habib-agahi. In *Aerospace Conference, 2011 IEEE*, pages 1–19. IEEE.
- [Hamann et al., 2011] Hamann, R. et al. (2011). *Systems Engineering & Technical Management Techniques*. TU Delft Faculty of Aerospace Engineering, issue 1 edition.
- [Heynderickx et al., 1998] Heynderickx, D., Quaghebeur, B., Fontaine, B., Glover, A., Carey, W. C., and Daly, E. J. (1998). New Features of Esa ' S Space Environment Information System Spenvis. *Nasa Technical Memorandum*.
- [Hut et al., 2003] Hut, P., Makino, J., Teuben, P., and Bischof, H. (2003). Moving stars around. *URL <http://www.artcompsi.org/msa/web/index.html>. Preliminary version of, 1.*
- [Jensen and Laursen, 2002] Jensen, H. and Laursen, J. (2002). Power conditioning unit for rosetta/mars express. *ESA SP*, pages 249–256.
- [Jensen, 2000] Jensen, J. (2000). Command and data handling subsystem design for the ionospheric observation nanosatellite formation (ion-f).
- [JPL, 2008] JPL (2008). Jupiter Europa Orbiter Mission Study 2008: Final Report. Technical report, JPL, California.
- [Karam, 1998] Karam, R. D. (1998). *Satellite thermal control for systems engineers*, volume 181. Aiaa.
- [Kraft,] Kraft, S. Highly intergrated payload architecture and instrumentation for future planetary missions. *Cosine Research B.V. SILAT*.
- [Luthi et al., 2004] Luthi, B. et al. (2004). The beagle 2 microscope. *Lunar and Planetary Science*, 35. Microimager for Beagle 2.
- [Makovsky et al., 2002] Makovsky, A., Barbriere, A., and Tung, R. (2002). Odyssey telecommunications.
- [Mazarico et al., 2015] Mazarico, E., Genova, A., Neumann, G., Smith, D., and Zuber, M. (2015). Simulated recovery of europas global shape and tidal love numbers from altimetry and radio tracking during a dedicated flyby tour.

-
- [McFadden et al., 2007] McFadden, L.-A., Weissman, P., and Johnson, T. (2007). *The Encyclopedia of the Solar System*. Elsevier.
- [Mills and Brown, 2000] Mills, F. P. and Brown, M. E. (2000). Thermal infrared spectroscopy of Europa and Callisto. *Journal of Geophysical Research*, 105:51–59.
- [Mooij, 2015] Mooij, E. (2015). Next stop Europa: Project guide design synthesis exercise.
- [Moon et al., 2009] Moon, S. et al. (2009). Towards a miniaturized photon counting laser altimeter and stereoscopic camera instrument suite for microsatellites. *7th IAA Symposium on Small Satellites for Earth Observation*. SILAT for Microsatellites.
- [Mukai et al., 2012] Mukai, R., Hansen, D., Mittskus, A., Taylor, J., and Danos, M. (2012). Juno telecommunications.
- [NASA, 1999] NASA (1999). *Guidelines for Thermal analysis of spacecraft hardware*.
- [NASA, 2011] NASA (August 2011). *Juno Launch Press Kit*. NASA.
- [Niebur et al., 2013] Niebur, C. et al. (2013). Icee team welcome briefing. Presented to the Europa Clipper Pre-Project Team.
- [Nouvellon et al.,] Nouvellon, S., Berthoud, L., and Rickwood, W. Thermal design of a lunar penetrator. *parameters*, 4(7):8.
- [Paranicas et al., 2007] Paranicas, C., Mauk, B. H., Khurana, K., Jun, I., Garrett, H., Krupp, N., and Roussos, E. (2007). Europa’s near-surface radiation environment. *Geophysical Research Letters*, 34(15):L15103.
- [Patel, 2004] Patel, M. (2004). *Spacecraft power systems*. CRC press.
- [Peterson et al., 2010] Peterson, S. B., Apt, J., and Whitacre, J. (2010). Lithium-ion battery cell degradation resulting from realistic vehicle and vehicle-to-grid utilization. *Journal of Power Sources*, 195(8):2385–2392.
- [Petropoulos et al., 2000] Petropoulos, A. E. et al. (2000). Trajectories to Jupiter via gravity assists from Venus, Earth, and Mars. *Spacecraft and Rockets*, 37:776 – 783.
- [Piascik et al., 2012] Piascik, B., Vickers, J., et al. (2012). *Materials, Structures, Mechanical Systems and Manufacturing Roadmap Technology Area 12*. National Aeronautics and Space Administration, Washington, DC 20546.
- [Planetary Systems Corporation, 2014] Planetary Systems Corporation (2014). *User’s Manual for Mark II Lightband*, revision e edition.
- [Poinas, 2004] Poinas, P. (2004). Satellite thermal control engineering. http://www.tak2000.com/data/Satellite_TC.pdf [Retrieved June 10, 2015].
- [Pope,] Pope, J. E. *Rules of thumb for mechanical engineers*. First edition.
- [Europa Study Team, 2012] Europa Study Team (2012). Europa study 2012 report. Technical Report JPL D-71990, National Aeronautics and Space Administration.
- [European Cooperation for Space Standardization, 1996] European Cooperation for Space Standardization (1996). Space project management: Project phasing and planning.
- [Pipeline and Hazardous Materials Safety Administration, 2015] Pipeline and Hazardous Materials Safety Administration (16 March 2015). Hazardous materials table. <http://www.phmsa.dot.gov/portal/site/PHMSA> [Retrieved May 10, 2015].
- [U.S. Department of Health and Human Services, 2012] U.S. Department of Health and Human Services (2012). Guidance for industry: Pyrogen and endotoxins testing: Questions and answers.
- [Richardson and Chan, 2007] Richardson, R. and Chan, J. (2007). Advanced Stirling radioisotope generator development. In *First Annual NASA Science Technology Conference*.

-
- [RuizTorres et al., 2010] RuizTorres, A. J., Zhang, J., Zapata, E., Pennathur, A., Rhodes, R., McCleskey, C., and Cowen, M. (2010). A reliability, maintainability, and safety model to support the assessment of space vehicles. *International Journal of Quality & Reliability Management*, 27(4):486–504.
- [Santos et al.,] Santos, J. C. D., dos Santos Carvalho, J. P., and de Moraes, R. V. Stable low-altitude polar orbits around europa.
- [Sciver and W.,] Sciver, V. and W., S. *Helium Cryogenics*. Edition number 2 edition.
- [Seltzer, 1979] Seltzer, S. (1979). Electron, Electron-Bremsstrahlung and Proton Depth-Dose Data for Space-Shielding Applications. *IEEE Transactions on Nuclear Science*, 26(6):4896–4904.
- [Shambayati, 2009] Shambayati, S. (2009). A comparison of the ka-band deep-space link with the x-band link through emulation.
- [Smith et al., 1976] Smith, E., Davis, J., and Jones, D. (1976). Jupiter’s magnetic field and magnetosphere. *Jupiter*, pages 788–829.
- [Strobl et al., 2000] Strobl, G., Uebele, P., Tentscher, K., Kern, R., Rasch, K., Bogus, K., Robben, T., and LaRoche, G. (2000). Thin hi-eta (η) space silicon solar cells with improved end-of-life performance. In *Photovoltaic Specialists Conference, 2000. Conference Record of the Twenty-Eighth IEEE*, pages 1289–1292. IEEE.
- [Technologies, 2013] Technologies, B. S. (2013). ST-200 Miniaturised Autonomous Star Tracker. Technical report, BST, Berlin.
- [Thomas et al., 2003] Thomas, N. et al. (2003). The microscope for the beagle 2 lander on esa’s mars express. *A Sixth international Conference on Mars*, 48. Microimager for Beagle 2.
- [Truscott et al., 2010] Truscott, P., Heynderickx, D., Nartallo, R., Lei, F., Sicard-piet, A., and Bourdarie, S. (2010). The JORE2M2 Project : Jupiter Environment , Effects and Shielding Prediction Models for SPENVIS Effects of the Jovian Radiation Environment. (21290).
- [United Launch Alliance, 2010] United Launch Alliance (2010). *Atlas V Launch Services User’s Guide*, revision 11 edition.
- [Vijendran et al., 2014] Vijendran, S. et al. (2014). *Europa Penetrator Design and Full Scale Survivability Testing*. Airbus Defence and Space.
- [Wahr et al., 2006] Wahr, J., Zuber, M., Smith, D., and Lunine, J. (2006). Tides on europa, and the thickness of europa’s icy shell. *J. Geophys. Res.*
- [Wakker, 2015] Wakker, K. F. (2015). *Fundamentals of Astrodynamics*. Institutional Repository, Library, Delft University of Technology.
- [Weiss et al., 2011] Weiss, P., Yung, K., Komle, N., Ko, S., Kaufmann, E., and Kargl, G. (2011). Thermal drill sampling system onboard high-velocity impactors for exploring the subsurface of europa. *Advances in Space Research*, 48(-):743–754. Thermal drill.
- [Wertz et al., 2011] Wertz, J. R., Everett, D. F., and Puschell, J. J. (2011). *Space Mission Engineering: The New SMAD*. Microcosm Press.
- [Willis, 2006] Willis, P. B. (2006). Europa Mission: Generic Materials Test Methodology. Pasadena.
- [Zandbergen, 2010] Zandbergen, I. (February 2010). *Thermal Rocket Propulsion*. TUDelft.

A. Work Distribution

Table A.1: Work distribution

Section	Title	Responsible	Helped by
-	Preface	Roy	-
-	Executive Overview	Roy	All (own subsystem)
1	Introduction	Roy	-
2	Concept Description & Top Level Req.	Floor	-
3	Design Considerations		
3.1	Mission Functions	Vincent	-
3.2	Resource Allocation and Budget Breakdown	Floor	-
4	Astrodynamic Characteristics	Valentin	Roy
5	GNC Subsystem	Boris & Stijn	-
6	Propulsion Subsystem	Nick	-
7	Scientific Instrumentation	Roy	Jonathan
8	Power Subsystem	Floor	-
9	TC&DH Subsystem	Jonathan	Roy
10	Thermal Control Subsystem	Gijsbert	-
11	Structural Subsystem	Vincent	-
12	Radiation	Tommy	-
13	Technical Risk Assessment	Gijsbert & Nick	All (own subsystem)
14	System Performance		
14.1	Spacecraft System Characteristics	Floor	-
14.2	Spacecraft Configuration	Nick	Vincent
14.3	Compliance Matrix	Floor	-
14.4	Sensitivity Analysis	Gijsbert	-
15	Mission Development & Operations		
15.1	Manufacturing, Assembly and Integration Plan	Stijn	-
15.2	Operations and Logistic Concept Description	Boris	-
15.3	RAMS Analysis	Valentin	-
15.4	Sustainable Development Strategy	Stijn	-
15.5	Market Analysis	Tommy	
16	Programmatics		
16.1	Project Design & Development Logic	Tommy	-
16.2	Cost Break-down Structure	Roy	-
17	Conclusion	Floor	-
18	Recommendation	Roy	-
A	Work Distribution	Gijsbert	-